

Engineering Materials

Guangming Jiang *Editor*

Microbiologically Influenced Corrosion of Concrete Sewers

Mechanisms, Measurements, Modelling
and Control Strategies

 Springer

Engineering Materials

This series provides topical information on innovative, structural and functional materials and composites with applications in optical, electrical, mechanical, civil, aeronautical, medical, bio- and nano-engineering. The individual volumes are complete, comprehensive monographs covering the structure, properties, manufacturing process and applications of these materials. This multidisciplinary series is devoted to professionals, students and all those interested in the latest developments in the Materials Science field, that look for a carefully selected collection of high quality review articles on their respective field of expertise.

Indexed at Compendex (2021) and Scopus (2022)


Guangming Jiang
Editor

Microbiologically Influenced Corrosion of Concrete Sewers

Mechanisms, Measurements, Modelling
and Control Strategies

 Springer

Editor

Guangming Jiang 

School of Civil, Mining, Environmental
and Architectural Engineering
University of Wollongong
Wollongong, NSW, Australia

ISSN 1612-1317

ISSN 1868-1212 (electronic)

Engineering Materials

ISBN 978-3-031-29940-7

ISBN 978-3-031-29941-4 (eBook)

<https://doi.org/10.1007/978-3-031-29941-4>

© The Editor(s) (if applicable) and The Author(s), under exclusive license to Springer Nature Switzerland AG 2023

This work is subject to copyright. All rights are solely and exclusively licensed by the Publisher, whether the whole or part of the material is concerned, specifically the rights of translation, reprinting, reuse of illustrations, recitation, broadcasting, reproduction on microfilms or in any other physical way, and transmission or information storage and retrieval, electronic adaptation, computer software, or by similar or dissimilar methodology now known or hereafter developed.

The use of general descriptive names, registered names, trademarks, service marks, etc. in this publication does not imply, even in the absence of a specific statement, that such names are exempt from the relevant protective laws and regulations and therefore free for general use.

The publisher, the authors, and the editors are safe to assume that the advice and information in this book are believed to be true and accurate at the date of publication. Neither the publisher nor the authors or the editors give a warranty, expressed or implied, with respect to the material contained herein or for any errors or omissions that may have been made. The publisher remains neutral with regard to jurisdictional claims in published maps and institutional affiliations.

This Springer imprint is published by the registered company Springer Nature Switzerland AG
The registered company address is: Gewerbestrasse 11, 6330 Cham, Switzerland

*This book is dedicated to my parents,
Daijun Jiang and Xiuqiong Zhang.*

*And, to my wife Emma and my children
Jayden and Isabella for their love.*

Foreword

Corrosion is the interaction of materials with the environment, resulting in changes in the material, which can eventually lead to considerable impairment of the function. It has been estimated that the total cost of corrosion worldwide is 3.4% of global gross national product. A conservative estimate is that approximately 20% of all corrosion in aqueous systems is microbiologically influenced corrosion (MIC). MIC is defined as a mechanism in which the kinetics of the corrosion process are influenced by microorganisms, directly or indirectly. MIC can significantly compromise the integrity of industry assets (e.g. oil and gas, water and wastewater processing, pulp and paper mills and maritime infrastructure) when biofilms are established and grow on the surfaces.

Industry assets with abundant, active and diverse microbial populations, ineffective corrosion control, and those with periods of water stagnation or low flow conditions can accelerate microbial growth and increase the threat of MIC on concrete surfaces. Concrete corrosion in sewers involves a combination of physical, chemical and biological processes and is commonly termed microbiologically influenced concrete corrosion (MICC).

This book provides the most recent knowledge about MICC mechanisms, measurements, modelling and control strategies. Corrosion causes loss of concrete mass and deteriorates the structural capacity, leading to cracking of sewer pipes and ultimately structural collapse. The rehabilitation and replacement of damaged sewers are very costly. In the USA alone, corrosion is causing sewer asset losses estimated at around \$14 billion per year. MICC can significantly reduce the lifetime of concrete structures, e.g. from an expected 100 years down to 30–50 years, and in extreme cases, to 10 years or less.

The editors and authors of this book have been actively carrying out research in collaboration with water utilities worldwide for more than a decade. A massive volume of updated and novel knowledge is being generated globally by different research groups, including those from Australia, Europe, the USA and China.

This book is a cross-disciplinary monograph covering physical, chemical, biological processes involved in concrete corrosion, corrosion rate measurements and characterisation methods, control of environmental factors, corrosion prediction models, corrosion mitigation and control strategies, and the development of corrosion-resistant concrete.

The book is highly relevant and useful for civil engineers, environmental engineers, microbiologists, concrete experts and sewer operators and managers. The book not only provides fundamental knowledge of how corrosion develops but also collates different control measures that are economically and environmentally sustainable. Academics, researchers, engineers and managers of water utilities will all find this book informative as it contains up-to-date information and technologies, practical feasibilities and the most recent advancements in the field.

To deal with the massive problems resulting from MICC in our society, we need outstanding experts like the editor and authors of this book, up-to-date industry standards, latest knowledge, groundbreaking innovation and funding for research in the field of MIC in general and in MICC in particular.

I trust, that this book will pave the road for such developments and investments in the years to come!

January 2023

Dr. Torben Lund Skovhus
Research Center for Built Environment,
Energy, Water and Climate
VIA University College
Horsens, Denmark

Contents

Corrosion Processes and Mechanisms

Concrete Sewer Systems and Wastewater Processes Related to Concrete Corrosion	3
Guangming Jiang, Xuan Li, and Yarong Song	
Mechanisms and Processes of Concrete Corrosion in Sewers	21
Xuan Li, Guangming Jiang, Cyrill Grengg, and Florian Mittermayr	

Corrosion Measurements

Testing of Sulfide Uptake Rate (SUR) and Its Applications	37
Xiaoyan Sun, Guangming Jiang, Jurg Keller, Philip Bond, and Xuan Li	
Concrete Corrosion Characterization Using Advanced Microscopic and Spectroscopic Techniques	59
Florian Mittermayr, Gregor J. G. Gluth, Cyrill Grengg, Ulf Garbe, and Guangming Jiang	
Characterization of Corrosion Microbial Communities	99
Xuan Li and Guangming Jiang	

A Systematic Laboratory Testing of Concrete Corrosion Resistance in Sewers	113
Guangming Jiang, Xiaoyan Sun, Jurg Keller, Xuan Li, Yarong Song, Markus Schmid, and Günther Walenta	

Modelling of Concrete Sewer Corrosion

Controlling Environmental Factors of Microbiologically Influenced Concrete Corrosion in Sewers	141
Guangming Jiang, Xiaoyan Sun, Xuan Li, Yarong Song, and Jurg Keller	

Mathematical Modelling for the Concrete Corrosion of Sewer Systems 159
Guangming Jiang, Yiqi Liu, Xuan Li, and Xiaoyan Sun

Corrosion Control Strategies

Advances on Corrosion-Resistant Concrete for Sewers 185
Fengming Yang, Yazhou Zhao, Tian Wang, Yarong Song, Guangming Jiang, and Min Wu

Corrosion Resistance of Calcium Aluminate Cements in Sewer Environments 219
Neven Ukrainczyk and Cyrill Grengg

Alkali-Activated Materials for Sewers 233
Cyrill Grengg, Gregor J. G. Gluth, and Florian Mittermayr

Surface Treatment for Corroding Concrete Sewers 249
Xuan Li and Guangming Jiang

Contributors

Philip Bond Australian Centre for Water and Environmental Biotechnology, The University of Queensland, Brisbane, QLD, Australia

Ulf Garbe Australia's Nuclear Science and Technology Organisation, The Australian Centre for Neutron Scattering (ACNS), Lucas Heights, NSW, Australia

Gregor J. G. Gluth Division 7.4 Technology of Construction Materials, Bundesanstalt für Materialforschung und -prüfung (BAM), Berlin, Germany

Cyrill Grengg Institute of Applied Geosciences, Graz University of Technology, Graz, Austria

Guangming Jiang School of Civil, Mining, Environmental and Architectural Engineering, University of Wollongong, Wollongong, NSW, Australia

Jurg Keller Australian Centre for Water and Environmental Biotechnology, The University of Queensland, Brisbane, QLD, Australia

Xuan Li School of Civil and Environmental Engineering, Centre for Technology in Water and Wastewater, University of Technology Sydney, Ultimo, Sydney, NSW, Australia

Yiqi Liu School of Automation Science and Engineering, South China University of Technology, Guangzhou, China

Florian Mittermayr Institute of Technology and Testing of Building Materials, Graz University of Technology, Graz, Austria

Markus Schmid Calucem GmbH, Mannheim, Germany

Yarong Song Australian Centre for Water and Environmental Biotechnology, The University of Queensland, St. Lucia, Brisbane, QLD, Australia

Xiaoyan Sun School of Civil Engineering, Sun Yat-sen University, Zhuhai, China

Neven Ukrainczyk Institute of Construction and Building Materials, Technische Universität Darmstadt, Darmstadt, Germany

Günther Walenta Calucem GmbH, Mannheim, Germany

Tian Wang Department of Chemical and Biochemical Engineering, Technical University of Denmark, Denmark, Lyngby, Denmark

Min Wu Department of Civil and Architectural Engineering, Aarhus University, Aarhus, Denmark

Fengming Yang Department of Civil and Architectural Engineering, Aarhus University, Aarhus, Denmark;
School of Materials Science and Engineering, Southeast University, Nanjing, China

Yazhou Zhao Department of Civil and Architectural Engineering, Aarhus University, Aarhus, Denmark;
College of Harbour, Coastal and Offshore Engineering, Hohai University, Nanjing, China

Corrosion Processes and Mechanisms

Concrete Sewer Systems and Wastewater Processes Related to Concrete Corrosion



Guangming Jiang, Xuan Li, and Yarong Song

Abstract Sewer systems is the cornerstone of modern urbanisation by providing wastewater collection and transport, which enables not only the recovery of water and resources but also the control of odour and harmful pathogens. Sewer systems are primarily composed of rising main pipes, gravity flow pipes, pumping stations and other associated facilities. Complicated physical, chemical, and biological processes are occurring in the phases of water, air and concrete, and their interfaces. These processes significantly affect the concrete durability due to microbiologically influenced corrosion.

1 Introduction of Sewer Systems

Sanity sewers are the underground carriage system to collect and transport wastewater from home or industry to treatment at wastewater treatment plants (WWTPs) and/or disposal. A sewer system generally consists of pipelines, pump stations, and auxiliaries such as inlet/collection structures, manholes etc. The first appearance of sewer dates back to many ancient civilizations (Fig. 1), including the ancient Roman, Egyptian, Greek, and Chinese [21, 29]. These early sewers were mainly used to conduit storm water and to prevent flooding. It was not until the middle of

G. Jiang (✉) · X. Li

School of Civil, Mining, Environmental and Architectural Engineering, University of Wollongong, Wollongong, NSW 2522, Australia
e-mail: gjiang@uow.edu.au

X. Li

e-mail: xuan.li@uts.edu.au

X. Li

School of Civil and Environmental Engineering, Centre for Technology in Water and Wastewater, University of Technology Sydney, Ultimo, NSW 2007, Australia

Y. Song

The Australian Centre for Water and Environmental Biotechnology, The University of Queensland, St. Lucia, QLD 4072, Australia
e-mail: yarong.song@uq.edu.au

© The Author(s), under exclusive license to Springer Nature Switzerland AG 2023

G. Jiang (ed.), *Microbiologically Influenced Corrosion of Concrete Sewers*, Engineering Materials, https://doi.org/10.1007/978-3-031-29941-4_1

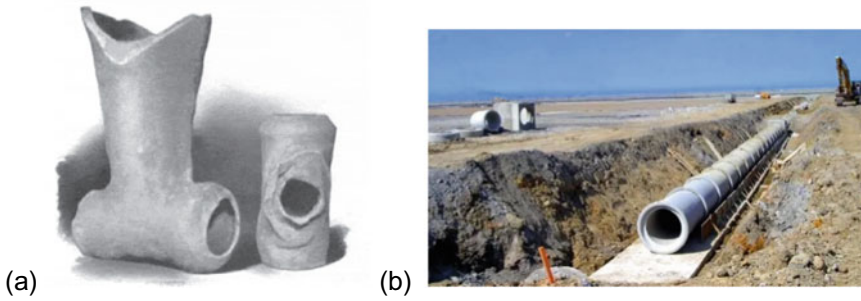


Fig. 1 **a** Knee and T joints made about 4000 B.C., found in the excavation of the Temple of Bl at Nippur, Babylonia. *Source* Cast Iron Pipe, by United States Cast Iron Pipe and Foundry Company, 1914. **b** Reinforced concrete sewer pipes under construction (<https://theconstructor.org/concrete/design-concrete-pipes-sewers/17652/>)

the nineteenth century did sewer systems become a hygienic and sanitary installation in cities that can reduce the spreading of epidemic diseases. In the last 100 years, separate systems, i.e., sanitary and storm sewers, were constructed in modern cities along with the construction of WWTPs. The old, combined sewers were also reformed by the installation of tanks to detain high storm flow and reduce the combined sewer overflow (CSO).

With the continuous urbanization and population explosion, the scale of sewer systems keeps on expanding in both developed and developing countries. Nowadays, it is one of the indispensable components in modern urban water/wastewater infrastructure. The total asset value of these networks is estimated to be about one trillion dollars in the USA and \$100 billion in Australia [7]. Sewer systems play an important role in protecting against water pollution, ensuring better public health, and water resource conservation. With the process of urbanization and the construction of more WWTPs, more and more sewer pipes have been installed all over the world. Most of OECD countries have more than 80% population connected to urban sewer systems (Fig. 2). However, many cities still have no sewers and only 15% of the urban population in low-income nations had sewer connections in 2020 (United Nations Statistics).

Sewers were built with a range of different materials including pottery, stone, and bricks in early days of human history. Over time, sewer pipes were made of different materials due to their availability, such as bored log, casted iron, and PVC pipes etc. Since the invention of Portland cement in 1824, due to its low-cost, high strength and easy shapeability, concrete becomes the most widely used construction materials in building sewer systems. Nowadays, many sewer structures, including sewer pipes, manholes and pumping stations, were mainly constructed using reinforced concrete. The total length of sewer pipes in Australia is about 117,000 km, and approximately 40% of this network is constructed with concrete [11]. Also, concrete is the first choice in constructing large-scale trunk (which receive wastewater flow from smaller collection sewers) and interception sewers. Especially, many mega-sized deep tunnel

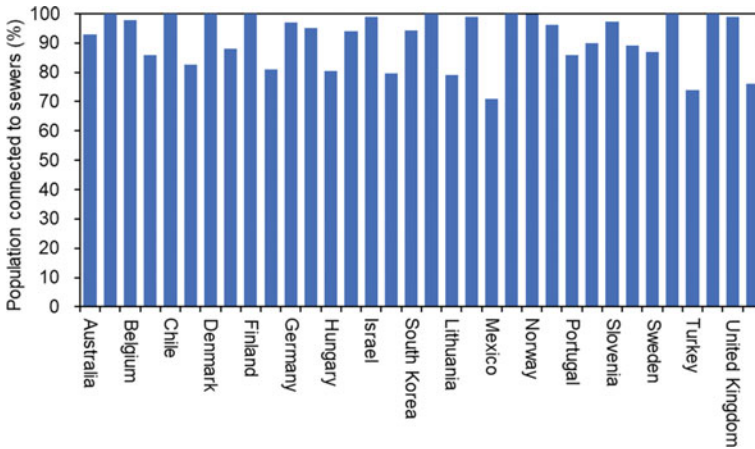


Fig. 2 Total public sewerage (% of resident population connected to urban wastewater collecting system) in different OECD countries. Most countries have data up to 2019. Data was extracted on 31 Jan 2022 from OECD Stat

sewer systems (DTSS), which are buried deep underground (20–200 m), are being constructed with concrete in well-developed and densely-populated cities, such as Hong Kong, Dubai, and Guangzhou [28, 41].

Flow in sanitary sewer can be controlled by either gravity (gravity sewers) or pressure (pressure sewers or rising main sewers). In partially filled gravity sewers, wastewater is partially aerobic due to the existence of aeration across the air–water interface. In contrast, anaerobic conditions typically dominate fully filled pressure sewers because of the lack of aeration. The most well-known problems caused by the anaerobic processes in pressurized sewers are odour and corrosion, although the latter is less noticed [69, 79, 82]. The sewer corrosion causes loss of concrete mass and deteriorates the structural capacity, leading to cracking of sewer pipes and ultimately structural collapse. The rehabilitation and replacement of damaged sewers is very costly. In the USA alone, corrosion is causing sewer asset losses estimated at around \$14 billion per year [7]. This cost is expected to increase as the aging infrastructure continues to fail [78, 82].

2 In-Sewer Processes Leading to Concrete Corrosion

Sewer systems are reactors in a broad sense because the retention of wastewater in sewers allows various physical, chemical and biological processes to occur [2, 46]. Generally, there are five phases in a sewer pipe: the suspended water phase, the biofilms, the sediments, the air phase (in partially-filled gravity sewer), and the sewer walls [29]. Microbial processes mainly happen in the water phase, biofilms, and sediments. The exchange of biological substrates and products between different

phases keeps up the microbial processes. The microbial processes not only produce odorous compounds and alter the quality and constituents in the wastewater, but also cause severe concrete corrosion problems.

The wastewater in sewers is rich in organic substances, which are electron donors for heterotrophic processes. The type of microbial transformation occurring depends on the availability of electron acceptors under different redox conditions (Table 1). Aerobic wastewater conditions arise in gravity sewers because of aeration across the air–water interface. In contrast, anaerobic wastewater conditions exist when dissolved oxygen is depleted for the degradation of easily degradable organic substances, in the absence of aeration. Anoxic wastewater condition becomes possible when oxidized inorganic nitrogen substances (NO_x) are added to the wastewater to supplement as electron acceptor in the absence of oxygen. Otherwise, sulfate becomes a candidate of electron acceptor in anaerobic wastewater. This results in the production of an important odorous and corrosion-causing compound: hydrogen sulfide (H_2S). The fermentation processes under anaerobic conditions also produce significant odour compounds like volatile sulfur compounds.

Bacteria tend to attach to wet surfaces, to multiply and embed themselves in a slimy matrix composed of extracellular polymer substances (EPS), thus forming a biofilm [13, 74]. The pressure sewer systems are covered with significant amount of biofilms, with a thickness of several hundred μm depending on the wastewater flow velocity and its shear stress. Biofilm offers cells many advantages such as improved survival during starvation, restricted exposure to toxins/biocides and fluctuating environmental factors. Biofilm cells can also form synergistic relationships by complementary metabolisms among different microbial populations. There are also adverse aspects like limitation of substrate diffusion into thick biofilms.

Figure 3 depicts the sewer biofilms in both pressure and gravity sewers. Anaerobic biofilms prevail in pressure sewers, conducting fermentation, sulfate reduction, and methane production in wastewater. There are two types of biofilms in gravity sewers

Table 1 Electron acceptors, oxidation–reduction potential (ORP), and corresponding conditions for microbial processes in sewer systems

Electron acceptors	ORP (mV)	Microbial processes	Typical sewer systems
O_2	> + 50	Oxic (aerobic)	Partially filled gravity sewer
NO_3^- , NO_2^-	+ 50 to – 50	Anoxic (anaerobic)	Pressure sewer with nitrate/nitrite addition
SO_4^{2-}	< – 50 to – 200	Sulfate reduction (anaerobic)	Pressure sewer
Organic compound CHO	< – 100	Fermentation (Mixed acids and alcohol production)	Full-flowing gravity sewer
CHO, CO, CO_2 , H_2	< – 300	Fermentation (Methane production)	Gravity sewer with low slope and deposits

Compiled from Gerardi [18] and Hvitved-Jacobsen et al. [29]

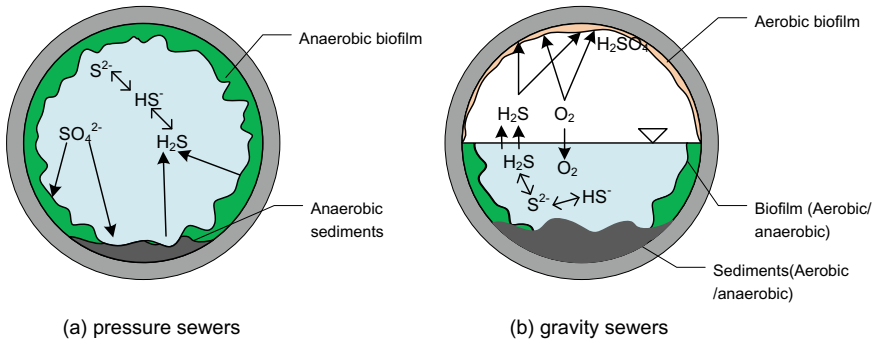


Fig. 3 Distinct biofilms and sediments developed in pressure (a) and gravity (b) sewers, respectively. The major sulfur transformation pathways are also shown

depending on their locations being below or above the water surface. The aerobic biofilm above water surface carries out sulfide oxidation to sulfuric acid (source of sewer concrete corrosion). The biofilm below water surface can be either aerobic or anaerobic depending on the strength of reaeration. The deep layer of biofilms and sediments in gravity sewer are permanently anaerobic although the condition of water phase varies between aerobic and anaerobic [29].

Among all the possible microbial processes, sulfide and methane formation occur in anaerobic biofilms (e.g., those primarily developed around pressure sewer pipes). In anaerobic pressure sewers, the organic matter (e.g., sugars, proteins) in wastewater sustains fermentation, methanogenesis (methane formation), and sulfate respiration (sulfide production) (Fig. 4). Sulfate-reducing bacteria (SRB) primarily reside in the biofilms rather than wastewater because they have low growth rate [53]. Sulfate can penetrate biofilm due to concentration gradient along the biofilm depth. Generally, methanogenic processes need the absence of sulfate and thus mainly happen in deep layers of biofilms and sediments. It was claimed that methane formation is of minor importance in sewers without significant sediments [29]. More recent research found significant methane formation by sewer biofilms in both lab-scale reactors and real sewer systems [23, 24, 33, 34, 42, 43]. The depletion of sulfate due to long retention time in sewer pipes, or the development of very thick biofilms can facilitate the methane formation in wastewater.

Anaerobic hydrolysis degrades hydrolysable organic matter into fermentable substrate like amino acids, sugars, and long chain fatty acids, etc. Fermentation further degrades easily degradable substances into alcohols and volatile fatty acids (VFA). Sulfate-reducing bacteria can use a wide range of organic matter produced by hydrolysis and fermentation processes in wastewater (Fig. 4). In contrast, methanogens primarily use acetate or hydrogen to form methane. The interaction between anaerobic carbon and sulfur transformation in sewers are thus of great importance to produce corrosion-causing hydrogen sulfide. Many wastewater-related properties like pH, temperature, and chemical oxygen demand (COD) play important roles in the possible microbial processes [45, 54].

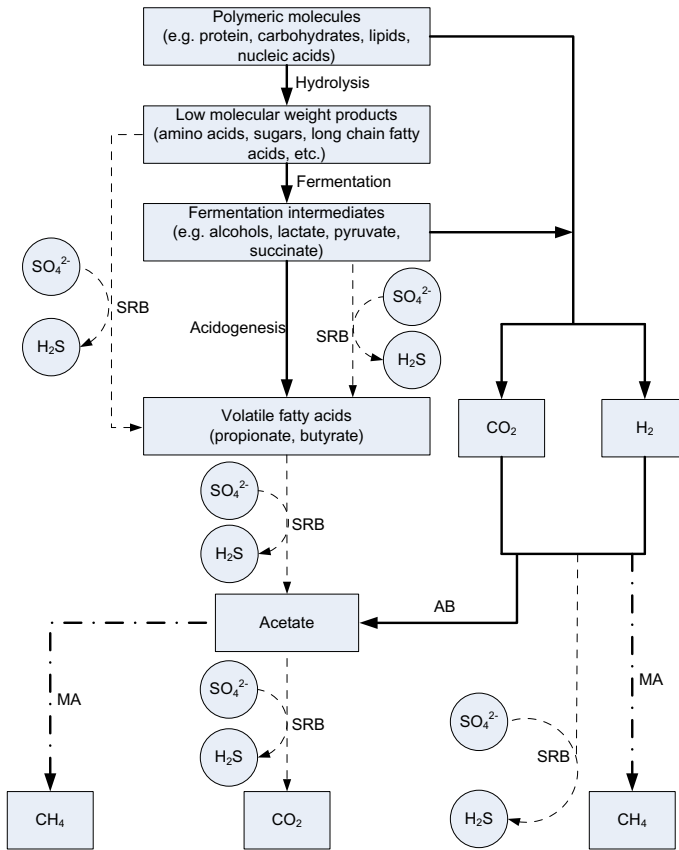


Fig. 4 A simplified concept for anaerobic transformations of organic matter and sulfur in wastewater and biofilms of a sewer system Modified from Gibson [19] and Hvitved-Jacobsen et al. [29]. AB: Acetogenic bacteria; SRB: Sulfate-reducing bacteria; MA: Methanogens

Once hydrogen sulfide is generated by sewer biofilms, a part diffuses through the air–water interface in gravity sewers and becomes a component in sewer gas. The concentration of H_2S in wastewater is largely dependent on the wastewater pH because hydrogen sulfide is a weak acid, with pK_{a1} value of 7 and pK_{a2} ranging from 11.96 to 17.00 [39]. Lower sewage pH could lead to more hydrogen sulfide emission.



Aside from the wastewater pH, other factors, such as high wastewater temperature and high turbulence intensity (high flow velocity or vigorous agitation) can also

promote the hydrogen sulfide emission from wastewater [9]. Thus, parameters associated with the sewers and their operations are also important for H₂S concentration in the gas phase, e.g., the turbulence flow (reaeration), ventilation (H₂S gas release), water depth ratio, water flow rate and sheer force, etc. [14, 29, 55].

Once being emitted in the gas phase, H₂S is absorbed in the condensation layer of the exposed pipe surface (sides and crown region), followed by the biological oxidation of H₂S and the production of sulfuric acid [64–68], which is responsible for the corrosive attack on the concrete [30, 31]. Recent studies have identified various microorganisms, primarily sulfide-oxidizing bacteria (SOB), involved in this acid production [10, 26, 38, 40, 52, 57, 72].

3 Concrete Corrosion in Sewers

3.1 Concrete Sewers

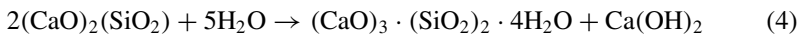
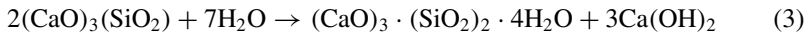
The concrete used to construct sewer is a mixture of water, cement binders, and aggregates of various sizes. Depending on the purpose of concrete pipe, different types of concrete are designed with a range of compositions and curing conditions to meet specific requirements of mechanical properties and durability [4]. The most used type of cement, i.e., Portland cement, has five main compounds, as listed in Table 2.

Table 2 Major constituents and composition of Portland cement

Compound	Composition	Abbreviation	Roles
Tricalcium silicate	3CaO · SiO ₂	C ₃ S	Hydrates and hardens rapidly. Responsible for initial set and early strength of the concrete
Dicalcium silicate	2CaO · SiO ₂	C ₂ S	Hydrates and hardens slowly. Contributes to later age strength (> 7 days)
Tricalcium aluminate	3CaO · Al ₂ O ₃	C ₃ A	Releases heat during the first few days. Contributes slightly to the early strength development
Tetracalcium aluminoferrite	4CaO · Al ₂ O ₃ · Fe ₂ O ₃	C ₄ AF	Hydrate rapidly but contributes little to strength. Hydrated cement looks grey due to ferrite hydrates
Gypsum	CaSO ₄		Controls the rate of hardening of fresh cement

Adapted from American Concrete Institute International Organization [1]

In anhydrous form, compounds listed in Table 2 are soluble in water. The hydration of these compounds, triggered by combining cement with water, generate insoluble products and bind the aggregate components together, forming a solid concrete [27]. Upon combining with water, C_3S inside cement reacts instantaneously with water, producing calcium hydroxide. Once calcium hydroxide becomes saturated in the system, it starts to crystallize, forming calcium silicate hydrate (C–S–H) (Eq. 1) [17]. Hydration process of C_2S proceeds is similar to that of C_3S , with the production of calcium hydroxide and a rigid C–S–H gel (Eq. 2).



The C–S–H matrix usually accounts for 50–60% volume of solids in a completely hydrated Portland cement paste and is considered as a critical contribution to the strength of hydrated cement paste [17]. The hydration of C_3S and C_2S also produces a large amount of calcium hydroxide, which results in the high alkalinity of concrete. Generally, the pH of hardened concrete is around 13 [36].

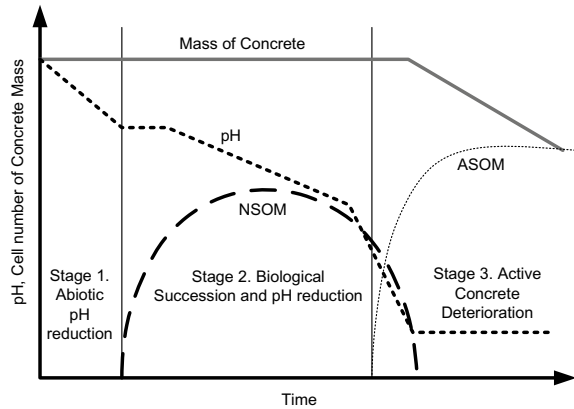
3.2 Concrete Corrosion

Concrete sewer pipelines and other metal installations are prone to corrosion from the day they are in service. Ideally, sewer pipes can serve for 50–100 years with minimal maintenance considering the durability of concrete buried underground [47]. However, the corrosion of sewer pipeline was reported by Olmstead and Hamlin [58] for the first time and they identified sulfuric acid as the cause of the corrosion. Later, hydrogen sulfide was recognized as the primer of sulfuric acid and thus the consequent sewer concrete corrosion [6]. The underlying mechanisms and its nature as a microbial process were revealed by systematic research in the middle of the twentieth century [61–64, 68]. More recently, active research in the sewer odour and corrosion field has led to more in-depth understanding of the microorganisms involved, corrosion processes and impacting factors [22, 35, 40].

Once sulfide is produced by sulfate-reducing bacteria, some of the hydrogen sulfide will be released into the sewer atmosphere. The hydrogen sulfide gas will be dissolved in the thin water film on the sewer wall surface above the water level. Hydrogen sulfide will then be oxidized to sulfuric acid by autotrophic sulfide-oxidizing bacteria [85]. Sulfuric acid thus formed is the real factor that causes corrosion of the sewer concrete. The presence of hydrogen sulfide, oxygen, and moisture are the necessary conditions for microbiologically influenced corrosion (MIC) to happen. Unfortunately, these conditions are commonly found in the sewer systems.

However, the microbiologically influenced concrete corrosion is developed through a few stages [30, 70]. The first stage is the abiotic pH reduction (Fig. 5).

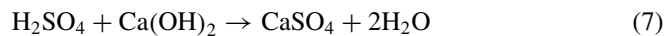
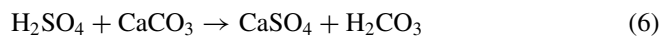
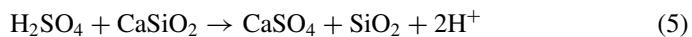
Fig. 5 Theoretical changes in the biological and physical properties of concrete with time during the microbiologically influenced corrosion process. Adapted from Islander et al. [30]. Neutrophilic sulfide-oxidizing microorganisms (NSOM); acidophilic sulfide-oxidizing microorganism (ASOM)



The surface pH of new concrete pipe is generally in the range of 11–13 after curing, storage, transportation and installation [85]. In addition, cement contains calcium hydroxide which neutralizes the acids and inhibits growth of sulfide oxidizing bacteria when the concrete is new. Hydrogen sulfide (H_2S) and carbon dioxide (CO_2) present in the air phase of the sewer systems can chemically reduce the concrete pH due to the fact that they are both weak acid [79]. As sewer pipe ages, the neutralizing capacity of the concrete is consumed, the surface pH drops. This makes the surface amenable for the succession of sulfuric acid-producing bacteria.

When the concrete surface pH is reduced to about 9, some neutrophilic sulfide-oxidizing microorganisms (NSOM) start to colonize. NSOM, and probably some fungi, dominate the community and go through a biological succession until the pH falls down to 3 [30]. Once the pH is lower than 3, acidophilic sulfide oxidation microorganisms (ASOM) become the protagonist in the sewer corrosion biofilm due to both the low pH and the sulfur products produced by NSOM. Sulfur generated by NSOM is an essential substrate for ASOM, which produce significant amounts of sulfuric acid. The active corrosion in Stage 3 drives the pH further down.

The final step of the corrosion process is the chemical reaction between the concrete materials (calcium hydroxide, calcium silicate hydrate gel (C-S-H), calcium carbonate (CaCO_3)) with the biogenic sulfuric acid (see equations below). This reaction produces a layer of wetted gypsum ($\text{CaSO}_4 \cdot 2\text{H}_2\text{O}$), which is easily eroded by the flush of wastewater. As the gypsum layer being washed away, new surfaces of concrete will be exposed for further erosion.



The formation of gypsum and ettringite ($3\text{CaO} \cdot \text{Al}_2\text{O}_3 \cdot \text{CaSO}_4 \cdot 12\text{H}_2\text{O}$ or $3\text{CaO} \cdot \text{Al}_2\text{O}_3 \cdot 3\text{CaSO}_4 \cdot 31\text{H}_2\text{O}$) during the acid reaction process aggravates the corrosion problem due to their expansive nature, with significantly higher volumes than the intact concrete, ranging from 124 to 700% [37, 40, 49, 59, 87]. Ettringite expansion causes internal cracking and pitting, which produces a larger surface area for the chemical reaction to occur.

A recent study examined the micro-cracking at the concrete corrosion front, through the cycle of iron dissolution in the highly acidic corrosion layer and the precipitation at the corrosion front [36]. The iron thus facilitates the concrete corrosion through the cycling process that creates more cracking at the corrosion front (Fig. 6). This will also provide further sites of penetration of the acid into the concrete. It was found that the ASOM and unidentified heterotrophs move into the concrete with the corroding layer, but the NSOM do not [12]. This suggests that the microbial succession is a surface phenomenon, and once the surface pH is low enough for the ASOM to survive and produce acid, ASOM follow the acid into the concrete. The designed structural integrity of sewer pipes is weakened by the conversion of the concrete to gypsum and ettringite. The reduced load bearing capacity of the concrete can result in the eventual collapse of the sewer.

Problems associated with corrosion caused by hydrogen sulfide occur in many parts of the world and particularly where sewage temperatures are high, such as the Middle East, Australia, USA, South Africa and India [79, 81, 82]. However, problems also exist in temperate climates and have been reported in Germany, Holland and the UK.

Many studies reported a corrosion rate between 1–10 mm per year (Table 3), resulting a sewer pipe service time as short as 20 years [82]. Some improved or modified concrete can be more resistant to corrosion, inducing a lower corrosion rate. Portland fly ash concrete was reported to be resistant to sulfide-oxidizing bacteria (SOB), thus the lifetime of Portland fly ash concrete sewer can last over 100 years [48]. A recent study shows that geopolymer sewer pipes have nearly ten times higher resistance to corrosion than ordinary Portlandite cement pipes [20].

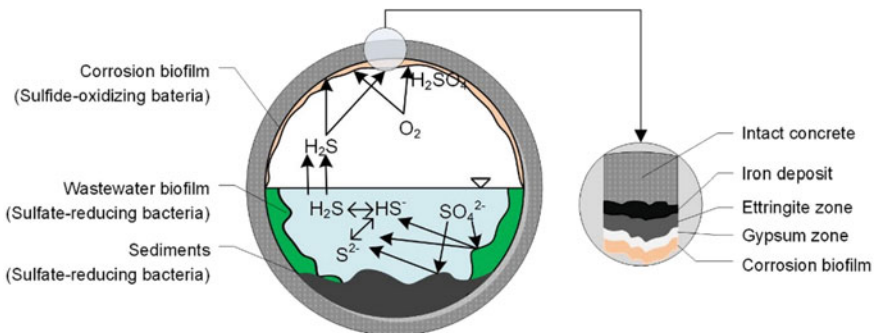


Fig. 6 A simple schematic of the microorganisms, their sulfur transformation processes, and distribution of corrosion products involved in concrete corrosion of sewers

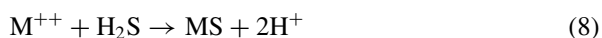
Table 3 Corrosion rate and lifetime of sewer pipes [86]

Corrosion rate (mm/year)	Lifetime ^a (year)	References
2.5–10	20–70	[82]
2.7	65	[51]
4.3–4.7	35–45	[50]
2–4	45–90	[31]
3.1	55	[12]
1.0–1.3	130–170	[48]
1.1–1.8	90–160	[84]

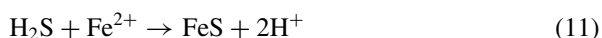
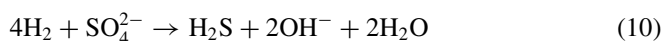
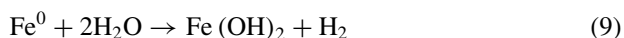
^a The lifetime is the ratio of concrete sewer pipes thickness to corrosion rate

3.3 Rebar and Metal Corrosion

Concrete is not the only target of sulfuric acid attack, most metals, including many stainless steel alloys, can also be attacked and destroyed by exposure to sulfuric acid [85]. Unlike concrete corrosion induced by sulfuric acid, metal corrosion can be caused by two ways of attack: direct chemical attack from hydrogen sulfide and acidic decomposition by exposure to sulfuric acid produced by SOB. Most metal can react with hydrogen sulfide gas resulting in metal sulfide and two hydrogen ions, which lower the pH and increase the corrosion rate. It is reported that the direct contact with H₂S can encourage steel corrosion to a level of 12.8 mm/year [80], and sulfides are intensive corrosion stimulators [25].



Another possible mechanism was revealed for the metal corrosion caused by anaerobic sulfate-reducing bacteria [3]. The iron reacts spontaneously with water under moist condition, forming a thin, protective double layer of ferrous hydroxide and hydrogen. Sulfate-reducing bacteria remove the hydrogen produced by using it as an electron donor to produce sulfide. Sulfide in turn, attacks the iron structures to form ferrous sulfide precipitates, and more hydrogen gas. Metallic iron structures are corroded gradually by chemical and biological processes in this manner [3].



Concrete sewer pipes, especially for pipes with diameters larger than 0.6 m, are usually reinforced with a sufficient number of steel bars designed to withstand both

internal pressure and external loads [22, 56]. Reinforced concrete pipes can be manufactured in a wide range of diameters (30–180 mm) and are relatively more corrosion resistant than metallic pipes. They are also more popular than ductile iron, vitrified clay, polyvinyl-chloride (PVC), composite fiber reinforced polymer (FRP) and high density polyethylene (HDPE) pipes [83]. When the protecting concrete cover of rebar is deteriorated by cracking or seriously corroded, rebar corrosion occurs because of the reduced cement alkalinity, ingress of aggressive substances, and the direct exposure after the concrete scaling [15, 32]. Rebar corrosion may in turn reduce sewer durability and its service life similar to other reinforced concrete structures [77].

The steel rebar corrosion is due to a combination of chemical factors: the reduced alkalinity of corroding concrete, at a pH level around 2–4 due to the biogenic sulfuric acid produced in the corrosion process [32, 36]; the ingress of H_2S , CO_2 , oxygen and wastewater through concrete cracks to rebar surface [60]; the direct exposure of rebar by regional concrete scaling or spalling that may occur in the later stages of service life [15].

Rebar corrosion is a major cause of durability problems in reinforced concrete structures such as concrete buildings, bridge decks, marine structures, slabs and floors [44]. The electrochemical process causes the dissolution of iron to form various corrosion products, such as iron oxides, hydroxides and hydrated oxides, the nature of the products being dependent on the exposure environment [5, 44]. Usually, chloride ions are considered as one of the major causes of the steel corrosion [71]. The dissolved chlorides from the external environment could permeate through sound concrete or cracks to the steel surface thus inducing corrosion of the steel bar [22]. In sewers, however, gaseous H_2S and the biogenic sulfuric acid, produced in corrosion biofilms [61, 62], are commonly accepted to be the corrosive substances rather than chlorides [16].

An early study [71] proposes that H_2S produced in the sewer could diffuse to the metal surface and form FeS . Recently, some long-term studies (45 months) were carried out to investigate the rebar corrosion mechanisms when the concrete cover was gradually removed due to concrete corrosion [76, 75]. It was found that H_2S and the biogenic sulfuric acid may not directly participate in the corrosion reactions of rebar covered by concrete or exposed completely to sewer atmosphere. Chloride ions play a significant role in initiating rebar corrosion in concrete sewers, resulting as a thin chloride-enriched layer at the steel/rust interface. Instead, oxygen is more likely responsible for rebar corrosion in sewers. When evident cracks occur inside concrete, H_2S that can reach the depth of rebar might play a minor role in the steel corrosion process.

The rebar rusts at the rebar/concrete interface may obtain a volume 2–6 times of the original rebar, thus causing the macro-level concrete cracking [83]. In addition, the cracking of the concrete cover was influenced by the micro-cracking accelerated by the dissolution, diffusion, and deposition of Fe precipitates at the concrete corrosion front [76]. The predominant corrosion products and potential reactions of exposed rebar or partially covered by poor-conditioned concrete were complicated and varied with the exposure time and the development of concrete corrosion. The

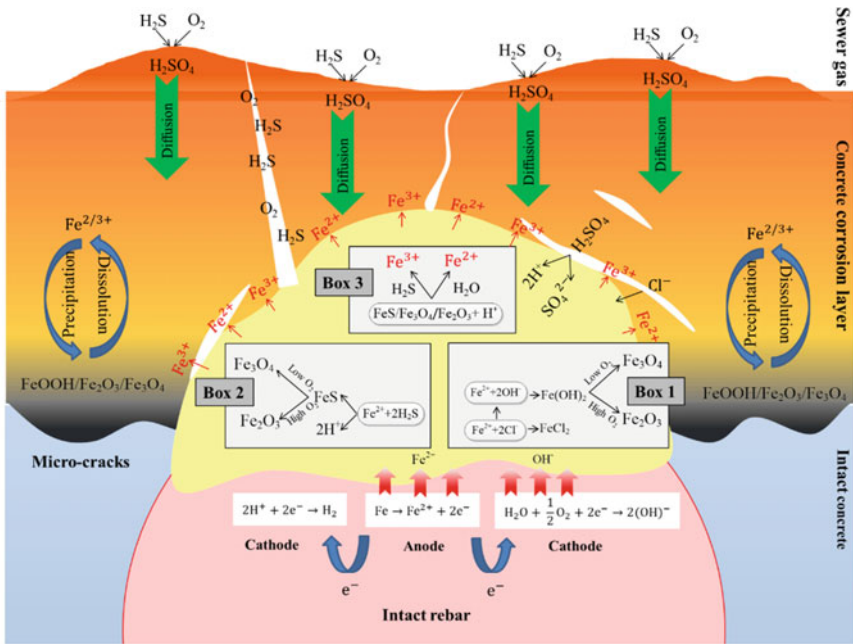


Fig. 7 A conceptual model describing the corrosion reactions of rebar and the cracking of concrete in reinforced sewers. Reproduced from Song et al. [76] with permission from Elsevier

major corrosion products observed include iron oxides (Fe_2O_3 , Fe_3O_4), iron oxyhydroxides (FeOOH , lepidocrocite, goethite), iron sulfides (FeS , Fe_3S_4 , FeS_2), iron chlorides ($\text{FeCl}_x(\text{H}_2\text{O})_z$) and iron sulfate ($\text{Fe}_2(\text{SO}_4)_3(\text{H}_2\text{O})_z$) (Fig. 7).

4 Summary

This chapter briefly discussed the history of sewer systems and why concrete is predominantly used to construct sewer structures. As an essential and expensive infrastructure, the durability of concrete sewer thus becomes critical for modern societies. The chapter also presented wastewater processes that leads to the production of hydrogen sulfide and its subsequent role in causing the biological production of sulfuric acid. The strong acid chemically reacts with alkaline cementitious material, leading to the reduction of concrete surface pH, formation of loosely bound corrosion products with little mechanical strength, and thus loss of mass and eventually structural failure of the concrete pipes. Rebar corrosion occurs and interacts with concrete corrosion, further reduces the durability of sewer systems. Severe concrete

corrosion can lead to the exposure of steel rebars, of which the metal corrosion can interact with concrete corrosion itself. Recent studies revealed more knowledge about the processes involved and distribution of various corrosion products.

Sulfide induced concrete corrosion in sewer systems leads to early structural failure and shortened life expectancy of pipes and other structures (pump wells, manholes, etc.). The corrosion damaged sewer infrastructure is costly to replace or rehabilitate. Control strategies need to be implemented to remedy the corrosion problems caused by sulfate reduction in anaerobic sewers. Many chemical dosing technologies in wastewater have been developed and applied by water industry to control hydrogen sulfide production, emission and the corrosion of concrete sewer systems [86]. In addition, gas-phase technologies like biofilter, bio-trickling filters and activated carbon adsorption systems were used widely to remove hydrogen sulfide from sewer atmosphere [8, 73]. Most importantly, different cementitious materials and concrete design were devised to enhance the corrosion resistance in harsh sewer environment [22].

References

1. ACI Committee, A.C.I. and Standardization, I.O.F.: Building Code Requirements for Structural Concrete (ACI 318-08) and Commentary. American Concrete Institute (2008)
2. Abdul-Talib, S., Hvitved-Jacobsen, T., Vollertsen, J., Ujang, Z.: Anoxic transformations of wastewater organic matter in sewers—process kinetics, model concept and wastewater treatment potential. *Water Sci. Technol.* **45**, 53–60 (2002)
3. Atlas, R.M., Bartha, R.: The sulfur cycle. In: Fogel, L., Wong, G. (eds.) *Microbial Ecology, Fundamentals and Applications*, 4th edn. Wesley Longman, California, Addison (1998)
4. Baran, I., Cinar, K., Ersoy, N., Akkerman, R., Hattel, J.H.: A review on the mechanical modeling of composite manufacturing processes. *Arch. Comput. Methods Eng.* **24**, 365–395 (2017)
5. Bertolini, L., Elsener, B., Pedferri, P., Redaelli, E., Polder, R.B.: *Corrosion of steel in concrete: prevention, diagnosis, repair*. Wiley (2013)
6. Bowlus, F., Banta, A.: Control of anaerobic decomposition in sewage transportation. *Water Works Sewerage* **79**, 369 (1932)
7. Brongers, M.P.H., Virmani, P.Y., Payer, J.H.: *Drinking Water and Sewer Systems in Corrosion Costs and Preventative Strategies in the United States*. United States Department of Transportation Federal Highway Administration (2002)
8. Bu, H., Carvalho, G., Yuan, Z., Bond, P., Jiang, G.: Biotrickling filter for the removal of volatile sulfur compounds from sewers: a review. *Chemosphere* **277**, 130333 (2021)
9. Carrera, L., Springer, F., Lipeme-Kouyi, G., Buffiere, P.: A review of sulfide emissions in sewer networks: overall approach and systemic modelling. *Water Sci. Technol.* **73**, 1231–1242 (2015)
10. Cayford, B.I., Dennis, P.G., Keller, J., Tyson, G.W., Bond, P.L.: High-throughput amplicon sequencing reveals distinct communities within a corroding concrete sewer system. *Appl. Environ. Microbiol.* **78**, 7160–7162 (2012)
11. Cayford, B.I.: Investigation of the microbial community and processes responsible for the corrosion of concrete in sewer systems. The degree of Doctor of Philosophy, University of Queensland (2012)
12. Davis, J.L., Nica, D., Shields, K., Roberts, D.J.: Analysis of concrete from corroded sewer pipe. *Int. Biodeterior. Biodegradation* **42**, 75–84 (1998)
13. De Beer, D., Stoodley, P., Lewandowski, Z.: Liquid flow and mass transport in heterogeneous biofilms. *Water Res.* **30**, 2761–2765 (1996)

14. Dunsmore, B.C., Jacobsen, A., Hall-Stoodley, L., Bass, C.J., Lappin-Scott, H.M., Stoodley, P.: The influence of fluid shear on the structure and material properties of sulphate-reducing bacterial biofilms. *J. Ind. Microbiol. Biotechnol.* **29**, 347–353 (2002)
15. Fandrich, R., Gu, Y., Burrows, D., Moeller, K.: Modern SEM-based mineral liberation analysis. *Int. J. Miner. Process.* **84**, 310–320 (2007)
16. Fernandes, I., Pericao, M., Hagelia, P., Noronha, F., Ribeiro, M., Maia, J.: Identification of acid attack on concrete of a sewage system. *Mater. Struct.* **45**, 337–350 (2012)
17. Gartner, E., Young, J., Damidot, D., Jawed, I.: Hydration of Portland cement. *Struct Perform Cem* **13**, 978 (2002)
18. Gerardi, M.H.: 3 methane-forming bacteria. In: Gerardi, M.H. (ed.) *The Microbiology of Anaerobic Digesters*. Wiley, Hoboken, New Jersey (2003)
19. Gibson, G.R.: Physiology and ecology of the sulfate-reducing bacteria. *J. Appl. Bacteriol.* **69**, 769–797 (1990)
20. Gourley, J.T., Johnson, G.B.: The corrosion resistance of geopolymer concrete sewer pipe. *Concr. Aust.* **43**, 38–43 (2017)
21. Gray, H.F.: Sewerage in ancient and mediaeval times. *J. Sewage Works* **12**, 939–946 (1940)
22. Grengg, C., Mittermayr, F., Ukrainczyk, N., Koraimann, G., Kienesberger, S., Dietzel, M.: Advances in concrete materials for sewer systems affected by microbial induced concrete corrosion: a review. *Water Res.* **134**, 341–352 (2018)
23. Guisasola, A., de Haas, D., Keller, J., Yuan, Z.: Methane formation in sewer systems. *Water Res.* **42**, 1421–1430 (2008)
24. Guisasola, A., Sharma, K.R., Keller, J., Yuan, Z.Q.: Development of a model for assessing methane formation in rising main sewers. *Water Res.* **43**, 2874–2884 (2009)
25. Heitz, E., Flemming, H.-C., Sand, W.: *Microbially Influenced Corrosion of Materials: Scientific and Engineering Aspects*. Springer (1996)
26. Hernandez, M., Marchand, E.A., Roberts, D., Peccia, J.: In situ assessment of active *Thiobacillus* species in corroding concrete sewers using fluorescent RNA probes. *Int. Biodeterior. Biodegradation* **49**, 271–276 (2002)
27. Hewlett, P., Liska, M.: *Lea's Chemistry of Cement and Concrete*. Butterworth-Heinemann (2019)
28. Huang, D., Liu, X., Jiang, S., Wang, H., Wang, J., Zhang, Y.: Current state and future perspectives of sewer networks in urban China. *Front. Environ. Sci. Eng.* **12**, 2 (2018)
29. Hvitved-Jacobsen, T., Vollertsen, J., Nielsen, A.H.: *Sewer Processes: Microbial and Chemical Process Engineering of Sewer Networks*, 2nd edn. CRC Press, Boca Raton, FL, USA (2013)
30. Islander, R.L., Deviny, J.S., Mansfeld, F., Postyn, A., Shih, H.: Microbial ecology of crown corrosion in sewers. *J. Environ. Eng.* **117**, 751–770 (1991)
31. Ismail, N., Nonaka, T., Noda, S., Mori, T.: Effects of carbonation on microbial corrosion of concretes. *J. Constr. Manag. Eng.* **20**, 11–138 (1993)
32. Jahani, F., Deviny, J., Mansfeld, F., Rosen, I., Sun, Z., Wang, C.: Investigations of sulfuric acid corrosion of concrete. I: modeling and chemical observations. *J. Environ. Eng.* **127**, 572–579 (2001)
33. Jiang, G., Gutierrez, O., Sharma, K.R., Keller, J., Yuan, Z.: Optimization of intermittent, simultaneous dosage of nitrite and hydrochloric acid to control sulfide and methane productions in sewers. *Water Res.* **45**, 6163–6172 (2011)
34. Jiang, G., Gutierrez, O., Sharma, K.R., Yuan, Z.: Effects of nitrite concentration and exposure time on sulfide and methane production in sewer systems. *Water Res.* **44**, 4241–4251 (2010)
35. Jiang, G., Sun, J., Sharma, K.R., Yuan, Z.: Corrosion and odor management in sewer systems. *Curr. Opin. Biotechnol.* **33**, 192–197 (2015)
36. Jiang, G., Wightman, E., Donose, B.C., Yuan, Z., Bond, P.L., Keller, J.: The role of iron in sulfide induced corrosion of sewer concrete. *Water Res.* **49**, 166–174 (2014)
37. Joseph, A.P., Keller, J., Bustamante, H., Bond, P.L.: Surface neutralization and H₂S oxidation at early stages of sewer corrosion: influence of temperature, relative humidity and H₂S concentration. *Water Res.* **46**, 4235–4245 (2012)

38. Kelly, D.P., Wood, A.P.: Reclassification of some species of *Thiobacillus* to the newly designated genera *Acidithiobacillus* gen. nov., *Halothiobacillus* gen. nov and *Thermithiobacillus* gen. nov. *Int. J. Syst. Evol. Microbiol.* **50**, 511–516 (2000)
39. Lens, P., Pol, L.H.: *Environmental Technologies to Treat Sulfur Pollution*. IWA Publishing (2000)
40. Li, X., Kappler, U., Jiang, G., Bond, P.L.: The ecology of acidophilic microorganisms in the corroding concrete sewer environment. *Front. Microbiol.* **8** (2017)
41. Liang, Z.S., Sun, J., Chau, H.K.M., Leong, E.I.M., Wu, D., Chen, G.H., Jiang, F.: Experimental and modelling evaluations of sulfide formation in a mega-sized deep tunnel sewer system and implications for sewer management. *Environ. Int.* **131** (2019)
42. Liu, Y., Ni, B.-J., Sharma, K.R., Yuan, Z.: Methane emission from sewers. *Sci. Total Environ.* **524–525**, 40–51 (2015)
43. Liu, Y., Sharma, K.R., Fluggen, M., O'Halloran, K., Murthy, S., Yuan, Z.: Online dissolved methane measurement in sewers. *Water Res.* (2014) (under review)
44. Lu, Y.-Y., Hu, J.-Y., Li, S., Tang, W.-S.: Active and passive protection of steel reinforcement in concrete column using carbon fibre reinforced polymer against corrosion. *Electrochim. Acta* (2018)
45. Mathioudakis, V.L., Aivasidis, A.: Effect of temperature on anoxic sulfide oxidation and denitrification in the bulk wastewater phase of sewer networks. *Water Sci. Technol.* **59**, 705–712 (2009)
46. Mohanakrishnan, J.: Role of anaerobic biofilm in sewer biotransformations. Ph.D. thesis. The University of Queensland (2008)
47. Monteiro, P.J., Kurtis, K.E.: Time to failure for concrete exposed to severe sulfate attack. *Cem. Concr. Res.* **33**, 987–993 (2003)
48. Monteny, J., de Belie, N., Vincke, E., Verstraete, W., Taerwe, L.: Chemical and microbiological tests to simulate sulfuric acid corrosion of polymer-modified concrete. *Cem. Concr. Res.* **31**, 1359–1365 (2001)
49. Monteny, J., Vincke, E., Beeldens, A., de Belie, N., Taerwe, L., van Gemert, D., Verstraete, W.: Chemical, microbiological, and in situ test methods for biogenic sulfuric acid corrosion of concrete. *Cem. Concr. Res.* **30**, 623–634 (2000)
50. Mori, T., Nonaka, T., Tazaki, K., Koga, M., Hikosaka, Y., Noda, S.: Interactions of nutrients, moisture and pH on microbial corrosion of concrete sewer pipes. *Water Res.* **26**, 29–37 (1992)
51. Morton, R.L., Yanko, W.A., Graham, D.W., Arnold, R.G.: Relationships between metal concentrations and crown corrosion in Los-Angeles-county sewers. *Res. J. Water Pollut. Control Fed.* **63**, 789–798 (1991)
52. Nica, D., Davis, J.L., Kirby, L., Zuo, G., Roberts, D.J.: Isolation and characterization of microorganisms involved in the biodeterioration of concrete in sewers. *Int. Biodeterior. Biodegradation* **46**, 61–68 (2000)
53. Nielsen, P.H., Hvitved-Jacobsen, T.: Effect of sulfate and organic-matter on the hydrogen-sulfide formation in biofilms of filled sanitary sewers. *J. Water Pollut. Control Fed.* **60**, 627–634 (1988)
54. Nielsen, A.H., Vollertsen, J., Hvitved-Jacobsen, T.: Chemical sulfide oxidation of wastewater—effects of pH and temperature. *Water Sci. Technol.* **50**, 185–192 (2004)
55. Nielsen, A.H., Vollertsen, J., Jensen, H.S., Wium-Andersen, T., Hvitved-Jacobsen, T.: Influence of pipe material and surfaces on sulfide related odor and corrosion in sewers. *Water Res.* **42**, 4206–4214 (2008)
56. Nnadi EO, Lizarazo-Marriaga J (2013) Acid corrosion of plain and reinforced concrete sewage systems. *J Mater Civil Eng* **25**:1353–1356
57. Okabe, S., Odagiri, M., Ito, T., Satoh, H.: Succession of sulfur-oxidizing bacteria in the microbial community on corroding concrete in sewer systems. *Appl. Environ. Microbiol.* **73**, 971–980 (2007)
58. Olmstead, W.M., Hamlin, H.: Converting portions of the Los Angeles outfall sewer into a septic tank. *Eng. News* **44**, 317 (1900)

59. Parande, A., Babu, B.R., Pandi, K., Karthikeyan, M., Palaniswamy, N.: Environmental effects on concrete using ordinary and Pozzolana Portland cement. *Constr. Build. Mater.* **25**, 288–297 (2011)
60. Parande, A., Ramsamy, P., Ethirajan, S., Rao, C., Palanisamy, N.: Deterioration of reinforced concrete in sewer environments. In: *Proceedings of the Institution of Civil Engineers-Municipal Engineer*, pp. 11–20. Thomas Telford Ltd. (2006)
61. Parker, C.: The corrosion of concrete 1. The isolation of a species of bacterium associated with the corrosion of concrete exposed to atmospheres containing hydrogen sulphide. *Aust. J. Exp. Biol. Med. Sci.* **23** (1945)
62. Parker, C.: The corrosion of concrete 2. The function of *Thiobacillus concretivorus* (nov. spec.) in the corrosion of concrete exposed to atmospheres containing hydrogen sulphide. *Aust. J. Exp. Biol. Med. Sci.* **23** (1945)
63. Parker, C.D.: The corrosion of concrete. *Aust. J. Exp. Biol. Med. Sci.* **23**, 81–90 (1945)
64. Parker, C.T.: Species of sulphur bacteria associated with the corrosion of concrete. *Nature* **159**, 439–440 (1947)
65. Parker, D.: The corrosion of concrete. 2. The function of *Thiobacillus concretivorus* (Nov-spec) in the corrosion of concrete exposed to atmospheres containing hydrogen sulfide. *Aust. J. Exp. Biol. Med. Sci.* **23**, 91–98 (1945)
66. Parker, D.: The corrosion of concrete. I. The isolation of a species of bacterium associated with the corrosion of concrete exposed to atmospheres containing hydrogen sulphide. *Aust. J. Exp. Biol. Med. Sci.* **23**, 81–90 (1945)
67. Parker, D.: Species of sulphur bacteria associated with the corrosion of concrete. *Nature* (London), 159 (1947)
68. Pomeroy, R., Bowlus, F.D.: Progress report on sulfide control research. *Sewage Works J.* **18**, 597–640 (1946)
69. Pomeroy, R.D.: *The Problem of Hydrogen Sulphide in Sewers*. Clay Pipe Development Association Limited, London (1990)
70. Roberts, D.J., Nica, D., Zuo, G., Davis, J.L.: Quantifying microbially induced deterioration of concrete: initial studies. *Int. Biodeterior. Biodegradation* **49**, 227–234 (2002)
71. Sanchez-Silva, M., Rosowsky, D.V.: Biodeterioration of construction materials: state of the art and future challenges. *J. Mater. Civ. Eng.* **20**, 352–365 (2008)
72. Santo Domingo, J.W., Revetta, R.P., Iker, B., Gomez-Alvarez, V., Garcia, J., Sullivan, J., Weast, J.: Molecular survey of concrete sewer biofilm microbial communities. *Biofouling* **27**, 993–1001 (2011)
73. Shammay, A., Sivret, E.C., Le-Minh, N., Lebrero Fernandez, R., Evanson, I., Stuetz, R.M.: Review of odour abatement in sewer networks. *J. Environ. Chem. Eng.* (2016)
74. Simoes, M., Simoes, L.C., Vieira, M.J.: A review of current and emergent biofilm control strategies. *LWT Food Sci. Technol.* **43**, 573–583 (2010)
75. Song, Y., Wightman, E., Tian, Y., Jack, K., Li, X., Zhong, H., Bond, P.L., Yuan, Z., Jiang, G.: Corrosion of reinforcing steel in concrete sewers. *Sci. Total Environ.* **649**, 739–748 (2019)
76. Song, Y., Wightman, E., Kulandaivelu, J., Bu, H., Wang, Z., Yuan, Z., Jiang, G.: Rebar corrosion and its interaction with concrete degradation in reinforced concrete sewers. *Water Res.*, 115961 (2020)
77. Sutrisno, W., Suprobo, P., Wahyuni, E.: Investigation of non-uniform rust distribution and its effects on corrosion induced cracking in reinforced concrete. In: *MATEC Web of Conferences*, p. 02013. EDP Sciences (2017)
78. Sydney, R., Esfandi, E., Surapaneni, S.: Control concrete sewer corrosion via the crown spray process. *Water Environ. Res.* **68**, 338–347 (1996)
79. Thistlethwayte, D.K.B.: *The control of Sulphides in Sewerage Systems*. Butterworth Pty. Ltd., Sydney (1972)
80. Tiller, A.: Biocorrosion in civil engineering. In: *Microbiology in Civil Engineering*, pp. 24–38. London (1990)
81. US EPA: *Process Design Manual for Sulfide Control in Sanitary Sewer Systems* (1974)

82. US EPA: Hydrogen sulphide corrosion in wastewater collection and treatment system. Technical report (1991)
83. Vahidi, E., Jin, E., Das, M., Singh, M., Zhao, F.: Environmental life cycle analysis of pipe materials for sewer systems. *Sustain. Cities Soc.* **27**, 167–174 (2016)
84. Vincke, E., van Wanseele, E., Monteny, J., Beeldens, A., de Belie, N., Taerwe, L., van Gemert, D., Verstraete, W.: Influence of polymer addition on biogenic sulfuric acid attack of concrete. *Int. Biodeterior. Biodegradation* **49**, 283–292 (2002)
85. WERF: In: Apgar, D., Witherspoon, J., Easter, C., Bassrai, S., Dillon, C., Torres, E., Bowker, R.P.G., Corsi, R., Davidson, S., Wolstenholme, P., Forbes, B., Quigley, C., Ward, M., Joyce, J., Morton, R., Weiss, J., Stuetz, R. (eds.) *Water Environment Research Fundation*, London, UK (2007)
86. Zhang, L., de Schryver, P., de Gussemme, B., de Muynck, W., Boon, N., Verstraete, W.: Chemical and biological technologies for hydrogen sulfide emission control in sewer systems: a review. *Water Res.* **42**, 1–12 (2008)
87. Zivica, V.R., Bajza, A.: Acidic attack of cement based materials—a review: part 1. Principle of acidic attack. *Constr. Build. Mater.* **15**, 331–340 (2001)

Mechanisms and Processes of Concrete Corrosion in Sewers



Xuan Li, Guangming Jiang, Cyrill Grengg, and Florian Mittermayr

Abstract Concrete corrosion in sewers is caused by the combination of chemical and biological processes including sulfide and carbon dioxide generation and partition in wastewater, sulfide oxidation, neutralizing reactions of carbon dioxide, hydrogen sulfide, and its oxidation products (mainly sulfuric acid) with concrete. Wastewater is a sulfate-rich environment with sufficient carbon sources. The metabolism of sulfate-reducing bacteria leads to the formation of hydrogen sulfide in wastewater under anaerobic conditions. During wastewater transport through the sewers, depending on the dissolved oxygen concentrations and pH in wastewater, hydrogen sulfide can be chemically or biologically oxidized in wastewater, or partition into sewer gas in gravity sewers. Due to the alkaline and porous nature of concrete sewer pipes, the hydrogen sulfide reacts with intact concrete and reduces the concrete pH, lowering the concrete surface pH through chemically induced corrosion. The additional outgassing of CO₂ from the wastewater further accelerates these processes. The reduction of surface pH facilitates the colonization of sulfide-oxidizing microorganisms on concrete surfaces. Sulfide-oxidizing microorganisms can further biologically

X. Li · G. Jiang (✉)

School of Civil, Mining, Environmental and Architectural Engineering, University of Wollongong, Wollongong, NSW 2522, Australia
e-mail: gjiang@uow.edu.au

X. Li

e-mail: xuan.li@uts.edu.au

X. Li

School of Civil and Environmental Engineering, Centre for Technology in Water and Wastewater, University of Technology Sydney, Ultimo, NSW 2007, Australia

C. Grengg

Institute of Applied Geosciences, Graz University of Technology, Rechbauerstraße 12, 8010 Graz, Austria
e-mail: cyrill.grengg@tugraz.at

F. Mittermayr

Institute of Technology and Testing of Building Materials, Graz University of Technology, Inffeldgasse 24, 8010 Graz, Austria
e-mail: f.mittermayr@tugraz.at

oxidize hydrogen sulfide into sulfuric acid, leading to microbiologically influenced concrete corrosion. This chapter describes and discusses the mechanisms of these processes in sewers.

1 The Sulfur Cycle in Sewers

As described in Chapter “Concrete Sewer Systems and Wastewater Processes Related to Concrete Corrosion”, modern sewers majorly consist of two types of sewers: rising main and gravity sewers. In rising main sewers, pipes are fully filled with wastewater and operated with no gas phase under anaerobic conditions. In some cases, at the entry of the rising main sewers, there will be an aerobic phase but along the distance in the pipe, the wastewater becomes anoxic [14], and anaerobic due to the consumption of oxygen as the electron acceptor for microbial processes [21]. Gravity regions are usually partially filled, where wastewater flows downstream due to gravity. In gravity sewers, both aerobic and anaerobic conditions can occur below the water surface depending on the wastewater temperature, turbulence and flow rates of the wastewater (i.e. determined by the slope, size of the pipe, and hydraulic load), ventilation (i.e. either natural or forced) and the water depth-to-diameter ratio of gravity sewers [1, 20]. The rising main sewer contains four main components: (1) wastewater; (2) biofilms; (3) sewer sediments; (4) sewer walls. While gravity sewers contain all these four components with one additional important component: the sewer gas.

Within the sewer system, the sulfur cycle is one of the most complex nutrient cycles. Wastewater is inherently a sulfate-rich environment, where the concentration of dissolved sulfate is typically 20–200 mg-S/L in wastewater [47]. The major source for this high sulfate concentration was identified as the coagulant used for the production of drinking water (52%), source water (38%), and other human wastes [37]. The change of sewer conditions alters the electron acceptors for chemical and biological reactions and products. Due to the dissolution and oxidation of sulfide, various sulfur compounds exist in sewers (Table 1).

Table 1 Inorganic sulfur species and the sulfur oxidation states adapted from Suzuki [42]

Oxidation state				
- 2	0	+ 2	+ 4	+ 6
H ₂ S hydrogen sulfide	S ⁰ elemental sulfur	(SO) sulfur monoxide	SO ₂ sulfur dioxide	SO ₃ sulfur trioxide
HS ⁻ bisulfide		H ₂ SO ₂ sulfoxylic acid	H ₂ SO ₃ sulfurous acid	H ₂ SO ₄ sulfuric acid
		S ₂ O ₃ ²⁻ thiosulfate	SO ₃ ²⁻ sulfite	SO ₄ ²⁻ sulfate
		S ₄ O ₆ ²⁻ tetrathionate		

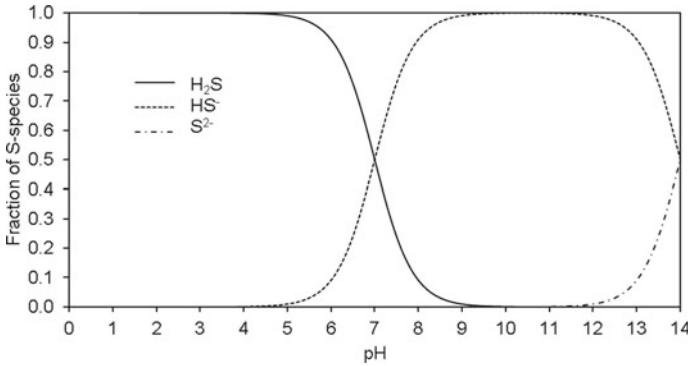
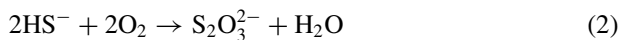


Fig. 1 The impact of the wastewater pH on the dissolved sulfide speciation (pK_{a1} of 7 and pK_{a2} of 14)

For both abiotic and biotic reactions, water is the major medium that allows the reaction to happen. In anaerobic parts of sewers (i.e. rising main sewer and anaerobic part of gravity sewer), sulfate becomes the main electron acceptor, where hydrogen sulfide is biologically produced by sulfate-reducing bacteria (SRB) [10]. In rising main sewers, the oxidation of sulfur happens in the wastewater phase; while in gravity sewers, it can occur in both the wastewater phase and moist sewer pipe surfaces in contact with oxygen [22]. Under both conditions, the dissociation of hydrogen sulfide is crucial for the distribution and oxidation of sulfide species, primarily controlled by the pH of the system. As described in Chapter “Concrete Sewer Systems and Wastewater Processes Related to Concrete Corrosion”, sulfide is a weak acid with pK_{a1} value of 7 and pK_{a2} value ranging from 11.96 to 17.00 [10, 36]. The pH dependent dissociation of hydrogen sulfide is shown in Fig. 1.

In normal wastewater conditions (7.5–8.5), bisulfide is the dominant sulfide species (Fig. 1). The main products of chemical sulfide oxidation with oxygen are thiosulfate ($S_2O_3^{2-}$) and sulfate (SO_4^{2-}), depending on the availability of oxygen in wastewater [32]. When oxygen is limiting, thiosulfate is the main product. The further oxidation of thiosulfate to sulfate mainly takes place in sewer pipes with long hydraulic retention times (HRT) [31]. Chemical oxidation of sulfide with oxygen also produces common intermediates such as elemental sulfur (S^0) and sulfite (SO_3^{2-}) [18]. The latter is rapidly oxidized by oxygen to sulfate and is often negligible in wastewater. Elemental sulfur, thiosulfate, sulfite, and sulfate are formed according to Eqs. (1)–(4) [31]:





Temperature and pH are important parameters affecting the abiotic oxidation of sulfide in aqueous environments. Studies performed on inactivated wastewater showed that chemical sulfide oxidation rates increase with increasing temperature [5, 32]. The pH of the solution also showed a significant impact on the abiotic oxidation process [5]. In acidic solutions with $\text{pH} < 6$, where H_2S is the predominating sulfide species (Fig. 1), the chemical oxidation rate of sulfide is very slow. The specific rate increases greatly as pH increases through 7 to a maximum of pH 8.0, then decreases to a minimum near pH 9, increases again to a second maximum about equal to first near pH 11, and finally decreases again in more alkaline solutions [5]. Similarly, a reaction pattern is also observed in [27], where the half-time ($t_{1/2}$) for the oxidation of H_2S by O_2 is estimated as 50 ± 16 h at 26 ± 9 °C in water with a pH of 8. Thus, the chemical oxidation of sulfide is generally considered a slow process.

In aqueous environments, biological sulfide oxidation can occur by sulfur-oxidizing microorganisms (SOM) at a faster rate than chemical oxidation [10]. Biological sulfide oxidation in the solution mainly occurs when sulfide generated in the upstream sections (i.e. rising mains) is transferred to the aerobic sections (i.e. gravity sewers) or when sulfide generated in the anaerobic part of biofilms diffuses to the aerobic part of biofilms [10]. The oxidation products are impacted by the sulfide and dissolved oxygen (DO) concentration. Under limited DO conditions, sulfide in water is oxidized by SOMs to elemental sulfur [30]. When DO concentration is sufficient, besides elemental sulfur, sulfate can be produced by SOM with thiosulfate, thirithionate, and tetrathionate as intermediates [35]. High concentrations of sulfide are toxic to some SOM [3]. Although elemental sulfur can be produced in both chemical and biological reactions, it is worthy to note that the elemental sulfur produced from chemical oxidations of sulfide is hardly used by SOMs [11]. This might be related to the particle size and surface properties of the elemental sulfur produced. In particular, the elemental sulfur produced by abiotic oxidation of sulfide is found quite hydrophobic but biologically produced elemental is hydrophilic, which is easier for the colonization and development of SOMs [19].

When the DO concentration is insufficient (normally < 0.5 mg/L) for either abiotic or biotic oxidation of sulfide, sulfide start to accumulate in the wastewater, which eventually leads to the partition of hydrogen sulfide to sewer gas in gravity sewers [10]. Among the sulfide species (Table 1), hydrogen sulfide is the only specie that can partition into the sewer gas phase. Hydrogen sulfide is moderately soluble in water ranging from 4 g/L at 20 °C to 6.3 g/L at 4 °C [2]. The partition process of H_2S is highly pH dependent. As shown in Fig. 1, at pH values below 8, hydrogen sulfide will present and can partition into the headspace [33]. Lower wastewater pH leads to a higher hydrogen sulfide release into the sewer atmosphere. Generally, Henry's law describes the partition of gases across the air–water interface. However, this steady state relationship does not apply to the dynamic partition of sulfide into the sewer atmosphere due to ever-changing conditions such as the occurrence of ventilation (either natural or forced), intermittent wastewater flow, and turbulence in sewer

systems. Furthermore, the overall mass transfer increases with higher temperature, thereby resulting in an increase in the ratio between hydrogen sulfide concentrations in the gas phase and in the liquid phase [4]. More importantly, the emission and subsequent oxidation of H₂S also leads to the chemically and microbiologically influenced corrosion in gravity sewers, which significantly shortens the service life of sewer pipes [13]. The details of chemically and microbially influenced corrosion are discussed in the following sections.

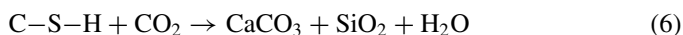
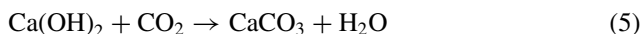
2 Chemically Induced Concrete Corrosion

2.1 The Impact of Corrosive Environment in Sewers

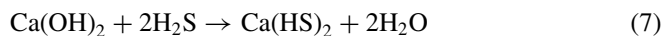
The corrosion of concrete in the sewer environment is attributed to two parts: the corrosive environment in sewers (i.e., H₂S, CO₂, relative humidity, wastewater etc.) and the physical and chemical properties of concrete. As mentioned in Chapter “Concrete Sewer Systems and Wastewater Processes Related to Concrete Corrosion”, concrete is a multicomponent, inorganic, porous material which for the most parts consist of the hardened cement paste and aggregates. The hydrated cement paste forms a network of hydration products consisting of calcium silicate hydrates (C–S–H), calcium hydroxide (CH) and minor quantities calcium aluminates (AFm) and ettringite (Aft) [7, 43].

The pH of the pore solution of hardened concrete made from OPC is usually > 13 [16, 43, 44]. Little microbial activity occurs at this stage due to the prevailing high alkalinity. According to the three-stage theory [11], this phase is named the initial acidification stage, where the pH is abiotically reduced from ~ 13 to ~ 9 through carbonation and hydrogen sulfide dissolution, within the condensate of the surface near pore structure.

The carbonation of the concrete surface starts from the manufacturing time of concrete sewer pipes. Directly contacted with the surface of concrete pipes or absorbed in pores, CO₂ reacts with calcium hydroxide and hydrated calcium silicate (C–S–H) in concrete and produces calcium carbonate (Eqs. 5 and 6) [9].

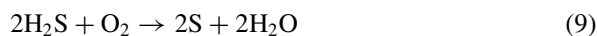


In a laboratory test setup with 5–50 ppm H₂S, 18–30 °C, and 85–100% relative humidity, it was shown that carbonation decreases the surface pH from 13 to about 10 [17]. Then, H₂S had a significant role in the initial abiotic pH reduction, and directly reacts with Ca(OH)₂ in concrete (Eq. 7), which further reduces the pH of concrete to around 8.



In contrast, on-site measurements within several corroded sewer basins in Austria reported high CO_2 concentrations of up to 6500 ppm, implying a central role of CO_2 within the initial abiotic pH reduction of concrete due to ongoing carbonation of the cementitious matrix [8]. The diffusion of CO_2 into the pore solution triggers a dissolution of Ca(OH)_2 , Ca depletion of the C–S–H phases and concurrent formation of calcium carbonates. Described chemical reactions are accompanied with a pH reduction to as low as 8.0. In this context the overall impact of CO_2 on the corrosion process is strongly associated with the overall relative humidity and corresponding water saturation of the pores since strongly controlling the diffusion kinetic of CO_2 . Accordingly, carbonation induced pH reduction may dominate in systems exhibiting lower relative humidity levels and/or high daily and/or seasonal changes in relative humidity (e.g. sewer manholes vs. sewer pipes).

Apart from direct reactions between corrosive sewer gases (i.e. CO_2 and H_2S) with concrete, due to the presence of oxygen, H_2S can be chemically oxidized on concrete surfaces. To date, the understanding of abiotic/chemical sulfide oxidation on concrete surfaces is limited. Few studies have investigated the chemical oxidation of H_2S on concrete surfaces. In laboratory-controlled corrosion chambers with H_2S below 50 ppm, elemental sulfur was found as the major oxidation product, with the presence of sulfate (< 10%) [17]. The oxidation of H_2S may thus occur according to Eq. (8) or Eq. (9).



In sewer systems affected by MICC, the reduction of pH during the initiation stage is usually followed by the development of biofilms on the concrete surfaces and corresponding biologically controlled sulfur oxidation reactions [11]. However, in systems exhibiting very high H_2S concentrations chemical oxidation of H_2S may remain the dominant process of concrete deterioration. Within a pilot-scale study with gaseous H_2S concentrations of 1100 ± 100 ppm, concrete samples were rapidly corroded in 20 days. The initial surface pH > 10 was rapidly reduced to around pH 3. Newly formed Ca-sulfate precipitates were identified as the main corrosion products [24]. This rapid corrosion was found to be caused by the chemical oxidation of H_2S to sulfuric acid. The fast and direct formation of sulfate through abiotic sulfide oxidation under alkaline conditions was further confirmed by aerated water containing fresh concrete powder, where more than 70% of the sulfide was oxidized within 4 h in this study. The sulfide uptake test of the concrete coupon further revealed that the chemical sulfide oxidation on the concrete surface followed exponential kinetics at H_2S concentration between 500–1500 ppm [24]. However, with ongoing pH reduction towards acidic conditions, the chemical oxidation rate of sulfide was found to

slow down due to the formation of corrosion layer [24]. Thus, this rapid chemically induced corrosion is likely still serving as a precedent stage for the development of advanced microbial corrosion, which requires future investigations. In real sewers, the H_2S concentration varies from several ppm to hundreds of ppm [22]. Such high concentrations H_2S (i.e. 500–1000 ppm) has been frequently detected in many sewers, which potentially accounts for higher corrosion rates than previously assumed [46]. Therefore, chemical concrete corrosion due to the interaction with H_2S and CO_2 can be an important deterioration process in sewers.

In regard to the factors affecting the chemically induced corrosion, H_2S concentration played an important role in both studies as mentioned above, where a quicker pH reduction and higher amount of corrosion products (sulfide oxidation products) were observed under higher H_2S concentrations [17, 24]. In the laboratory study, higher temperature, and relative humidity also facilitate the corrosion process [12, 15, 17]. As detailed in Sect. 1, the chemical oxidation of H_2S in water is enhanced under higher temperatures. Furthermore, a higher temperature in sewer gas is also associated with a higher water evaporation rate, which together with relative humidity impacts the moisture level and condensation water layer on concrete (Sect. 1).

2.2 *The Impact of Concrete Properties*

Concrete is a porous material (Fig. 2a). Accordingly, the pore structure and volume play an essential role in respect to the material response within diffusion-based deterioration processes [34, 39]. The formation of the pore structure in concrete is closely related to the hydration processes of concrete. The hydration process is triggered once the cement is in contact with water and further developed during the curing process when concrete is fully immersed in water or water-based solutions (i.e., lime water). During the hydration process, the hydration products bind the aggregates with the cement matrix and occupy the pore spaces (i.e., the air voids introduced due to the mixing) (Fig. 2b). After the curing process, the hydration process continues until the excess water in the pores evaporates and leaves the pores empty or unsaturated.

The overall amount and structure of pores is controlled by the water to binder ratio (w/b), the cement chemistry and the curing conditions applied. Pores in concrete can be isolated or interconnected from one another. The interconnected pores are capable of transporting aggressive species, such as moisture, carbon dioxide (CO_2), and hydrogen sulfide within the cement paste, which thereby influences the corrosion development on concrete [26]. Based on the pore size distribution and relevant assumptions, Wells and Melchers [46] built a model for the relationship between concrete moisture level and relative humidity. It shows that the higher the relative humidity, the greater the increase of concrete moisture level, especially for the relative humidity range from 95 to 100%. At higher humidity levels, moisture in sewer gas condenses initially within the smaller diameter pores and then progressively

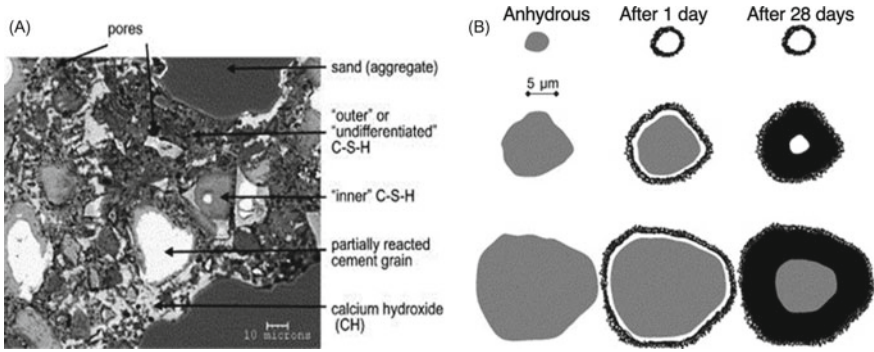


Fig. 2 **a** Backscattered (BSE) electron micrograph of an Ordinary Portland Cement mortar (200 days old, $w/c = 0.4$), with the microstructural constituents distinguished. **b** Schematic illustration of the formation of hydration shells according to grain size. Adapted from Scrivener [38] with permission from Elsevier

in larger diameter pores with further humidity increases until eventually, at 100% humidity, the pore space is fully filled. At this point, a condensate film forms on the concrete surface of the pipe [46]. Therefore, higher temperature and relative humidity in sewer gas allows an earlier and denser formation of condensation layer (as visually observed by Joseph et al. [17], which provides the suitable conditions for chemical oxidation of sulfide. In addition, the concrete chemical and physical properties are also dependent on the concrete materials and manufacture process, which subsequently affects the chemically induced corrosion [8, 25] (Fig. 3).

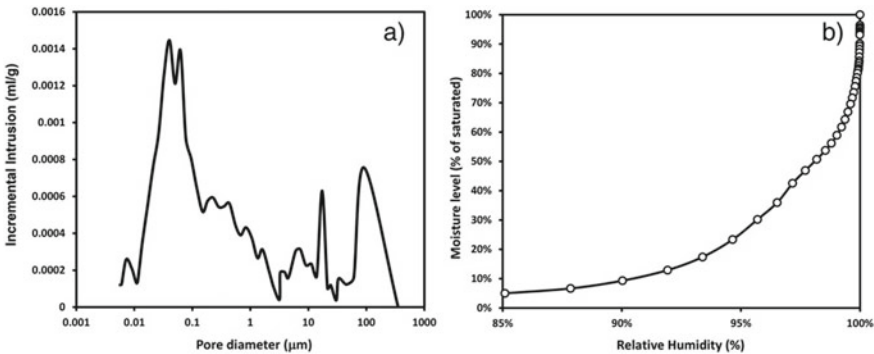
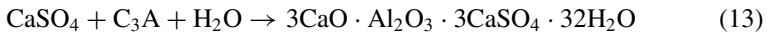
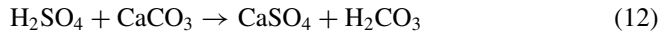
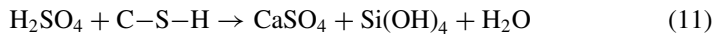
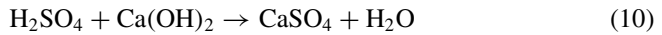


Fig. 3 **a** Pore size distribution of a concrete coupon and **b** the calculated response of concrete moisture level to changes in sewer gas relative humidity. Reproduced from Wells and Melchers [46] with permission from Elsevier

3 Microbiologically Influenced Concrete Corrosion (MICC)

Once the surface pH reaches about 9, neutrophilic sulfur-oxidizing microorganisms (NSOM) colonize the concrete surface [11]. NSOM are typical sulfur oxidizers that could biologically oxidize sulfur compounds to sulfuric acid. Sulfuric acid either produced by microorganisms or by chemical oxidization (discussed in Sect. 2) reacts with the cementitious phases and, if present carbonate aggregates, causing dissolution of the microstructure and the precipitation of expansive secondary minerals as Eqs. (10)–(13), where calcium sulfates (i.e., anhydrite, basanite and gypsum), ettringite and amorphous silica are found as the major corrosion products.



Continuous biotic acid production by NSOM lead to a further pH reduction within the corrosion horizons of the concrete to below 4. With the decrease of pH, the microbial community on the concrete surface gradually changes, which leads to the start of stage 3 of the corrosion. In stage 3, acidophilic sulfur-oxidizing microorganisms (ASOM) colonize and become the dominant microbe on the concrete surface, where the biological formation of large amounts of sulfuric acid occurs.

In contrast to chemically induced corrosion, numerous studies have investigated the development of microbiologically influenced concrete corrosion, where location, H_2S concentrations, relative humidity, temperature are found as critical factors affecting corrosion development in sewers. Depending on the availability of sewer gases and wastewater, MICC commonly occurs at two hot spots, namely crown regions and tidal regions in the sewer pipes (Fig. 4). Crown regions are the ceiling of the sewer headspace, while tidal regions are just above the wastewater flow level [22]. In manholes, corrosion also occurs in the regions next or the wastewater line (similar to the tidal regions), and manhole walls (similar to the crown regions). The availability of sewer gas and contact with wastewater varies greatly in these two locations. In crown regions, concrete contacts with wastewater very occasionally (e.g., during flooding), the sewer gases thereby become the major source of ‘food’ for microorganism development. The diffusion of gases (i.e., CO_2 , H_2S , O_2) provides volatile substrates and nutrients for the development of NSOM and ASOM [12]. Furthermore, water content, a critical compound for microbial activities, is also provided by the moisture from sewer gas for crown regions. The water content in crown regions is majorly provided by the condensation from sewer gas with high relative humidity

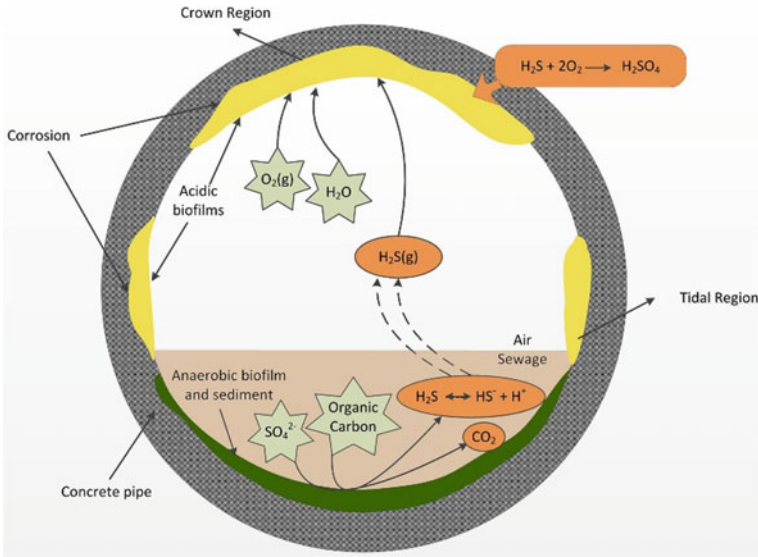


Fig. 4 A diagram of a cross-section of a sewer gravity concrete pipe summarizing the major processes that lead to the acid formation in the aerobic biofilms and the onset of sewer corrosion at two major hot spots, i.e., tidal and crown regions [22] (open access)

(as discussed in Sect. 2). In tidal regions, concrete walls receive frequent contact with wastewater, which provides the frequent replenishment of nutrients, microbial inoculum, and moisture. The abrasive effect of wastewater flow also removes the loss corrosion layers [40]. This results in more severe corrosion in tidal regions than the crown regions [12, 29].

It has been observed for a long time that the microbiologically influenced corrosion was positively correlated with the H_2S levels in sewers globally. For instance, in the crown of a sewer in Japan with 5–400 ppm H_2S and 10–30 °C, the average corrosion rate was around 4.3–4.7 mm/year, but around 2 mm/year in another sewer with 10–50 ppm H_2S and 22 °C in Australia [28, 45]. However, these studies are commonly conducted in different sewers or laboratory setups, where other factors including the relative humidity, temperature, and the concrete type vary from study to study. This greatly hinders the understanding of the exact role of H_2S concentration in corrosion development. In the last decade, several well-controlled laboratory studies in conjunction with the field observations greatly improved the understanding of H_2S on corrosion development. In a laboratory study, the corrosion loss of concrete was found to follow the nth-order kinetics as Eq. (14).

$$C_r = k \times [H_2S]^n \times f_{BET}(RH) + C_{ri} \tag{14}$$

where n is the model constant estimated from the experimental data; $f_{BET}(RH)$ is a Brunauer–Emmett–Teller sorption isotherm of relative humidity and C_{ri} represents

the corrosion caused due to historical exposure prior to the experiment. In this study, the n was estimated to around 0.5, suggesting a dominant role of H_2S concentration on the corrosion loss [12]. A similar observation was reported in a field study in Australia, where the corrosion rate followed n th order kinetics of H_2S concentration with an n value of 0.5–1.0 [45].

As discussed in Sect. 2, the increase of relative humidity and temperature facilitate the formation of a condensation layer on the concrete surface. Similar to the chemically induced corrosion, the increase of relative humidity enhanced the microbial development on concrete in crown regions [12]. While within tidal regions, where frequent wastewater contact is provided by the wastewater stream, the increase of relative humidity showed negligible impacts on the corrosion development [12]. Furthermore, as discussed in Sect. 2, the temperature increase also leads to faster biological oxidation of sulfide. Thus, the microbiologically influenced corrosion is found generally accelerated at higher temperatures. For instance, in sewer biofilms, the sulfide oxidation rates at 25 °C were found to be about 15% higher than those at 20 °C [41]. In laboratory-scale corrosion chambers with controlled conditions, the increase of temperature from 20 to 30 °C also led to a faster acid generation and higher corrosion loss [12]. The details of SOM and their contributions to the microbiologically influenced corrosion will be further discussed in Chapter “[Characterization of Corrosion Microbial Communities](#)”. In addition, the concrete chemical and physical properties also affects the MICC [6, 23].

4 Summary

This chapter discussed the mechanisms and processes involved in the corrosion of concrete sewers in the context of sulfur cycle and carbonation. The corrosion of concrete sewers is closely related to the corrosive environments in gravity sewers and the alkaline and porous nature of concrete. Wastewater is rich in sulfate and carbon sources, which creates conditions similar to a ‘microbial reactor’ where substances are transformed and degraded through chemical and biological processes. The concrete corrosion in sewers is majorly caused by the presence of H_2S , and to a lesser extend CO_2 , in the sewer gas in gravity sections of sewer transportation networks, pumping stations and sewage plants.

The occurrence of H_2S in the sewer gas is related to the metabolism of sulfate-reducing bacteria in anaerobic sections of sewers such as rising main sewers. Due to the low dissolved oxygen levels in wastewater, sulfate become the major electron donor, leading to the biological formation of hydrogen sulfide. During wastewater transportation, the sulfide generated can be either chemically or biological oxidized in wastewater, or partition into sewer gas due to changes in water pressure, turbulences, temperature and pH. The chemical or biological oxidation of sulfide in wastewater results in the formation of various oxidation products including elemental sulfur, thiosulfate, and sulfate. The partition of gaseous hydrogen sulfide from wastewater into sewer gas is highly pH-dependent although further factors such as turbulences,

temperature, and sewer pipe design also play a role. The hydrogen sulfide in the sewer gas leads to chemically and microbiologically influenced concrete corrosion.

Intact concrete usually has a high pH of around 13, which is not suitable for the colonization of most microorganisms. The H₂S in sewer gas reacts with the alkaline concrete directly, leading to the dissolution of portlandite and corresponding pH reduction. While under extreme H₂S concentrations, H₂S can be chemically oxidized directly to sulfuric acid. These reactions reduce the surface pH of concrete, leading to microbiologically influenced concrete corrosion.

The microbiologically influenced concrete corrosion starts when sulfur-oxidizing microorganisms colonize concrete surfaces. Through the biological oxidation of H₂S, biologically produced sulfuric acid on concrete surfaces leads to the formation of corrosion products such as calcium sulfates (i.e., anhydrite, basanite, and gypsum), ettringite and amorphous silica. These corrosion products are of expansive nature, inducing micro- and macro cracking, while providing minimum structural strength and resulting in the mass loss. Very high concrete corrosion rates of > 1 cm/a will eventually lead to a failure of the affected concrete structures.

References

1. Apgar, P., Witherspoon, J.: *Minimization of Odors and Corrosion in Collection Systems* (2008)
2. Boon, A.G.: Septicity in sewers: causes, consequences and containment. *Water Sci. Technol.* **31**, 237–253 (1995)
3. Buisman, C., Uspeert, P., Janssen, A., Lettinga, G.: Kinetics of chemical and biological sulphide oxidation in aqueous solutions. *Water Res.* **24**, 667–671 (1990)
4. Carrera, L., Springer, F., Lipeme-Kouyi, G., Buffiere, P.: A review of sulfide emissions in sewer networks: overall approach and systemic modelling. *Water Sci. Technol.* **73**, 1231–1242 (2016)
5. Chen, K.Y., Morris, J.C.: Kinetics of oxidation of aqueous sulfide by oxygen. *Environ. Sci. Technol.* **6**, 529–537 (1972)
6. Chetty, K., Xie, S., Song, Y., McCarthy, T., Garbe, U., Li, X., Jiang, G.: Self-healing bioconcrete based on non-axenic granules: a potential solution for concrete wastewater infrastructure. *J. Water Process Eng.* **42**, 102139 (2021)
7. Gartner, E., Young, J., Damidot, D., Jawed, I.: Hydration of Portland cement. *Struct. Perform. Cem.* **13**, 978 (2002)
8. Grengg, C., Ukrainczyk, N., Koraimann, G., Mueller, B., Dietzel, M., Mittermayr, F.: Long-term in situ performance of geopolymer, calcium aluminate and Portland cement-based materials exposed to microbially induced acid corrosion. *Cem. Concr. Res.* **131**, 106034 (2020)
9. Houst, Y.F.: The role of moisture in the carbonation of cementitious materials. *Int. Z. Bauinstandsetzen Baudenkmalpflege* **2**, 49–66 (1996)
10. Hvitved-Jacobsen, T., Vollertsen, J., Matos, J.S.: The sewer as a bioreactor—a dry weather approach. *Water Sci. Technol.* **45**, 11–24 (2002)
11. Islander, R.L., Deviny, J.S., Mansfeld, F., Postyn, A., Shih, H.: Microbial ecology of crown corrosion in sewers. *J. Environ. Eng.* **117**, 751–770 (1991)
12. Jiang, G., Keller, J., Bond, P.L.: Determining the long-term effects of H₂S concentration, relative humidity and air temperature on concrete sewer corrosion. *Water Res.* **65**, 157–169 (2014)
13. Jiang, G., Keller, J., Bond, P.L., Yuan, Z.: Predicting concrete corrosion of sewers using artificial neural network. *Water Res.* **92**, 52–60 (2016)

14. Jiang, G., Sharma, K.R., Guisasaola, A., Keller, J., Yuan, Z.: Sulfur transformation in rising main sewers receiving nitrate dosage. *Water Res.* **43**, 4430–4440 (2009)
15. Jiang, G., Sun, X., Keller, J., Bond, P.L.: Identification of controlling factors for the initiation of corrosion of fresh concrete sewers. *Water Res.* **80**, 30–40 (2015)
16. Jiang, G., Wightman, E., Donose, B.C., Yuan, Z., Bond, P.L., Keller, J.: The role of iron in sulfide induced corrosion of sewer concrete. *Water Res.* **49**, 166–174 (2014)
17. Joseph, A.P., Keller, J., Bustamante, H., Bond, P.L.: Surface neutralization and H₂S oxidation at early stages of sewer corrosion: influence of temperature, relative humidity and H₂S concentration. *Water Res.* **46**, 4235–4245 (2012)
18. Keller-Lehmann, B., Corrie, S., Ravn, R., Yuan, Z., Keller, J.: Preservation and simultaneous analysis of relevant soluble sulfur species in sewage samples. In: *Proceedings of the Second International IWA Conference on Sewer Operation and Maintenance*, p. 28. Citeseer (2006)
19. Kleinjan, W., de Keizer, A., Janssen, A.: Elemental sulfur and sulfur-rich compounds I. *Top. Curr. Chem.* **230**, 167–188 (2003)
20. Kulandaivelu, J., Choi, P.M., Shrestha, S., Li, X., Song, Y., Li, J., Sharma, K., Yuan, Z., Mueller, J.F., Wang, C., Jiang, G.: Assessing the removal of organic micropollutants from wastewater by discharging drinking water sludge to sewers. *Water Res.* **181**, 115945 (2020)
21. Kulandaivelu, J., Gao, J., Song, Y., Shrestha, S., Li, X., Li, J., Doederer, K., Keller, J., Yuan, Z., Mueller, J.F.: Removal of pharmaceuticals and illicit drugs from wastewater due to ferric dosing in sewers. *Environ. Sci. Technol.* (2019)
22. Li, X., Jiang, G., Kappler, U., Bond, P.: The ecology of acidophilic microorganisms in the corroding concrete sewer environment. *Front. Microbiol.* **8**, 683 (2017)
23. Li, X., Kulandaivelu, J., O'Moore, L., Wilkie, S., Hanzic, L., Bond, P.L., Yuan, Z., Jiang, G.: Synergistic effect on concrete corrosion control in sewer environment achieved by applying surface washing on calcium nitrite admixed concrete. *Constr. Build. Mater.* **302**, 124184 (2021)
24. Li, X., O'Moore, L., Song, Y., Bond, P.L., Yuan, Z., Wilkie, S., Hanzic, L., Jiang, G.: The rapid chemically induced corrosion of concrete sewers at high H₂S concentration. *Water Res.* **162**, 95–104 (2019)
25. Li, X., O'Moore, L., Wilkie, S., Song, Y., Wei, J., Bond, P.L., Yuan, Z., Hanzic, L., Jiang, G.: Nitrite admixed concrete for wastewater structures: mechanical properties, leaching behavior and biofilm development. *Constr. Build. Mater.* **233**, 117341 (2020)
26. Mehta, P.K.: *Concrete. Structure, Properties and Materials* (1986)
27. Millero, F.J., Hubinger, S., Fernandez, M., Garnett, S.: Oxidation of H₂S in seawater as a function of temperature, pH, and ionic strength. *Environ. Sci. Technol.* **21**, 439–443 (1987)
28. Mori, T., Nonaka, T., Tazaki, K., Koga, M., Hikosaka, Y., Noda, S.: Interactions of nutrients, moisture and pH on microbial corrosion of concrete sewer pipes. *Water Res.* **26**, 29–37 (1992)
29. Nica, D., Davis, J.L., Kirby, L., Zuo, G., Roberts, D.J.: Isolation and characterization of microorganisms involved in the biodeterioration of concrete in sewers. *Int. Biodeterior. Biodegradation* **46**, 61–68 (2000)
30. Nielsen, A.H., Hvitved-Jacobsen, T., Vollertsen, J.: Kinetics and stoichiometry of sulfide oxidation by sewer biofilms. *Water Res.* **39**, 4119–4125 (2005)
31. Nielsen, A.H., Vollertsen, J., Hvitved-Jacobsen, T.: Determination of kinetics and stoichiometry of chemical sulfide oxidation in wastewater of sewer networks. *Environ. Sci. Technol.* **37**, 3853–3858 (2003)
32. Nielsen, A.H., Vollertsen, J., Hvitved-Jacobsen, T.: Kinetics and stoichiometry of aerobic sulfide oxidation in wastewater from sewers—effects of pH and temperature. *Water Environ. Res.* **78**, 275–283 (2006)
33. Nielsen, A.H., Vollertsen, J., Jensen, H.S., Madsen, H.I., Hvitved-Jacobsen, T.: Aerobic and anaerobic transformations of sulfide in a sewer system—field study and model simulations. *Water Environ. Res.* **80**, 16–25 (2008)
34. Page, C.L., Page, M.M.: *Durability of Concrete and Cement Composites*. Elsevier (2007)
35. Parker, C.: The corrosion of concrete 2. The function of *Thiobacillus concretivorus* (nov. spec.) in the corrosion of concrete exposed to atmospheres containing hydrogen sulphide. *Aust. J. Exp. Biol. Med. Sci.* **23** (1945)

36. Pikaar, I., Rozendal, R., Yuan, Z., Keller, J., Rabaey, K.: Electrochemical Sulfide Abatement in Sewer Systems (2011)
37. Pikaar, I., Sharma, K.R., Hu, S., Gernjak, W., Keller, J., Yuan, Z.: Reducing sewer corrosion through integrated urban water management. *Science* **345**, 812–814 (2014)
38. Scrivener, K.L.: Backscattered electron imaging of cementitious microstructures: understanding and quantification. *Cem. Concr. Compos.* **26**, 935–945 (2004)
39. Song, Y., Chetty, K., Garbe, U., Wei, J., Bu, H., O’Moore, L., Li, X., Yuan, Z., McCarthy, T., Jiang, G.: A novel granular sludge-based and highly corrosion-resistant bio-concrete in sewers. *Sci. Total Environ.* **791**, 148270 (2021)
40. Song, Y., Tian, Y., Li, X., Wei, J., Zhang, H., Bond, P.L., Yuan, Z., Jiang, G.: Distinct microbially induced concrete corrosion at the tidal region of reinforced concrete sewers. *Water Res.* **150**, 392–402 (2019)
41. Sublette, K.L., Kolhatkar, R., Raterman, K.: Technological aspects of the microbial treatment of sulfide-rich wastewaters: a case study. *Biodegradation* **9**, 259–271 (1998)
42. Suzuki, I. (1999) Oxidation of inorganic sulfur compounds: chemical and enzymatic reactions. *Can. J. Microbiol.* **45**, 97–105
43. Taylor, H.F.W.: *Cement Chemistry* (1997)
44. Vollpracht, A., Lothenbach, B., Snellings, R., Haufe, J.: The pore solution of blended cements: a review. *Mater. Struct.* **49**, 3341–3367 (2016)
45. Wells, T., Melchers, R., Joseph, A., Bond, P., Vitanage, D., Bustamante, H., De Grazia, J., Kuen, T., Nazimek, J., Evans, T.: A collaborative investigation of the microbial corrosion of concrete sewer pipe in Australia. In: *OzWater-12 Australia’s National Water Conference and Exhibition*, pp. 8–10, May, 2012
46. Wells, T., Melchers, R.E.: Modelling concrete deterioration in sewers using theory and field observations. *Cem. Concr. Res.* **77**, 82–96 (2015)
47. Zhang, L., de Schryver, P., de Gussem, B., de Muynck, W., Boon, N., Verstraete, W.: Chemical and biological technologies for hydrogen sulfide emission control in sewer systems: a review. *Water Res.* **42**, 1–12 (2008)

Corrosion Measurements

Testing of Sulfide Uptake Rate (SUR) and Its Applications



Xiaoyan Sun, Guangming Jiang, Jurg Keller, Philip Bond, and Xuan Li

Abstract This chapter introduces a methodology to measure the rate of gaseous H_2S transferring from sewer atmosphere to the exposed concrete surface. This facilitates the monitoring of sulfide-induced corrosion processes on concrete at various corrosion stages. In comparison to many existing methods, this methodology has the advantages of rapid measurement and non-destruction of the concrete sample. The H_2S uptake rate (SUR) for a concrete coupon can be determined by measuring the gaseous H_2S concentrations over time in a temperature- and humidity-controlled gas-tight reactor. The reliability of this method was evaluated by carrying out repeated tests on concrete coupons previously exposed to different corrosion conditions. The method could be applied to perform various research activities related to microbiologically influenced concrete corrosion, for instance, (1) understand sulfide uptake activity by concrete; (2) differentiate chemical and biological driven sulfide uptake activity; (3) evaluate the effectiveness of concrete control techniques; (4) estimate concrete corrosion rate in sewer systems; (5) investigate important factors affecting sulfide-induced concrete corrosion, particularly temperature, fluctuating gaseous H_2S concentrations, oxygen concentrations, surface pH and relative humidity (RH).

X. Sun

School of Civil Engineering, Sun Yat-sen University, Zhuhai 519082, China
e-mail: sunxy55@mail.sysu.edu.cn

G. Jiang (✉)

School of Civil, Mining, Environmental and Architectural Engineering, University of Wollongong, Wollongong, NSW 2522, Australia
e-mail: gjiang@uow.edu.au

J. Keller · P. Bond

Australian Centre for Water and Environmental Biotechnology, The University of Queensland, Brisbane, QLD 4072, Australia
e-mail: j.keller@uq.edu.au

X. Li

School of Civil and Environmental Engineering, Centre for Technology in Water and Wastewater, University of Technology Sydney, Ultimo, NSW 2007, Australia
e-mail: xuan.li@uts.edu.au

1 Method Development

1.1 *Characteristics of Key Corrosion Indicators*

The sulfide induced concrete corrosion process leads to pH reduction of the concrete surface, formation of loosely bound corrosion products with little mechanical strength, and thus the loss of concrete mass and eventually the structural failure of the concrete pipes. Various approaches have been used to monitor and analyze the corrosion processes in sewers. They include determining the concrete surface pH, monitoring the mass loss, analyzing corrosion products, and characterizing microbes within the corrosion layer. The availability and usefulness of these methods can be limited.

In terms of pH measurement, it could be difficult to monitor corrosion progress through pH measurement in corroded concrete as surface pH may remain constant at pH 3–4 due to the partial neutralization of the acid production by alkalinity released from the corroding concrete and the wastewater spray onto concrete surface. Consequently, surface pH is only indirectly related to the corrosion process and not a good indicator of corrosion rate. Measuring the mass loss of concrete may take years of monitoring activity during which in situ conditions driving the corrosion rate likely change. The composition of corrosion products is complicate, and the quantification is costly and time consuming. Microbial analysis is arduous, time consuming and costly and currently even quantitative microbial population analysis has not been successfully correlated with the corrosion rates. In addition, the understanding of microbial communities related to corrosion processes is still limited. Recently employed advanced sequencing techniques revealed unexpected microbial groups to be abundant in some situations. Finally, most microbiological investigations are restricted to severely corroded concrete and consequently the early-stage microbial populations are not well studied.

1.2 *Detailed Procedures of SUR Measurement*

It is important to develop quick and non-invasive methods to readily measure the corrosion rate of concrete at various corrosion stages. A reactor to measure the H₂S uptake rate (SUR) on sewer concrete blocks and assess the corresponding corrosion activities was designed. With temperature and humidity controlled, gaseous H₂S can be intermittently injected into the reactor to various levels and the corresponding SUR of the concrete surfaces determined. The method utilizes the fact that the overall corrosion process is largely driven by the sulfide adsorption and oxidation to sulfuric acid.



Fig. 1 Top front view of the mounting coupons in a stainless-steel casing. Reproduced from Sun et al. [24] with permission from Elsevier

(1) Introduction of the H_2S uptake reactor

Concrete coupons were arranged in pairs and embedded in a stainless-steel casing using epoxy (Fig. 1). The upper rim of the stainless-steel casing provided a reference point to determine the reduction in coupon thickness due to corrosion.

The reactor for the H_2S uptake tests was constructed from glass to minimize reaction/absorbance with H_2S (Fig. 2a). The reactor was designed to neatly fit around the coupon pairs and stainless-steel casings used in the corrosion chamber experiments. The stainless-steel casing had no contact with the gas in the reactor. The volume of reactor was designed to be as small as possible to facilitate fast rates of H_2S uptake (i.e., higher detection limit) in the experiments. The two coupons, e.g., a pre-corroded and a fresh concrete coupon, were exposed in two separate compartments through the top rectangular opening. In each compartment, one H_2S sensor was mounted on the side wall to monitor the gas phase H_2S concentrations (Fig. 2a). One humidity sensor was mounted to detect the relative humidity (RH) in the gas phase (Fig. 2a). Each compartment had an internal electric fan to maintain homogenous gas phase conditions.

The coupon pairs were clamped to the top of the uptake reactor, so the exposed coupon surfaces were sealed within the reactor. The interfaces between the two compartments and between the coupon edges and reactor surfaces were packed with foam to provide gas-tight seals between the casing and the reactor, as well as between the two compartments each with one coupon exposed to the gas phase conditions. Polypropylene slabs placed on top of the coupon and at the bottom of the reactor were bolted together to form a tight seal for the whole assemblage. Gas tightness was confirmed by immersing the complete assembly in water and checking for any gas bubbles emerging under slight pressure. Gaseous H_2S was generated in situ with

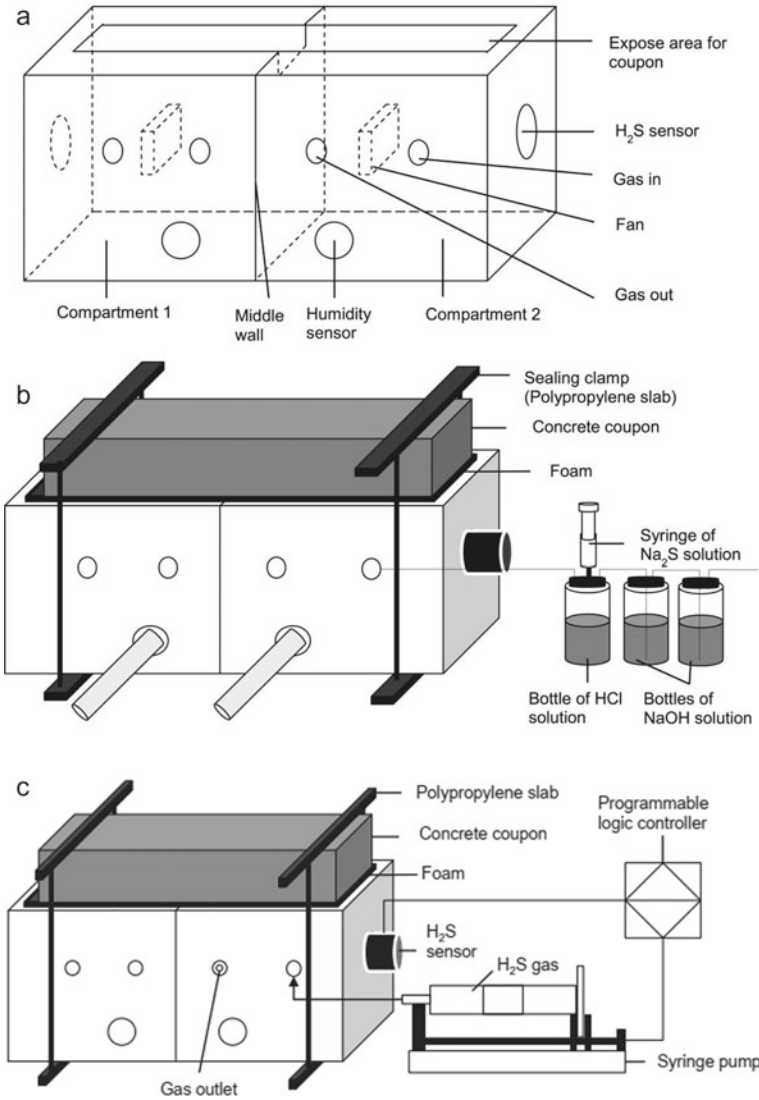


Fig. 2 An outline of the glass reactor (a) for gaseous H₂S uptake measurements. The reactor dimensions are 290 mm length × 110 mm width × 100 mm height. The experimental setup for the manual measurement of SUR is outlined in (b), through which a concrete coupon pair was clamped to the reactor and controlled levels of H₂S gas can be introduced to the reactor through injecting known amounts of Na₂S to the bottle of HCl solution and connecting the gas phase from this bottle to the reactor to enable the transfer of the generated H₂S gas into the reactor. The experimental setup for the automatic measurement of SUR is outlined in (c), where gaseous H₂S can be injected into the reactor through a syringe pump regulated by a programmable logic controller. Reproduced from Sun et al. [24] with permission from Elsevier

a system composed of a syringe filled with sodium sulfide solution (Na_2S , 0.3 M), a bottle containing hydrochloric acid (HCl , 6 M) and two bottles connected in series containing sodium hydroxide solution (NaOH , 1 M). To achieve a given level of H_2S in the reactor, Na_2S solution was gradually injected into the acid bottle and the generated H_2S gas transferred into the reactor compartment (Fig. 2b). After reaching the specified H_2S concentration, the reactor was isolated from the H_2S generation bottles. Due to the toxicity of the residual H_2S in the acid bottle, the acid bottle was connected to the two bottles with sodium hydroxide solution to avoid leakage of H_2S to the atmosphere. The seal between the compartments was tested through injection of H_2S to the separate compartments sequentially.

Alternatively, to repeatedly measure the SUR at a specific H_2S concentration, the addition of gaseous H_2S into the reactor can be performed by a syringe pump regulated by a programmable Logic Controller (PLC) (Fig. 2c). The PLC was employed to monitor the H_2S concentration inside the reactor and to trigger the syringe pump to add further gaseous H_2S . This setup can be used to run a pre-determined sequence of low and high H_2S concentrations at a specified frequency. To avoid the build-up of pressure inside the reactor during the dosing of gaseous H_2S , a small gas outlet from the reactor was kept open through a needle (0.5 mm in diameter) inside a rubber stopper with a non-metallic lure lock connector on the inside of the reactor (to avoid the potential of metal (needle) catalyzed sulfide oxidation).

(2) Conducting a typical H_2S uptake test

After being exposed to a specific sewer environment, e.g. 50 ppm H_2S , 30 °C and 100% RH for 32–33 months, the concrete coupon pair can be retrieved to measure the SUR. Prior to mounting the coupon pair to the uptake reactor, 1 mL of deionized water was sprayed on the bottom of the reactor to obtain 100% RH in the sealed reactor. Internal leakage between the compartments was checked in every experiment for compartments 1 and 2. This was done by adding H_2S gas into one compartment at a starting level of 150 ppm and the reactor internal airtightness was indicated by maintaining a constant 0 ppm H_2S reading in the adjacent compartment. This test was repeated to confirm there was no leakage from both compartments.

Following this initial testing, it took 2–3 min to inject H_2S simultaneously into both compartments to the level specified by the uptake tests. After injection, H_2S concentration gradually decreased due to the combined effects of sulfide sorption and chemical and biological oxidation. Further injections could be applied to reach various levels of H_2S in each compartment.

After several batches of H_2S injection, the background uptake rates of H_2S were determined by removing the coupon pair, resealing the reactor with a piece of foam panel and a stainless-steel sheet and repeating the H_2S injection and monitoring process. This background uptake rate of the whole reactor (but without the coupons) was then subtracted from the measured H_2S uptake rate with the coupons in place to get a net uptake rate for the concrete coupons. H_2S uptake rate was determined by calculating the slope of the measured H_2S concentration versus time:

$$r = -\frac{d[\text{H}_2\text{S}]}{dt} \quad (1)$$

where $[\text{H}_2\text{S}]$ is H_2S gas phase concentration (ppm), t is time (h). Then, the rate was converted into a surface specific H_2S uptake rate using Eq. (2).

$$r_{\text{H}_2\text{S}} = -\frac{d[\text{H}_2\text{S}]}{dt} \times 101.325 \times \frac{32 \text{ g/mol}}{RT} \times \frac{V}{S} \quad (2)$$

where $r_{\text{H}_2\text{S}}$ is the surface-specific H_2S uptake rate ($\text{mg-S m}^{-2} \text{ h}^{-1}$), R is the universal gas constant ($\text{J K}^{-1} \text{ mol}^{-1}$), T is the absolute temperature (K), V is the total gas volume in the reactor (m^3), S is the concrete surface exposed to the reactor atmosphere (m^2).

(3) Background H_2S uptake rate of the reactor

The background SUR of the reactor is likely due to adsorption and/or oxidation of H_2S in the moist air and on the reactor materials (walls, sensors, etc.) in the absence of a coupon, and was required for the correct interpretation of the H_2S uptake data of the concrete coupons. Background rates were determined in the presence of either dry air (about 75% RH), air with 100% RH or when air was replaced with nitrogen gas to exclude oxidation reactions (about 30% RH). These background SUR were much lower than what was typically observed in the presence of coupons. Thus, the sulfide uptake rate by the reactor without coupon but in the presence of air and 100% RH, which is the same humidity level as with the coupons, was used as the background uptake rate. This background SUR was measured in each experimental run and was subtracted from the measured profiles to determine the net SUR for the coupons alone.

1.3 Reliability of the SUR Test

Concrete coupons, previously prepared from fresh and pre-corroded concrete, were actively corroding after incubation in the corrosion chamber for 33 months in the presence of 50 ppm H_2S at 30 °C and 100% RH. Typical H_2S concentrations profiles and the corresponding uptake rates are illustrated in Fig. 4. Nine repeated injections of H_2S to the level of about 150 ppm were applied in one experimental run and then the background uptake due to moist air was measured after removing the coupon (Fig. 4a). The coupon SUR was highly reproducible over the nine repeat experiments providing good confidence in the experimental results (Fig. 4b).

To examine the reproducibility of the method, SUR were determined on the pre-corroded coupon after exposure to 50 ppm H_2S , 30 °C and 100% RH for 32 months and then again after a further 1 month exposure at the same conditions (Fig. 4c).

After 32 and 33 months of exposure, little difference was seen on the H₂S uptake rates of the same coupon. The results clearly indicate that the method can be applied to measure coupon uptake rates accurately and reproducibly.

2 Application in Corrosion Development Monitoring

2.1 Understanding Sulfide Uptake Activity by Concrete

(1) Fitting H₂S uptake data into various models

The SUR can be related to the concentration of gaseous H₂S, using various models. In a previous study, the H₂S uptake results were fit to Exponential, Monod and Power functions using the Sigma Plot Scientific Graphing System, version 12.0 and the value of various coefficients were determined (Table 1) [24]:

$$r_{\text{H}_2\text{S}} = \mu_{\text{max}}(1 - e^{-K[\text{H}_2\text{S}]}), \quad \text{Exponential function} \quad (3)$$

$$r_{\text{H}_2\text{S}} = \frac{\mu_{\text{max}}[\text{H}_2\text{S}]}{K_s + [\text{H}_2\text{S}]}, \quad \text{Monod function} \quad (4)$$

$$r_{\text{H}_2\text{S}} = K_r[\text{H}_2\text{S}]^n, \quad \text{Power function} \quad (5)$$

where μ_{max} is the maximum uptake rate (mg-S m⁻² h⁻¹), K is an empirical coefficient (ppm⁻¹), K_s is the half velocity constant (ppm), K_r is the rate constant (mg-S m⁻² h⁻¹ (ppm)⁻ⁿ) and n is the reaction order (-).

The fitting of H₂S uptake data in the exponential function had the highest value of R^2 and the lowest value of the sum of residual squares (Table 1). It suggests that the

Table 1 Kinetic parameters determined for various models

Coefficients	Exponential	Monod	Power
μ_{max} (mg-S m ⁻² h ⁻¹)	497	760	-
K (ppm ⁻¹)	0.0135	-	-
K_s (ppm)	-	108	-
K_r (mg-S m ⁻² h ⁻¹ ppm ⁻ⁿ)	-	-	14
N (-)	-	-	0.70
R^2 (-)	0.9960	0.9946	0.9888
Sum of residual squares (based on $r_{\text{H}_2\text{S}}$)	9933	13,250	54,741
$\sum_{i=1}^n (r_{i\text{-monitored}} - r_{i\text{-simulated}})^2 ((\text{mg-S m}^{-2} \text{ h}^{-1})^2)$			

Reproduced from Sun et al. [24] with permission from Elsevier

Exponential function predicted the data with the highest accuracy, though no apparent saturation of the uptake rates was observed even at 140 ppm of H_2S . The power law function also provided a good fit to the H_2S uptake data. It was evident that the H_2S uptake rate did not follow a zero (constant rate) or first order (linear) reaction rate in relation to the H_2S concentration but showed an intermediate reaction rate as is often observed for combined diffusion and reaction processes on surfaces (e.g. in solids combustion, biofilms etc.) [8]. The reaction order n was found to be 0.70, which is within the range (0.45–0.75) reported for oxidation of H_2S on corroding concrete surfaces [27]. It is also consistent with the expected diffusion/reaction profiles within the corrosion layer, whereby diffusion of one of the substrates (likely sulfide in this case) will be limiting the reaction in the inner part of the corrosion layer [20].

Similar uptake rate curves have been obtained through measurements of H_2S uptake of corroded concrete exposed to H_2S with levels ranging from 1000 to 0 ppm [27]. With the increase of H_2S levels, no tendency towards a constant maximal uptake rate (saturation) was observed even at 1000 ppm H_2S . Given the very high H_2S concentrations applied in these reported experiments, the microorganisms within the corrosion layer of the experimental pipe could differ considerably from real sewers [5, 4]. Hence, the biological sulfide oxidation kinetics could also vary.

(2) Differentiate chemical and biological driven sulfide uptake activity

With the intensification of concrete corrosion, the relative importance of chemical and biological driven corrosion activities vary. The relative importance of biological and chemical sulfide oxidation processes can be determined through measuring and comparing the SUR of the specific concrete coupon prior to and after deactivating/removing microbes in the corrosion layer. SUR can be used as a reliable detection indicator to help us conduct efficient analysis.

For example, previous studies showed SUR and the ratio of live/dead cells of corroded concrete decreased following the nitrite spray [15, 23]. An explanation for this is that the remaining low SUR after nitrite spray is resulting from physicochemical interactions on the concrete surface that may include the physical adsorption of sulfide, chemical oxidation of sulfide and reactions between sulfide and alkaline compounds in corrosion layer. In addition, the relationship between SUR and H_2S concentration follow orders of about 0.5 and 1.5 before and after nitrite spray [fitting the data into power function as shown in Eq. (5)], respectively. These observations support the idea that the reactions are mostly biological before the nitrite spray and are nonbiological following the spray.

Similarly, the SUR were determined before and after high pressure washing of the concrete coupons [25]. The SUR decreased immediately after high pressure washing probably due to the loss of sulfide oxidizing bacteria (SOB) and thus decrease of the microbial sulfide oxidizing activity. The remaining SUR after washing is likely driven by chemical sulfide oxidation and the residual microbial catalyzed sulfide oxidation.

There was larger decrease of SUR on the more severely corroded coupon, which was probably due to the higher degree of SOB activity on that corrosion layer prior to washing. This facilitates the detailed understanding of the key driving force of concrete corrosion activities.

In addition, the SUR of more significantly corroded concrete (usually with lower surface pH) is generally higher (Fig. 4) [24]. The results suggest that biological oxidation of H_2S is the main factor driving SUR on the severely corroded concrete samples. Therefore, the evolution of concrete corrosion activity could be determined by comparing the SUR of concrete at the same H_2S concentration.

2.2 Understanding Corrosion Activity Development

Concrete corrosion is a complex process. As a reliable evaluation index of concrete corrosion, SUR facilitates us to evaluate the effectiveness of concrete control techniques and estimate the concrete corrosion rate.

(1) Evaluating the effectiveness of concrete control techniques

SUR test has been applied to evaluate the performance of concrete corrosion control techniques. In general, the SUR of concrete at a specific concentration of gaseous H_2S prior to and after subjecting the concrete corrosion control technique can be measured intermittently. The corresponding SUR can be analyzed to understand the corrosion mitigation and re-establishment.

Example 1. SUR of Concrete Subject to Nitrite Spray

A previous study investigated the effectiveness of nitrite on concrete corrosion control in laboratory corrosion chamber environment [23]. As shown in Fig. 5, for the coupon with nitrite spray on day 0 (coupon No. 1), the SUR was intermittently measured over 4 months before the spray and over 12 months after the spray. For the other sprayed coupon (coupon No. 2), the SUR was intermittently measured over 10 months before spray and 6 months after spray. The SUR of the experimental coupons prior to application of the nitrite spray and the control coupons was relatively constant over the 4 months of measurement. Particularly, experimental coupon No. 1 (nitrite sprayed on Day 0) and the 3 control coupons had similar SUR prior to free nitrous acid (FNA) treatment. These SUR indicate the corrosion activity was relatively steady. The other experimental coupon, No. 2, had a higher SUR at $107 \pm 6 \text{ mg-S m}^{-2} \text{ h}^{-1}$, which is likely coinciding with a higher microbial activity on this coupon.

Following the application of nitrite on both coupons No. 1 and No. 2 there was a large decrease in the SUR of 84% and 92%, respectively. Likely the FNA had significantly suppressed/inhibited the microbial sulfide uptake activity in concrete corrosion layer. Importantly, no obvious recovery of SUR by the coupons was observed over nearly one year after the nitrite spray. In contrast, over the 16 months of analyses, the SUR of coupons without nitrite spray was relatively stable, mostly remaining

above $60 \text{ mg-S m}^{-2} \text{ h}^{-1}$. Given that the coupons with and without FNA treatment had similarly high SUR at the start of the experiment, the results implicate that a single application of FNA can effectively mitigate the H_2S uptake rate of these active concrete corrosion layers for a period of at least one year.

A further study investigated the effectiveness of nitrite on concrete corrosion control in real sewer pipe environment [15]. The SUR of control coupons reached around $200 \text{ mg-S m}^{-2} \text{ h}^{-1}$ at height H and M and around $300 \text{ mg-S m}^{-2} \text{ h}^{-1}$ at height L after 12 months (Fig. 6). These levels of SUR are similar to that of the coupons achieved in laboratory chambers and real sewers [14], suggesting that all the control coupons were at the active corrosion stage during the whole experimental period. Furthermore, the SUR observed at height L was about 100% higher than that of coupons at both heights H and M at the 12th month, and about 17% higher than coupons at both heights H and M at the 21st month. Similarly, for type B coupons, the SUR observed at height L was about 100% higher at the 12th month and 40% higher at the 21st month than that of coupons at both height M and H (Fig. 6). In comparison to control coupons, 6 months after the spray, around $34.0 \pm 1.3\%$ and $29.4 \pm 2.0\%$ reduction of SUR were observed on nitrite sprayed coupons of type A and type B, respectively (Fig. 4a, b), suggesting reduced sulfide oxidizing activities on the surface of coupons due to the sprayed nitrite. However, with the increase of exposure time, the SUR reduction ratio decreased to $8.5 \pm 4.0\%$ and $12.3 \pm 3.4\%$ for type A and type B, respectively at the 21st month. This lower SUR reduction confirms the recovery/re-development of corrosion on sprayed coupons with the exposure time.

Example 2. SUR of Nitrite-Admixed Concrete

A previous study demonstrated the increased resistance of nitrite-admixed concrete to microbially induced corrosion in in real sewer environment [14]. Specifically, the SUR of all the coupons increased gradually with the increase of exposure time for both control and nitrite coupons (Fig. 7). After 6–9 months, the SUR of all the coupons at 50 ppm of H_2S reached and gradually became stable at $200\text{--}400 \text{ mg-S m}^{-2} \text{ h}^{-1}$. This SUR level is similar to the levels achieved by coupons after 500-day exposure in a laboratory chamber under 25 ppm H_2S and suggests that the coupons have reached the active corrosion stage caused by the development of sulfide oxidizing microorganisms (SOM). In this study, the SUR of the admixed concrete was 30% lower in comparison to that of the control coupons. With the development of SOM, the higher SUR values at the later stage of all the coupons resulted in a higher actual difference in SUR between nitrite coupons and control coupons.

Example 3. SUR of Concrete Subject to Surface Washing

A study evaluated the potential of mitigating sulfide induced sewer concrete corrosion by surface washing. Washing interrupted the corrosion activity of concrete coupons by increasing the surface pH and decreasing the SUR (Fig. 8). The SUR recovered to the level prior to washing within 60–140 days. The slowest recovery rate was from the most severely corroded coupon.

(2) Estimate the corrosion rate

If it is assumed that the entire H_2S taken up from the gas phase is oxidized to sulfuric acid and contributes to the corrosion of concrete, then it is possible to compare the corrosion rates observed by water utilities and reported in literature with the corrosion rates calculated from the laboratory measured H_2S uptake rates. Based on these considerations it follows that the mass balance for H^+ consumption per square meter of concrete exposed to sewer atmosphere gives:

$$C \times 10^{-3} \frac{\text{m}}{\text{mm}} \times 1 \text{ m}^2 \times A = \frac{r_{\text{H}_2\text{S}} \times 2 \times \frac{24 \text{ h}}{\text{day}} \times \frac{365 \text{ day}}{\text{year}} \times 10^{-3} \frac{\text{g}}{\text{mg}}}{M_{\text{S}}} \times 1 \text{ m}^2 \quad (6)$$

where C is the annual loss of concrete (mm year^{-1}), A is the buffering capacity of concrete ($\text{mol-H}^+ (\text{m}^3 \text{ concrete})^{-1}$, here $2400 \text{ mol-H}^+ (\text{m}^3 \text{ concrete})^{-1}$ was used), M_{S} is the molar mass of sulfur (32 g mol^{-1}), and the factor '2' is the amount of H^+ generated per mole of H_2S uptaken.

The SUR measured can be converted to the corresponding corrosion rates according to Eq. (6). These rates are listed in Table 2 together with the actual corrosion rates observed at two different field sites and previously reported laboratory studies, as well as corrosion rates calculated from the reported SUR.

In a real sewer in Melbourne, Australia, the temperature ranged between 18 and 22 °C, the average gaseous H_2S levels was 8 ppm (ranged between 5 and 60 ppm) and the corrosion rate of pre-corroded coupons exposed therein was measured at 6–7 mm per year between 2009 and 2013 (personal communication, Melbourne Water). The corrosion rates observed in the Melbourne sewer were comparable but lower than those calculated from the SUR of the laboratory coupons (Table 2). However, at a sewer in Perth, Australia, where the average concentration of H_2S was approximately

Table 2 Comparison between corrosion rates of laboratory coupons, real sewers and values reported from literature [24]

Location	H_2S (ppm)	Corrosion rate (mm year^{-1})	References
Laboratory concrete coupon	8	8.9 ± 0.5	[24]
	10	11.2 ± 5.2	
	20	29.2 ± 5.9	
	80	76.0 ± 1.4	
	100	83.3 ± 2.1	
Melbourne sewer	8	6.0–7.0	[24]
Perth sewer	80	12.0	[28]
Laboratory concrete coupon	15–25	~ 14.0	[1]
Pilot scale sewer reactor in Denmark	10	4.1–41.1	[27]
	100	8.2–164.2	

Reproduced with permission from Elsevier

80 ppm [29], the SUR determined at the same H₂S levels in laboratory experiments correspond to acid generation that would cause a higher corrosion rate than that was actually observed. The calculated rates at 20 ppm H₂S are more than double the corrosion rates reported by Aesoy et al. [1]. In the above cases the over prediction of the corrosion rates indicates that not all of the H₂S taken up is immediately utilized in the corrosion process, i.e. some is converted to other forms of sulfur and/or is returned to the wastewater stream before it can react with the concrete. In the high H₂S situation in Perth, it is also likely that the humidity is not typically at 100% (estimated around 90% based on short-term measurements), which may significantly influence the actual SUR due to the limitation of the microbial activity under such 'dry' conditions. In a pilot scale sewer reactor, without temperature control, the SUR of concrete pipe segments exposed to H₂S with levels ranging from 1000 to 0 ppm were measured [27]. Using Eq. (6), the corresponding corrosion rates are estimated to be between a few mm per year to well over 100 mm per year (Table 2) in extreme cases.

In summary, the corrosion rate calculated from Eq. (6) provides the rate that the concrete coupon can maximally achieve under the optimal conditions. The actual corrosion rates may be limited at times by factors like low humidity or H₂S concentrations, the method provides a reasonable estimation of the likely expected corrosion rate at H₂S concentrations that are typical case for most sewers.

2.3 *Understanding Key Factors Affecting Sulfide Uptake*

The important factors affecting sulfide uptake include temperature, fluctuating gaseous H₂S concentrations, RH, oxygen concentration and surface pH.

(1) **Temperature**

When the concentration of H₂S in sewers reaches a certain level, the SUR will be accelerated with the increase of temperature. However, if the temperature exceeds a certain limit, some key microorganisms in the pipe may be inactivated, resulting in a decrease in the SUR. Many studies show that the SUR at 30 °C are slightly higher than at 25 °C for H₂S concentrations above 5 ppm (Table 3) [24]. For example, at the H₂S exposure level of 50 ppm, the SUR are 303 ± 13 and 58 ± 6 mg-S m⁻² h⁻¹, which are about 17% and 26% higher than those at 25 °C, for the pre-corroded and fresh coupons respectively.

The increase in SUR with temperature could be due to increasing rate of diffusion of H₂S in air or water [26] or increasing chemical and biological sulfide oxidation rates [17, 19]. Additionally, the SOB within the corrosion layer will have been adapted to a temperature if the concrete coupons experienced long term exposure conditions at the temperature. This may also contribute to the influence of temperature on SUR. The dependency of sulfide oxidation on temperature reported in previous studies varies considerably. For instance, an earlier study of sulfide oxidation in water found

Table 3 H₂S uptake rates of pre-corroded and fresh coupon at two temperature levels [24]

H ₂ S (ppm)	H ₂ S uptake rates (mg-S m ⁻² h ⁻¹)			
	25 °C		30 °C	
	Pre-corroded	Fresh	Pre-corroded	Fresh
5	14 ± 7	8 ± 1	13 ± 8	7 ± 2
10	53 ± 25	19 ± 1	67 ± 10	22 ± 1
20	128 ± 26	29 ± 1	155 ± 8	41 ± 1
50	259 ± 22	46 ± 3	303 ± 13	58 ± 6
75	321 ± 18	57 ± 4	372 ± 13	65 ± 8
100	362 ± 14	66 ± 5	413 ± 17	70 ± 11

Reproduced with permission from Elsevier

the increase of the rate constant (pseudo-first-order reaction) can be up to 160% with a temperature increase from 25 to 30 °C [17]. Another study of a wastewater biofilm showed an increase of about 15% in the sulfide oxidation rate with a temperature increase from 20 to 25 °C [18].

(2) Fluctuating gaseous H₂S concentrations

Large fluctuations of gaseous H₂S concentrations occur in sewers due to the diurnal profiles of sewage flow and retention times and the necessity of intermittent pumping of sewage from pressure pipes into gravity pipes. The fluctuating gaseous H₂S concentrations include deprivation and high load of H₂S. A few studies examined the behavior of H₂S uptake by concrete under various high load and deprivation of H₂S [21, 22].

Both short- and long-term high H₂S load events decrease the SUR of concrete coupons. The latter leads to a larger temporary reduction of SUR whereas they cause similar persistent inhibition effects (Fig. 9) [21]. In addition, sequential exposures to elevated H₂S levels create a cumulative effect on the SUR, which is more pronounced if there is a rapid initial increase rather than a gradual increase in H₂S. The sensitivity of SUR by the corrosion layer towards high H₂S loads is largely dependent on the historical H₂S exposure levels. For a specific, actively corroding concrete surface higher average H₂S concentrations create more corrosive conditions than lower levels. Due to the rapid decrease and slow recovery effect of H₂S spikes on the SUR, an estimation of the corrosion effect purely on the average H₂S concentrations may result in an overestimation of the total H₂S uptake and thus probably an overestimation of the concrete corrosion rates [21, 23].

In comparison to the baseline SUR, exposing the concrete coupon to 0 ppm of H₂S for 1 h consistently caused a temporary increase of the SUR (i.e. 3.2–12.5%) following re-supply of H₂S at baseline levels. With the continuous re-supply of H₂S, there was gradual and steady decrease of SUR to the level close to the baseline SUR. However, for the case after deprivation of H₂S for 12 h, the SUR was 5.1% lower than baseline SUR and gradually increased to a level similar to the baseline SUR

during the 20–30 min of continuous re-supply of H_2S . In addition, the simultaneous deprivation of H_2S and O_2 for 1 h had negligible impact on the SUR (Fig. 10). Further analysis suggests that the historically accumulated intermediates of sulfide oxidation could act as electron donors for SOB. The replenishment of the intermediates upon the re-supply of H_2S could play a key role in the increase of SUR after short-term deprivation of H_2S . However, the activity of SOB could be diminished after long-term deprivation of H_2S , although the sulfur intermediates still could be available. Estimating the sulfide uptake by concrete using the SUR of the average H_2S concentration could lead to overestimation of the sulfide uptake. There could be more significant overestimation for the case with longer deprivation of H_2S .

(3) Relative humidity

On concrete surface, the condensation water layer provides the essential medium for the chemical and biological sulfide oxidation reactions [16]. The RH in the sewer atmosphere has significant impact on the water condensation of concrete surface and hence the corrosion rate [12, 10, 13]. In addition, RH could affect the chemical oxidation of sulfide [24]. For example, the SUR were determined in the presence of air with 75% RH and 100% RH and nitrogen gas with 30% RH (Fig. 3a). The results show that the H_2S concentration decreased faster in air with higher RH. This suggests that physical adsorption of H_2S by the moisture and chemical oxidation of sulfide in the presence of air took place. However, the impact of RH on the SUR of concrete needs to be investigated through further study.

(4) Oxygen

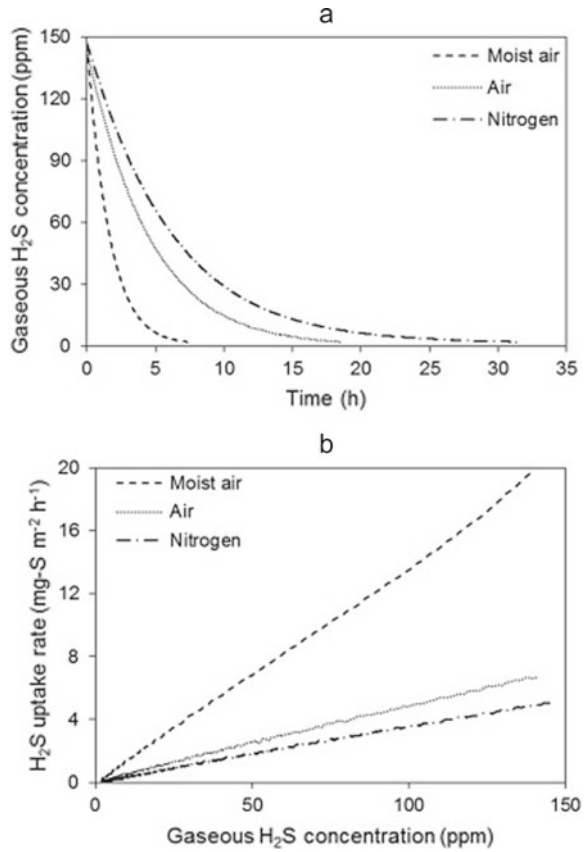
O_2 is an important electron acceptor for SOB during sulfide oxidation. Though other electron acceptors such as nitrate and ferrous can also be utilized by SOB, their concentration in the corrosion layer would be negligible and the relative abundance of the microbes (e.g. *Acidithiobacillus ferrooxidans*) using these alternative electron acceptors may be low [3, 11]. Previous studies confirmed that these oxidation processes have a key influence on the H_2S uptake kinetics by the corroding concrete coupon (Fig. 10) [22]. During the deprivation of gaseous H_2S and O_2 , there could be little oxidation of sulfur intermediates in the corrosion layer considering the limited electron acceptors available.

The dissolved oxygen concentration in the sewer network and along the depth of corrosion layer varies significantly [6, 20]. Previous studies showed dissolved oxygen concentration affect the chemical and biological oxidation of sulfide in sewer corrosion layers [9]. However, due to the difficulty of simulating different gaseous O_2 concentration in experimental setup, the knowledge related to the impact of gaseous oxygen on the H_2S uptake kinetics is still limited.

(5) Surface pH

pH has significant impact on the chemical sulfide oxidation kinetics. In acidic solutions, the chemical oxidation rate is slow at $\text{pH} < 6$, but increases greatly when the

Fig. 3 Temporal profiles of gaseous H₂S concentrations (a) and the corresponding H₂S uptake rates (b) measured in the reactor filled with (i) nitrogen at about 30% relative humidity, (ii) dry air at about 75% relative humidity, and (iii) moist air at 100% relative humidity. The surface area of the pre-corroded coupon was used in graph (b) to determine the surface-specific uptake rates. Reproduced from Sun et al. [24] with permission from Elsevier



pH increases through 7–11 [2, 7]. It is reported that the newly manufactured concrete sewers, that have high surface pH, are susceptible to the corrosion caused by chemical oxidation of sulfide at high H₂S concentrations (Li et al. 2019). In addition, pH affects the microbial community structure in corrosion layer and relative abundance of SOB, hence the biological oxidation of sulfide.

3 Summary

This chapter introduces the development, evaluation, and applications of a novel, non-destructive method to monitor the corrosion activity of concrete in sewer environment due to hydrogen sulfide. It is based on the measurement of the gaseous hydrogen sulfide concentration profile under specific conditions and then the calculation of the sulfide uptake rate. The sulfide uptake rate is theoretically proportional to the acid production and thus the corrosion rate of concrete. It has been applied for different

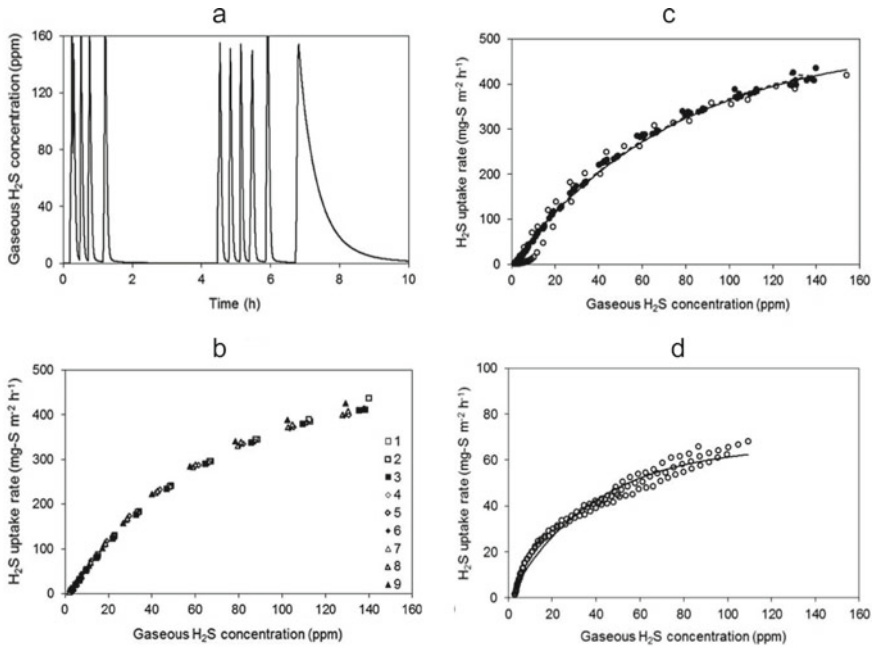


Fig. 4 The temporal profiles of H_2S concentrations at 25°C (a) and the corresponding surface-specific H_2S uptake rates (b) of a pre-corroded coupon after exposure for 33 months to 50 ppm H_2S at 30°C and 100% relative humidity. The last peak in a is the measurement of the background uptake rate without concrete coupons and the corresponding rate has been subtracted from the measured uptake rates with coupons to determine the net uptake rates shown in (b). The comparison between the measured (open/closed circles) and the exponential function fitted (solid/dashed lines) surface-specific H_2S uptake rates of this coupon after exposure for 32 months (open circles and solid line) and 33 months (close circles and dashed line) is shown in (c). The measured (open circles) and simulated (solid line) surface-specific H_2S uptake rates at 25°C for a fresh coupon after being exposed for 32 months to 50 ppm H_2S , at 30°C and 100% relative humidity is shown in (d). Reproduced from Sun et al. [24] with permission from Elsevier

purposes related to concrete corrosion, such as the use of chemical spray, surface washing and nitrite admixture to control the corrosion. It has also been demonstrated as an important research tool to understand the detailed sulfide uptake processes under realistic conditions with fluctuating hydrogen sulfide concentrations.

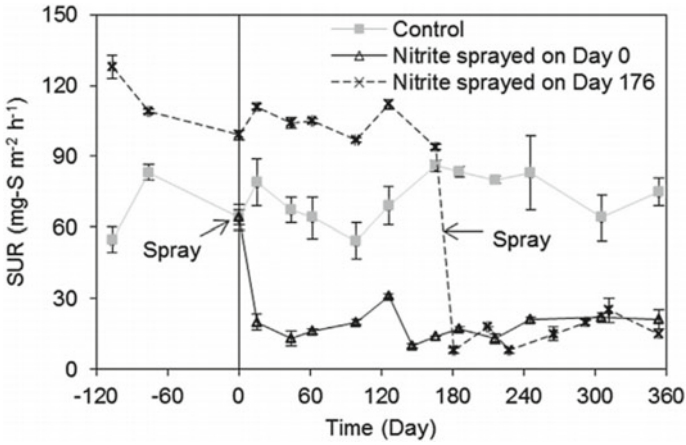


Fig. 5 The H₂S uptake rates of two experimental concrete coupons, coupon No. 1 with nitrite spray on day 0 and coupon No. 2 with nitrite spray on day 176, and three control coupons without nitrite spray. The SUR of Control shown in the figure prior to day 0 was averaged from the SUR of 3 control coupons and coupon No. 1. Reproduced from Sun et al. [23] with permission from Elsevier

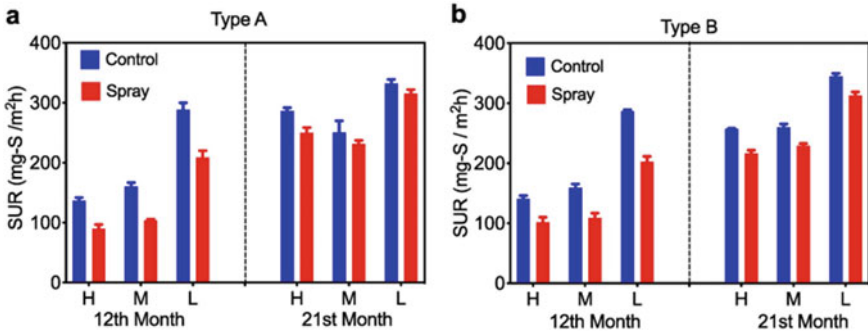


Fig. 6 Sulfide uptake rate (SUR) of nitrite sprayed coupons and control coupons at the 12th month (6 months after the spray) and the 21st month (15 months after the spray) for type A concrete (a) and type B concrete (b) [15]. Reproduced with permission from Elsevier

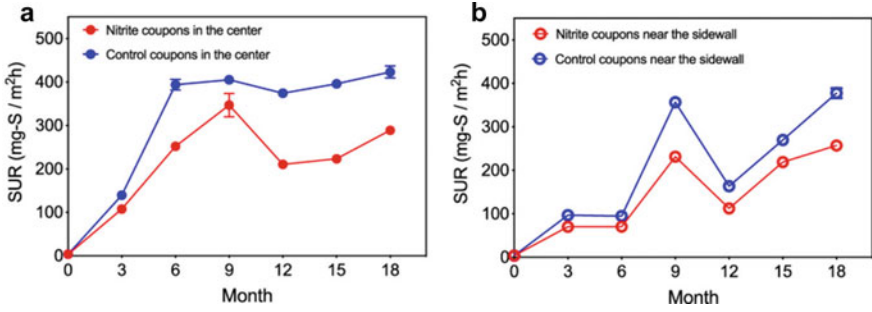


Fig. 7 Sulfide uptake rates of concrete coupons exposed (a) in the center of the manhole and (b) near the sidewall of the manhole [14]. Reproduced from with permission from Elsevier

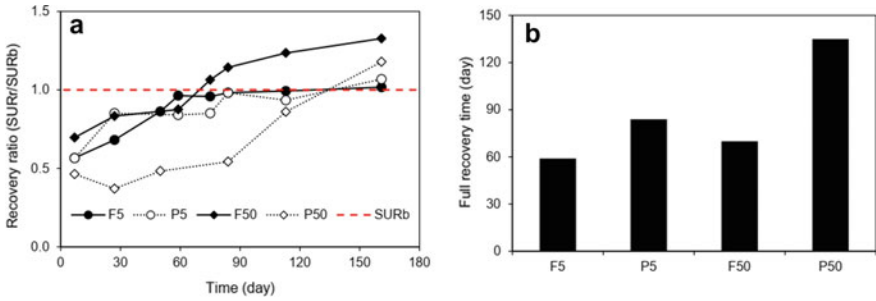


Fig. 8 Recovery ratio (SUR_b and SUR_r indicate the SUR of coupon prior to and after washing, respectively) of the coupon F5, P5, F50 and P50 (F and P indicate fresh and pre-corroded coupon, respectively, 5 and 50 indicate the H₂S concentration (ppm) in the exposure chamber) after the high pressure washing is shown in figure (a) and the full SUR recovery time of the four concrete coupons after washing is shown in figure (b). Reproduced from Sun et al. [25] with permission from Elsevier

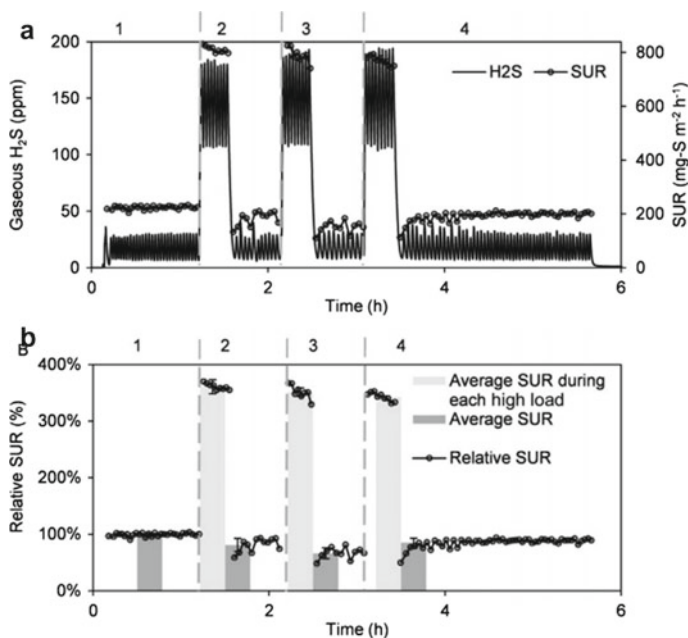


Fig. 9 The H₂S uptake profiles of the concrete coupon (exposure history: 15 ppm H₂S, 22–25 °C, 100% relative humidity for 54 months), the corresponding SUR at its baseline H₂S level (i.e. 15 ppm) and high H₂S levels (i.e. 130 ppm) are shown in figure (a) and the relative SUR and the average relative SUR at each stage is shown in figure (b). Different experimental stages (1–4) are listed above the plotted data in sub-plot (a) and (b) and the error bars in b represent standard deviations [21]. Reproduced with permission from Elsevier

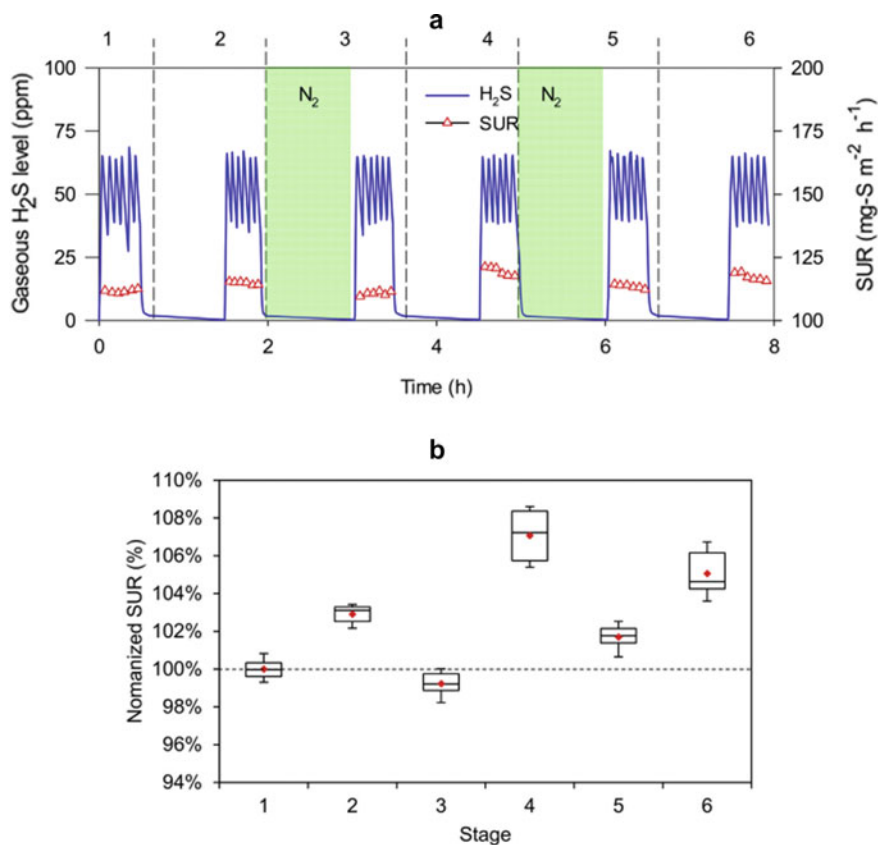


Fig. 10 **a** The H₂S uptake profiles (solid line) and the corresponding SUR (triangles) were shown of a coupon previously exposed to 50 ppm H₂S, 100% relative humidity and 22–25 °C for 28 months. The numbers above **a** represented the stages and the green areas labelled 'N₂' represented the periods of time with deprivation of O₂. **b** The boxplots of the normalized SUR values at each stage relative to the baseline SUR (dotted line) and the average of the normalized SUR at each stage (red diamond) were shown [21]. Reproduced with permission from Elsevier

References

1. Aesoy, A., Osterhus, S.W., Bentzen, G.: Controlled treatment with nitrate in sewers to prevent concrete corrosion. *Water Sci. Technol. Water Supply* **2**, 137–144 (2002)
2. Buisman, C., Uspeert, P., Janssen, A., Lettinga, G.: Kinetics of chemical and biological sulphide oxidation in aqueous solutions. *Water Res. (Oxford)* **24**, 667–671 (1990)
3. Cayford, B.I., Dennis, P.G., Keller, J., Tyson, G.W., Bond, P.L.: High-throughput amplicon sequencing reveals distinct communities within a corroding concrete sewer system. *Appl. Environ. Microbiol.* **78**, 7160–7162 (2012)
4. Cayford, B.I., Jiang, G., Keller, J., Tyson, G., Bond, P.L.: Comparison of microbial communities across sections of a corroding sewer pipe and the effects of wastewater flooding. *Biofouling* **33**, 780–792 (2017)

5. Cayford, B.I., Dennis, P.G., Tyson, G.W., Bond, P.L.: Microbial communities involved in the corrosion of concrete sewer infrastructure. In: 14th International Symposium on Microbial Ecology (ISME14) (2012)
6. Chen, G.-H., Leung, D.H.-W.: Utilization of oxygen in a sanitary gravity sewer. *Water Res.* **34**, 3813–3821 (2000)
7. Chen, K.Y., Morris, J.C.: Kinetics of oxidation of aqueous sulfide by oxygen. *Environ. Sci. Technol.* **6**, 529–537 (1972)
8. Harremoës, P.: The significance of pore diffusion to filter denitrification. *J. Water Pollut. Control Fed.* **42**, 377–388 (1976)
9. Jensen, H.S., Lens, P.N.L., Nielsen, J.L., Bester, K., Nielsen, A.H., Hvitved-Jacobsen, T., Vollertsen, J.: Growth kinetics of hydrogen sulfide oxidizing bacteria in corroded concrete from sewers. *J. Hazard. Mater.* **189**, 685–691 (2011)
10. Jiang, G., Sun, X., Keller, J., Bond, P.L.: Identification of controlling factors for the initiation of corrosion of fresh concrete sewers. *Water Res.* **80**, 30–40 (2015)
11. Jiang, G., Zhou, M., Chiu, T.H., Sun, X., Keller, J., Bond, P.L.: Wastewater-enhanced microbial corrosion of concrete sewers. *Environ. Sci. Technol.* **50**, 8084–8092 (2016)
12. Jiang, G., Bond, P., Keller, J.: Long term investigation of concrete corrosion processes in sewers. In: *Ozwater'13*, pp. 1–5 (2013)
13. Joseph, A.P., Keller, J., Bustamante, H., Bond, P.L.: Surface neutralization and H₂S oxidation at early stages of sewer corrosion: influence of temperature, relative humidity and H₂S concentration. *Water Res.* **46**, 4235–4245 (2012)
14. Li, X., Bond, P.L., O'Moore, L., Wilkie, S., Hanzic, L., Johnson, I., Mueller, K., Yuan, Z., Jiang, G.: Increased resistance of nitrite-admixed concrete to microbially induced corrosion in real sewers. *Environ. Sci. Technol.* **54**, 2323–2333 (2020)
15. Li, X., Johnson, I., Mueller, K., Wilkie, S., Hanzic, L., Bond, P.L., O'Moore, L., Yuan, Z., Jiang, G.: Corrosion mitigation by nitrite spray on corroded concrete in a real sewer system. *Sci. Total Environ.* **806**, 151328 (2022)
16. Li, X., O'Moore, L., Song, Y., Bond, P.L., Yuan, Z., Wilkie, S., Hanzic, L. and Jiang, G.: The rapid chemically induced corrosion of concrete sewers at high H₂S concentration. *Water Res.* **162**, 95–104 (2019)
17. Millero, F.J., Hubinger, S., Fernandez, M., Garnett, S.: Oxidation of H₂S in seawater as a function of temperature, pH, and ionic strength. *Environ. Sci. Technol.* **21**, 439–443 (1987)
18. Nielsen, A.H., Hvitved-Jacobsen, T., Vollertsen, J.: Kinetics and stoichiometry of sulfide oxidation by sewer biofilms. *Water Res.* **39**, 4119–4125 (2005)
19. Nielsen, A.H., Vollertsen, J., Jacobsen, T.H.: Chemical sulfide oxidation of wastewater—effects of pH and temperature. *Water Sci. Technol.* **50**, 185–192 (2004)
20. Satoh, H., Odagiri, M., Ito, T., Okabe, S.: Microbial community structures and in situ sulfate-reducing and sulfur-oxidizing activities in biofilms developed on mortar specimens in a corroded sewer system. *Water Res.* **43**, 4729–4739 (2009)
21. Sun, X., Jiang, G., Bond, P.L., Keller, J.: Impact of fluctuations in gaseous H₂S concentrations on sulfide uptake by sewer concrete: the effect of high H₂S loads. *Water Res.* **81**, 84–91 (2015)
22. Sun, X., Jiang, G., Bond, P.L., Keller, J.: Periodic deprivation of gaseous hydrogen sulfide affects the activity of the concrete corrosion layer in sewers. *Water Res.* **157**, 463–471 (2019)
23. Sun, X., Jiang, G., Bond, P.L., Keller, J., Yuan, Z.: A novel and simple treatment for control of sulfide induced sewer concrete corrosion using free nitrous acid. *Water Res.* **70**, 179–187 (2015)
24. Sun, X., Jiang, G., Bond, P.L., Wells, T., Keller, J.: A rapid, non-destructive methodology to monitor activity of sulfide-induced corrosion of concrete based on H₂S uptake rate. *Water Res.* **59**, 229–238 (2014)
25. Sun, X., Jiang, G., Chiu, T.H., Zhou, M., Keller, J., Bond, P.L.: Effects of surface washing on the mitigation of concrete corrosion under sewer conditions. *Cem. Concr. Compos.* **68**, 88–95 (2016)
26. Tamimi, A., Rinker, E.B., Sandall, O.C.: Diffusion coefficients for hydrogen sulfide, carbon dioxide, and nitrous oxide in water over the temperature range 293–368 K. *J. Chem. Eng. Data* **39**, 330–332 (1994)

27. Vollertsen, J., Nielsen, A.H., Jensen, H.S., Wium-Andersen, T., Hvitved-Jacobsen, T.: Corrosion of concrete sewers—the kinetics of hydrogen sulfide oxidation. *Sci. Total Environ.* **394**, 162–170 (2008)
28. Wells, T., Melchers, R.: An observation-based model for corrosion of concrete sewers under aggressive conditions. *Cem. Concr. Res.* **61**, 1–10 (2014)
29. Wells, P.T., Melchers, R.: Findings of a 4 year study of concrete sewer pipe corrosion. In: *Corrosion and prevention*. Darwin, Northern Territory, Australia (2014)

Concrete Corrosion Characterization Using Advanced Microscopic and Spectroscopic Techniques



Florian Mittermayr, Gregor J. G. Gluth, Cyrill Grengg, Ulf Garbe,
and Guangming Jiang

Abstract The aim of this chapter is to give an overview of basic and advanced state-of-the-art microstructural and spectroscopic analytics to investigate inorganic material corrosion in the context of biochemically aggressive sewers. The chapter covers optical methods, electron beam, X-ray and neutron techniques (SEM, MLA, XRF, XRD, CT, Neutron radiography and tomography), and spectroscopic methods (MAS-NMR, FT-IR, and Raman). For each technique, a short section on the fundamental scientific background of the method precedes and examples of data output from the latter in respect to the corrosion of cementitious materials including reinforced concrete is presented.

F. Mittermayr (✉)

Institute of Technology and Testing of Building Materials, Graz University of Technology,
Inffeldgasse 24, 8010 Graz, Austria

e-mail: f.mittermayr@tugraz.at

G. J. G. Gluth

Division 7.4 Technology of Construction Materials, Bundesanstalt für Materialforschung und
-prüfung (BAM), Unter den Eichen 87, 12205 Berlin, Germany

e-mail: gregor.gluth@bam.de

C. Grengg

Institute of Applied Geosciences, Graz University of Technology, Rechbauerstraße 12, 8010 Graz,
Austria

e-mail: cyrill.grengg@tugraz.at

U. Garbe

Australia's Nuclear Science and Technology Organisation, The Australian Centre for Neutron
Scattering (ACNS), New Illawarra Rd, Lucas Heights, NSW 2234, Australia

e-mail: ulg@ansto.gov.au

G. Jiang

School of Civil, Mining, Environmental and Architectural Engineering, University of
Wollongong, Wollongong, NSW 2522, Australia

e-mail: gjiang@uow.edu.au

1 Optical Methods

1.1 *Optical Evaluation and Light Microscopy*

When investigating corrosion on cementitious materials, a first evaluation is commonly performed with the naked eye. An optical comparison of (i) the same samples before and after specific time intervals of corrosion and/or (ii) different materials (e.g., CEMI, CEMIII and CAC based mortars as shown in Fig. 1. For further details, the reader is referred to Chapter “[Corrosion Resistance of Calcium Aluminate Cements in Sewer Environments](#)”).

Basically, all studies dealing with microbiologically influenced concrete corrosion (MICC) included optical evaluation. Authors are describing changes in colors, surface properties and the structural nature. Thereby appearances of dissolution features, lost material or total disintegration as well as swelling and neoformation of e.g. crystalline phases or biofilms are described [31, 38, 39, 41, 42, 61, 67]. Many of these studies further applied optical light microscopy to study the observed optical corrosion features in more details and combined it with other more sophisticated methods such as epifluorescence analyses.

1.2 *Surface pH Measurement and Imaging*

MICC is a multistep process that is accompanied by a strong decrease of surface pH of the cementitious materials caused by sulfur oxidizing bacteria. Pore solutions of OPC based concretes typically have a pH of around 13.5 [95]. Meanwhile, for the initial stages of MICC, the pH of the surface (and near surface area) is of importance. Due to natural carbonation after production, concrete surfaces commonly have a lower pH in the range of 11–13 before going into service in sewers. Although the surface pH, being of central importance for the controlling and understanding MICC, it is not straightforward to measure. The pH describes the concentration of H^+ ions in aqueous solutions. Consequently, a direct pH measurement of a dry concrete surface is not possible. Besides the decrease of pH with the depth away from the surface into the cementitious materials is of high significance for analyzing the progress of MICC.

Typical approaches for pH measurements for cementitious materials comprise (i) flat surface electrodes, (ii) (sprayable) indicator solutions and (iii) expressing pore solutions [2, 6, 68]. For studies on MICC several studies have used these techniques. For instance Jiang et al. [41] have drilled profiles through corroded concrete samples, mixed the dust powder with pure water and measured the respective pH values using a generic pH probe (Fig. 2a). Using a flat surface electrode, Grengg et al. [31] have measured the pH on the outer surface of four different materials after being exposed to an aggressive sewer system (Fig. 2b).



Fig. 1 Comparison of CEMI, CEMIII and CAC samples before, after 1 and 4 years of exposure in a sewer system. Adapted from Herisson et al. [39] with permission from Elsevier

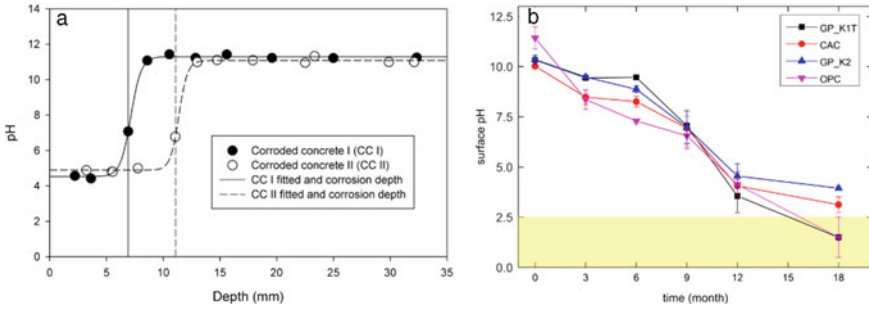


Fig. 2 a A pH depth profile of a concrete subjected to corrosion [41]. b Surface pH values measured on 4 different cementitious materials with flat surface electrodes on samples exposed to MICC [31]. Both diagrams reproduced with permission from Elsevier

The use of flat surface electrodes has some concerns in case of dry samples, a (small) amount of pure water is required which may causes dilution effects and interactions of deeper regions (with higher pH) in the material. This is potentially also altering the actual surface pH. Secondly, the relatively large spot size of the electrodes (roughly 10 mm) may cause unprecise results and thirdly, uneven and highly porous surfaces, that typically occur on heavily corroded concrete, cause further challenges as the flat top needs to have full contact. Accordingly, for measuring pH-profiles into degraded samples these techniques are sometimes limited as the spatial resolution is too low.

For studying the corrosion depth of cementitious materials, the indicator dye phenolphthalein (PHPHT) is often applied. While having the advantages of simple application, quick analytical results and cost-efficiency, the downside is that only information on areas above and below the inflection point of the indicator can be revealed (the pK_a value of PHPHT is at about pH 10). Khan et al. [46, 48, 49] studied different OPC-based, CAC-based and alkali-activated materials after exposure in real sewer environments and in the lab. They evaluated neutralization depths by spraying PHPHT on freshly split samples (Fig. 3).

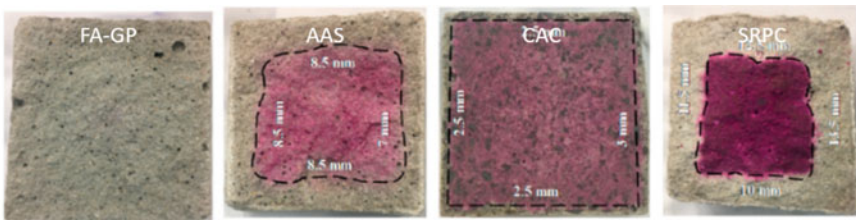


Fig. 3 Neutralization depth on mortars determined by phenolphthalein. From left to right the following mortar materials were investigated: fly ash geopolymer (FA-GP), alkali activated slag (AAS), calcium aluminate cement (CAC) and sulfate resistant ordinary Portland cement (SRPC) after 6 months of a MICC mimicking test. Image modified after [49] with permission from Elsevier

Table 1 Composition (major ions), electric conductivity and pH values from expressed interstitial solutions from heavily deteriorated concrete taken out of the manholes from two gravity sewers

Sample ID	pH	EC	Na ⁺	NH ₄ ⁺	K ⁺	Mg ²⁺	Ca ²⁺	Cl ⁻	NO ₃ ⁻	SO ₄ ²⁻	PO ₄ ³⁻
		mS/cm	mg/l	mg/l	mg/l	mg/l	mg/l	mg/l	mg/l	mg/l	mg/l
GS1-3-PF1	0.9	59.5	97.8	296	122	115	680	44.6	29.0	13,605	198
GS1-4-PF1	0.9	64.2	91	152	266	243	584	168	15.0	18,139	156
GS1-5-PF1	2.4	5.7	182	80.8	33.3	51.8	577	120	8.75	2719	0.89
GS1-5-PF2	3.1	4.6	167	62.7	55.2	61.9	638	112	11.7	2730	0.50
GS1-6-PF1	2.7	8.7	109	236	186	309	542	15.4	52.2	7127	3.74
GS1-6-PF2	1.6	20.4	103	315	163	206	621	15.9	45.1	9951	17.02
GS1-6-PF3	2.3	11.3	100	341	194	343	508	23.4	45.1	9436	15.08
GS1-6-PF4	1.6	18.3	75.4	370	111	126	494	20.8	28.5	7750	7.19
GS1-6-PF5	1.8	12.7	59.2	284	108	92.2	469	17.0	22.4	6092	7.06
GS2-1-PF1	1.0	102.0	2978	2994	1383	4322	551	1648	6.58	104,210	555
GS2-1-PF2	1.1	69.5	404	635	534	1521	575	316	1.99	44,090	345
GS2-1-PF3	0.7	101.0	573	210	330	990	567	376	5.35	40,818	161
GS2-1-PF4	0.9	66.4	523	198	346	931	520	380	3.85	32,717	141

Data modified after Grengg et al. [28]

Measurements of expressed pore- or interstitial solution avoid some of the above-mentioned problems as the pH values are being precisely measurable with either electrodes or by titration. As for MICC this methodology has a clear limitation during all stages of corrosion before the cementitious material is completely destroyed for the reason that it is a bulk measurement technique. Only larger sample amounts (typically several hundreds of grams) can be expressed to generate enough fluid for the pH analytics [12, 62]. Grengg et al. [28] have expressed interstitial solutions from completely altered concrete regions taken from a sewer network displaying extremely low pH values of 0.7–3.1 (Table 1).

To overcome most of the limitation from the before mentioned methods, new pH analytics based on optical sensor foils containing luminescent and pH sensitive dyes for quantification and imaging have recently been developed and also applied to studying MICC [12, 21, 22, 30, 64]. On the one hand, by using this technique in needle size sensors tips, lower amounts of pure water addition and much higher spatial resolution compared to flat top electrodes can be achieved. On the other hand, large sensor foils (up to 6 × 6 cm) have been successfully applied to determine pH mappings of cut corroded samples. Müller et al. [64] first used a large sensor foil to measure the pH on a cross-section of an ultra-high performance fiber reinforced concrete (UHPFRC) after being exposed for 12 months to a heavily corrosive sewer system. Grengg et al. [31] analyzed OPC-, CAC, and two different geopolymers using the same t-DLR technique to image the pH distribution on the respective cross sections after being exposed to an aggressive sewer environment for 18 months (see Fig. 4).

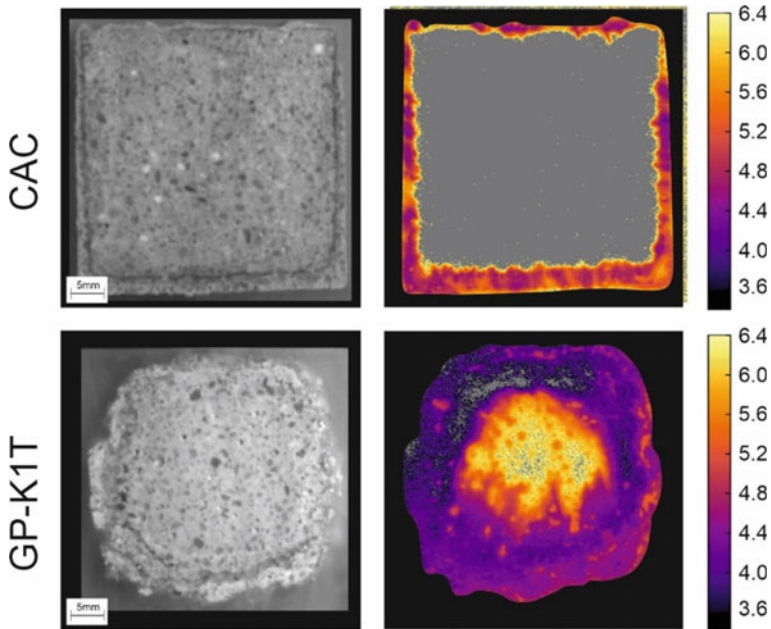


Fig. 4 pH images (right side) of calcium aluminate cement based (CAC)- and geopolymer mortar (GP-K1T) cross sections after being subjected to MICC for 18 months. Grey areas represent out of calibration i.e. $\text{pH} > 6.4$ or < 3.6 . Images on the left side photographs of the respective surfaces. Figure adapted from Grengg et al. [31] with permission from Elsevier

Although, in recent years advances have been made in measuring the pH during progressing MICC, further research will be required to establish a suitable set of techniques for this purpose.

2 Beam (Electron, X-Ray and Neutron) Techniques for Studying MICC

In the upcoming subchapters several “beam methods” for studying materials in the context of MICC are briefly introduced to the readers and some applications and results from studies are summarized. The first beam methods to be introduced are electron beam techniques such as scanning electron microscopy (SEM), environmental scanning electron microscopy (ESEM) and electron probe micro analyser (EPMA). Secondly, methods that interact with X-rays with the sample of interest are described. These comprise micro-X-ray fluorescence (μXRF), X-ray diffraction (XRD), micro X-ray diffraction (μXRD) and micro computed tomography (μCT). And finally, a subchapter on neutron analyses is presented.

2.1 Scanning Electron Microscopy

The three methods highlighted here are SEM, ESEM and EPMA. They all have very similar features as a high voltage focused electron beam (typically 1–30 kV for materials instigated for MICC) is scanning over the sample, interacting with its components and producing signals that can produce images of high magnification. Typical magnifications are between 40 and 100,000-fold. When the electrons from the beam interact with atoms in the sample elastic and inelastic scattering occurs and lead to secondary electrons (SE) and back-scattered electrons (BSE) generated at different depths of the sample. SE are used to generate highly detailed images of the samples surface while BSE images are commonly acquired from polished sample surfaces giving information about the elemental composition of the scanned region. SEM and EPMA are operated under high vacuum and require prior drying and a conductive sample surface. In contrast, ESEM can investigate moist samples at low vacuum conditions.

In addition to these two image-generating modes, several others exist with limited use for the investigation of MICC. Moreover, a third electron beam-sample interaction leads to the characteristic X-rays, which are emitted when electrons from the beam kick out inner shell electrons from the sample. They are important for MICC investigations. Characteristic X-rays signals can be recorded in either energy or wavelength dispersive X-ray spectrometers and aid in obtaining detailed information of the chemistry on the microscale level. This can on the one hand be used to acquire in situ analyses that have, depending on the beam condition, usually a spot size of $\sim 1 \mu\text{m}$. On the other hand, stringing together multiple spots in x and y-direction of the sample surface can be used to produce elemental mappings.

For further details on the physical background of the electron beam techniques the interested readers are referred to textbooks such as “Scanning Electron Microscopy and X-Ray Microanalysis” [27] and “Electron Microprobe Analysis and Scanning Electron Microscopy in Geology” [71]. For the specific use of electron beam techniques for cementitious materials including advices for sample preparation the readers are further referred to the textbook “A Practical Guide to Microstructural Analysis of Cementitious Materials” [77].

In the context of MICC many research studies have applied electron beam methods mainly to identify, describe and compare (i) organic neoformation (i.e. biofilms, bacteria, fungi, etc.) and (ii) inorganic (mineral) neoformation and dissolution features on actual material surfaces [13, 28, 43, 57, 63, 84–86] (see examples in Fig. 5). (iii) In addition, researchers also used electron beam methods to investigate material cross sections on (polished) cementitious samples to study (i) and (ii) with increasing sample depth to ultimately quantify the corrosion depth and speed, as well as gaining advanced understanding of the corrosion process mechanisms [13, 28, 29, 31, 32, 41, 46, 49, 55, 83, 85, 86] (see examples in Fig. 6).

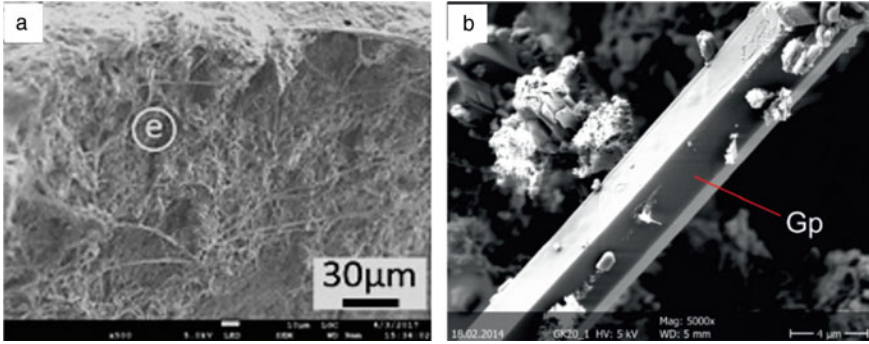


Fig. 5 Secondary electron images of a biofilm that had developed on an OPC paste after 133 days of exposure in the BAC test (a). Image modified from Buvignier et al. [13] with permission from Elsevier. **b** A newly formed gypsum crystal in a concrete damaged by MICC. Image modified from Grengg et al. [28] with permission from Elsevier

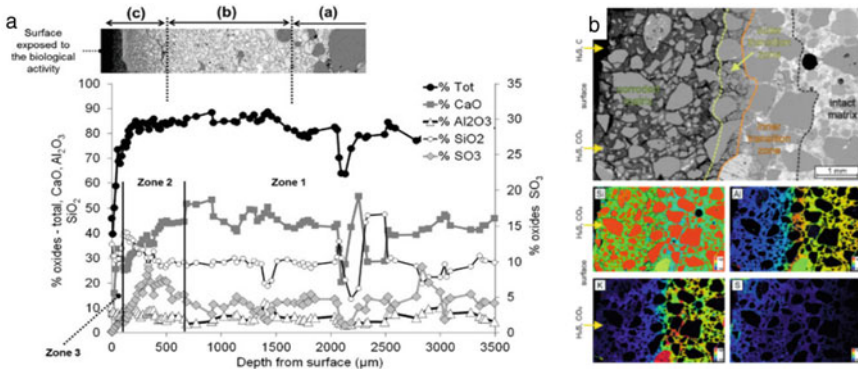


Fig. 6 BSE cross section and chemical composition profiles recorded by EPMA. The displayed sample is from a cementitious sewer pipe lining that was exposed to the BAC test (a). Image replicated from Lavigne et al. [55] with permission from Elsevier. **b** A BSE cross section image and elemental distribution images of Al, K, Si and S of the transition between the corroded and the intact areas of a low-Ca metakaolin-based AAM mortar after being exposed to a highly corrosive sewer environment for 18 months. The image was replicated from Grengg et al. [32] with permission from Elsevier

2.2 Image Analysis and Mineral Liberation Analysis of SEM/EPMA Data

The visualization and quantification of the proportions of different phases on the microstructural level is certainly of interest in geo and material sciences including the field of cement and concrete [77]. Mineral liberation analysis (MLA) can be used for such purposes. MLA provides the mass proportion or association of the target mineral either occurring as liberated (degree of liberation) or not liberated. It was

mostly and widely used in metallurgy for mineral processing which requires detailed characterization of the ore and plant feed during the design and operation [19]. MLA was also used on concrete and on associated corrosion products generated by MICC for their quantitative mineral compositions, as demonstrated in some recent corrosion studies of concrete and rebar in sewers, and granular sludge-based bioconcrete [41, 84–86].

Mineral liberation was conventionally done using optical microscopes, which was time-consuming and semi-quantitative for small samples. Recent development in electron microscopy, especially scanning electron microscopy (SEM), ever-increasing computing power, and the development of advanced image processing software allowed fast (within hours) and highly quantitative results. Automation of the analysis, including particle segregation, X-ray analysis and database searching, significantly reduced the time and increased the accuracy and texture resolution, which is $< 1 \mu\text{m}$. The modern Mineral Liberation Analyzer is an automated SEM-based mineralogical characterization tool that harness the power of backscattered electron (BSE) intensity and X-ray analysis to identify minerals present in particles on prepared and polished sections. The particles on the sections are usually identified by the BSE image and thus the boundaries of mineral phases are defined accordingly. For each of segmented mineral phases, an Energy-dispersive X-Ray spectrum (EDS or EDX) is then collected and used for offline processing to identify the mineral or phase based on its chemical composition. In instances where phases cannot be separated by grey levels of BSE images, X-ray mapping at an accelerating voltage of 25 kV can be used [19].

High resolution and quantitative data will be useful when investigating the distribution of corrosion products and the corrosion progression at the interfaces between intact materials (concrete, rebar) and corrosion layers (gypsum, ettringite, and other minerals). MLA were usually obtained from polished mounts or sections made from the various size samples produced by cutting, embedding, and grinding procedures [41]. As shown in Fig. 7, MLA can provide a suite of data to facilitate the interpretation of the corrosion development and processes based on the sample BSE image, a false-color classified particle map (mineral mapping) and a particle and grain-based dataset which can be used to determine modal mineralogy, elemental department, mineral grain size and association and mineral liberation.

The use of MLA on concrete sections with corrosion makes it possible to quantitatively determine the distribution of corrosion products at the corrosion front. In combination with the elemental distribution using EDS and vertical profile of concrete pH, it greatly supported the conceptual model of concrete corrosion [41, 84–86].

In another MICC study, the deterioration mechanism of alkali-activated materials in sulfuric acid were investigated [33]. Spot analyses, BSE images and quantified elemental mappings were recorded by EPMA wavelength dispersive X-ray spectroscopy. The data was further processed using the XMapTools software [54] in order to produce phase maps of the transition between the corroded outer zones and the uncorroded matrix (Fig. 8). However, the full power of image analysis such as MLA in investigating concrete corrosion is yet to be explored.

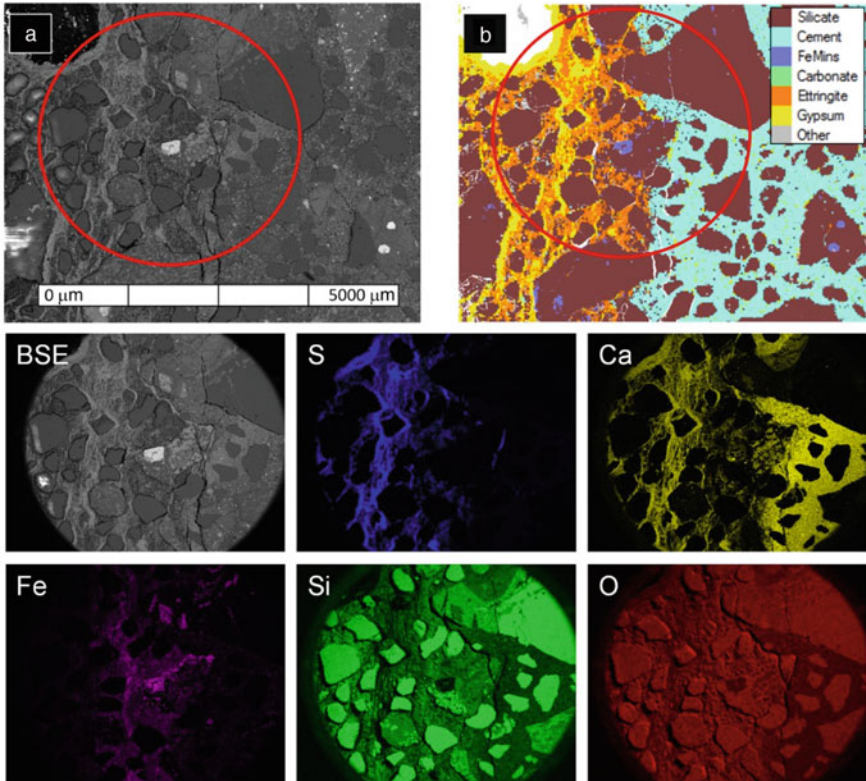


Fig. 7 BSE image (a) and MLA mineral mapping (b) Images in the second and third row shows BSE image and EDS element mapping of S, Ca, Fe, Si, and O respectively for the area marked with red circle in A and B. Reproduced from Jiang et al. [41] with permission from Elsevier

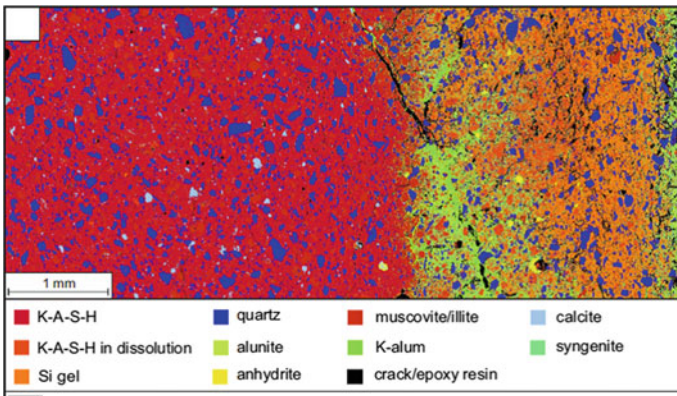


Fig. 8 Mineral phase distribution image, of an alkali activated material that was immersed in sulfuric acid at pH 2 for 5 weeks, produced with the XMapTools software. Image modified after [33]

Data recorded by X-ray analytical methods such as μ XRF and μ CT can also be used for quantification of different phases by image analyses [4]. These X-ray techniques will be briefly introduced in the following section.

2.3 (Micro)-XRF

Besides electron beam methods, investigations with X-rays are commonly used in material sciences. X-rays beams (radiation) for material characterization possess high-energies, very short wavelengths and are produced when electrons interact with metals from the anode (typically copper or cobalt). X-ray fluorescence (XRF) describes the effect when the sample of interest is excited with primary X-rays from the source and then emits secondary characteristic X-rays for detection. Thereby the bulk (XRF) and spatial resolved (μ XRF) chemical composition of materials can be analyzed. For further details on the physical backgrounds readers are referred to the textbook “Handbook of Practical X-Ray Fluorescence Analysis” [5]. Since knowledge on the chemical composition is of great interest when investigating concrete materials and specifically their corrosion, XRF is a widely used technique. For instance, studies have used XRF and μ XRF to investigate chloride diffusion into concrete [11, 50, 70]. Even though μ XRF being a promising technique to investigate the in situ chemical composition on relatively large samples (up to 50 cm) with low sample preparation effort required and fast data recording speeds, it has not been applied to samples from sewers where MICC had occurred. However, it has been used in MICC related studies. E.g. [90] exposed OPC based mortar, concrete and ready mix concrete in a sulfuric acid environment at pH 1 and analyzed the chemical composition with μ XRF on unpolished cross sections after 1, 3 and 6 months (see Fig. 9a, b).

2.4 (Micro)-X-Ray Diffraction

2.4.1 Background

X-ray diffraction (XRD) has been one of the fundamental techniques to characterize the mineralogical structure and phase composition of crystalline materials for decades. It is based on the principle of the Bragg’s equation [10] describing the reflection of a collimated X-ray beam on a crystal plane creating characteristic X-ray diffraction patterns, which can be assigned to specific mineral phases. The Bragg’s law describes this correlation based on the wavelength λ and the spacing of the crystal lattice planes d .

$$n\lambda = 2d \sin \theta \quad (1)$$

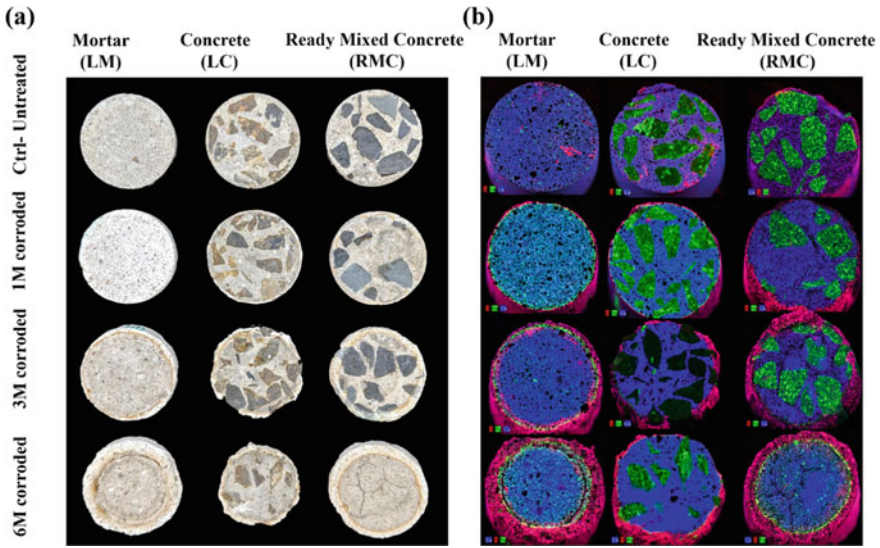


Fig. 9 **a** Images of cross-sections of the specimens after sulfuric acid immersion at pH 1; **b** μ -XRF elemental distribution maps of S, Ca, Fe (green color represents Fe, blue Ca and red S). Images reproduced from Taheri et al. [90] with permission from Elsevier

where, n represents the diffraction order and θ the angle of incidence of the X-ray beam. Conventional XRD analyses are conducted on powdered bulk samples, limiting the information on spatial phases changes. Micro-XRD (μ XRD) analyses are based on the same principles, however also enabling the measurement on a microscopic scale, in either small volumes of powdered samples or on solids with a high spatial resolution (small sample area). This is achieved by advanced polycapillary focusing optics concentrating the excitation beam to a diameter in the range of a few tens of microns [20]. In this context it has to be distinguished between traditional, lab-based equipment using a standard X-ray source and synchrotron μ XRD, which is frequently coupled with μ X-ray fluorescence analytics, and provides significantly higher resolution and lower detection limits due to the high energy source [72].

2.4.2 Characterization of Mineral Phase Changes Within Corroding Cementitious Materials Using MXRD

Only a few studies applied μ XRD analytics to characterize location-bound mineralogical changes in corroded cement-based construction materials. Serdar et al. [78] resolved the mineralogy and spatial distribution of nano-crystalline corrosion products forming at and in the concrete-steel interface during the chloride-induced corrosion of stainless steel in concrete. Synchrotron μ XRD analyses revealed goethite and akaganeite to be the main corrosion products forming, whereas goethite mainly

forms close to the surface of the steel due to the higher amounts of chloride present (Fig. 10).

Similar findings are reported by Grousset et al. [34] who conducted in situ analyses of mineral phase precipitation during chloride attack within steel reinforced hydraulic binders from historic monuments. They correlated the local precipitation of ferric oxyhydroxides, such as akageneite and goethite, via the transformation of a metastable chlorinated green rust, to the spatial distribution of iron accumulations with ongoing corrosion.

Finally, [29] characterized the mineralogical changes throughout a, up to, 4 cm thick corrosion layer of a strongly deteriorated concrete collected from a concrete manhole exhibiting intensive biochemically aggressive conditions. Therein, using μ XRD in combination with EPMA analyses, the dissolution behavior of the cementitious matrix and accompanying changes in the mineralogical phase assemblages was assessed. The transition between the intact matrix and the corrosion horizons was attributed to a strong decrease in cementitious phases such as portlandite, ettringite and calcite accompanied by the precipitation of aluminum- and iron (oxy-)hydroxides (gibbsite, goethite, lepidocrocite, parautlerite). Whereas gypsum and anhydrite were found as the main phases within the strongly corroded concrete layers.

Micro-XRD was also employed to differentiate the crystallized compositions of rust at selected spots of reinforced steel in concrete [83]. Point mineralogical analysis was carried out on the polished cross-sectional surface of the steel/concrete interface. Three typical regions, including the steel/rust interface, the intact rust area and the cracking or external rust layer, were identified. Rusts at the interface were primarily

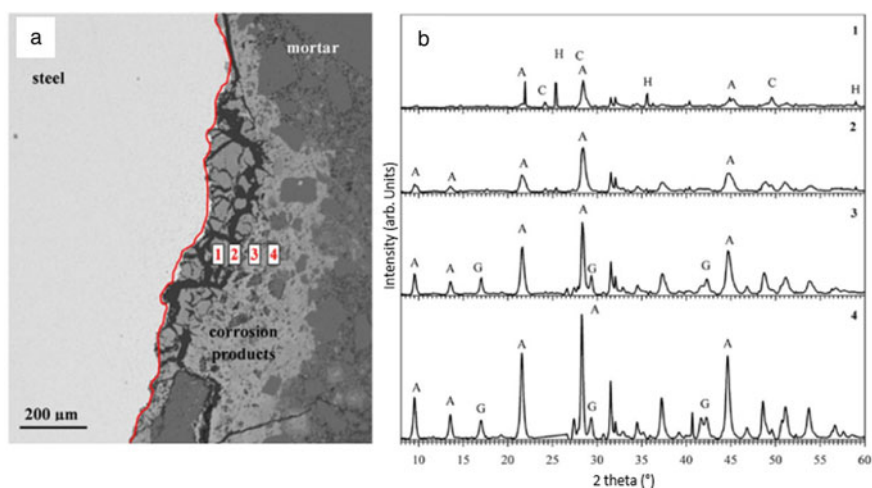


Fig. 10 a BSE image of the corroded steel–concrete interface. Numbers marked present the position of μ XRD diffraction patterns presented in (b), showing characteristic peaks of akageneite (A), goethite (G), chromite (C) and halite (H). Data adopted from Serdar et al. [78] with permission from Elsevier

composed of Fe, Fe₃O₄, FeCl₂ and its hydrated compounds. The intact rusts showed the formation of Fe₃O₄, α-FeOOH and γ-FeOOH.

Another study used Micro-XRD as an accurate method for the identification of localized compositions of tidal regions of concrete sewers [84]. Results showed that various forms of iron sulfides as major compositions of the rebar rusts. Additionally, iron oxides or hydroxides were scattered at the rust surface together with a small amount of iron sulfate and iron chlorides. In a study about the rebar corrosion products in concrete exposed to a pilot scale sewer pipe, micro-XRD results showed they were a mixture of iron oxyhydroxide (FeOOH), iron oxides (Fe₂O₃, Fe₃O₄), Fe_xS_y (FeS, Fe₃S₄, FeS₂), FeCl_x(H₂O)_z and Fe₂(SO₄)₃(H₂O)_z [85].

2.5 *Micro Computed Tomography*

In accordance with the two before mentioned methods, Micro Computed Tomography (μCT) also applies X-ray radiation. In contrast the X-rays are used to produce cross sections of materials potentially allowing to 3D reconstruct the sample or certain features therein (e.g., porosity). The source generates X-rays which penetrate the sample. There they might either be absorbed or attenuated depending on various factors such as sample density, atomic number, thickness and linear attenuation coefficient. The attenuated X-rays passing the sample are collected by detectors and produce a radiograph for a specific angular position. Fully rotating the sample and collecting multiple radiographs allows for a 3D reconstruction of the investigated region of interest [41]. In material sciences today, μCT is a well-established non-destructive method and requires little to no sample preparation. This is very advantageous when dealing with corroded materials and further allows to combine results recorded by other (destructive) methods as what have been mentioned before in this chapter.

Recently, μCT is increasingly used in studies related to building materials including concrete damaging mechanisms such as corrosion [3, 89, 98, 99]. In a related context, which is acid corrosion of cultural heritage building materials, Gibeaux et al. [26] have studied the corrosion of the natural Savonnières limestone (SV) and the reconstituted stone (Rs) where cement was used. The 3D reconstructions of the respective samples are shown in Fig. 11.

X-ray CT was used in MICC of concrete in sewers to show that the corrosion layer had a cloudier appearance than intact concrete, which implies it had a lower density due to the material expansion occurring in the corrosion layer [41]. Although μCT has not been widely used for studies on MICC, the methodology has great potential to further explore the corrosion mechanisms and depths of different cementitious materials in a non-destructive manner (Fig. 12).

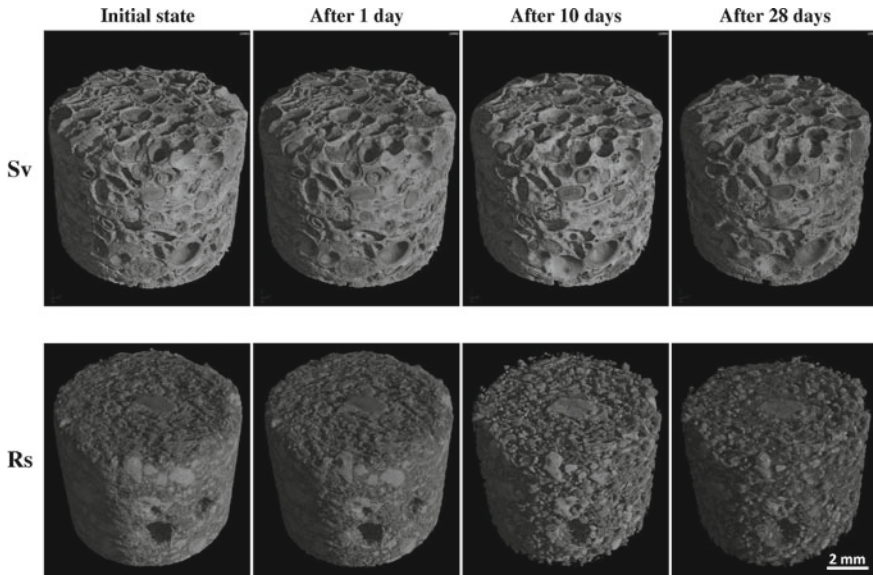


Fig. 11 3D reconstruction of samples before and after 1, 10 and 28 days of mixed acid solution treatment. Image reproduced from Gibeaux et al. [26] with permission from Elsevier

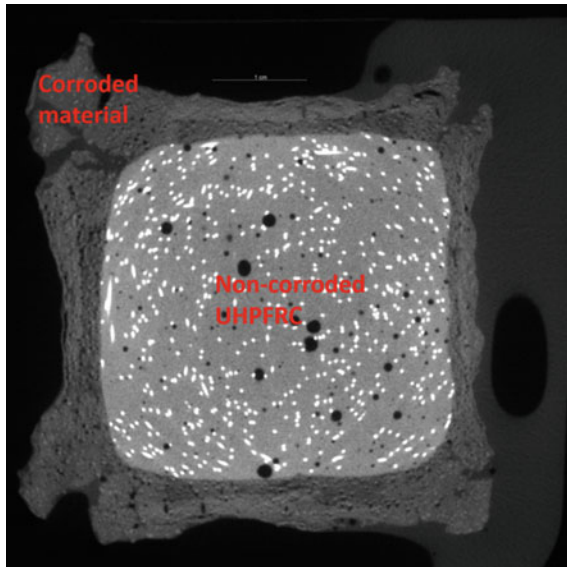


Fig. 12 Cross-section through an ultra-high-performance fibre reinforced concrete prisms after being outsourced for 2 years in a MICC environment

2.6 Neutron Imaging in Cement and Concrete Research

Neutron radiation is used world-wide in quality control of explosive devices for mining, defense and industrial applications, for example to assess oil and water flow in sedimentary rock reservoirs, assessing water damage in aircraft components to name a few examples. The user community varies from industrial or material research, non-destructive testing, geology, archaeology, and fundamental research. The facility can provide two-dimensional “shadow” images of objects (radiography) and three-dimensional neutron tomography. Neutron radiography and tomography stations at facilities world-wide like PSI, FRM 2, HZB and NIST have shown a high impact in industrial and commercial research. In Australia a new cutting-edge neutron imaging instrument DINGO [23] was built from 2011 to 2014 to facilitate the area of neutron imaging research and industry support. Research related to concrete and cement paste became a strong field of interest over several years of operation and has shown the advantages of neutron radiation [24]. A large range of applications is utilizing neutron radiation instead of X-rays, because of their strong penetration depth and different absorption compared to x-rays as shown in Fig. 13a, b.

Another major advantage of neutron radiation over X-rays and other imaging methods like MRI is its high sensitivity to hydrogen or water inside metals, ceramics, or concrete. Generally, light elements provide stronger contrast in neutron imaging than with X-rays, which helps to visualize water/moisture or organic material next to concrete or cement paste. Depending on the application neutron radiography or neutron tomography can be used to analyze concrete samples. Neutron radiography has been mainly used to monitor water intake or distribution in cement paste samples, as shown in Fig. 14.

The advantage of radiography is the possible fast time resolution. Only one image at the time is required and can lead to a time resolution of up to 10 images per second. The examples in Fig. 14 were taken with 15 s exposure time and a pixel size of 25 μm. The samples are cement paste cylinders standing in a water bath. Water diffusion into the cement paste is monitored over time. The high absorption of water compared

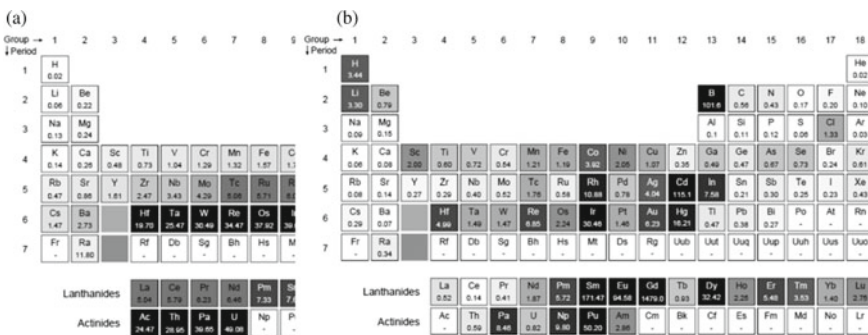
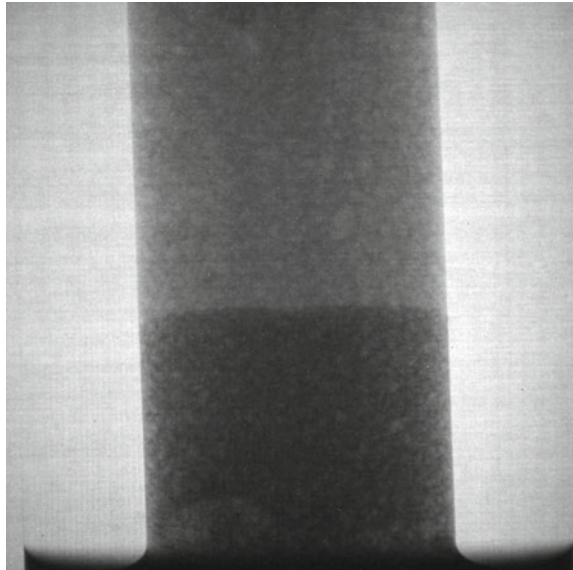


Fig. 13 a Attenuation coefficient for x-rays (left side). b Attenuation coefficient for thermal neutron (right side)

Fig. 14 Water intake of a cement paste detected by using neutron radiography



to cement darkens the cylinder. Fast measurements for kinetic experiments where concrete damage will be observed require larger pixel size up to $200\ \mu\text{m}$ to achieve 10 fps time resolution. Unfortunately, radiographs do not deliver any in depth 3D information.

Therefore a tomography scan is required, which can take 30 min, with large pixel size and low counting statistics, or 36 h and more in case of pixel sizes smaller than $10\ \mu\text{m}$ and good counting statistics. Applications like porosity analysis require high counting statistics to distinguish between pores and noise if detection limit of $2 \times 2 \times 2$ voxel should be reached. Figure 15 shows a test piece of a drill core. The tomographic 3D data was analyzed with the software package VGStudio (Volume Graphics) to detect porosity in the sample focusing on the region around the reinforcement steel. This is an area which can not be imaged with other methods like X-rays or synchrotron radiation. Due to the strong penetration depth into steel only for neutron radiation, pores close to steel are visible. The red area in Fig. 15 is in touch with the steel. The color coding is according to the size of the pore, from red for large pores to blue, small pores [24].

Further investigation on drill cores taken from the pacific highway near Port Macquarie in Australia have shown some large pores developing. During these measurements it turned out, that the maximum is around 50 mm in diameter which can be analysed with neutron radiation. Any larger diameter leads to reconstruction artifacts or cannot be reconstructed at all. In case with high moisture content the diameter must be much smaller, down to 20–30 mm, due to neutron absorbing of hydrogen. The length of the sample can be up to one meter on DINGO. Such long sample will be measured in section on 200 mm and stitched after reconstruction. A core sample with 50 mm diameter and 150 mm length is shown in Fig. 16.

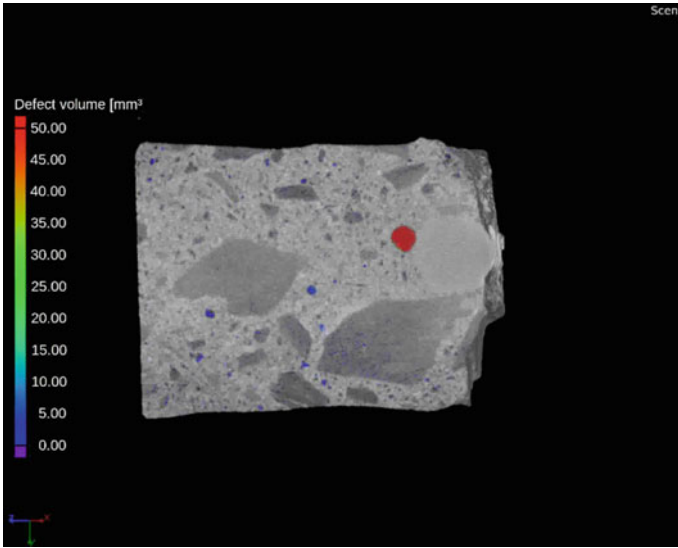


Fig. 15 Concrete drill core with reinforcement steel detected by using neutron tomography. From Garbe et al. [24] reproduced with permission from Elsevier

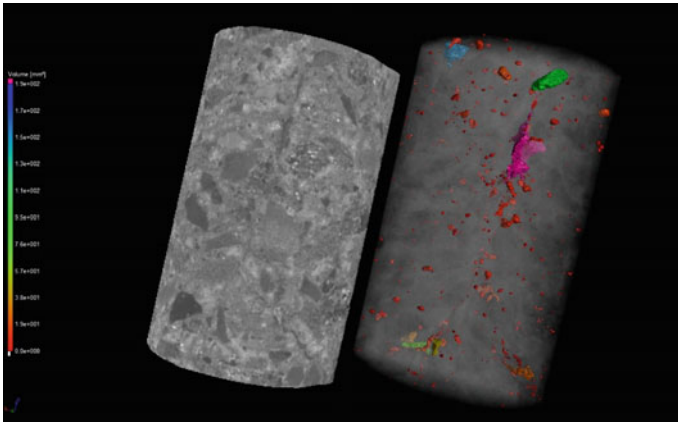


Fig. 16 Drill core from Pacific highway near Port Macquarie detected by using neutron tomography

The left part shows the full 3D representation of the sample after reconstruction. The right part is the same sample under different transparency setting in VGStudio. VGStudio and other rendering software packages allow to set the density or transparency of the 3D object to visualize the inner part and still showing the outer shape. This is a great tool to visualize the position of pores inside the sample. It makes it easy to show the relation of pore size with sample size, one of the very important characteristics of concrete.

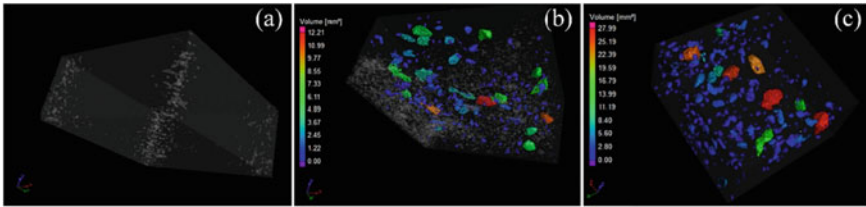


Fig. 17 The volume and distribution of granular sludge particles in control coupon-C0 (a), bio-concrete-B1 (b) and B2 (c). From Song et al. [86] reproduced with permission from Elsevier

The third example of neutron imaging in concrete and cement research targets the identification of organic material (granular sludge) as part of the mixture [86]. Bio-concrete plays an important role in corrosion resistant concrete, because of its self-healing ability. The local distribution of the granular sludge is important to its self-healing abilities. Neutron radiation is very sensitive to organic material because the incorporated hydrogen is a strong neutron absorber and creates a strong contrast (it darkens the image at its location). In the first study utilizing neutron imaging, the position and size distribution of granular sludge was measured. Figure 17 shows the control sample C0 without any granular sludge and the sample B1 and B2 with 1 and 2% granular sludge in the mix. The colour coding represents the large particles in red and the small one in blue.

The rendering technique of increased transparency of the 3D sample helps to show the position of the sludge relative to the sample dimension. The examples above are just a small selection of the work which has been done in concrete and cement paste research using neutron imaging to visualise moisture, porosity and organic material distribution. The specific nature of neutron radiation makes it possible to penetrate large samples non-destructively and be sensitive to organic material and moisture, because of the strong neutron absorption by hydrogen.

In an MICC related study [90] investigated uncorroded and sulfuric acid immersed concrete samples after 1, 3 and 6 months with 3D neutron tomography. Thereafter the samples were 3D reconstructed to decipher the corrosion mechanisms of different materials at the respective time of immersion.

3 Spectroscopic Methods

3.1 Nuclear Magnetic Resonance Spectroscopy

3.1.1 Background

In nuclear magnetic resonance (NMR) spectroscopy, a sample is exposed to a strong magnetic field and the responses of atomic nuclei in the sample to pulses of electromagnetic radiation are measured [17, 45, 60, 81]. To obtain NMR spectra of solids with a high resolution, it is required to spin the sample at a specific angle relative to the applied magnetic field ($\theta_m = 54.74^\circ$, the “magic angle”); the resulting technique is referred to as magic-angle spinning nuclear magnetic resonance (MAS NMR) spectroscopy, or high-resolution solid-state NMR spectroscopy.

For a nucleus to be amenable to NMR spectroscopy it needs to possess a nuclear spin, i.e., it must have an odd mass number, or even mass number and odd charge. This includes isotopes of essentially all elements that are relevant for cement chemistry, for example ^1H , ^{13}C , ^{17}O , ^{23}Na , ^{25}Mg , ^{27}Al , ^{29}Si , ^{31}P , ^{33}S , ^{39}K , and ^{43}Ca . Since the major phases of most cements are silicates, aluminosilicates and/or aluminates, ^{29}Si and ^{27}Al have been most often studied. The basic single-pulse MAS NMR experiment yields information about the fractions of sites with different chemical environments (coordination number, distortion of coordination polyhedron, nearest-neighbor elements, next-nearest-neighbor elements etc.). A prerequisite to obtain spectra that contain such quantitative information is that the experimental conditions are chosen appropriately [17, 45, 60, 81]. Several other, more sophisticated NMR experiments (e.g., cross-polarization MAS NMR, REDOR, TRAPDOR, REAPDOR, and multiple-quantum MAS NMR) have been devised that make it possible to obtain additional information about a compound or material [17, 60]. Except for cross-polarization (CP) MAS NMR, these advanced techniques have not yet been applied to study the degradation of cements subject to MICC or under related conditions, and thus will not be discussed here.

Compared to diffraction methods, NMR spectroscopy can provide more detailed information about amorphous and semi-crystalline phases, which is particularly helpful in the context of the degradation of cementitious materials, as will be discussed below. Compared to several other spectroscopic methods, a considerable advantage of NMR spectroscopy is that it is element-specific, i.e., the measured spectra contain only information about the response of the element under study, which can greatly simplify analysis of the spectra in some cases.

3.1.2 Data Presentation

NMR spectroscopy differs from other spectroscopic methods in that it is standard to present the spectra as plots of intensity versus chemical shift. The chemical shift, δ , is defined as

$$\delta = \frac{\nu - \nu_{\text{ref}}}{\nu_{\text{ref}}} \quad (2)$$

where ν is the frequency (in Hz) of the line in question, and ν_{ref} is the frequency (in Hz) of an agreed reference compound. Because of the small numerical values of δ , they are usually quoted in parts per million (ppm). The usual reference compound for ^1H and ^{29}Si is tetramethylsilane (Me_4Si or TMS) in solution, and for ^{27}Al it is $\text{Al}(\text{NO}_3)_3$ in solution [i.e., $\text{Al}(\text{H}_2\text{O})_6^{3+}$]; reference compounds for other nuclei, common secondary reference compounds, and the agreed reference sample conditions have been compiled [37, 60]. The graphical presentation of the spectra is such that δ increases to the left.

A distinction has to be made between the observed shift, δ or δ_{obs} , and the isotropic chemical shift, δ_{iso} . While the isotropic chemical shift is characteristic of the site under study (i.e., it is the “true” chemical shift), the observed chemical shift of that site (i.e., the position of the corresponding line maximum or center of gravity in a measured spectrum) can be displaced from δ_{iso} , the magnitude of the displacement depending on the experimental conditions. The isotropic chemical shift can be obtained from measurement of a series of spectra under systematically varied conditions and simulation of the line shape, or analysis of the spinning sidebands [17, 81]. However, this is not always feasible (nor necessary); thus, in many cases only the observed chemical shifts are reported.

3.1.3 Nomenclature and Basic Concepts Applicable to NMR Spectroscopy of Cements

For silicates, the established nomenclature system is the so-called “Q nomenclature” [58]. In this system, SiO_4 tetrahedra are denoted $\text{Q}^n(m\text{Al})$, where n is the number of oxygen bridges (Si–O–Si or Si–O–Al) to neighboring SiO_4 and AlO_4 tetrahedra, and $m \leq n$ denotes the number of AlO_4 of these tetrahedra; for $m = 0$, the expression in parentheses is omitted. For example, $\text{Q}^3(1\text{Al})$ denotes SiO_4 tetrahedra connected to two SiO_4 tetrahedra and one AlO_4 tetrahedron via oxygen bridges. The chemical shift ranges of SiO_4 tetrahedra in solids, including unhydrated and hydrated cements, are summarized in Table 2. In addition, chemical shift values have been compiled for many minerals [60] and cement phases [81, 97]. It can be noted from Table 2 that, in general, there is a systematic downfield shift by approx. 5 ppm for each additional AlO_4 tetrahedron bonded to a SiO_4 site. Much of the overlap of the Q^n sites with no AlO_4 is due to the presence of differing amounts of AlO_6 in different compounds; for Al-free silicates, the chemical shift ranges the Q^n sites are considerably narrower [51]. It should further be noted that there is almost complete overlap between the chemical shifts of Q^n sites, $\text{Q}^4(m\text{Al})$ sites, and $\text{Q}^3(m\text{Al})$ sites; this means that an assignment of a resonance to one of these sites always requires knowledge (or an assumption) about the presence of AlO_4 sites in the material under study.

For Al units in aluminosilicates and aluminates, often only the coordination number of the Al is indicated (Al^{IV} or AlO_4 , Al^{V} or AlO_5 , and Al^{VI} or AlO_6 , for

Table 2 Typical chemical shift ranges of Q^n , $Q^4(mAl)$, and $Q^3(mAl)$ sites in silicates and aluminosilicates

Site	Chemical shift range (vs. TMS) (ppm)
Q^0	– 60 to – 88
Q^1	– 68 to – 84
Q^2	– 74 to – 93
Q^3	– 91 to – 101
Q^4	– 101 to – 116
$Q^4(4Al)$	– 81 to – 92
$Q^4(3Al)$	– 85 to – 94
$Q^4(2Al)$	– 90 to – 100
$Q^4(1Al)$	– 95 to – 107
$Q^3(3Al)$	approx. – 77
$Q^3(2Al)$	– 82 to – 85
$Q^3(1Al)$	– 85 to – 90

Data from Kirkpatrick et al. [51], MacKenzie and Smith [60] and Walkley and Provis [97]

4-, 5-, and 6-coordinated Al, respectively). Sometimes the connectivity of AlO_4 tetrahedra in aluminosilicates is indicated by denoting them as q^n , analogously to the Q-nomenclature for SiO_4 tetrahedra. For example, q^4 denotes AlO_4 tetrahedra connected to four SiO_4 tetrahedra via Al–O–Si bonds. The chemical shift ranges of Al units in aluminosilicates and some aluminates, including cements, are summarized in Table 3. It should be noted that in other compounds, e.g., aluminium phosphates and aluminium borates, the chemical shift ranges of Al sites can differ considerably from those given in the Table 3 [60]. Chemical shift values have been compiled for minerals [60] and cement phases [81, 97].

An important concept helpful in the interpretation of ^{29}Si MAS NMR spectra of aluminosilicates is the Loewenstein rule. This rule states that in crystalline aluminosilicates, two AlO_4 tetrahedra cannot be bonded to each other via Al–O–Al bonds, i.e., of two neighboring tetrahedra connected via an oxygen bridge only one can have

Table 3 Typical chemical shift ranges of Al sites in aluminosilicates, aluminium oxides, and aluminium hydroxides

Site	Chemical shift range [vs. $Al(H_2O)_6^{3+}$] (ppm)
AlO_4 in aluminium oxides	90–62
AlO_4 in aluminosilicates: q^3	80–70
AlO_4 in aluminosilicates: q^4	69–50
AlO_4 , strongly distorted	50–20
AlO_5	50–20
AlO_6	20 to – 10

Data from MacKenzie and Smith [60], Müller et al. [65] and Walkley and Provis [97]

Al as the central atom [59]. Importantly, this implies that in a material with Si/Al < 1, not all aluminum can be in the tetrahedral network; instead, AlO₆ sites must exist in the structure of the aluminum silicate, or some or all of the Al is in an additional phase.

Based on the Loewenstein rule, Engelhardt and colleagues derived an equation to compute the Si/Al ratio of zeolites from the intensities of the Q⁴(mAl) and Q⁴ sites in their ²⁹Si MAS NMR spectra [18]:

$$\frac{\text{Si}}{\text{Al}} = \frac{\sum_{m=0}^4 I_{Q^4(m\text{Al})}}{\sum_{m=0}^4 0.25 \times m \times I_{Q^4(m\text{Al})}} \quad (3)$$

where $I_{Q^4(m\text{Al})}$ is the intensity of the line of the respective Q⁴(mAl) site ($m = 0$: Q⁴ site). This equation can be applied to other crystalline tectosilicates with substitution of Al for Si. The computed value may serve as an independent check of the Si/Al ratio obtained by other analyses.

In amorphous aluminosilicates, such as glasses and gels, the Loewenstein rule is not strictly obeyed, i.e., some Al–O–Al bonds can occur between AlO₄ sites. However, in several amorphous aluminosilicates, these Al–O–Al bonds comprise only a small fraction of the oxygen bridges [56, 96]; thus, the concept is called “aluminum avoidance principle”, and the Engelhardt equation might remain applicable, though not perfectly accurate, for these compounds.

3.1.4 NMR Spectroscopy Applied to the Corrosion of Cementitious Materials

Gutberlet et al. [36] applied single-pulse ²⁷Al and ²⁹Si MAS NMR spectroscopy to hardened ordinary Portland cement (OPC)-pastes exposed to hydrochloric acid (HCl) or sulfuric acid (H₂SO₄) at pH-values of 2, 3 and 4, for several weeks. For both acids, they observed a polymerization (increase of mean chain length) of the C–A–S–H, including an increase of the connectivity of the AlO₄ tetrahedra, and the eventual formation of Q³ and Q⁴ sites in the material (Fig. 18). The latter was interpreted to indicate the complete degradation of the C–A–S–H and the formation of an amorphous silica gel. ²⁷Al MAS NMR spectroscopy showed that the amount of ettringite, relative to AFm phase, was increased after acid exposure (Fig. 18); after 28 days in HCl at pH = 2, both ettringite and AFm were completely dissolved. Comparison of the spectra obtained from samples exposed to the two acids indicated that the deterioration mechanism of the cement pastes was essentially the same in HCl and H₂SO₄, but the rate of deterioration was faster in HCl.

The deterioration of alkali-activated materials (AAMs) with low or intermediate Ca-content in sulfuric acid was studied by Sturm et al. [88]. Using ²⁹Si MAS NMR spectroscopy, these authors found that in these materials, too, exposure to H₂SO₄ caused deterioration of the major phase(s) (N–A–S–H gel in the low-Ca AAMs;

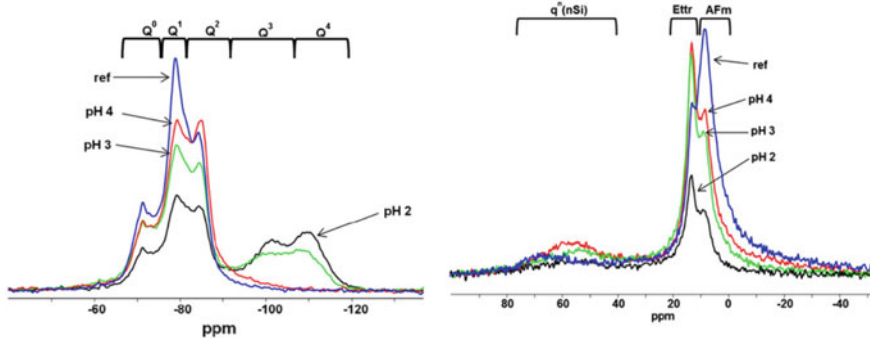


Fig. 18 ^{29}Si MAS NMR (left panel) and ^{27}Al MAS NMR (right panel) single-pulse spectra of hardened OPC pastes exposed to sulfuric acid (pH indicated) for 28 days. Sample *ref* was stored under inert gas for 28 days before the measurements. The AlO_6 resonances assigned to ettringite and AFm phase are labelled *Ettr* and *AFm*, respectively. Figure from Gutberlet et al. [36] with permission from Elsevier

likely some additional C–A–S–H in one of the intermediate-Ca AAMs). The deterioration products contained virtually only Q^3 and Q^4 units, indicative of silica gel. In the ^1H – ^{29}Si CP MAS NMR spectra of the corroded materials, the Q^3 sites were considerably enhanced (Fig. 19), indicating that the silica gel was highly hydrated, i.e., that the gel particles had a small size and a correspondingly high surface area. Based on comparison with published spectra [14] and additional evidence, the authors concluded that the silica gel had formed by precipitation rather than by incremental dealumination and polymerization of the N–A–S–H and C–A–S–H gel during acid attack [88]. A subsequent study [33] provided additional evidence for this deterioration mechanism for potassium silicate-activated metakaolin-based AAMs, and, using ^{27}Al MAS NMR spectroscopy, identified AlO_6 , assigned to K-alum, in the deteriorated layer of the materials.

The carbonation of cementitious materials is relevant in the present context, because the sulfuric acid attack on cementitious materials in sewers is usually preceded by an abiotic attack including carbonation (Chapter “Mechanisms and Processes of Concrete Corrosion in Sewers”). In addition, the carbonation of cementitious materials can be understood as a form of acid attack, since the dissolution of CO_2 in the pore solution leads to the formation of carbonic acid (H_2CO_3) and a concomitant decrease of the pH; accordingly, results obtained for carbonated cementitious materials may be partly transferable to materials corroded in sulfuric acid. In line with this, Groves et al. [35] found by ^{29}Si MAS NMR that exposure of hardened C_3S pastes to 100% CO_2 or to air led to an increase of the fraction of Q^2 units, relative to the fraction of Q^1 units, and for the pastes exposed to 100% CO_2 eventually to the occurrence of Q^3 and Q^4 units, i.e., the formation of silica gel. A subsequent study found by ^{27}Al and ^{29}Si MAS NMR that the decalcification of C–S–H during carbonation occurs in two steps (first, removal of Ca from the interlayer; second,

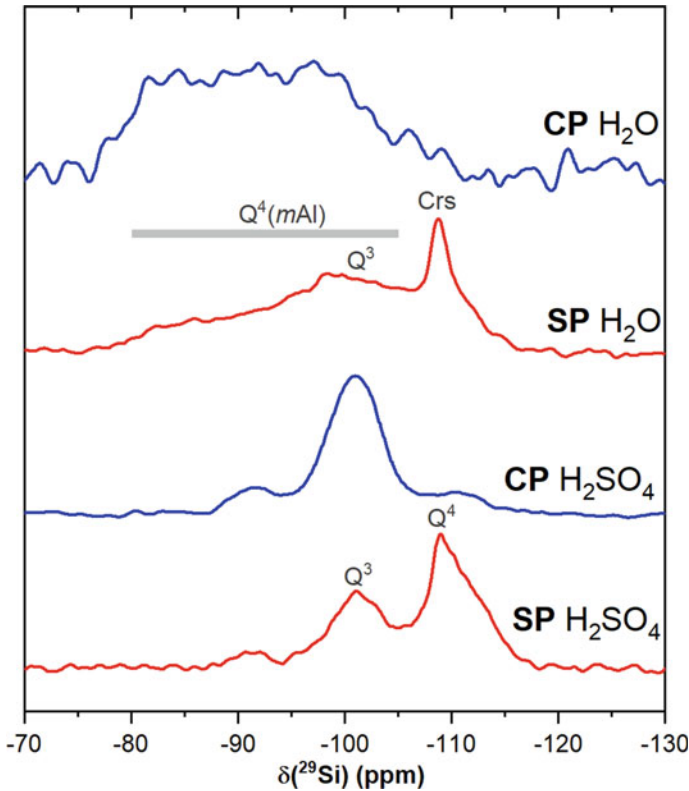


Fig. 19 ^{29}Si MAS NMR single-pulse spectra (*SP*; red lines) and ^1H - ^{29}Si CP MAS NMR spectra (*CP*; blue lines) of low-Ca AAM pastes after 70-day immersion in water (H_2O) or after 70-day immersion in sulfuric acid ($\text{pH} = 1$; H_2SO_4). The grey bar in the SP spectra marks the approximate chemical shift range of $\text{Q}^4(\text{mAl})$ species with $m = 1 \dots 4$. The comparatively narrow peak at -109 ppm is due to cristobalite (*CrS*) from the starting material. Data from Sturm et al. [88] with permission from Elsevier

removal of Ca from the principal layer and formation of amorphous silica), and that aluminum from C-A-S-H is incorporated in the resulting amorphous silica as q^4 units [79].

The above examples demonstrate that NMR spectroscopy can reveal information about the degradation of the major cementitious phases, the degradation products, the fate of specific elements during the process, and, in favorable cases, can provide clues about the degradation mechanism of the acid corrosion of cementitious materials. Though all examples relate to abiotic attack, it is obvious that NMR spectroscopy will also be a very useful tool to study the degradation of cementitious materials under MIC conditions.

3.2 Infrared Spectroscopy

3.2.1 Background

In infrared (IR) spectroscopy, the absorption of electromagnetic radiation in the infrared range ($130,000\text{--}10\text{ cm}^{-1}$) by matter is measured. The mid-infrared region spans the wavenumber range $4000\text{--}400\text{ cm}^{-1}$; this is the region which is most often considered in IR spectroscopy of cementitious materials, and which will be discussed here. There are several methods to split up (disperse) the radiation that passes the sample before it is detected [40, 87], but in modern IR spectrometers, this is usually done using an interferometer and Fourier transformation of the obtained signal; the instruments employing this method are called Fourier-transform infrared (FTIR) spectrometers. Likewise, there are several ways to expose the sample to the radiation [40, 87], but in many FTIR spectrometers this is done utilizing total internal reflection, i.e., in a set-up in which the radiation is reflected at the interface between the sample and a crystal, whereby some of the radiation is absorbed by the sample; this technique is called attenuated total reflectance Fourier-transform infrared (ATR-FTIR) spectroscopy. A different method is to mix the sample powder with an alkali halide (often potassium bromide, KBr) and compressing the powder mix produce a transparent disc; this disc is then exposed to the IR radiation to record the spectrum in transmission.

The basis for selective absorption of electromagnetic radiation and, thus, the emergence of a useful spectrum in IR spectroscopy is the vibration of molecules (or of the nuclei in a solid); specifically, the electric dipole moment of the molecule must change during the vibration to cause infrared absorption. Transitions between such vibrational energy levels cause the absorption of specific wavelengths of electromagnetic radiation. A peak in the IR spectrum that is related to a vibrational transition is usually called a “band”, while the term “line” refers to features of the fine structure of spectra (associated with transitions between rotational energy levels) of samples in the gas phase; however, for liquids and solids, where a fine structure cannot be observed, these two terms are sometimes used interchangeably [40]. Polyatomic molecules vibrate in complex ways that can be described using the concept of normal modes of vibration, which in turn requires the theory of molecular symmetry. A polyatomic molecule has more than one normal mode of vibration, i.e., it will generally absorb infrared radiation at more than one wavelength, and there exist an agreed nomenclature to refer to these different vibrational modes. The above principles, theories and nomenclature rules form the basis of the interpretation of IR spectra; descriptions of these are available at various levels of sophistication (e.g., [40, 87]).

In solids, all nuclei interact with each other via the bonds between them; thus, in a strict sense, no individual molecule with a tractable number of atoms can be identified. However, a similar approach as for molecules in the gas phase can in some cases be applied, since, as a first approximation, specific units in solids (e.g., common oxyanions in salts, such as the sulfate, the nitrate and the carbonate ion) can be treated as if they absorb the infrared radiation individually [87, 92]. Considerations about

the degree to which this approximation is valid for coordination polyhedra in solids led to the concept of condensed and isolated units and the assignment of specific wavenumber ranges that are typically absorbed by these units; for example, major absorption bands of SiO_4 units are generally found in the range $1200\text{--}800\text{ cm}^{-1}$, those of AlO_4 units in the range $900\text{--}650\text{ cm}^{-1}$, and those of AlO_6 units in the range $680\text{--}400\text{ cm}^{-1}$ [91, 92]. Similarly, the vibrations of specific molecular groups (group vibrations), such as OH groups, usually cause absorption at similar wavelengths for all compounds in which they occur [40, 87]. Due to the interactions between the nuclei in a solid, however, the bands assigned to the above units, and often also the bands of the group vibrations, are considerably broadened, compared to related bands of molecules in the gas phase.

3.2.2 Data Presentation

It is common practice to present infrared spectra as plots of transmittance versus wavenumber of the radiation, with transmittance increasing to the top, i.e., with the absorption bands pointing to the bottom. The transmittance, T , is defined as

$$T = \frac{I}{I_0} \quad (4)$$

where I_0 is the intensity of the radiation entering the sample, and I is the intensity of the radiation transmitted through sample.

The negative logarithm of T is called the absorbance, A :

$$A = -\log_{10}\left(\frac{I}{I_0}\right) = \log_{10}\left(\frac{I_0}{I}\right) = \log_{10}(I_0) - \log_{10}(I) \quad (5)$$

The absorbance of a band is proportional to the concentration of the compound causing the absorbance in the sample (Beer–Lambert law); thus, it is sometimes used instead of the transmittance for the presentation of IR spectra, particularly in contexts where IR spectroscopy is applied in analytical chemistry.

The wavenumber, $\tilde{\nu}$, of electromagnetic radiation is defined as the reciprocal of its wavelength, i.e.

$$\tilde{\nu} = \frac{1}{\lambda} = \frac{\nu}{c} \quad (6)$$

where λ is the wavelength, ν is the frequency, and c is the speed of light. In the context of IR spectroscopy, the wavelength is usually quoted in units of cm^{-1} (reciprocal centimeters), and it is common to present IR spectra with the wavenumber increasing to the left, though this convention is not always followed.

3.2.3 FTIR Spectroscopy Applied to the Corrosion of Cementitious Materials

Khan et al. [47] exposed mortars based on calcium aluminate cement (CAC) or a sulfate-resistant special-purpose composite cement (CEM V) for 24 months to a sewer environment and studied their degradation, *inter alia* using FTIR spectroscopy. They identified $\text{Al}(\text{OH})_3$ (bands assigned at 1025 and 967 cm^{-1}), gypsum (bands at 1685, 1625 and 1122 cm^{-1}) and calcite (bands at 1485, 875 and 856 cm^{-1}) in the corroded regions of the CAC mortar (Fig. 20). In the CEM V mortar, gypsum (bands assigned at 1685, 1625 and 1120 cm^{-1}) and polymorphs of CaCO_3 (bands at 1481, 1415–1410, 875 and 855 cm^{-1}) were identified; bands at 1160, 1075, 1055, 960 and in the range 750–650 cm^{-1} were attributed to C–S–H, and their shift in the spectra of the corroded regions was interpreted to indicate its alteration (Fig. 21). Reference IR spectra of the aforementioned degradation products and other relevant minerals can be found in the RRUFF database [53, 75], and in the compilation by Chukanov [15].

In their study of the corrosion of OPC pastes and slag/fly ash-based AAM pastes in 5% sulfuric acid, Aiken et al. [1] found by FTIR spectroscopy that portlandite (identified through a band at 3635 cm^{-1}) and ettringite (identified through a shoulder at 1105 cm^{-1}) in the OPC pastes had dissolved, and that gypsum had formed in all pastes that contained either OPC or slag but not in the AAM pastes based on only fly ash; in addition, in all pastes the main band between approx. 950 and 1000 cm^{-1}

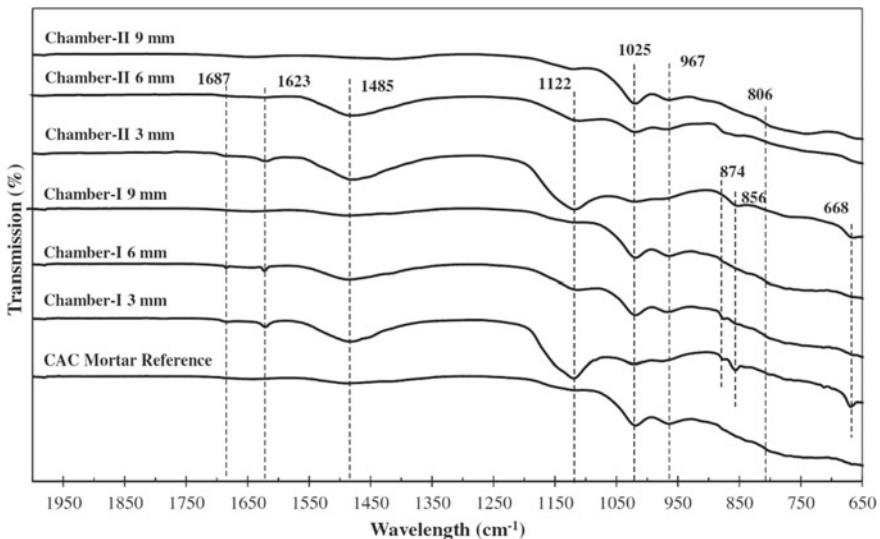


Fig. 20 FTIR spectra of corroded regions of a CAC mortar exposed to a sewer environment for 24 months. *Chamber I* and *Chamber II* denote the two different overflow chambers in which the specimens were placed; *Reference* denotes a specimen not exposed to the sewer environment. Figure from Khan et al. [47] with permission from Elsevier

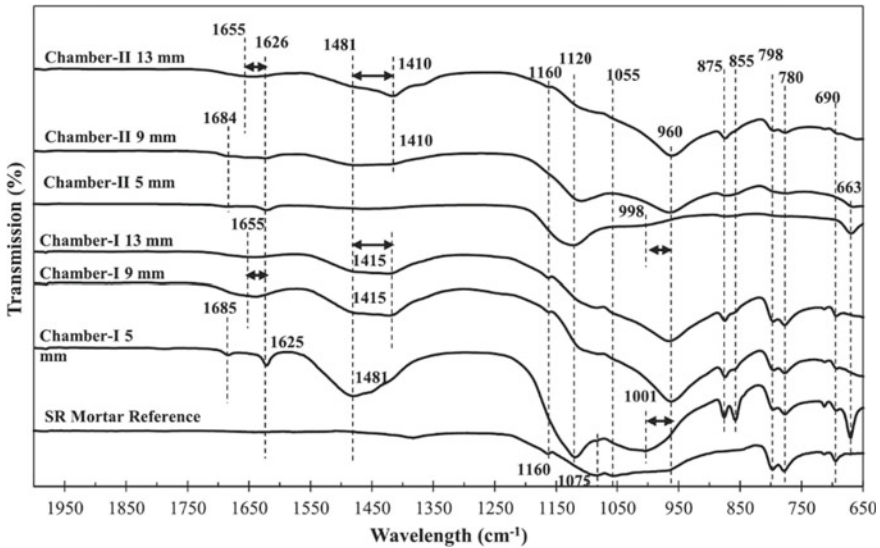


Fig. 21 FTIR spectra of corroded regions of a sulfate-resistant composite cement (CEM V) mortar (SR) exposed to a sewer environment for 24 months. *Chamber I* and *Chamber II* denote the two different overflow chambers in which the specimens were placed; *Reference* denotes a specimen not exposed to the sewer environment. Figure from Khan et al. [47] with permission from Elsevier

had shifted to higher wavenumbers after exposure to sulfuric acid, indicating partial decalcification and/or dealumination during acid attack. Broadly similar conclusions were drawn by Vogt et al. [94] and Khan et al. [48], who used FTIR spectroscopy to study the corrosion of metakaolin-based AAMs in sulfuric acid and the corrosion of AAM mortars and sulfate-resistant composite cement (CEM V) mortars in sulfuric acid and in a sewer environment, respectively. Bernal et al. [8] studied the degradation of Portland cement pastes and alkali-activated slag pastes in acetic acid using FTIR spectroscopy and found that the C–A–S–H gel in the alkali-activated slag was significantly less affected (less decalcified) by the acid attack than the C–S–H gel in the Portland cement paste.

As demonstrated by the above examples, IR spectroscopy is a versatile tool that can provide information about the dissolution of cement phases, the formation of secondary degradation products as well as alterations of the main cement phases (C–S–H, C–A–S–H, N–A–S–H). However, it should be born in mind that the band positions of specific compounds and molecular groups can vary between samples and that the bands of different phases can overlap, making interpretation of IR spectra sometimes ambiguous. Thus, in the context of cement degradation, IR spectroscopy is often used in conjunction with other methods that allow the identification of phases in the initial and the degraded material, such as X-ray diffraction, to facilitate assignments of bands in the spectra. Nevertheless, because of the comparatively low experimental effort to obtain IR spectra, it may be useful to analyze a large number of

samples that would otherwise be inaccessible; in addition, in certain cases, amorphous or semi-crystalline phases (e.g., carbonates and sulfates), that would not be detected with diffraction methods may be observed with IR spectroscopy.

3.3 *Raman Spectroscopy and Microscopy*

3.3.1 Background

Raman spectroscopy is related to IR spectroscopy in that it is concerned with energy level transitions in the range approx. $4000\text{--}400\text{ cm}^{-1}$, i.e., transitions between vibrational energy levels of molecules. However, the mechanism underlying the transitions that gives rise to Raman spectra as well as the experimental setup that is required to record Raman spectra are different from those on which IR spectroscopy is based [40, 82]. In Raman spectroscopy, the sample is irradiated with a laser, i.e., with radiation with a single frequency, and the radiation that is scattered by the sample is recorded. While most of the radiation undergoes elastic scattering (Rayleigh scattering), i.e., scattering that involves no change of frequency, a small fraction of the photons will interact with the sample in a way that the frequency of the scattered radiation is shifted, which is called Raman scattering. This process involves excitation of a molecule to a so-called virtual state and its return to an accessible vibrational energy level. If it returns to a higher energy level than before the scattering process, energy is absorbed from the scattered radiation (Stokes scattering); if it returns to a lower energy level than before the scattering process, the energy of the scattered radiation will be increased (anti-Stokes scattering). Usually, Stokes scattering is more intense than anti-Stokes scattering, and therefore only the Stokes spectrum is considered in most cases. Raman scattering requires that the molecular vibration that is involved in the process causes a change of the polarizability of the molecule. Since another property, the electric dipole moment, needs to change during vibration to cause absorption in IR spectroscopy, most vibrations are more intense in either Raman spectra or IR spectra (or do not occur in IR spectra or Raman spectra at all); these vibrations are called Raman-active and infrared-active, respectively. As with IR spectroscopy, detailed interpretation of the Raman spectra of molecules involves the theory of normal modes of vibration [40], while some oxyanions, molecular groups, and coordination polyhedra in solids can, as a first approximation, be treated as if Raman scattering from these units occurs individually [82].

A major advantage of Raman spectroscopy is that Raman spectrometers can be coupled to a microscope; the resulting technique is called Raman microscopy or μ -Raman spectroscopy. This technique allows one to analyze samples in situ without extensive prior sample preparation, and, particularly useful in the context of the degradation of cementitious materials, allows to produce images or maps of samples, for example to locate specific compounds in the corroded regions of a material. A difficulty with Raman spectroscopy and Raman microscopy is that problems with sample degradation and fluorescence can occur, which may even prevent the collection of

meaningful Raman spectra at all. These problems can in some cases be avoided or mitigated by an appropriate choice of laser wavelength, laser energy, and irradiation time [82], but these measures are not always successful.

3.3.2 Data Presentation

Raman spectra are usually presented as plots of scattered intensity versus Raman shift in units of cm^{-1} (reciprocal centimeters). The Raman shift is the difference between the energy of the irradiated laser light and the energy of the scattered radiation; it can be calculated, expressed as wavenumber difference, $\Delta\tilde{\nu}$, as follows:

$$\Delta\tilde{\nu} = \frac{1}{\lambda_{\text{laser}}} - \frac{1}{\lambda_{\text{scattered}}} \quad (7)$$

where λ_{laser} is the wavelength of the incident laser light, and $\lambda_{\text{scattered}}$ is the wavelength of the scattered radiation. If the wavelengths are inserted in units of nm, and the Raman shift is sought in units of cm^{-1} , the equation becomes:

$$\Delta\tilde{\nu}(\text{in cm}^{-1}) = \left(\frac{1}{\lambda_{\text{laser}}(\text{in nm})} - \frac{1}{\lambda_{\text{scattered}}(\text{in nm})} \right) \times 10,000,000 \quad (8)$$

The graphical presentation of Raman spectra is sometimes such that $\Delta\tilde{\nu}$ increases to the left (analogously to IR spectroscopy), and sometimes such that $\Delta\tilde{\nu}$ increases to the right.

3.3.3 Raman Spectroscopy Applied to the Corrosion of Cementitious Materials

Raman spectroscopy can be employed for the structural characterization of C–S–H and C–A–S–H [25, 52, 74] as well as to follow the transformations of the silicate structure that occurs during their degradation [9, 66]. A compilation of Raman bands of some units relevant for cements and cement degradation is shown in Table 4. However, the intensity of the Raman bands of the relevant units in amorphous and semi-crystalline (alumino)silicates, such as C–S–H, C–A–S–H and alkali aluminosilicate gels, is generally much lower than the intensity of the bands of other oxides and oxyanions that occur in cementitious systems, and often their bands are in the same wavenumber range (Table 4), making it difficult or impossible to identify the bands of the silicate and aluminate units of interest (e.g., [44, 80]).

Because of the aforesaid, Raman spectroscopy and Raman microscopy appears to be more useful to identify or map compounds such as sulfates, carbonates, iron oxides, organic compounds etc. in studies of MIC and related degradation processes of cementitious materials. The identification of these compounds is greatly aided by the RRUFF database [53, 75], which contains a comprehensive collection of

Table 4 Typical wavelength ranges of Raman bands of Si and Al units in silicate and aluminosilicate glasses, hydrous semi-crystalline silicates and aluminosilicates, and hydrous semi-crystalline and crystalline aluminates, and of some oxyanions

Range (cm ⁻¹)	Structural unit	Vibration
430–500	SiO ₂ /Q ⁴	Si–O symmetric stretching
~ 440	AlO ₄ ⁵⁻	Al–O stretching
490–550	AlO ₆ ⁹⁻	Al–O stretching
580–630	Si ₂ O ₅ ²⁻ /Q ³	Si–O–Si motion (incl. bending)
620–680	Si ₂ O ₆ ⁴⁻ /Q ²	Si–O–Si motion (incl. bending)
~ 700	Si ₂ O ₇ ⁶⁻ /Q ¹	Si–O–Si motion (incl. bending)
710–730	NO ₃ ⁻	N–O degenerate symmetric stretching/planar angular deformation
830–860	SiO ₄ ⁴⁻ /Q ⁰	Si–O symmetric stretching
880–910	Si ₂ O ₇ ⁶⁻ /Q ¹	Si–O symmetric stretching
~ 890	Si(OAl) ₄ /Q ⁴ (4Al)	(Si, Al)–O stretching
940–1010	Si ₂ O ₆ ⁴⁻ /Q ²	Si–O symmetric stretching
~ 925	(SiO)–Si(OAl) ₃ /Q ⁴ (3Al)	(Si, Al)–O stretching
980–995	SO ₄ ^{2-b}	S–O symmetric stretching
~ 1000	(SiO) ₂ –Si(OAl) ₂ /Q ⁴ (2Al)	(Si, Al)–O stretching
1010–1025	SO ₄ ^{2-c}	S–O symmetric stretching
1040–1070	NO ₃ ⁻	N–O symmetric stretching
1050–1100	Si ₂ O ₅ ²⁻ /Q ³	Si–O symmetric stretching
~ 1060 (w) ^a	SiO ₂ /Q ⁴	Si–O asymmetric stretching
1065–1090	CO ₃ ^{2-d}	C–O symmetric stretching
~ 1140	(SiO) ₃ –Si(OAl)/Q ⁴ (1Al)	(Si, Al)–O stretching
1190–1250 (w)	SiO ₂ /Q ⁴	Si–O asymmetric stretching
1340–1385	NO ₃ ⁻	N–O asymmetric stretching

Adapted from the compilation in Simon et al. [80], extended using data for sulfates and carbonates from Bensted et al. [7], Potgieter-Vermaak et al. [69], Renaudin et al. [73] and Torr ns-Mart n et al. [93]

^a (w): weak band

^b Sulfate ion in hydrous calcium sulfoaluminates (ettringite, monosulfate) or thenardite

^c Sulfate ion in calcium sulfates (gypsum, hemihydrate, anhydrite)

^d Carbonate ion in hydrous calcium carboaluminates (monocarbonate, hemicarbonat) or calcium carbonates (calcite, aragonite, vaterite)

Raman spectra of relevant minerals. An example is provided by Khan et al. [46], who identified thenardite, gypsum and calcite in the deteriorated layers of AAM mortars after corrosion in overflow chambers of a sewer system (Fig. 22). In addition, Raman spectroscopy of proteins and of naturally occurring lipids, some of which may be relevant in the context of MIC, has been reviewed [16, 76]. Thus, though Raman spectroscopy has so far only occasionally been applied to the analysis of MIC of

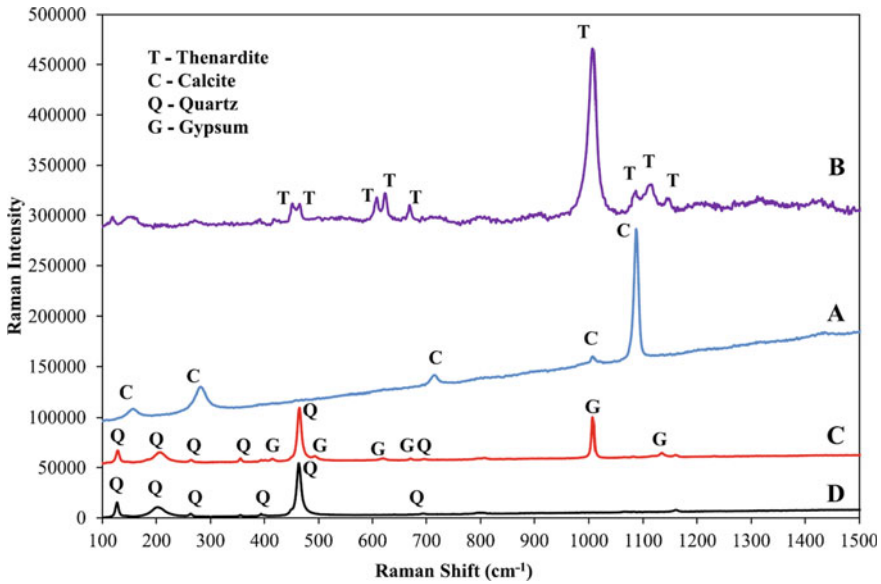


Fig. 22 Raman spectra of the corroded regions of AAM mortars exposed to a sewer environment for 12 months, indicating the presence of thenardite, calcite, and gypsum. Figure from Khan et al. [46] with permission from Elsevier

cementitious materials, this technique, particularly if applied as Raman microscopy, has considerable potential for obtaining relevant information, and it is expected that future MIC studies will benefit significantly from applying them.

4 Summary

Microbiologically influenced corrosion of concrete sewers is a complex multistep chain of reactions that ultimately lead to the destruction of (usually) very durable (reinforced) structures way before their expected lifespan. In order to decipher these complex reaction mechanisms a combination of sophisticated methods is required. In this chapter an overview of currently used basic and state of the art methodologies that are applied to explore the fascinating field of microbiologically influenced corrosion of concrete sewers are presented. Optical evaluations to highly sophisticated microstructural and spectroscopic methods are included, comprising (optical) pH measurement methods, electron beam, X-ray and neutron techniques (SEM, MLA, XRF, XRD, CT, Neutron radiography and tomography), and spectroscopic methods (MAS-NMR, FT-IR, and Raman).

References

1. Aiken, T.A., et al.: Effect of slag content and activator dosage on the resistance of fly ash geopolymer binders to sulfuric acid attack. *Cem. Concr. Res.* **111**, 23–40 (2018). Available at: <https://doi.org/10.1016/j.cemconres.2018.06.011>
2. Alexander, M., Bertron, A., De Belie, N.: Performance of cement-based materials in aggressive aqueous environments: state-of-the-art report, RILEM TC 211-PAE (2013)
3. Artioli, G., et al.: X-ray diffraction microtomography (XRD-CT), a novel tool for non-invasive mapping of phase development in cement materials. *Anal. Bioanal. Chem.* **397**(6), 2131–2136 (2010). Available at: <https://doi.org/10.1007/s00216-010-3649-0>
4. Barker, R.D., et al.: Quantitative mineral mapping of drill core surfaces I: a method for μ XRF mineral calculation and mapping of hydrothermally altered, fine-grained sedimentary rocks from a carlin-type gold deposit. *Econ. Geol.* **116**(4), 803–819 (2021). Available at: <https://doi.org/10.5382/econgeo.4803>
5. Beckhoff, B., et al. (eds.): *Handbook of Practical X-ray Fluorescence Analysis*, 1st edn. Springer, Berlin, Heidelberg (2006). Available at: <https://doi.org/10.1007/978-3-540-36722-2>
6. Behnood, A., Van Tittelboom, K., De Belie, N.: Methods for measuring pH in concrete: a review. *Constr. Build. Mater.* **105**, 176–188. Available at: <https://doi.org/10.1016/J.CONBUILDMAT.2015.12.032>
7. Bensted, J.: Uses of Raman spectroscopy in cement chemistry. *J. Am. Ceram. Soc.* **59**(3–4), 140–143 (1976). Available at: <https://doi.org/10.1111/j.1151-2916.1976.tb09451.x>
8. Bernal, S.A., et al.: Performance of alkali-activated slag mortars exposed to acids. *J. Sustain. Cem. Based Mater.* **1**(3), 138–151. Available at: <https://doi.org/10.1080/21650373.2012.747235>
9. Black, L., et al.: Structural features of C–S–H(I) and its carbonation in air—a Raman spectroscopic study. Part II: carbonated phases. *J. Am. Ceram. Soc.* **90**(3), 908–917 (2007). Available at: <https://doi.org/10.1111/j.1551-2916.2006.01429.x>
10. Bragg, W.: The diffraction of short electromagnetic waves by a crystal. *Proc. Camb. Philos. Soc.* **17**, 43–57 (1913)
11. Bran-Anleu, P., et al.: Standard and sample preparation for the micro XRF quantification of chlorides in hardened cement pastes. *Microchem. J.* **141**, 382–387 (2018). Available at: <https://doi.org/10.1016/J.MICROC.2018.05.040>
12. Briendl, L.G., et al.: In situ pH monitoring in accelerated cement pastes. *Cem. Concr. Res.* **157**, 106808 (2022). Available at: <https://doi.org/10.1016/j.cemconres.2022.106808>
13. Buvignier, A., et al.: Resistance to biodeterioration of aluminium-rich binders in sewer network environment: study of the possible bacteriostatic effect and role of phase reactivity. *Cem. Concr. Res.* **123**, 105785 (2019). Available at: <https://doi.org/10.1016/J.CEMCONRES.2019.105785>
14. Chuang, I.-S., Maciel, G.E.: A detailed model of local structure and silanol hydrogen bonding of silica gel surfaces. *J. Phys. Chem. B* **101**, 3052–3064 (1997). Available at: <https://doi.org/10.1021/jp9629046>
15. Chukanov, N.V.: *Infrared Spectra of Mineral Species*, 1st edn. Springer, Dordrecht (2014)
16. Czamara, K., et al.: Raman spectroscopy of lipids: a review. *J. Raman Spectrosc.* **46**, 4–20 (2015). Available at: <https://doi.org/10.1002/jrs.4607>
17. Duer, M.J.: *Introduction to Solid-State NMR Spectroscopy*. Blackwell, Oxford (2004)
18. Engelhardt, G., et al.: ^{29}Si -NMR-Untersuchungen zur Verteilung der Silicium- und Aluminiumatome im Alumosilicatgitter von Zeolithen mit Faujasit-Struktur TT— ^{29}Si NMR investigations of silicon-aluminum ordering in the aluminosilicate framework of Faujasite-type zeolites. *Z. Anorg. Allg. Chem.* **482**, 49–64 (1981). Available at: <https://doi.org/10.1002/zaac.19814821106>
19. Fandrich, R., et al.: Modern SEM-based mineral liberation analysis. *Int. J. Min. Proc.* **84**(1–4), 310–320 (2007). Available at: <https://doi.org/10.1016/J.MINPRO.2006.07.018>
20. Flemming, R.L.: Micro X-ray diffraction (μ XRD): a versatile technique for characterization of earth and planetary materials. *Can. J. Earth Sci.* **44**(9), 1333–1346 (2007). Available at: <https://doi.org/10.1139/E07-020>

21. Galan, I., et al.: Continuous optical in-situ pH monitoring during early hydration of cementitious materials. *Cem. Concr. Res.* **150**, 106584 (2021). Available at: <https://doi.org/10.1016/J.CEMCONRES.2021.106584>
22. Galan, I., et al.: Amorphous and crystalline CaCO₃ phase transformation at high solid/liquid ratio—insight to a novel binder system. *J. Cryst. Growth* **580**, 126465 (2022). Available at: <https://doi.org/10.1016/J.JCRYSGRO.2021.126465>
23. Garbe, U., et al.: A new neutron radiography/tomography/imaging station DINGO at OPAL. *Phys. Proc.* **69**, 27–32 (2015). Available at: <https://doi.org/10.1016/j.phpro.2015.07.003>
24. Garbe, U., et al.: Industrial application experiments on the neutron imaging instrument DINGO. *Phys. Proc.* **88**, 13–18 (2017). Available at: <https://doi.org/10.1016/j.phpro.2017.06.001>
25. Garbev, K., et al.: Structural features of C–S–H(I) and its carbonation in air—a Raman spectroscopic study. Part I: fresh phases. *J. Am. Ceram. Soc.* **90**(3), 900–907 (2007). Available at: <https://doi.org/10.1111/j.1551-2916.2006.01428.x>
26. Gibeaux, S., et al.: Weathering assessment under X-ray tomography of building stones exposed to acid atmospheres at current pollution rate. *Constr. Build. Mater.* **168**, 187–198 (2018). Available at: <https://doi.org/10.1016/J.CONBUILDMAT.2018.02.120>
27. Goldstein, J.I., et al. (eds.): *Scanning Electron Microscopy and X-Ray Microanalysis*, 4th edn. Springer, New York, NY (2018). Available at: <https://doi.org/10.1007/978-1-4939-6676-9>
28. Grengg, C., et al.: Microbiologically induced concrete corrosion: a case study from a combined sewer network. *Cem. Concr. Res.* **77**, 16–25 (2015). Available at: <https://doi.org/10.1016/J.CEMCONRES.2015.06.011>
29. Grengg, C., et al.: The decisive role of acidophilic bacteria in concrete sewer networks: a new model for fast progressing microbial concrete corrosion. *Cem. Concr. Res.* **101** (2017). Available at: <https://doi.org/10.1016/j.cemconres.2017.08.020>
30. Grengg, C., et al.: High-resolution optical pH imaging of concrete exposed to chemically corrosive environments. *Cem. Concr. Res.*, 116 (2019). Available at: <https://doi.org/10.1016/j.cemconres.2018.10.027>
31. Grengg, C., et al.: Long-term in situ performance of geopolymer, calcium aluminate and Portland cement-based materials exposed to microbially induced acid corrosion. *Cem. Concr. Res.* **131**, 106034 (2020). Available at: <https://doi.org/10.1016/J.CEMCONRES.2020.106034>
32. Grengg, C., et al.: Cu- and Zn-doped alkali activated mortar—properties and durability in (bio)chemically aggressive wastewater environments. *Cem. Concr. Res.* **149**, 106541 (2021). Available at: <https://doi.org/10.1016/J.CEMCONRES.2021.106541>
33. Grengg, C., et al.: Deterioration mechanism of alkali-activated materials in sulfuric acid and the influence of Cu: a micro-to-nano structural, elemental and stable isotopic multi-proxy study. *Cem. Concr. Res.* **142**, 106373 (2021). Available at: <https://doi.org/10.1016/j.cemconres.2021.106373>
34. Grousset, S., et al.: In situ monitoring of corrosion processes by coupled micro-XRF/micro-XRD mapping to understand the degradation mechanisms of reinforcing bars in hydraulic binders from historic monuments. *J. Anal. Atom. Spectrom.* **30**(3), 721–729 (2015). Available at: <https://doi.org/10.1039/c4ja00370e>
35. Groves, G.W., et al.: Progressive changes in the structure of hardened C₃S cement pastes due to carbonation. *J. Am. Ceram. Soc.* **74**(11), 2891–2896 (1991). Available at: <https://doi.org/10.1111/j.1151-2916.1991.tb06859.x>
36. Gutberlet, T., Hilbig, H., Beddoe, R.E.: Acid attack on hydrated cement—effect of mineral acids on the degradation process. *Cem. Concr. Res.* **74**, 35–43 (2015). Available at: <https://doi.org/10.1016/j.cemconres.2015.03.011>
37. Harris, R.K., et al.: NMR nomenclature. Nuclear spin properties and conventions for chemical shifts (IUPAC recommendations 2001). *Pure Appl. Chem.* **73**, 1795–1818 (2001). Available at: <https://doi.org/10.1351/pac200173111795>
38. Herisson, J., et al.: Toward an accelerated biodeterioration test to understand the behavior of Portland and calcium aluminate cementitious materials in sewer networks. *Int. Biodeterior. Biodegradation* (2013) [Preprint]. Available at: <https://doi.org/10.1016/j.ibiod.2012.03.007>

39. Herisson, J., et al.: Influence of the binder on the behaviour of mortars exposed to H₂S in sewer networks: a long-term durability study. *Mater. Struct.* **50**(1), 8 (2016). Available at: <https://doi.org/10.1617/s11527-016-0919-0>
40. Hollas, J.M.: *Modern Spectroscopy*, 3rd edn. Wiley, Chichester (1996)
41. Jiang, G. et al.: The role of iron in sulfide induced corrosion of sewer concrete. *Water Res.* **49**, 166–174 (2014). Available at: <https://doi.org/10.1016/J.WATRES.2013.11.007>
42. Jiang, G., Keller, J., Bond, P.L.: Determining the long-term effects of H₂S concentration, relative humidity and air temperature on concrete sewer corrosion (2014). Available at: <https://doi.org/10.1016/j.watres.2014.07.026>
43. Joseph, A.P., et al.: Surface neutralization and H₂S oxidation at early stages of sewer corrosion: influence of temperature, relative humidity and H₂S concentration. *Water Res.* (2012) [Preprint]. Available at: <https://doi.org/10.1016/j.watres.2012.05.011>
44. Ke, X., et al.: Alkali aluminosilicate geopolymers as binders to encapsulate strontium-selective titanate ion-exchangers. *Dalton Trans.* **48**, 12116–12126 (2019). Available at: <https://doi.org/10.1039/C9DT02108F>
45. Keeler, J.: *Understanding NMR Spectroscopy*, 2nd edn. Wiley, Chichester (2010)
46. Khan, H.A., et al.: Deterioration of alkali-activated mortars exposed to natural aggressive sewer environment. *Constr. Build. Mater.* **186**, 577–597 (2018). Available at: <https://doi.org/10.1016/J.CONBUILDMAT.2018.07.137>
47. Khan, H.A., et al.: Durability of calcium aluminate and sulphate resistant Portland cement based mortars in aggressive sewer environment and sulphuric acid. *Cem. Concr. Res.* **124**, 105852 (2019). Available at: <https://doi.org/10.1016/j.cemconres.2019.105852>
48. Khan, H.A., Castel, A., Khan, M.S.H.: Corrosion investigation of fly ash based geopolymer mortar in natural sewer environment and sulphuric acid solution. *Corros. Sci.* **168**, 108586 (2020). Available at: <https://doi.org/10.1016/J.CORSCI.2020.108586>
49. Khan, H.A., Yasir, M., Castel, A. (2022). Performance of cementitious and alkali-activated mortars exposed to laboratory simulated microbially induced corrosion test. *Cem. Concr. Compos.* **128**, 104445. Available at: <https://doi.org/10.1016/J.CEMCONCOMP.2022.104445>
50. Khanzadeh Moradillo, M., Hu, Q., Ley, M.T.: Using X-ray imaging to investigate in-situ ion diffusion in cementitious materials. *Constr. Build. Mater.* **136**, 88–98 (2017). Available at: <https://doi.org/10.1016/J.CONBUILDMAT.2017.01.038>
51. Kirkpatrick, R.J., et al.: Solid-state nuclear magnetic resonance spectroscopy of minerals. *Annu. Rev. Earth Planet. Sci.* **13**, 29–47 (1985)
52. Kirkpatrick, R.J., et al.: Raman spectroscopy of C–S–H, tobermorite, and jennite. *Adv. Cem. Based Mater.* **5**(3–4), 93–99 (1997). Available at: [https://doi.org/10.1016/S1065-7355\(97\)00001-1](https://doi.org/10.1016/S1065-7355(97)00001-1)
53. Lafuente, B., et al.: The power of databases: the RRUFF project. In: Armbruster, T., Danisi, R.M. (eds.) *Highlights in Mineralogical Crystallography*, pp. 1–29. De Gruyter, Berlin (2015)
54. Lanari, P., et al.: Quantitative compositional mapping of mineral phases by electron probe micro-analyser. *Geol. Soc. Lond. Spec. Publ.* **478**(1), 39–63 (2019). Available at: <https://doi.org/10.1144/SP478.4>
55. Lavigne, M.P., et al.: Innovative approach to simulating the biodeterioration of industrial cementitious products in sewer environment. Part II: validation on CAC and BFSC linings. *Cem. Concr. Res.* **79**, 409–418 (2016). Available at: <https://doi.org/10.1016/J.CEMCONRES.2015.10.002>
56. Lee, S.K., Stebbins, J.F.: The degree of aluminium avoidance in aluminosilicate glasses. *Am. Miner.* **84**, 937–945 (1999)
57. Li, X., et al.: The rapid chemically induced corrosion of concrete sewers at high H₂S concentration. *Water Res.* **162**, 95–104 (2019). Available at: <https://doi.org/10.1016/J.WATRES.2019.06.062>
58. Lippmaa, E., et al.: Structural studies of silicates by solid-state high-resolution ²⁹Si NMR. *J. Am. Chem. Soc.* **102**(15), 4889–4893 (1980). Available at: <https://doi.org/10.1021/ja00535a008>

59. Loewenstein, W.: The distribution of aluminium in the tetrahedra of silicates and aluminates. *Am. Miner.* **39**(1–2), 92–96 (1954)
60. MacKenzie, K.J.D., Smith, M.E.: *Multinuclear Solid-State NMR of Inorganic Materials*, Pergamon Materials Series. Pergamon, Oxford (2002)
61. Magniont, C., et al.: A new test method to assess the bacterial deterioration of cementitious materials. *Cem. Concr. Res.* (2011) [Preprint]. Available at: <https://doi.org/10.1016/j.cemconres.2011.01.014>
62. Mittermayr, F., et al.: Evaporation—a key mechanism for the thaumasite form of sulfate attack. *Cem. Concr. Res.* **49**, 55–64. Available at: <https://doi.org/10.1016/J.CEMCONRES.2013.03.003>
63. Monteny, J., et al.: Chemical, microbiological, and in situ test methods for biogenic sulfuric acid corrosion of concrete. *Cem. Concr. Res.* **30**(4), 623–634 (2000). Available at: [https://doi.org/10.1016/S0008-8846\(00\)00219-2](https://doi.org/10.1016/S0008-8846(00)00219-2)
64. Müller, B., et al.: Wide-range optical pH imaging of cementitious materials exposed to chemically corrosive environments. *RILEM Tech. Lett.* **3**(0 SE-), 39–45 (2018). Available at: <https://doi.org/10.21809/rilemtechlett.2018.72>
65. Müller, D., et al.: Solid-state aluminium-27 nuclear magnetic resonance chemical shift and quadrupole coupling data for condensed AlO_4 tetrahedra. *J. Chem. Soc. Dalton Trans.*, 1277–1281 (1986). Available at: <https://doi.org/10.1039/DT9860001277>
66. Ortoboy, S., et al.: Effects of CO_2 and temperature on the structure and chemistry of C–(A–)S–H investigated by Raman spectroscopy. *RSC Adv.* **7**, 48925–48933 (2017). Available at: <https://doi.org/10.1039/c7ra07266j>
67. Peyre Lavigne, M., et al.: Innovative approach to simulating the biodeterioration of industrial cementitious products in sewer environment. Part II: validation on CAC and BFSC linings. *Cem. Concr. Res.* (2015) [Preprint]. Available at: <https://doi.org/10.1016/j.cemconres.2015.10.002>
68. Plusquellec, G., et al.: Determination of the pH and the free alkali metal content in the pore solution of concrete: review and experimental comparison. *Cem. Concr. Res.* **96**, 13–26 (2017). Available at: <https://doi.org/10.1016/J.CEMCONRES.2017.03.002>
69. Potgieter-Vermaak, S.S., Potgieter, J.H., Van Grieken, R.: The application of Raman spectrometry to investigate and characterize cement, part I: a review. *Cem. Concr. Res.* **36**, 656–662 (2006). Available at: <https://doi.org/10.1016/j.cemconres.2005.09.008>
70. Proverbio, E., Carassiti, F.: Evaluation of chloride content in concrete by X-ray fluorescence. *Cem. Concr. Res.* **27**(8), 1213–1223 (1997). Available at: [https://doi.org/10.1016/S0008-8846\(97\)00108-7](https://doi.org/10.1016/S0008-8846(97)00108-7)
71. Reed, S.J.B.: *Electron Microprobe Analysis and Scanning Electron Microscopy in Geology*. Cambridge University Press (2005). Available at: <https://doi.org/10.1017/CBO9780511610561>
72. Reiche, I., Chalmin, E.: Synchrotron methods: color in paints and minerals. In: Holland, H.D., Turekian, K.K. (eds.) *Treatise on Geochemistry*, 2nd edn., pp. 209–239. Elsevier, Oxford (2014). Available at: <https://doi.org/10.1016/B978-0-08-095975-7.01216-X>
73. Renaudin, G., et al.: A Raman study of the sulfated cement hydrates: ettringite and monosulfaluminate. *J. Adv. Concr. Technol.* **5**(3), 299–312 (2007). Available at: <https://doi.org/10.3151/jact.5.299>
74. Renaudin, G. et al.: Structural characterization of C–S–H and C–A–S–H samples—part II: local environment investigated by spectroscopic analyses. *J. Solid State Chem.* **182**, 3320–3329 (2009). Available at: <https://doi.org/10.1016/j.jssc.2009.09.024>
75. RRUFF Project: RRUFF project, database of Raman spectroscopy, X-ray diffraction and chemistry of minerals (RRUFF database) (2022). Available at: <https://rruff.info/>. Accessed: 6 May 2022
76. Rygula, A., et al.: Raman spectroscopy of proteins: a review. *J. Raman Spectrosc.* **44**, 1061–1076 (2013). Available at: <https://doi.org/10.1002/jrs.4335>
77. Scrivener, K., Snellings, R., Lothenbach, B. (eds.): *A Practical Guide to Microstructural Analysis of Cementitious Materials*. 1st edn (2016). Available at: <https://doi.org/10.1201/b19074>

78. Serdar, M., et al.: Spatial distribution of crystalline corrosion products formed during corrosion of stainless steel in concrete. *Cem. Concr. Res.* **71**, 93–105 (2015). Available at: <https://doi.org/10.1016/j.cemconres.2015.02.004>
79. Sevelsted, T.F., Skibsted, J.: Carbonation of C–S–H and C–A–S–H samples studied by ^{13}C , ^{27}Al and ^{29}Si MAS NMR spectroscopy. *Cem. Concr. Res.* **71**, 56–65 (2015). Available at: <https://doi.org/10.1016/j.cemconres.2015.01.019>
80. Simon, S., Bertmer, M., Gluth, G.J.G.: Sol–gel synthesis and characterization of lithium aluminate (L–A–H) and lithium aluminosilicate (L–A–S–H) gels. *Int. J. Appl. Ceram. Technol.* **19**(6), 3179–3190 (2022). Available at: <https://doi.org/10.1111/ijac.14187>
81. Skibsted, J.: High-resolution solid-state nuclear magnetic resonance spectroscopy of Portland cement-based systems. In: Scrivener, K., Snellings, R., Lothenbach, B. (eds.) *A Practical Guide to Microstructural Analysis of Cementitious Materials*, pp. 213–286. CRC Press, Boca Raton (2016)
82. Smith, E., Dent, G.: *Modern Raman Spectroscopy: A Practical Approach*, 2nd edn. Wiley, Hoboken (2019)
83. Song, Y., Wightman, E., et al.: Corrosion of reinforcing steel in concrete sewers. *Sci. Total Environ.* **649**, 739–748 (2019). Available at: <https://doi.org/10.1016/J.SCITOTENV.2018.08.362>
84. Song, Y., Tian, Y., et al.: Distinct microbially induced concrete corrosion at the tidal region of reinforced concrete sewers. *Water Res.* **150**, 392–402 (2019). Available at: <https://doi.org/10.1016/J.WATRES.2018.11.083>
85. Song, Y., et al.: Rebar corrosion and its interaction with concrete degradation in reinforced concrete sewers. *Water Res.* **182**, 115961 (2020). Available at: <https://doi.org/10.1016/J.WATRES.2020.115961>
86. Song, Y., et al.: A novel granular sludge-based and highly corrosion-resistant bio-concrete in sewers. *Sci. Total Environ.* **791**, 148270 (2021). Available at: <https://doi.org/10.1016/j.scitotenv.2021.148270>
87. Stuart, B.: *Infrared Spectroscopy: Fundamentals and Applications*. Wiley, Chichester (2004)
88. Sturm, P. et al.: Sulfuric acid resistance of one-part alkali-activated mortars. *Cem. Concr. Res.* **109**, 54–63 (2018). Available at: <https://doi.org/10.1016/j.cemconres.2018.04.009>
89. Suzuki, T., Shiotani, T., Ohtsu, M.: Evaluation of cracking damage in freeze-thawed concrete using acoustic emission and X-ray CT image. *Constr. Build. Mater.* **136**, 619–626 (2017). Available at: <https://doi.org/10.1016/J.CONBUILDMAT.2016.09.013>
90. Taheri, S., et al.: Migration and formation of an iron rich layer during acidic corrosion of concrete with no steel reinforcement. *Constr. Build. Mater.* **309**, 125105 (2021). Available at: <https://doi.org/10.1016/J.CONBUILDMAT.2021.125105>
91. Tarte, P.: Applications nouvelles de la spectrométrie infrarouge à des problèmes de cristalochimie. *Silic. Indus.* **28**, 345–354 (1963)
92. Tarte, P.: Infra-red spectra of inorganic aluminates and characteristic vibrational frequencies of AlO_4 tetrahedra and AlO_6 octahedra. *Spectrochim. Acta Part A* **23**(7), 2127–2143 (1967)
93. Torrén-Martín, S., et al.: Raman spectroscopy of anhydrous and hydrated calcium aluminates and sulfoaluminates. *J. Am. Ceram. Soc.* **96**, 3589–3595 (2013). Available at: <https://doi.org/10.1111/jace.12535>
94. Vogt, O., Ukrainczyk, N., Koenders, E.: Effect of silica fume on metakaolin geopolymers' sulfuric acid resistance. *Materials* (2021). Available at: <https://doi.org/10.3390/ma14185396>
95. Vollpracht, A., et al.: The pore solution of blended cements: a review. *Mater. Struct.* **49**(8), 3341–3367 (2016). Available at: <https://doi.org/10.1617/s11527-015-0724-1>
96. Walkley, B., et al.: New structural model of hydrous sodium aluminosilicate gels and the role of charge-balancing extra-framework Al. *J. Phys. Chem. C* **122**, 5673–5685 (2018). Available at: <https://doi.org/10.1021/acs.jpcc.8b00259>
97. Walkley, B., Provis, J.L.: Solid-state nuclear magnetic resonance spectroscopy of cements. *Mater. Today Adv.* **1** (2019). Available at: <https://doi.org/10.1016/j.mtadv.2019.100007>
98. Yang, S., Cui, H., Poon, C.S.: Assessment of in-situ alkali-silica reaction (ASR) development of glass aggregate concrete prepared with dry-mix and conventional wet-mix methods by X-ray

- computed micro-tomography. *Cem. Concr. Compos.* **90**, 266–276 (2018). Available at: <https://doi.org/10.1016/J.CEMCONCOMP.2018.03.027>
99. Yuan, J. et al.: Investigating the failure process of concrete under the coupled actions between sulfate attack and drying–wetting cycles by using X-ray CT. *Constr. Build. Mater.* **108**, 129–138 (2016). Available at: <https://doi.org/10.1016/J.CONBUILDMAT.2016.01.040>

Characterization of Corrosion Microbial Communities



Xuan Li and Guangming Jiang

Abstract The corrosive conditions in sewers influence the corrosion development on concrete sewers. With the corrosion development, the continuous acid production alters the corrosion layer conditions and the microbial community. This chapter briefly discussed the dynamic corrosive conditions within sewers and their impacts on corrosion development. H₂S concentration, temperature, relative humidity, and contact with wastewater are critical environmental factors for corrosion development. The pH reduction due to corrosion development changed the corrosion layer conditions and corrosion microbial communities, where a temporal succession from neutrophilic sulfur-oxidizing microorganisms (NSOM) to acidophilic sulfide-oxidizing microorganisms (ASOM) occurs. Through culture-dependent and culture-independent detection approaches, a diverse range of NSOM and ASOM was detected in corrosion layers along with heterotrophic microbes. The functions and physiology of core members in corrosion communities, especially in relation to the corrosion process are summarized.

X. Li · G. Jiang (✉)

School of Civil, Mining, Environmental and Architectural Engineering, University of Wollongong, Wollongong, NSW 2522, Australia

e-mail: gjiang@uow.edu.au

X. Li

e-mail: xuan.li@uts.edu.au

X. Li

Centre for Technology in Water and Wastewater, School of Civil and Environmental Engineering, University of Technology Sydney, Ultimo, Sydney, NSW 2007, Australia

1 Development and Conditions of Concrete Corrosion Layers

From the moment of installation, newly manufactured concrete sewer pipes undergo various abiotic and biotic processes caused by the corrosive environments in sewers, which reduce the pH of intact concrete from 13 to below 3 [1, 2]. With the development of the corrosion processes, the corrosion layer conditions also change greatly. During the initiation stage of concrete corrosion, abiotic processes such as carbonation (CO_2) and H_2S acidification reduce the surface pH of concrete from ~ 13 to ~ 9 [2]. After the pH of the sewer surface is abiotically reduced to 9, neutrophilic sulfur-oxidizing microorganisms (NSOM) will colonize the surface and produce acid to eventually lower the pH to 5–3 [3]. Although corrosion is developed on the surface of the concrete with the reduction of surface pH and visual appearance of corrosion products, the mass loss of concrete is limited and no clear corrosion front between the corrosion layer and the un-corroded part of the specimens can be differentiated when pH is above 3 [1, 4]. However, the activity of NSOM establishes suitable surface conditions, which allows the subsequent colonization of acidophilic sulfide oxidation microorganisms (ASOM) on the concrete surface [1, 5]. Once the pH is lower than 3, ASOM becomes the protagonist and the active corrosion drives the pH further down, along with the massive corrosion loss of concrete. In microbiologically influenced concrete corrosion (MICC), concrete with a surface pH of 2–3 is generally regarded as reaching the active corrosion stage, where the corrosion layers are well-established [5]. In most of the corroding sewers, concrete stays in the active corrosion stage for most of their service life. Thus, the active corrosion stage, with corrosion layer and the associated ASOM available for sampling, has obtained more research focuses than other stages.

Once the corrosion is well developed, on the corroding concrete surface, a soft (cottage cheese-like) moist layer forms comprising largely of crystalline gypsum and other sulfur species. The microbial biofilms exist within the corrosion layer together with corrosion products (Fig. 1). Due to the paucity of some essential nutrients (such as organic nitrogen and phosphorus substances), which are innately absent from the concrete, the development of microorganisms mainly relies on sewer gases and wastewater. As mentioned in Chap. 2, microbiologically influenced corrosion majorly occurs in crown regions and tidal regions. The availability of sewer gas and wastewater contact varies greatly at these two locations. The hydraulic shaping and mixing of the wastewater flow also change the microstructures of corrosion layers. In crown regions, corrosion products tend to be non-uniform in size and loosely scattered or piled up on the intact cement matrix, while corrosion products are smaller and of more uniform sizes in the tidal regions [6]. Therefore, the microbial communities in crown regions and tidal regions are commonly different even within the same sewer pipe [6].

The corrosive conditions within sewers also differ temporally and spatially [8, 9]. Environmental factors such as H_2S , relative humidity (RH), and temperature of sewer gas play crucial roles in the corrosion process [2, 8, 10]. H_2S in the sewer gas phase is a

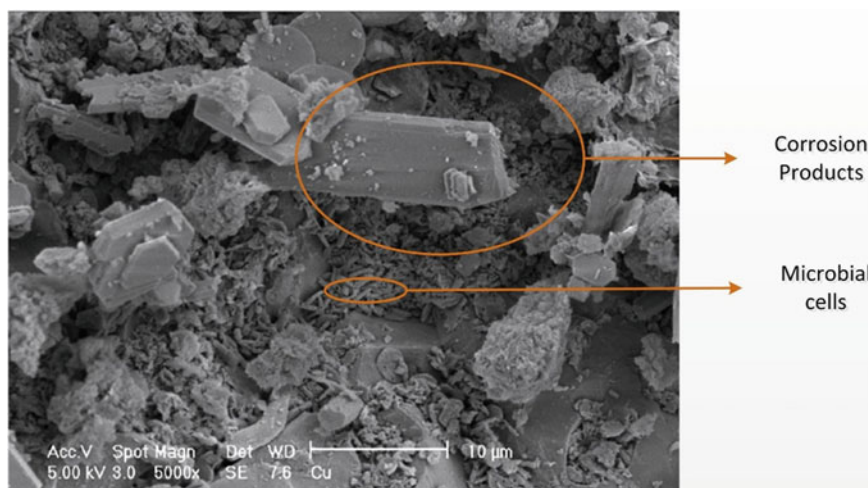


Fig. 1 Scanning electron microscopy image of the corroded concrete surface. Small elongated rod shapes are microbial cells, and angular crystal formations are sulfur-containing corrosion products, adapted from [7] (open access)

potential key energy source for chemolithotrophic sulfur-oxidizing microorganisms [11]. The H_2S levels in sewer gas are also found positively related to the sewer corrosion development and corrosion loss [8, 10]. H_2S levels above 2 ppm in sewer gas can cause corrosion [12]. In different sewers, average concentrations of H_2S vary greatly between a few ppm up to a few hundred ppm [11]. Seasonal and diurnal variations are also commonly observed in the same sewer. For instance, in a real sewer manhole in tropical regions of Australia, the average gaseous H_2S concentrations in the summer were about 8 ppm higher than the winter values (Fig. 2a). The household water usage also influences the real-time H_2S concentrations. In the same manhole, H_2S concentrations peaked at higher usages times at 40–60 ppm but remained low levels at low usage times at < 20 ppm (Fig. 2b). In some extreme conditions, H_2S concentrations of over 800 ppm are observed in a gravity pipe [9].

In a typical sewer system, the temperature in the sewer atmosphere is relatively stable during a short period (i.e., days and weeks) but has seasonal variations. Take the manhole in Australia as an example, sewer gas temperature showed negligible variations within 24 h but was about 5 °C higher in summers than in winters (Fig. 2). Geological differences in sewer air temperature have also been reported. For instance, the sewer gas temperature is about 19–22 °C in Queensland, Australia but 3–20 °C in Denmark, and 10–30 °C in Japan throughout the year [2, 13]. The sulfide oxidizing activity of ASOM increased by 15% when the temperature increased from 20 to 25 °C, but was inhibited when the temperature was below 15.6 °C [14]. In laboratory corrosion chambers, the increase of temperature from 13 to 30 °C showed no clear impact on the corrosion rate and possibly the acclimation of ASOM to temperature mitigated its effects. The moisture in sewer gas is measured by relative humidity. In

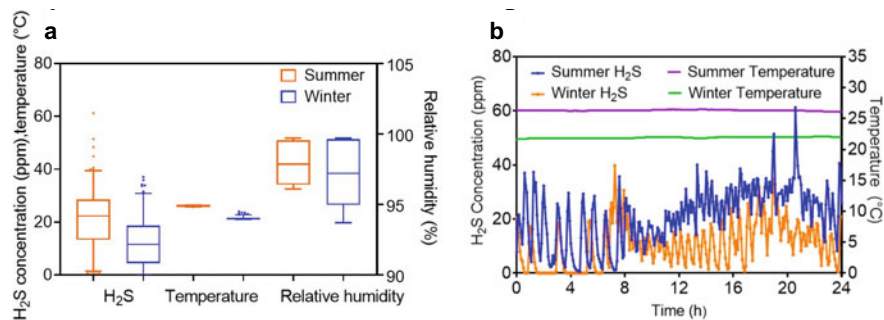


Fig. 2 **a** The profile of gaseous H₂S concentrations, temperature, and relative humidity in a sewer manhole in Australia. **b** Typical diurnal profiles of gaseous H₂S concentration and temperature of the sewer manhole in winter and summer

gravity sewers, the relative humidity typically ranges between 60 and 100% [15, 16]. Higher relative humidity levels also facilitate the corrosion development process in crown regions, but a negligible impact on the corrosion development in tidal regions due to their vicinity to wastewater [8, 10]. With the dynamic corrosive conditions in sewers, the corrosion development and relevant corrosion-inducing microorganisms vary temporally and spatially, the characterization and function of sewer corrosion microbial communities are discussed in the following sections.

2 Detection Approaches for Identifying Corrosion Microbial Communities

Conventionally, the identification of corrosion microbial communities relies on culture-dependent methods, where corrosion layer samples are used as inoculum in suitable culture media to facilitate their growth [17, 18]. Since the choice of growth substrates, supplements, and conditions for cultivation heavily influences what will grow, only a limited number of microorganisms that suit the culture media can be detected in individual culturing attempts. Thus, prior information for the suitable culture media is required for the target microorganism or microorganism group (Table 1). The selection of one or a group of targeted microorganisms can thereby be achieved by the selection of culture media [19]. However, only a small fraction (in the order of 1%) of bacteria present in the environment are readily obtained in pure culture in the laboratory [20]. This largely biases our view on the diversity of the corrosion microbial community.

The development of culture-independent methods has revolutionized studies of microbial ecology [21]. The application of culture-independent methods in the identification of corrosion communities has advanced greatly in the past decade and is providing revealing insight. This is especially with the application of high-throughput next-generation sequencing (NGS) of small-subunit rRNA gene amplicons (normally

Table 1 Detection approaches applied for the identification of corrosion microbial communities

Detection approach	Specificity	Throughputs	Functional information	Prior information	Amplification
Culture-dependent methods	Targeted one or a group of microorganisms	Low	Depends on the culture media	Culture media selection	N/A
16S rRNA genes sequencing	All the 16S rRNA genes	High	Not directly	Required for primer selection	Yes
Metagenomic sequencing	All DNA fragments	High	Direct	No	No
FISH	Target DNA fragments	Low	Yes	Yes	No

16S rRNA genes) for community profiling and of whole community DNA for metagenomics (Table 1). Most of the corrosion community profiling is based on sequences of the small subunit ribosomal genes, where 16S rRNA genes are used commonly for the detection of bacteria and archaea [11]. Using this approach, 16S rRNA genes in DNA samples extracted from corrosion layers are amplified by relevant primers using the polymerase chain reaction (PCR) and further analyzed against 16S databases, i.e., Greengenes, Silva, and EzBioCloud, for microorganism identification. This provides thousands of gene reads that represent operational taxonomic units (OTUs) within the sample. The 16S rRNA sequencing provides direct information regarding the taxonomic composition and phylogenetic diversity of corrosion layer samples. However, the reads obtained in 16S rRNA gene sequencing are short reads of a few hundred bases, so the resolution for identification of the OTU is limited to the order, family, or genus level at best [11]. The major bias of the 16S rRNA gene sequencing is introduced by the PCR amplification of genes from corrosion samples. It is reported that the success of the amplification can be variable, and this likely relates to the quality and quantity of DNA extracted from such samples and also the primer used for PCR [22]. The relatively low levels of microorganisms in the samples and the co-extraction of molecules inhibitory to the PCR amplification would challenge molecular-based studies.

Furthermore, 16S rRNA sequencing cannot directly identify metabolic or other functional capabilities of the microorganisms under study (Table 1). Some recent studies have extended these intuitions to predict the functional contribution of particular community members through different bioinformatic tools such as Tax4Fun and BugBase algorithms for selected Kyoto Encyclopedia of Genes and Genomes (KEGG) pathways [23]. The accuracy of such approaches has not been evaluated, but the correlation between gene content and phylogeny (excepting special cases such as laterally transferred elements and intracellular endosymbionts with reduced genomes) suggests that it may be possible to approximately predict the functional potential of microbial communities from phylogeny [24]. Nevertheless, the approach

has been extremely enlightening and has led to significant new insights into the microbial communities involved in sewer concrete corrosion.

Another culture-independent method for understanding microbial community composition and function is metagenomic sequencing. This approach sequences the total genomic component and utilizes bioinformatics tools to directly access the genetic content of the entire community [25]. Compared with the 16S rRNA gene method, metagenomics not only reveals the taxonomic diversity of a community but also allows the detection of functional genes and the compilation of complete and near-complete genomes of the microorganisms within a sample. Conversely, metagenomic sequencing aims to sample all genes from a community and can produce detailed metabolic and functional profiles [24]. However, metagenomic sequencing has a higher requirement for the quality and quantity of DNA extracted from such samples, longer handling time, and cost. In particular, the concrete corrosion layer is inherently low in biomass quantity but high in inorganic compounds such as corrosion products including gypsum and ettringite [11], which limits the application of metagenomic sequencing. To date, only one study has applied metagenomic sequencing for the characterization of corrosion microbial community in sewers [25].

Apart from DNA-based analysis, cells in corrosion layers can also be detected directly using probes targeting rRNA molecules by fluorescence in situ hybridization (FISH). This approach allows the real quantitative estimations of cells in samples and can target a couple of microorganisms or microorganism groups. The specificity of FISH relies on the choice of probes. By performing the hybridization in solution (rather than directly on samples dried onto microscope slides) and filtering portions of the solution onto black filters for microscopy, the total cell density and a key ASOM (i.e. *Acidithiobacillus*) were identified [26]. Another study also identified the density of *Acidithiobacillus* in corroded mortar samples [5]. Both studies managed to detect *Acidithiobacillus* using its specific genus level probes, the use of a more extensive range of probes is required to obtain a more complete picture of community compositions. Overall, this approach is rarely applied to characterize the corrosion community in sewers. FISH of concrete samples is conceivably a difficult procedure due to the combination of relatively meagre cell densities, variable cell activity, and interfering autofluorescence from mineral particles [11].

3 Microbial Communities in Concrete Corrosion Layers

3.1 *Neutrophilic Sulfur-Oxidizing Microorganisms in Corrosion Layers*

As mentioned in the above sections, the sulfur-oxidizing microorganisms are important protagonists of the corrosion process as they accelerate the reduction of surface pH through the production of various sulfur compounds including sulfuric acid

Table 2 Physiological characteristics of key NSOM detected in corrosion layers

NSOM	Range of pH for growth	Sulfur substrate	Products
<i>Thiobacillus thioeparus</i>	6–10	H ₂ S, S ⁰ , S ₂ O ₃ ²⁻	S ⁰ , Polythionic acids
<i>Halothiobacillus neapolitanus</i> (formerly <i>Thiobacillus neapolitanus</i>)	6–8	S ⁰ , S ₂ O ₃ ²⁻	Polythionic acids, SO ₄ ²⁻
<i>Thiobacillus plumbophilus</i>	4–6.5	H ₂ S	–
<i>Thiomonas sp.</i>	3–9	H ₂ S, S ₂ O ₃ ²⁻	SO ₄ ²⁻
<i>Thiobacillus novellus</i>	6–8	S ₂ O ₃ ²⁻	S ⁰

[11]. With the gradual decrease of the concrete surface pH, microbial communities in corrosion layers go through a temporal succession from NSOM to ASOM. Both NSOM and ASOM use reduced forms of sulfur as energy sources, but respectively, have a preference for growth at a neutral or acidic pH [1]. NSOM starts to colonize the surface once the pH of concrete is reduced to 9, and produces various sulfur compounds to eventually lower the pH to 5–3 [3]. Depending on the pH and availability of sulfur compounds in corrosion layers, various dominant NSOM species have been detected (Table 2) including *Thiobacillus thioeparus*, *Thiobacillus plumbophilus* (formally as *Sulfuriferula plumbophilus*) [27], *Thiomonas sp.*, *Thiobacillus novellus* and *Halothiobacillus neapolitanus* [5, 28, 29].

Thiothrix spp. and *Thiomonas* spp. can grow chemoorganoheterotrophically or chemolithoautotrophically using either organic carbon or the inorganic sulfur species H₂S, S₂O₃²⁻, and S⁰ as electron donors. In comparison, *Halothiobacillus sp.* are obligate chemolithoautotrophic sulfur-oxidizing bacteria. The initial activity of NSOM on the sewer surface provides suitable conditions for subsequent colonization by ASOM [1, 5, 17, 30, 31]. Some heterotrophic and neutrophilic bacteria, including *Psychrobacter fozii*, *Planococcus antarcticus*, *Polaromonas naphthalenivorans*, and *Acidovorax delafieldii*, were also detected at the end of the initiation stage when the pH of concrete was neutralized to around 8 [5, 32]. The role of these heterotrophic microbes has not been clearly revealed. Although they are not involved in the sulfur oxidation process, they can scavenge organic compounds produced by the growth and metabolic activities of NSOM [33].

3.2 Acidophilic Sulfur-Oxidizing Microorganisms in Corrosion Layers

Through culture-dependent methods, *Acidithiobacillus* is the most typical genus of ASOM detected in corrosion layers [11]. The prominent species of *Acidithiobacillus* include *Acidithiobacillus ferrooxidans*, *Acidithiobacillus thiooxidans*, and *Acidithiobacillus caldus* [5, 25, 28, 34, 35]. *Acidithiobacilli* are autotrophic

sulfur-oxidizing bacteria, which is an essential advantage in such an environment on concrete surfaces with low organic carbon availability and high levels of reduced sulfur compounds [33]. *Acidithiobacillus thiooxidans* is the most commonly cultured organism among the *Acidithiobacillus* from sewer concrete corrosion [1]. Recent culture-independent methods revealed a more diverse range of ASOMs in corrosion layers. However, there are instances where NGS analyses report low abundance or no detection of *A. thiooxidans* in sewer corrosion samples [22, 29]. *Mycobacterium* spp. are often detected as abundant in acidophilic communities of sewer corrosion layers [5, 22, 36]. In corrosion layers from two sewers in Sydney, *Acidiphilium* spp. and *Mycobacterium* spp. were the most dominant acidophilic microbial groups across the 10 samples examined, while *Acidithiobacillus* spp. was prominent in only one sample and made up < 3% of the total populations in all other samples [22]. In another study, in 5 of the 6 crown samples, *Mycobacterium* spp. dominated with the abundance of 45–98% among all the detected bacteria, while *Acidithiobacillus* spp. were prominent in only 2 crown samples with the abundance of 28–36% [36]. Previously, *Mycobacterium* were assumed to have a heterotrophic role in MICC, however, recently an acidophilic *Mycobacterium* sp. has been observed to oxidize sulfur and produce acid [37].

Significant proportions of *Xanthomonadales* spp., *Burkholderiales* spp., and *Sphingobacteriales* spp. were detected in wall and ceiling samples of the sewers [22]. The *Xanthomonadales* spp. have been reported in other sewer corrosion environments and are considered primarily as heterotrophs [25, 29, 35]. However, the *Xanthomonadales* sequence from Cayford et al. [22] phylogenetically affiliates with *Xanthomonadales* spp., which are capable of sulfur oxidation [38].

On one occasion *Ferroplasma* spp. are reported in severely corroded concrete biofilms with an extremely low pH [28]. *Ferroplasma* spp. are extreme acidophiles and versatile heterotrophs that can oxidize iron [39]. Heterotrophic fungi have also been detected in acidic corrosion layers (pH 2.6), and are found to exist in a symbiotic relationship with ASOM by oxidizing H₂S to thiosulfate and by utilizing organic compounds produced by the bacteria [40]. Another study isolated fungi from corroding concrete which was identified as a *Fusarium* sp. [41]. However, *Fusarium* sp. are not reported to be acidophilic, although they are suggested to contribute to the corrosion process by producing organic acids [41].

With the diversity of microorganisms detected in corrosion layers, the role of each microorganism is also of high interest for researchers. Under pH 2–3, the oxidation of reduced sulfur compounds would be the major energy source in the oxidative corrosion layers of the dark sewer, an environment that is low in other inorganic or organic electron-donating molecules. Reduced iron is another electron source that may be present mainly due to the reinforcing bar used in the concrete pipe. In relation to the limited types of electron donors, the important metabolic functions of different acidophilic microbes found in the sewer corrosion layer of concrete are thus summarized in Table 3.

Acidithiobacillus spp., as chemolithoautotrophs, are a keystone group in the corrosion community. This group undertakes the activities of sulfur-oxidation (and iron-oxidation for some species), carbon-fixation, production of extracellular polymeric

Table 3 Specific microorganisms detected in acidic concrete corrosion layers and their functions adapted from [11] (open access)

Species	Frequency of detection	Abundance	Potential functions
<i>Acidithiobacillus thiooxidans</i>	Nearly always	3–95%	Sulfur-oxidation Carbon-fixation Acid Production EPS formation
<i>Acidithiobacillus ferrooxidans</i>	Often	2–9%	Sulfur-oxidation Carbon-fixation Acid Production Iron-oxidation EPS formation
<i>Acidithiobacillus caldus</i>	Often	35–50%	Sulfur-oxidation Carbon-fixation Acid Production Iron-oxidation
<i>Acidiphilium</i> spp.	Often	50–70%	H ₂ S-oxidation Organic carbon utilization
<i>Mycobacterium</i> spp.	Often	17–45%	Possible H ₂ S-oxidation Organic carbon utilization
<i>Ferroplasma</i> spp.	Rarely	Not reported	Iron-oxidation Organic carbon utilization
<i>Xanthomonadaceae</i>	Occasionally	5–20%	Organic carbon utilization
<i>Fungi</i>	Occasionally	Not reported	H ₂ S-oxidation EPS formation

substances (EPS), and the generation of sulfuric acid. The production of EPS would be an important activity that enables the biofilms in the corrosion layer to exist. As a major component of the biofilm matrix, biofilm would provide favorable habitat for the EPS producers and for other non-EPS producing microorganisms [42]. It is estimated that *Acidithiobacillus* spp. excrete as much as 20% of the CO₂ they fix as small organic substances [43], and these excreted organic molecules can be inhibitory to their own growth [5]. Typically, the corrosion layer is expected to be low in organic carbon levels and the molecules excreted by *Acidithiobacillus* spp. would be an important organic carbon source for energy and growth of the heterotrophic members of the microbial communities.

Mutualistic relationships between *Acidithiobacillus* spp. and heterotrophs, that can degrade such inhibitory organic compounds, are proposed [40, 44]. Therefore, simple roles for the proposed heterotrophs, such as *Mycobacterium* spp., *Xanthomonadales*, *Ferroplasma* spp., and fungi found in the sewer corrosion communities, would be the degradation of the secreted organic compounds and the production of CO₂. These activities would maintain favorable conditions for the growth of the chemolithoautotrophs and enable their activities to continue, which would enhance the sewer corrosion. Based on these observations, a conceptual model for the corrosion layer is proposed (Fig. 3). The microbial biofilm is dense near the surface of

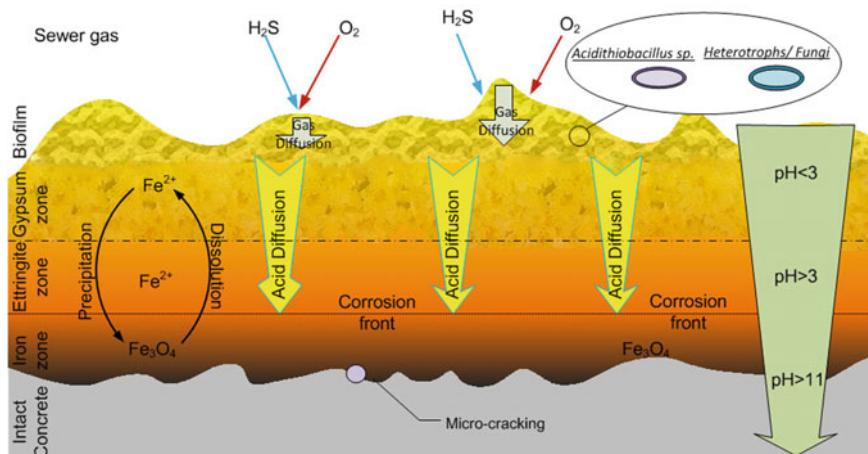


Fig. 3 A conceptual model for the sewer concrete corrosion layer. See the text for description of the activities within the zones. From [11] with open access

the corrosion layer where the diffused oxygen and H_2S levels are high. Sulfuric acid is generated by SOM in the biofilm, and this diffuses through the corrosion layer towards the surface of the intact concrete [5]. With the acid diffusion, the gypsum ($\text{pH} < 3$) and ettringite zones ($\text{pH} > 3$) are formed and as they are expansive, together with iron mineral precipitation, cause cracking of the intact concrete.

Some heterotrophs in this environment are also found to have the ability to oxidize H_2S or iron. *Acidiphilium* spp. are sulfur-oxidizing heterotrophs that are often detected in corrosion layer communities. Additionally, *Acidiphilium* are known to reduce ferric iron in anaerobic conditions [45], although, that activity is likely negligible in the aerobic concrete corrosion layers. *Leptospirillum* spp. are also detected in corroding concrete. They are common in very acidic, iron-rich environments, and are obligate iron oxidizers [45]. Their presence in this environment may be related to the dissolution of iron bar used for sewer pipe reinforcement.

Iron oxidation is considered less important with regard to concrete sewer corrosion as iron is generally in low concentrations in this environment. However, iron is often embedded in sewer pipes to reinforce the concrete, and during concrete loss, this becomes exposed to corroding conditions. Iron oxidizing microbes detected in sewer corrosion layers include *A. ferrooxidans* and *Ferroplasma* spp. (Table 3). *A. ferrooxidans* is the most well studied of all acidophiles with regard to iron oxidation. Through oxidation of ferrous to ferric iron in *A. ferrooxidans* electrons are transferred to reduce oxygen and this utilizes protons within the cell. *Ferroplasma* spp. also uses iron oxidation as an energy conservation process [46] through Fe(II) oxidation that transfers electrons for the intracellular reduction of O_2 [47]. In certain circumstances, it may be the case that acidophilic microorganisms in sewer corrosion are utilizing iron oxidation as the primary mechanism for energetic and growth requirements.

4 Summary

This chapter briefly introduced the corrosion development in concrete sewers and the change of corrosion layer conditions and microbial communities with the corrosion development. The corrosion development is largely affected by the corrosive conditions inside sewers, where environmental factors such as H₂S levels, relative humidity, temperature, and contact with wastewater play crucial roles in corrosion development. The corrosive conditions within sewers are dynamic with great temporal and spatial variations. Although the impact of each environmental parameter on the corrosion development still needs future investigations, the pH change of corrosion layers shows a direct indicator for the corrosion development and corrosion layer conditions.

During the corrosion process, no clear corrosion front can be differentiated from the concrete matrix until the surface reaches active conditions. Along with the reduction of surface pH, a temporal succession of key corrosion-inducing microorganisms from NSOM to ASOM also occurs. For the identification of microbial communities in corrosion layers, culture-dependent and culture-independent methods have been applied. NGS approaches greatly advanced the understanding of corrosion-inducing microbial communities and provided revealing insights. Diverse communities of ASOM and NSOM have been detected by NGS, along with heterotrophic bacteria. The core members of NSOM and ASOM along with their functions are summarized in this chapter. In aerobic sewer biofilms, the NSOM and ASOM play an important role in sulfur oxidation and carbon fixation, while heterotrophs degrade the extracellular organic molecules to support their growth, which also removes the presence of small organic molecules that may be toxic to NSOM and ASOM. The understanding of corrosion communities is crucial for the control and mitigation of sewer corrosion and preventing structure failure.

References

1. Islander, R.L., Devinny, J.S., Mansfeld, F., Postyn, A., Shih, H.: Microbial ecology of crown corrosion in sewers. *J. Environ. Eng.* **117**, 751–770 (1991)
2. Joseph, A.P., Keller, J., Bustamante, H., Bond, P.L.: Surface neutralization and H₂S oxidation at early stages of sewer corrosion: Influence of temperature, relative humidity and H₂S concentration. *Water Res.* **46**, 4235–4245 (2012)
3. Sand, W.: Importance of hydrogen sulfide, thiosulfate, and methylmercaptan for growth of thiobacilli during simulation of concrete corrosion. *Appl. Environ. Microbiol.* **53**, 1645–1648 (1987)
4. Kong, L., Lu, H., Fu, S., Zhang, G.: Effect of corrosion layer on the deterioration of concrete in gravity sewers. *Constr. Build. Mater.* **272**, 121663 (2021)
5. Okabe, S., Odagiri, M., Ito, T., Satoh, H.: Succession of sulfur-oxidizing bacteria in the microbial community on corroding concrete in sewer systems. *Appl. Environ. Microbiol.* **73**, 971–980 (2007)

6. Song, Y., Tian, Y., Li, X., Wei, J., Zhang, H., Bond, P.L., Yuan, Z., Jiang, G.: Distinct microbially induced concrete corrosion at the tidal region of reinforced concrete sewers. *Water Res.* **150**, 392–402 (2019)
7. Cayford, B.I.: Investigation of the microbial community and processes responsible for the corrosion of concrete in sewer systems. The degree of Doctor of Philosophy, University of Queensland (2012)
8. Jiang, G., Keller, J., Bond, P.L.: Determining the long-term effects of H₂S concentration, relative humidity and air temperature on concrete sewer corrosion. *Water Res.* **65**, 157–169 (2014)
9. Wells, T., Melchers, R.E.: Modelling concrete deterioration in sewers using theory and field observations. *Cem. Concr. Res.* **77**, 82–96 (2015)
10. Jiang, G., Sun, X., Keller, J., Bond, P.L.: Identification of controlling factors for the initiation of corrosion of fresh concrete sewers. *Water Res.* **80**, 30–40 (2015)
11. Li, X., Jiang, G., Kappler, U., Bond, P.: The ecology of acidophilic microorganisms in the corroding concrete sewer environment. *Front. Microbiol.* **8**, 683 (2017)
12. O’Dea, V.: Understanding biogenic sulfide corrosion. *Mater. Perform.* **46**, 36–39 (2007)
13. Vollertsen, J., Nielsen, A.H., Jensen, H.S., Wium-Andersen, T., Hvitved-Jacobsen, T.: Corrosion of concrete sewers—the kinetics of hydrogen sulfide oxidation. *Sci. Total Environ.* **394**, 162–170 (2008)
14. Sublette, K.L., Kolhatkar, R., Raterman, K.: Technological aspects of the microbial treatment of sulfide-rich wastewaters: A case study. *Biodegradation* **9**, 259–271 (1998)
15. Ward, M., Corsi, R., Morton, R., Knapp, T., Apgar, D., Quigley, C., Easter, C., Witherspoon, J., Pramanik, A., Parker, W.: Characterization of natural ventilation in wastewater collection systems. *Water Environ. Res.* **83**, 265–273 (2011)
16. Wells, T., Melchers, R., Joseph, A., Bond, P., Vitanage, D., Bustamante, H., De Grazia, J., Kuen, T., Nazimek, J., Evans, T.: A collaborative investigation of the microbial corrosion of concrete sewer pipe in Australia. In: *OzWater-12 Australia’s National Water Conference and Exhibition*, pp. 8–10 (2012)
17. Davis, J.L., Nica, D., Shields, K., Roberts, D.J.: Analysis of concrete from corroded sewer pipe. *Int. Biodeterior. Biodegradation* **42**, 75–84 (1998)
18. Keller, M., Zengler, K.: Tapping into microbial diversity. *Nat. Rev. Microbiol.* **2**, 141–150 (2004)
19. Grengg, C., Mittermayr, F., Koraimann, G., Konrad, F., Szabó, M., Demeny, A., Dietzel, M.: The decisive role of acidophilic bacteria in concrete sewer networks: A new model for fast progressing microbial concrete corrosion. *Cem. Concr. Res.* **101**, 93–101 (2017)
20. Staley, J.T., Konopka, A.: Measurement of in situ activities of nonphotosynthetic microorganisms in aquatic and terrestrial habitats. *Annu. Rev. Microbiol.* **39**, 321–346 (1985)
21. Ward, D.M., Weller, R., Bateson, M.M.: 16S rRNA sequences reveal numerous uncultured microorganisms in a natural community. *Nature* **345**, 63–65 (1990)
22. Cayford, B.I., Dennis, P.G., Keller, J., Tyson, G.W., Bond, P.L.: High-throughput amplicon sequencing reveals distinct communities within a corroding concrete sewer system. *Appl. Environ. Microbiol.* **78**, 7160–7162 (2012)
23. Mathews, E.R., Semene, L., Wood, J.L., Batinovic, S., Billington, N., Phillips, D., Barnett, D., Petrovski, S., Franks, A.E.: Sewer tidal biofilm communities are dominated by mix of acidophilic microorganisms at high H₂S producing sites. Exploring the effects of treatments for sewer corrosion on H₂S-producing microbial communities in an operational sewer, vol. 126 (2019)
24. Langille, M.G.I., Zaneveld, J., Caporaso, J.G., McDonald, D., Knights, D., Reyes, J.A., Clemente, J.C., Burkepile, D.E., Vega Thurber, R.L., Knight, R., Beiko, R.G., Huttenhower, C.: Predictive functional profiling of microbial communities using 16S rRNA marker gene sequences. *Nat. Biotechnol.* **31**, 814–821 (2013)
25. Gomez-Alvarez, V., Revetta, R.P., Santo Domingo, J.W.: Metagenome analyses of corroded concrete wastewater pipe biofilms reveal a complex microbial system. *BMC Microbiol.* **12**, 1 (2012)

26. Hernandez, M., Marchand, E.A., Roberts, D., Peccia, J.: In situ assessment of active *Thiobacillus* species in corroding concrete sewers using fluorescent RNA probes. *Int. Biodeterior. Biodegradation* **49**, 271–276 (2002)
27. Watanabe, T., Kojima, H., Fukui, M.: *Sulfuriferula multivorans* gen. nov., sp. nov., isolated from a freshwater lake, reclassification of '*Thiobacillus plumbophilus*' as *Sulfuriferula plumbophilus* sp. nov., and description of *Sulfuricellaceae* fam. nov. and *Sulfuricellales* ord. nov. *Int. J. Syst. Evol. Microbiol.* **65**, 1504–1508 (2015)
28. Ling, A.L., Robertson, C.E., Harris, J.K., Frank, D.N., Kotter, C.V., Stevens, M.J., Pace, N.R., Hernandez, M.T.: High-resolution microbial community succession of microbially induced concrete corrosion in working sanitary manholes. *PLoS ONE* **10**, e0116400 (2015)
29. Santo Domingo, J.W., Revetta, R.P., Iker, B., Gomez-Alvarez, V., Garcia, J., Sullivan, J., Weast, J.: Molecular survey of concrete sewer biofilm microbial communities. *Biofouling* **27**, 993–1001 (2011)
30. Jiang, G., Sun, J., Sharma, K.R., Yuan, Z.: Corrosion and odor management in sewer systems. *Curr. Opin. Biotechnol.* **33**, 192–197 (2015)
31. Mild, K., Sand, W., Wolff, W., Bock, E.: *Thiobacilli* of the corroded concrete walls of the Hamburg sewer system. *Microbiology* **129**, 1327–1333 (1983)
32. Parker, C. D.: The corrosion of concrete. *Aust. J. Exp. Biol. Med. Sci.* **23**(2) 81–90 (1945). <https://doi.org/10.1038/icb.1945.13>
33. Nica, D., Davis, J.L., Kirby, L., Zuo, G., Roberts, D.J.: Isolation and characterization of microorganisms involved in the biodeterioration of concrete in sewers. *Int. Biodeterior. Biodegradation* **46**, 61–68 (2000)
34. Jiang, G., Zhou, M., Chiu, T.H., Sun, X., Keller, J., Bond, P.L.: Wastewater-enhanced microbial corrosion of concrete sewers. *Environ. Sci. Technol.* **50**, 8084–8092 (2016)
35. Satoh, H., Odagiri, M., Ito, T., Okabe, S.: Microbial community structures and in situ sulfate-reducing and sulfur-oxidizing activities in biofilms developed on mortar specimens in a corroded sewer system. *Water Res.* **43**, 4729–4739 (2009)
36. Pagaling, E., Yang, K., Yan, T.: Pyrosequencing reveals correlations between extremely acidophilic bacterial communities with hydrogen sulphide concentrations, pH and inert polymer coatings at concrete sewer crown surfaces. *J. Appl. Microbiol.* **117**, 50–64 (2014)
37. Kusumi, A., Li, X.S., Katayama, Y.: Mycobacteria isolated from Angkor monument sandstones grow chemolithoautotrophically by oxidizing elemental sulfur. *Front Microbiol* **2**, 104 (2011)
38. Lee, C.S., Kim, K.K., Aslam, Z., Lee, S.-T.: *Rhodanobacter thiooxydans* sp. nov., isolated from a biofilm on sulfur particles used in an autotrophic denitrification process. *Int. J. Syst. Evol. Microbiol.* **57**, 1775–1779 (2007)
39. Ferrer, M., Golyshina, O.V., Beloqui, A., Golyshin, P.N., Timmis, K.N.: The cellular machinery of *Ferroplasma acidiphilum* is iron-protein-dominated. *Nature* **445**, 91 (2007)
40. Cho, K.-S., Mori, T.: A newly isolated fungus participates in the corrosion of concrete sewer pipes. *Water Sci. Technol.* **31**, 263–271 (1995)
41. Gu, J.-D., Ford, T.E., Berke, N.S., Mitchell, R.: Biodeterioration of concrete by the fungus *Fusarium*. *Int. Biodeterior. Biodegradation* **41**, 101–109 (1998)
42. Flemming, H.-C., Wingender, J.: The biofilm matrix. *Nat. Rev. Microbiol.* **8**, 623–633 (2010)
43. Karavaiko, G., Pivovarova, T.: Oxidation of elementary sulfur by *Thiobacillus thiooxydans*. *Mikrobiologiya* **42**, 389 (1973)
44. Peccia, J., Marchand, E.A., Silverstein, J., Hernandez, M.: Development and application of small-subunit rRNA probes for assessment of selected *Thiobacillus* species and members of the genus *Acidiphilium*. *Appl. Environ. Microbiol.* **66**, 3065–3072 (2000)
45. Hallberg, K.B., Johnson, D.B.: Biodiversity of acidophilic prokaryotes. *Adv. Appl. Microbiol.* **49**, 37–84 (2001)
46. Dopson, M., Lindström, E.: Analysis of community composition during moderately thermophilic bioleaching of pyrite, arsenical pyrite, and chalcopyrite. *Microb. Ecol.* **48**, 19–28 (2004)
47. Allen, E.E., Tyson, G.W., Whitaker, R.J., Detter, J.C., Richardson, P.M., Banfield, J.F.: Genome dynamics in a natural archaeal population. *Proc. Natl. Acad. Sci.* **104**, 1883–1888 (2007)

A Systematic Laboratory Testing of Concrete Corrosion Resistance in Sewers



Guangming Jiang, Xiaoyan Sun, Jurg Keller, Xuan Li, Yarong Song, Markus Schmid, and Günther Walenta

Abstract This chapter developed a Systematic Corrosion Resistance (SCORE) testing to determine the concrete corrosion resistance in urban wastewater systems, primarily sewers. Microbially induced concrete corrosion has a profound impact on the useful service life of concrete sewers, which leads to billions of dollars of economic loss annually. Concrete is widely used in the rehabilitation or construction of new wastewater infrastructure. It is vital to quantitatively measure the corrosion resistance for a reliable and sustainable design. The testing of corrosion resistance is primarily based on the measurements of initiation time and corrosion rate, in combination with corrosion development parameters including surface pH, sulfur

G. Jiang (✉) · X. Li

School of Civil, Mining, Environmental and Architectural Engineering, University of Wollongong, Wollongong, NSW 2522, Australia

e-mail: gjiang@uow.edu.au

X. Li

e-mail: xuan.li@uts.edu.au

X. Sun

School of Civil Engineering, Sun Yat-Sen University, Zhuhai 519082, China

e-mail: sunxy55@mail.sysu.edu.cn

J. Keller · Y. Song

Australian Centre for Water and Environmental Biotechnology, The University of Queensland, Brisbane, QLD 4072, Australia

e-mail: j.keller@uq.edu.au

Y. Song

e-mail: yarong.song@uq.edu.au

X. Li

Centre for Technology in Water and Wastewater, School of Civil and Environmental Engineering, University of Technology Sydney, Ultimo, Sydney, NSW 2007, Australia

M. Schmid · G. Walenta

Calucem GmbH, Besselstraße 8, 68219 Mannheim, Germany

e-mail: markus.schmid@calucem.com

G. Walenta

e-mail: gunther.walenta@calucem.com

© The Author(s), under exclusive license to Springer Nature Switzerland AG 2023

G. Jiang (ed.), *Microbiologically Influenced Corrosion of Concrete Sewers*, Engineering Materials, https://doi.org/10.1007/978-3-031-29941-4_6

compounds, and sulfide uptake rate. The different corrosion parameters support each other to make a cohesive comparison of different concrete products. Two newly developed Calucon concrete products were demonstrated with different corrosion resistance using this testing approach. In addition, advanced microscopic methods and microbial community analysis will help to optimize the concrete design by providing insights into the corrosion resistance. The systematic testing approach has been applied in large-scale concrete sewers and showed its effectiveness in supporting the service life design.

1 Introduction

Microbiologically influenced concrete corrosion induced by hydrogen sulfide in sewer systems leads to early structural failure and shortened life expectancy of pipes and other structures (pump wells, manholes, etc.) made of concrete [1–3]. The corrosion damaged concrete sewer infrastructure is costly to replace or rehabilitate. In sewers, hydrogen sulfide is mainly produced in the fully anaerobic conditions present in rising mains (pressure pipes) after pump stations or slowly flowing gravity driven sewer pipes. Sulfate-reducing bacteria residing in anaerobic sewer biofilms or sediments are the primary source of sulfide production [4]. Once the sulfide containing wastewater is discharged into the gravity pipes partially filled with sewage, the transfer of gaseous H_2S from the liquid phase to the head space of the pipe can take place. H_2S in the gas phase then transfers to the exposed surface of the concrete pipes above the wastewater line, where it is oxidized to sulfuric acid by mostly sulfide-oxidizing bacteria [5–8]. The sulfuric acid produced in this biological pathway can penetrate into the pores of concrete and react with the cement compounds (particularly the Ca and Al minerals) to form highly expansive minerals like gypsum and ettringite ($3CaO \cdot Al_2O_3 \cdot 3CaSO_4 \cdot 31H_2O$, or the monosulfate form $3CaO \cdot Al_2O_3 \cdot CaSO_4 \cdot 12H_2O$ when sulfate concentration is not high enough to stabilize the ettringite) [3, 9–11]. This process leads to concrete surface pH reduction, formation of loosely bound corrosion products with little mechanical strength, and thus loss of mass and eventually structural failure of the concrete pipes.

Model is a helpful tool to predict concrete corrosion in sewers. However, the relationship between H_2S concentration and concrete corrosion is unknown yet [12–14]. The types of concrete and their properties are also detrimental factors for the corrosion resistance, including its corrosion initiation time, active corrosion rate and other corrosion parameters [15]. The design and construction of new concrete sewer systems require the detailed characterization of concrete to be used in terms of its corrosion resistance, especially when sulfide induced MICC is the primary deterioration for the structure. Such corrosion resistance would be equally important for the operation, maintenance, and management of sewer systems to achieve the designed service life [16]. Water utilities need to measure the corrosion during sewer inspection and such accurate measurement does not exist yet due to the complexity of MICC and the destructive nature of many corrosion testing methods.

The concrete can be designed to use different binding materials (cement), ratios of water/cement, various admixtures, and curing conditions [17–20]. Many researchers have been working on the development of more corrosion-resistant and durable concrete for the corrosive sewer environments. For a specific concrete product, its corrosion resistance needs to be quantified experimentally through biocorrosion tests. However, due to the lack of a standard, various methods have been reported for the test of various concrete products. Experimental methods include chemical immersion tests, microbiological simulation tests, and *in-situ* tests [21–30]. Chemical immersion tests can only simulate the fast chemical reactions between concrete and acids. Thus, such tests provide a simple and accelerated way for the evaluation of concrete corrosion resistance to sulfuric acid. Major disadvantages are apparent since the tests are not based on the MICC mechanism and results from different studies are incomparable due to the different accelerations employed. Most importantly, chemical immersion tests cannot provide a meaningful corrosion rate as biological processes might be the rate-controlling steps in MICC, which are not taken into consideration in these tests.

In comparison to chemical immersion tests, microbiological simulation tests and *in-situ* tests incorporate both biological processes and chemical reactors, which can represent the MICC mechanisms better. Especially, microbiological simulation tests can be delivered in laboratory-scale corrosion chambers simulating different sewers under well-controlled conditions [31, 32]. The *in-situ* test is usually difficult to achieve as it requires a representative working sewer environment [33–35].

Another important consideration for the evaluation of corrosion resistance is the choice of corrosion parameters, which will require different analytical techniques. Previously, various approaches, e.g. measurement of concrete surface pH and corrosion layer thickness, analysis of corrosion products and microbial characterization within corrosion layer, were used to monitor and analyze the corrosion processes in sewers [36–38]. However, the availability and usefulness of these methods has limits. For example, it is difficult to monitor corrosion progress through pH measurement under acidic conditions (heavily corroded concrete) as the pH may stagnate when it decreases to about 3–5 [39, 40]. Therefore, surface pH is only indirectly related to the corrosion process, and thus not a good indicator of corrosion rate.

The corrosion rate may be determined by direct detection of the corrosion layer thickness. However, this requires removal of the surface corrosion layer, which is destructive, disrupting the continuous monitoring of the corrosion process. Additionally, detection of the corrosion layer thickness is technically very difficult. In the corrosion process the concrete samples will corrode and malform, this making it extremely difficult to maintain a point of reference so that the change in concrete thickness can be determined. Specialized approaches, such as imbedding non-corroding components are required, and these can be difficult and expensive to implement within concrete samples. Consequently, obtaining corrosion rates by direct detection requires years of monitoring activity and is very demanding on resources [37].

Microbial analysis is arduous, time consuming and costly and currently quantitative analysis has not been correlated with corrosion rates [40]. Moreover, the

understanding of corrosion microbial communities is still very limited, advanced sequencing techniques reveal that unexpected microbial types can be abundant [36], and most investigations are restricted to severely corroded concrete, thus early stage microbiology is not well studied.

Consequently, it is critical to develop a systematic microbiological simulation test with a set of corrosion parameters to be measured in order to fully quantify the corrosion resistance of a concrete product. This chapter presents such a systematic testing approach, with demonstrative results being obtained from some highly corrosion resistant concrete products to be used for the construction of a large-scale sewer system. A detailed design of the corrosion chamber, preparation of concrete samples, testing parameters and their interpretation were discussed in detail to encourage the development of this systematic approach as a standard corrosion resistance test in the future.

2 Material and Methods

This section describes all the required steps involved in a systematic evaluation of the corrosion resistance of concrete products, including preparing the sample, as well as the biocorrosion simulation chambers, testing parameters, analytical methods and data interpretation for the potential service life.

2.1 *Sample Preparation and Pre-Treatment*

The corrosion resistance test is conducted using multiple coupons of the same concrete products for two reasons: (1) temporal measurements at different exposure time to obtain corrosion rate and other parameters related to corrosion resistance; (2) some measurements are destructive or severely disturbing to the ongoing corrosion processes. Each concrete coupon is designed in a size of $100 \times 70 \times 50$ mm, to ensure enough depth (50 mm) to quantify the corrosion deterioration and enough exposure surface (100×70 mm) to obtain multiple sampling areas for parameters like surface pH and corrosion products for chemical and microbial analysis.

It is recommended to commission a concrete specialist provider or concrete research lab to cast the concrete product in a large block, which can then be cut to the required coupon size. This ensures that all concrete coupons are cast and cured at the same conditions and thus present replicates for each other. The cast and curing should be carried out according to the product-specific concrete design which is geared for maximum performance in application. As an example, beams (prisms) with dimensions of $400 \times 100 \times 100$ mm (L \times W \times H) are cast for the corrosion resistance test. Two beams were prepared for each type of concrete mix design. The beams are cut as shown in Fig. 1, to provide ten test specimens per beam, a total of 20 coupons per type of concrete. It is recommended to prepare surplus concrete

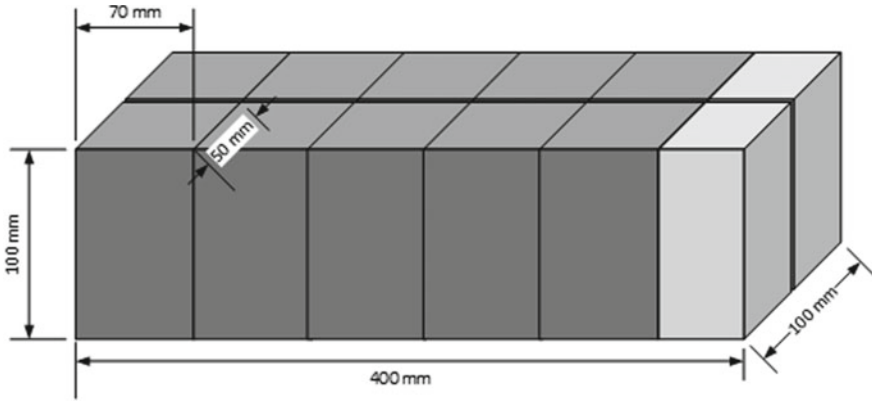


Fig. 1 Schematic of the concrete specimens cutting plan, to make 10 specimens from one standard $400 \times 100 \times 100$ mm concrete prism

specimens for each type of concrete in case of any imperfections or damages in some of the specimens. The two residual $50 \times 50 \times 100$ mm block (light grey in Fig. 1) can be discarded as left-over.

The bottom surface (100×70 mm) will be used as the exposure surface while the other surfaces of each specimen are covered by epoxy in the stainless-steel frame, as shown in Fig. 2. Maximum tolerance on specimen dimensions is $+ / - 3$ mm. After cutting and embedding in frames, these samples will be installed into corrosion chambers for bio-corrosion testing, which can determine corrosion resistance parameters including corrosion rate.

Concrete specimens can be water-saturated during the despatch to the corrosion chamber. However, precaution should be taken to not mix different types of concrete in one container to avoid cross-contamination. The test can cover both the corrosion initiation stage and the active deterioration stage. To skip the initiation stage, concrete coupons for corrosion resistance tests will be pre-treated to reduce surface pH by immersing or spraying the exposure surface with sulfuric acid. The surface pH should be acidic (2–4) to facilitate the growth of acidophilic microorganisms. After the pre-treatment with acid, the coupons will be placed in the corrosion chambers. For the first 2 months, the concrete coupons will be inoculated (spraying domestic wastewater on the concrete surface) with real wastewater weekly to induce active microbiologically influenced concrete corrosion. After the inoculation period, the corrosion development and activity will be monitored using surface pH, sulfide uptake rate (SUR), photogrammetry, weight change and sulfur compounds (as described below).

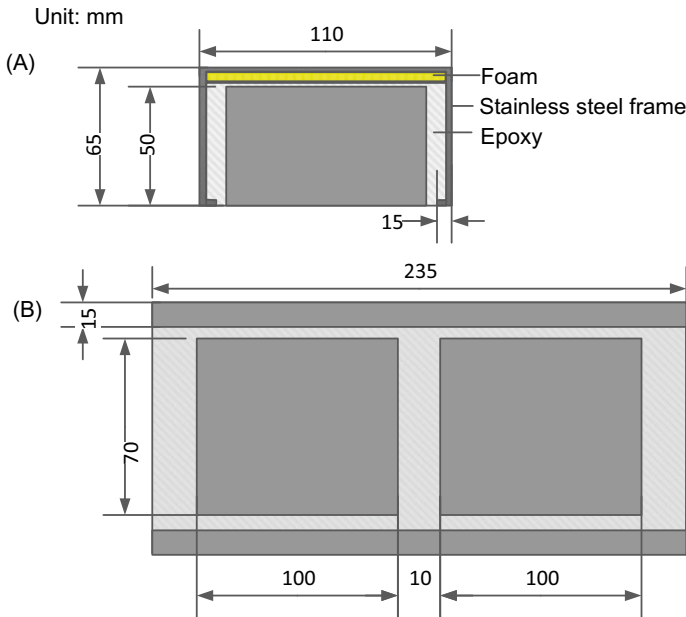


Fig. 2 The enclosure of two concrete coupons in one stainless steel frame with epoxy

2.2 Corrosion Chamber Design and Operation

The corrosion chamber is designed and constructed to simulate the corrosive environment of real sewer systems by controlling the temperature, relative humidity and gaseous hydrogen sulfide concentration. It is composed of a H_2S gas generator, a sewage circulation system, a cooling water system, a PLC controller and a chamber body to house concrete samples (Fig. 3). The corrosion chamber conditions can be adjusted according to the test requirement, e.g., the gas-phase temperatures at $30\text{ }^\circ\text{C}$ to mimic a tropical location, relative humidity of 100% for most gravity sewers, and H_2S gas concentration of 100 ppm for a severely inductive level. The level of H_2S is recommended to be 50–100 ppm for bio-corrosion tests as it simulates a highly corrosive sewer environment. The corrosion resistance determined under such high level of H_2S concentration would be highly supportive in selecting concrete products for many challenging sewer construction projects.

To achieve the specified H_2S gaseous concentrations in the corrosion chamber, Na_2S solution is injected into a container partially filled with acid (13% HCl), using a corrosion-resistant solenoid pump (Bio-chem Fluidics, model: 120SP2440-4TV) with a dispense volume of $40\text{ }\mu\text{L}$. The H_2S concentrations are monitored using two H_2S gas detectors with a range between 0 and 200 ppm (Acrolug Pty Ltd, Clontarf, Australia). A programmable logic controller (PLC) was employed to monitor the H_2S concentration and to trigger the dosing pump for Na_2S addition to maintain the specified H_2S concentrations (Fig. 1).

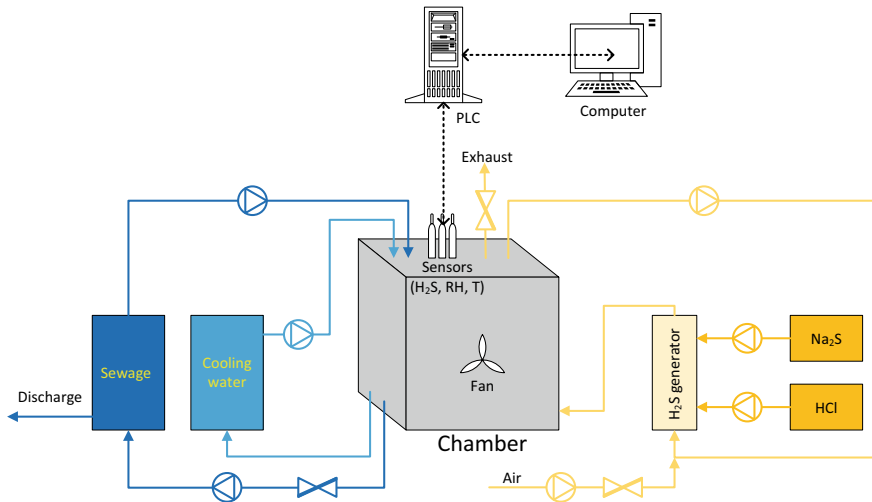


Fig. 3 Schematic of the corrosion chamber with gaseous H_2S concentration, relative humidity and gas temperature controlled by a PLC

The dimensions of the chamber room are 1336 mm (L) \times 1000 mm (D) \times 1286 mm (H), as shown in Fig. 4. Concrete coupons can be installed either with its exposure surface facing downwards but above the wastewater, i.e., gas phase coupons, or being partially submerged by wastewater with its exposure surface facing sideways, i.e., partially-submerged coupons. The chamber has 4 layers of trays for gas-phase concrete coupons, and 4 layers of trays for partially submerged concrete coupons. The eight liquid trays each hold 4 cm depth of real wastewater, which can be collected from a local sewer pumping station or wastewater treatment plant, and replaced every two weeks. The wastewater temperature and pH are regulated to maintain comparable conditions over time. The wastewater pH is maintained at around 7.5, a typical value for raw wastewater. The wastewater temperature is kept at the specified temperature and it creates the relative humidity in combination of the cooling water system.

Each sample tray has a capacity of 16 concrete coupons, with two in each stainless-steel frame (Fig. 4). Gas-phase coupons (a maximum capacity of 128 samples) enclosed in stainless steel frames are exposed to the gas phase within the chambers with the exposed surface facing downwards approximately 170 mm above the wastewater surface in the wastewater tray below. These gas-phase concrete coupons simulate the sewer pipe crown, a location which is reported to be highly susceptible to sulfide induced MICC. For all gas-phase coupons, cooling water will be circulated through the samples and help to create condensations on the exposure surface, that is critical for the development of sulfide-oxidizing biofilms.

Half of concrete coupons (a maximum capacity of 128 samples) can be placed at the bottom of the liquid trays, which were thus partially submerged (approx. 20 mm) in the wastewater simulating the concrete sewer pipe near the water level, which has been reported as a region of high corrosion activity. The partially-submerged samples

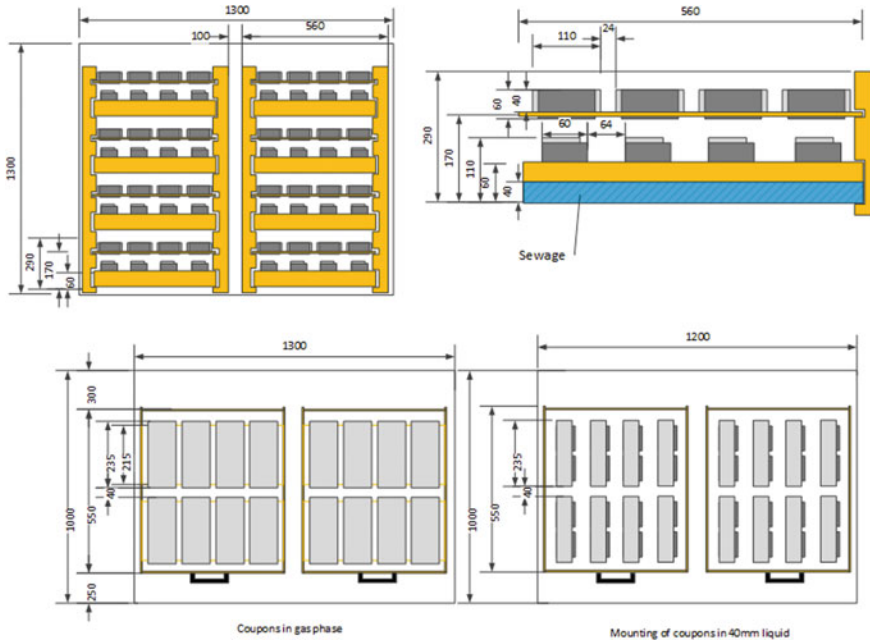


Fig. 4 Arrangement of gas-phase and partially-submerged concrete samples in the corrosion chamber for H_2S exposure

might experience much higher corrosion rates for different concrete types than gas-phase concrete samples, due to wastewater inoculation of nutrients and bacteria, in addition to high moisture levels [31].

2.3 Testing Schedule and Analytical Parameters

Once the concrete products to be tested are cast into concrete specimens, which will be cut into sub-samples or coupons ($100 \times 70 \times 50$ mm) to test the corrosion development over a period of 12 months. This testing period is determined based on a general assumption of 2 months for corrosion development and 10 months of active MICC induced concrete deterioration. For the determination of a meaningful and representative corrosion rate, at least 3 measurements of corrosion losses over 10 month is required. However, it can be possible to measure up to 5 corrosion losses in 10 months, but more frequent measurements are unnecessary. That also means the overall testing period can be shortened to 8 months if a faster turnaround of evaluation is required.

Table 1 Proposed analytical items and frequency for the monitoring of corrosion development in corrosion chambers over a 12-month exposure period

Item	Times	Frequency
Surface pH	13	Once every month
Sulfide uptake rate (SUR)	7	0, 2, 4, 6, 8, 10 and 12 months
Photogrammetry	4	0, 4, 8 and 12 months
Microbial community	3	4, 8 and 12 months
Weight change	4	0, 4, 8 and 12 months
Sulfur compounds	1	12 months

In general, the total number of samples is divided into two equal sets, one as the gas-phase coupons and one as the partially-submerged coupons. Pairs of concrete samples are embedded in epoxy inside stainless-steel 316 frames, to provide only one exposure surface to H_2S . These samples may be cast and provided in different batches. However, these embedded samples should be installed in the corrosion chambers at the same time to ensure comparable exposure to the H_2S containing corrosive environments. The proposed analytical parameters and monitoring items are listed in Table 1. For each parameter, duplicate samples will be used and usually multiple measurements on one sample should be carried out to obtain the average value and standard deviation.

Surface pH and SUR are non-destructive measurements which are useful in monitoring the corrosion initiation and development on concrete coupons. It is recommended to measure surface pH monthly and SUR bi-monthly. Periodically, at intervals specified in the testing schedule (2 to 4-month interval is recommended), one set of coupons (one gas-phase coupon and one partially submerged coupon) is retrieved from the corrosion chamber for detailed analysis of different corrosion parameters. A standard step-by-step procedure of various analysis is employed to measure surface pH, followed by sampling for sulfur species (primarily elemental sulfur and sulfate, as other sulfur compounds were found to be at nonsignificant levels), and then photogrammetry analysis (thickness change) and weight change (corrosion loss).

2.4 Analytical Methods

The corrosion resistance can be analyzed by many related corrosion development parameters, among them the performance related parameters are recommended but mechanism related parameters are supplementary in the evaluation of corrosion resistance. Surface pH, SUR, corrosion rate, weight loss are essential parameters. Sulfur compounds, microbial community and microscopic measurements are supportive parameters. However, as the whole test is quite time-consuming to organize, it would be prudent to include as many parameters as possible to obtain the best understanding

of the concrete product and its corrosion resistance. Table 2 listed all potential parameters to be chosen in the evaluation. The actual testing items can be decided according to the testing schedule discussed in Sect. 2.3.

Table 2 Parameters to be measured with the Systematic COrrOsion REsistance testing (SCORE) methodology. Detailed description of different analytical methods has been published in referred journals

Parameter	Unit	Method description
Surface pH	–	Flat surface pH electrode (Extech PH150-C concrete pH kit, Extech Instruments, USA) [37]
Sulfide uptake rate (SUR)	mg S/m ² h	The corrosion activity is measured using a SUR test, which is conducted using a reactor designed specifically for the dimension of concrete coupons [16]
Corrosion rate	mm/year	The corrosion rate, i.e., the decreased depth of concrete over time, is measured using a photogrammetry method [34]
Weight loss rate	kg/m ² year	The weight of each concrete coupon is measured at the start (0 month) and extraction date (e.g., 4, 8 and 12 months) of the exposure tests in corrosion chambers [7]
Advanced microscopic analysis	–	The corrosion products or intact concrete are prepared (drying, sectioning, coating per analytical requirements) and measured using electron microscopy (SEM, EDS, XRD, MLA) and neutron radiography [8, 10]
Sulfur compounds in corrosion products	g S/m ²	The sulfur content in the corrosion products is analyzed using a Dionex ICS-2000 IC with an AD25 absorbance (230 nm) and a DS6 heated conductivity detector (35 °C) [4]
Microbial community	–	The composition of microbial community: Total DNA was extracted using the FastDNA SPIN Kit for Soil (MP Biomedicals, CA, USA), as per the manufacturer's instructions. The 16S rRNA genes were amplified and sequenced on a Genome Sequencer FLX Titanium pyrosequencer (Roche 454 platform, CA, USA) or MiSeq Sequencing System (Illumina) [33, 31, 9] Inactivation of microorganisms in corrosion biofilm is determined by LIVE/DEAD staining kit [41]

2.4.1 Surface pH Measurement

A flat surface pH electrode (Extech PH150-C concrete pH kit, Extech Instruments, USA) is used to measure the coupon surface pH. The pH meter was allowed to reach steady reading after contacting the electrode with the measuring spots wetted by about 1 mL of milliQ water. Four measurements were made on randomly selected spots on the coupon surface (100 × 70 mm) to determine an average value for one coupon.

2.4.2 Sulfide Uptake Rate (SUR)

The SUR reactor for the H₂S uptake tests was constructed from glass in order to minimise reaction and absorbance of H₂S and was designed to neatly fit around the coupon pairs and stainless-steel frames used in the corrosion chamber experiments. A concrete coupon is extracted from the corrosion chamber and fitted on top of the SUR reactor to reach air-tight condition. H₂S is then injected to a level around the exposure concentration in the corrosion chamber. The decrease of H₂S gaseous concentration in the chamber is monitored using a H₂S sensor (App-Tek OdaLog® Logger L2, range of detection is 0–200 ppm). H₂S uptake rate is then determined by calculating the slope of the measured H₂S concentration versus time [42]:

$$r = \frac{d[H_2S]}{dt} \quad (1)$$

where [H₂S] is H₂S gas phase concentration (ppm), t is time (h). Then, the rate was converted into a surface specific H₂S uptake rate using Eq. (2).

$$r_{H_2S} = -\frac{d[H_2S]}{dt} \times 101.325\text{KPa} \times \frac{32\text{g/mol}}{RT} \times \frac{V}{A} \quad (2)$$

where r_{H_2S} is the surface-specific H₂S uptake rate (mg-S m⁻² h⁻¹), R is the universal gas constant (J K⁻¹ mol⁻¹), T is the absolute temperature (K), V is the total gas volume in the reactor (m³), A is the concrete surface exposed to the reactor atmosphere (m²).

2.4.3 Sulfur Compounds

After measuring the surface pH and SUR, the exposed surface of concrete coupons can be washed using a high-pressure washer (Kaercher K 5.20 M). Four litres of water is used for each coupon. The wash-off water is homogenized using a magnetic mixer for 2 h before subsamples taken into sulfide anti-oxidant buffer solution [43]. A Dionex ICS-2000 IC with an AD25 absorbance (230 nm) and a DS6 heated conductivity detector (35 °C) is used to measure the soluble sulfur species.

2.4.4 Photogrammetry

After concrete coupons being washed using a high-pressure washer (Kaercher K 5.20 M), five photos for each concrete coupon are taken to measure the coupon thickness using photogrammetry. A 3D cloud image of the exposed surface for each coupon is generated to calculate the surface height of the coupon relative to the stainless-steel frame as the reference plane.

The decrease in thickness after certain exposure time (e.g., 4, 8, 12 months) is then calculated by subtracting the average thickness after washing from the average thickness before exposure (0 month). This technique not only enables an accurate change in coupon thickness to be determined irrespective of the surface roughness but also provides a detailed record of the spatial distribution of the losses that occurred.

2.4.5 Weight Change

The weight of each concrete coupon pairs is measured at the start and finish of the exposure tests (e.g., 0, 4, 8, 12 months) in corrosion chambers. The change of coupon weight is thus used as an indicator of the mass loss due to corrosion. The measurement will be done for weights that have equilibrated with humidity in the corrosion chamber. However, the previous curing and storage conditions might affect the accuracy.

2.4.6 DNA Extraction and Microbial Community Analysis

The corrosion layers on the surface of each coupon are scraped with a sterile surgical scalpel directly into sterile 50 ml polypropylene containers. The wet samples are stored at 4 °C for less than 24 h until used for DNA extraction. To loosen the microbial cells from the corrosion layer matrix the samples are first sonicated on ice for 30 s followed by 30 s resting on ice and repeated twice. Sonicated samples are then loaded onto a sucrose density gradient and are washed in pyro-phosphate buffer (pH 4) and centrifuged to pellet the cells (18,000 g for 10 min at 4 °C). The cell pellets are finally resuspended in pyrophosphate buffer (pH 7.5) and then cells are lysed, and DNA extracted using the Fast DNA™ SPIN Kit for Soil.

To perform 16S rRNA gene amplicon sequencing, extracted DNA samples can be delivered to a sequencing provider, such as Australia Center for Ecogenomics (ACE, Brisbane, Australia). PCR amplifications are conducted in Q5 Hot Start High-Fidelity 2X Master Mix (New England Biolabs) in standard PCR conditions. Modified universal primers 28F and 519R are used for the amplification of 450 bp of the variable regions V1–V3 of the 16S rRNA gene. Amplification products are confirmed with eGels (Life Technologies, Grand Island, New York), and the confirmed products are sequenced on MiSeq Sequencing System (Illumina) using paired end (2 × 300 bp) sequencing with V3 chemistry in ACE according to manufacturer's protocol.

Sequences are quality filtered and dereplicated using the QIIME (qiime.org) script `split_libraries.py` with the homopolymer filter deactivated and checked for chimeras against the greengenes database using UCHIME ver. 3.0.617. Sequences are treated following the procedures using QIIME scripts with the default settings: (1) sequences are clustered at 97% similarity into operational taxonomic units (OTUs); (2) cluster representatives are selected; (3) Greengenes taxonomy is assigned to the cluster representatives using BLAST; (4) tables with the abundance of different OTUs and their taxonomic assignments in each sample are generated.

2.5 Estimation of a Scaling Factor to Real Sewers

The corrosion resistance testing results can be obtained using the lab-scale corrosion chamber to simulate the real sewer conditions. The test described above is thus not an accelerated test of corrosion resistance of concrete samples. The chamber was operated to simulate a controlled environment simulating that of sewers, i.e., at specific gas-phase temperatures, relative humidity and H₂S gas concentration. To apply the tested corrosion rates to other sewer conditions different from the testing chamber conditions will require the data being scaled based on a range of factors related to the actual conditions in the real sewer.

2.5.1 Different Levels of Hydrogen Sulfide Gaseous Concentration

For different H₂S gaseous concentrations, the corrosion rate is theoretically proportional to the sulfide oxidation rate, which is related to gaseous H₂S concentration (ppm) in a power function. In the equation, k is a constant coefficient, with n around 0.5 [6, 8].

$$r = k \cdot C_{H_2S}^n \quad (3)$$

2.5.2 Different Levels of Humidity

The relative humidity of the sewer gas has a big impact on the corrosion rate, which was regarded as a result of changing the moisture content in the concrete. If it is assumed that the rate of corrosion is directly proportional to the moisture content present in the concrete pore structure, then it follows that for a certain type of concrete [35].

$$r = k \cdot C_{H_2S}^n \times \left(\frac{0.1602RH - 0.1355}{1 - 0.9770RH} \right) \quad (4)$$

It should be noted that this equation changes for different types of concrete depending on their porosity and pore size distribution. In most sewer systems, the relative humidity is close to 100%. Therefore, it is not necessary to do this correction of relative humidity.

2.5.3 Different Levels of Temperature

The influence of gas phase temperature on the chemical, physiochemical and biological processes involved in sewer corrosion can be described as a function of the activation energy using the Arrhenius relationship [35]:

$$r = k \cdot C_{H_2S}^n \times \left(\frac{0.1602RH - 0.1355}{1 - 0.9770RH} \right) \times e^{\left(\frac{-45000}{RT} \right)} \quad (5)$$

2.5.4 Fluctuations of Hydrogen Sulfide Gaseous Concentration

In real sewers, large fluctuations of gaseous H₂S concentrations occur due to the diurnal profiles of sewage flow and retention times and the necessity of intermittent pumping of sewage from pressure pipes into gravity pipes. The peaks and troughs of H₂S profiles lead to lower corrosion in comparison to concrete exposed to a constant H₂S levels at the same average concentration (like the corrosion chambers) [26, 27]. It is estimated that the fluctuation of hydrogen sulfide can cause a decrease of corrosion by about 5–85%. To be on the safe side, it is recommended to use a scaling factor of 0.67 by assuming the chamber overestimates the corrosion rate by 50%.

2.5.5 Other Correction Factors

In addition to the well-studied and known factors contributing to the scaling factor, there are other processes that can affect the acid reaction with the concrete (e.g., the loss of acid before it reaches the concrete). The well-known Pomeroy equation [44] uses a correction factor of 0.3–1 in the calculation of corrosion rate. There is probably a similar factor that can be applied to the translation of rates obtained in chamber to real sewers.

Therefore, the scaling factor of the testing condition is about 3 due to constant H₂S concentration in the corrosion chamber and other corrections listed above. If the real sewer condition is different from the chamber, a scaling factor can be calculated using the above equations, e.g. the scaling factor of a real sewer condition (30 °C, 100% RH and 5 ppm H₂S) can be estimated to be 0.075. That means the measured rate is roughly 13.4 times higher than the expected rate in a real sewer. It should be

Table 3 Estimation of a scaling factor for the corrosion rates determined in the laboratory corrosion chamber tests

Factors	Laboratory corrosion chamber	Actual sewer condition	Scaling factor
Temperature	30 °C	30 °C	1
Relative humidity	100%	100%	1
H ₂ S concentration	100 ppm	20 ppm	2.24
H ₂ S fluctuations	Constant	Diurnal fluctuations	2
Loss of acid before it attacks concrete	Flat surface of gas-phase specimens	Curved surface	2
Overall scaling factor	$1 \times 1 \times 2.24 \times 2 \times 2 = 8.96$		

noted that this is not an acceleration factor but a scaling factor because the chamber test is not an accelerated corrosion test. Below is an example of how to estimate the overall scaling factor based on the scientific literature discussed above (Table 3).

The corrosion rates can be correlated with the service life. The service life (L , year), which is determined by the time for corrosion to initiate (t_i , month) and the corrosion rate (r , i.e. concrete depth lost over time, mm/year) [34].

$$L = \frac{t_i}{12} + \frac{D}{r} \quad (6)$$

where D is the concrete depth (mm) that can be sacrificed before the end of service life.

Although this section provides an approach to estimate the expected corrosion rate in certain sewer conditions based on the measured data, it is the responsibility of the person who does such extrapolation to conduct detailed investigation to ensure reasonable assumptions are taken. A good safety factor should be adopted for the design of the depth of concrete cover to ensure the 100-year service life. In addition to that, control strategies should be implemented to achieve operational target for the control of H₂S gas concentration and gas humidity through either chemical dosing in sewage or sewer air ventilation.

3 Results and Discussion

As a demonstration of the systematic evaluation of corrosion resistance, two different types of concrete products named SewerCem Concrete, i.e. SCC-I and SCC-II provided by Calucem Company, Germany, were tested. Two different concretes (a total of 24 samples, 12 samples each type of concrete) were cast for testing in Calucem's lab. The samples for this test were cast as cubes $150 \times 150 \times 150$ mm, five cubes per concrete. They were cured for at least 28 days before being sliced by

water-lubricated diamond saw into individual test specimens. Four such test specimens were prepared from each of the five replicate cubes per concrete, giving a total of 20 replicate specimens per concrete. The test surface on specimens from all cubes is 100×70 mm and represents the inside of the cube as-cast. In the end, twelve out of the twenty specimens were randomly chosen for the corrosion resistance testing. The corrosion chamber was operated at a highly corrosive condition, i.e. the gas-phase temperatures of 30°C , relative humidity of 100% and H_2S gaseous concentration of 100 ppm. This level of H_2S was used as it simulates a highly corrosive sewer environment and can provide measurable corrosion within limited exposure time. The level of H_2S employed in the corrosion chamber requires precautious lab management and risk controls according to occupational health and safety regulations.

3.1 Corrosion Chamber Conditions During the Test

Hydrogen sulfide (H_2S) and gas temperature profiles are recorded continuously through two Acrulog sensors (Acrulog Pty Ltd, Clontarf, Australia) in the corrosion chamber. The data were used to calculate the daily average concentrations, which are plotted in Figs. 5 and 6.

Domestic sewage was circulated through the chamber to simulate the wastewater flow in sewers. The sewage pH was monitored and adjusted to be similar to fresh sewage. The daily average profile is shown in Fig. 7. As the humidity sensor cannot handle continuous monitoring, we periodically monitor the humidity (which is ensured by the temperature control of sewage and cooling water system) when we change chemicals or wastewater, or during sampling events. The weekly measurements we did so far confirmed the RH to be around 99.5%.

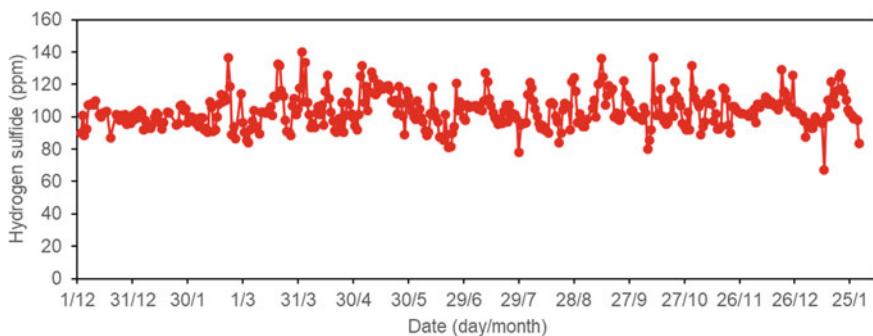


Fig. 5 Daily average hydrogen sulfide gaseous concentration in the corrosion chamber during the testing period

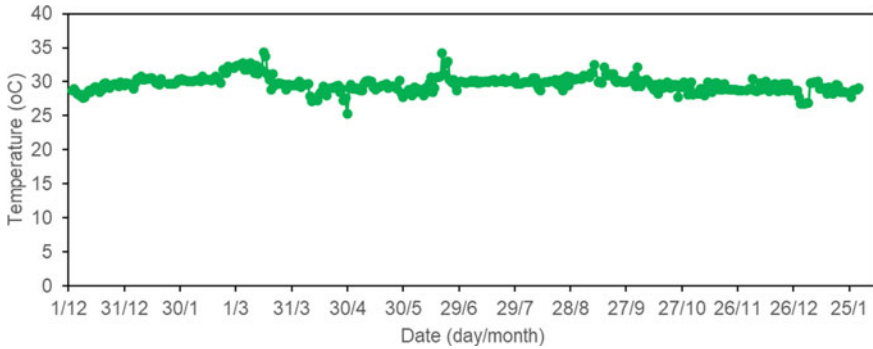


Fig. 6 Daily average of gas temperature in the corrosion chamber during the testing period

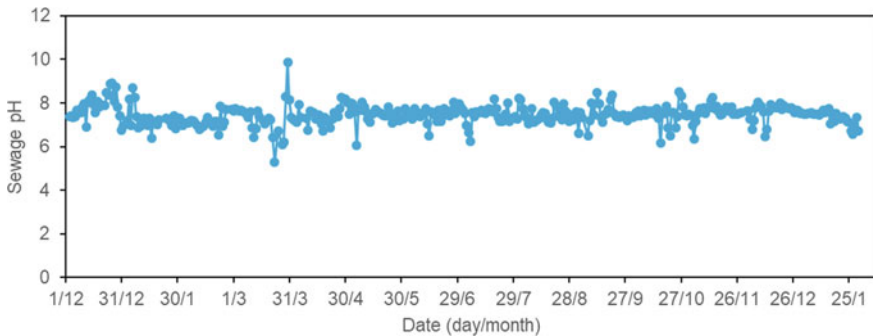


Fig. 7 Daily average of wastewater pH of the corrosion chamber

3.2 Testing of Calucem Concrete Samples

In the time period from January 2019 to January 2020, the above detailed corrosion resistance evaluation methodology was applied to test two concrete products (Fig. 8) as specified and provided by Calucem company, Germany. The purpose of the project was to determine the corrosion resistance (activated deterioration rate followed the surface pre-treatment) of two types of client-provided concrete samples in corrosion chambers simulating gravity sewer conditions.

Concrete samples were sent to the corrosion lab after being prepared (cast, curing, and cutting) by the product provider. Each concrete type (SCC-I, SCC-II) was tested for surface pH, sulfide uptake rate, corrosion rate, weight loss and sulfur compounds.

3.2.1 Summary of Corrosion Resistance Evaluation

Table 4 summarizes the results without applying a scaling factor to corrosion rates. After 12 month of exposure in the corrosion chamber, the surface pH of all concrete



Fig. 8 Photos of the embedded concrete coupons of two concrete products, i.e. SCC-I and SCC-II

samples has reached to 1.2–2.8, with the partially-submerged (PS) coupons showing pH values about 1–1.5 unit lower than the gas-phase (GP) coupons. Measurements on the two types of concrete were conducted after being exposed to the H₂S-containing corrosion chambers for 0, 2, 4, 6, 8, 10 and 12 months. It is clear that the surface pH of pre-treatment samples (test of activated corrosion) is reaching equilibrium around 2.5–2.8 and 1.2–1.6 for gas-phase and partially-submerged samples, respectively. This is typical for concrete with active sulfide induced corrosion. Test results of surface pH are graphically presented in Fig. 9. This suggests that corrosion-inducing acidophilic microorganisms were established on these coupons within 12 months after being placed into the corrosion chambers. The PS coupons were close to wastewater, which likely provides sufficient moisture, nutrients and inoculum for the succession of corrosion biofilms. Thus, the surface pH is generally lower for PS concrete coupons. The overall observation of surface pH is that all concrete are experiencing active biogenic acid corrosion.

The corrosion rates (Table 5) measured by photogrammetry are used to determine the corrosion resistance of the tested concrete samples, supported by the measurement of weight loss and SUR. It was found that SCC-II performed slightly better

Table 4 Summary of 12-month test results for concrete SCC-I and SCC-II. Results are given as an average value of triplicate measurements except for the sulfur compounds and weight loss. The ranking of corrosion resistance was primarily based on corrosion rate and weight loss, with other data as the supporting criteria

Concrete	Surface pH	SUR	Corrosion rate	Weight loss	Sulfate
	–	mg S/m ² h	mm/year	kg/m ² year	g S/m ²
<i>Gas-phase coupons simulating sewer crown</i>					
SCC-I	2.83	80.78	1.39	1.14	3.77
SCC-II	2.53	80.00	1.12	0.95	3.70
<i>Partially-submerged coupons simulating sewer tidal regions</i>					
SCC-I	1.66	163.58	4.11	3.50	38.41
SCC-II	1.20	150.83	3.49	3.34	33.50

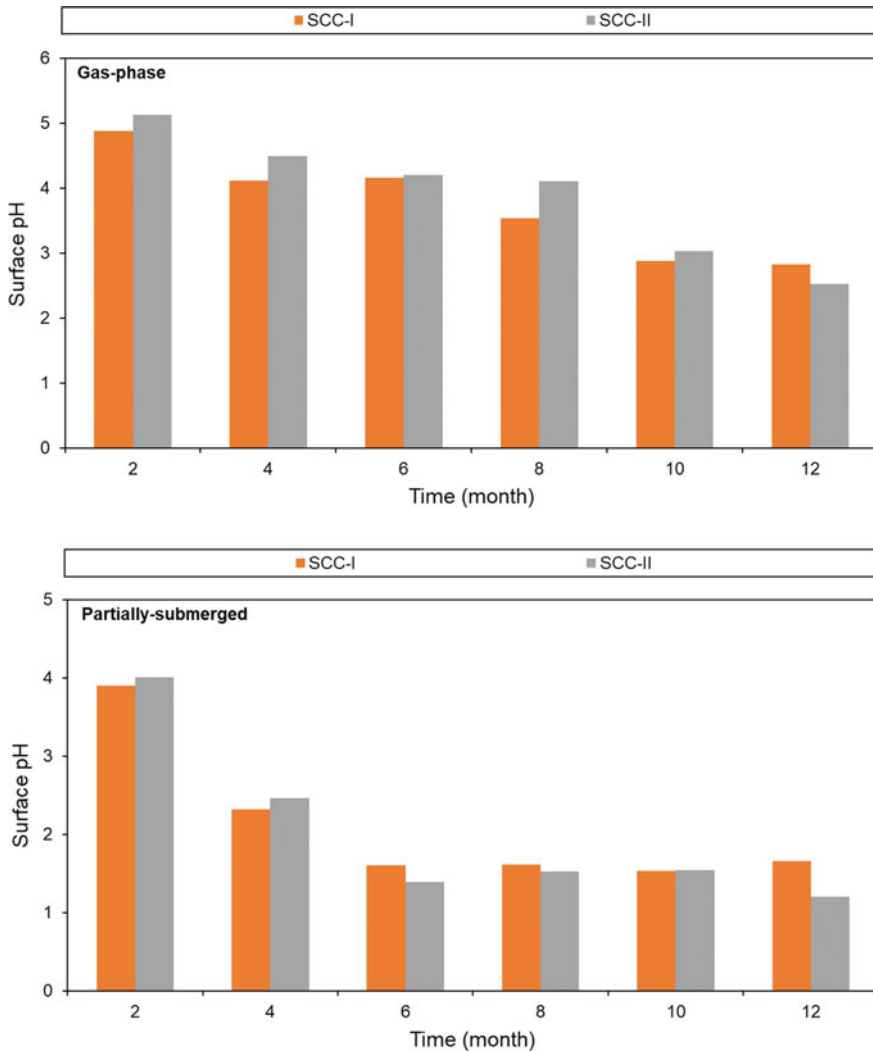


Fig. 9 Surface pH measured on concrete SCC-I and SCC-II after 2, 4, 6, 8, 10 and 12 months of exposure in the gas-phase (top) and partially-submerged (bottom) in sewage in the H₂S corrosion chambers

with a low corrosion rate around 1.1 mm/year and low weight loss in the gas phase of the corrosion chamber. For the partially-submerged condition, SCC-II also outperformed SCC-I with a corrosion rate around 3.5 mm/year. Overall, SCC-II has higher resistance than SCC-I, both in the gas-phase and partially-submerged phase.

The level of corrosion resistance is largely consistent with other parameters like SUR (Table 6), sulfate and surface pH. The slight discrepancy between different

Table 5 Corrosion rate measured on concrete SCC-I and SCC-II after 4, 8 and 12 months of exposure in the gas-phase (top) and partially-submerged (bottom) in sewage in the H₂S corrosion chambers. Results are given as average and standard sample deviation calculated from three individual measurements

Time (month)		4	8	12
Gas-phase	SCC-I	1.23 ± 0.19	1.91 ± 0.04	1.39 ± 0.01
	SCC-II	0.76 ± 0.06	1.36 ± 0.26	1.12 ± 0.19
Partially-submerged	SCC-I	5.18 ± 0.25	5.33 ± 0.05	4.11 ± 0.18
	SCC-II	3.96 ± 0.47	4.59 ± 0.04	3.49 ± 0.07

Table 6 Sulfide uptake rate measured on concrete SCC-I and SCC-II after 4, 8 and 12 months of exposure in the gas-phase (top) and partially-submerged (bottom) in sewage in the H₂S corrosion chambers. Results are given as average and standard sample deviation calculated from three individual measurements

Time (month)		4	8	12
Gas-phase	SCC-I	17.12 ± 3.45	72.62 ± 5.76	80.78 ± 11.25
	SCC-II	16.57 ± 3.57	62.67 ± 7.04	80.00 ± 3.72
Partially-submerged	SCC-I	30.39 ± 11.08	155.63 ± 14.54	163.58 ± 7.52
	SCC-II	35.58 ± 13.23	115.31 ± 11.80	150.83 ± 3.27

measured parameters might be due to the special mix design or mechanical properties of each concrete, which makes it non-sensitive to the wastewater effects or other corrosion processes. Due to the high corrosion rate in the chamber, the measured sulfate concentrations are semi-quantitative due to the likely loss of corrosion products.

The SUR results obtained on the coupons indicate how quickly the hydrogen sulfide was oxidized to sulfuric acid. In general, SUR is directly proportional to the instantaneous concrete corrosion rate. However, caution should be taken while interpreting this SUR results to long-term corrosion loss because SUR is an instantaneous measurement and it is unable to account for any factors affecting the long-term corrosion processes. Besides, the coefficient to convert SUR to actual corrosion rate ($\frac{17520 \times f}{A \times M_s}$) might be different for different types of concrete due to the different buffering capacity of concrete and/or sewer conditions. More accurate calculation can be done if concrete properties like acid neutralisation capacity are known.

In summary, the data obtained so far suggests that for the two types of concrete sample, SCC-II has better performance in resisting H₂S induced corrosion in a gravity sewer environment. The extrapolation of the testing results to different sewer environment need to consider a scaling factor, that should be determined based on the sewer environmental conditions (mainly H₂S concentration, temperature, relative humidity, wastewater location) and the concrete structural properties (mainly the porosity and pore size distribution).

3.2.2 Microbial Activity and Community Analysis

At the end of the exposure (4, 8 and 12 months) in the corrosion chamber, microbial analysis was carried out to determine the microbial community through DNA sequencing. For the determination of the microbial community, the corrosion layers on the surface of each coupon were scraped for DNA extraction using the Fast DNA™ SPIN Kit for Soil. Data generated from Illumina high-throughput sequencing were analysed via a pipeline that consisted of denoising and chimera detection followed by microbial diversity analysis.

Microbial community analysis was determined based on DNA sequencing on different samples and the top 10 abundant genera are shown in Fig. 10. Considering the low pH on those samples, the typical corrosion-causing acidophilic bacteria such as *Acidithiobacillus* (or *Thiobacillus*), *Ferroplasma*, *Sulfobacillus* and *Mycobacterium* dominated the microbes detected on the concrete exposed to the corrosion chamber.

Acidithiobacillus and *Acinetobacter* were the highest abundant genera at 4-month of exposure. The relative abundance of *Acidithiobacillus/Thiobacillus* was 71.4% and 55.2% on the partially-submerged samples of SCC-I and SCC-II, respectively. The next most abundant bacteria were *Acinetobacter*, which is an acid producer and is often detected from corrosion environment. However, the abundance of *Ferroplasma* dominated for the 8-months and 12-months of exposure, followed by *Acidithiobacillus* on the partially-submerged samples and one gas-phase sample (SCC-II). The rest of samples showed a more even distribution of microbial community. This temporal change might be due to the development of the corrosion and change of surface conditions on specific concrete samples.

Acidithiobacillus, the most frequently reported sulfide-oxidizing bacteria in corroding sewers, only showed dominant abundance after 4-months exposure. *Ferroplasma*, also a known Archaea causing concrete corrosion, emerged at high abundance after 8-months exposure. For 8-months and 12-months samples, *Ferroplasma* is the leading bacteria. This might be due to the fact that *Ferroplasma* is more adapted to the active corrosion environment and the specific corrosion products formed on those concrete samples.

After 4 months of exposure, it was noted that Fungi was also detected at a level around 10.5% for SCC-I concrete samples in the gas phase, indicating the importance of Fungi for this type of concrete. However, Fungi disappeared from the 8-months analysis. *Sulfobacillus* were also sulfur oxidizing bacteria contributing to the concrete corrosion in the liquid phase samples during the 8-months and 12-months exposure. Other bacteria were detected mostly due to the vicinity to wastewater substrates and nutrients, which were originated from wastewater or human gut as real sewage was used in the chambers. Some other bacteria like *Alicyclobacillus* were originated from wastewater or human gut as real sewage was used in the chambers.

Collectively speaking, the microbial communities showed temporal change and comparable differences on different types of concrete. The variation in microbial communities might be due to the specific concrete properties of the concrete, which support the development of different microbial communities.

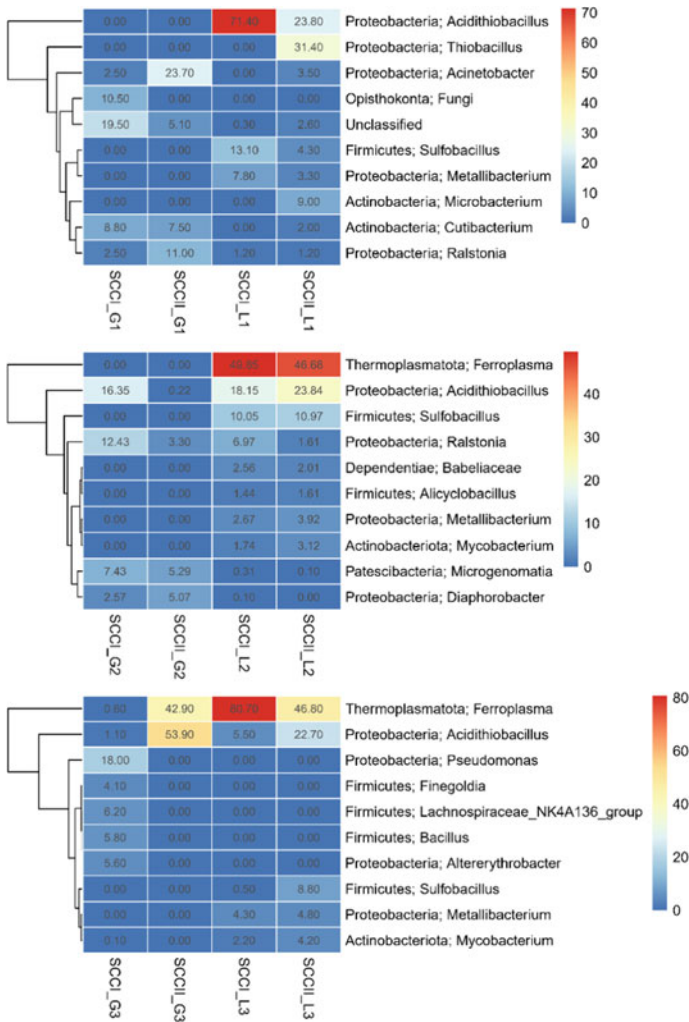


Fig. 10 Microbial community of relative abundance (%) measured on concrete SCC-I and SCC-II after 4 (top), 8 (middle) and 12 (bottom) months of exposure in the gas-phase or partially submerged in sewage of the H₂S corrosion chambers

4 Conclusions

This chapter presented a systematic approach to determine the corrosion resistance of concrete products experimentally in lab-scale sewer corrosion chambers and discussed how to apply these results to different real sewer conditions by estimating a scaling factor to the measured corrosion rate. The systematic approach was demonstrated on two real concrete products provided by Calucem Company, which showed

that one product has a higher corrosion resistance than the other. It is thus an effective and quantitative evaluation method for various concrete products to be used in sewer systems. The corrosion resistance data can be used by civil and environmental engineers in designing new concrete sewer systems to meet their specific service life by providing adequate cover depth on rebar.

The biocorrosion testing method is advantageous compared to acid immersion tests and in-situ tests due to its well-controlled conditions, together with the modelling tools to extrapolate results to different application scenarios. All the analytical methods have been published in top quality academic journals and thus will provide scientific data to support the comparison of corrosion resistances. It is anticipated that the proposed testing approach will be standardized and widely accepted and applied by the concrete and water industry.

References

1. Jiang, G., Sun, J., Sharma, K.R., Yuan, Z.: Corrosion and odor management in sewer systems. *Curr. Opin. Biotechnol.* **33**, 192–197 (2015)
2. Li, X., Kappler, U., Jiang, G., Bond, P.L.: The ecology of acidophilic microorganisms in the corroding concrete sewer environment. *Front. Microbiol.* **8** (2017)
3. Song, Y., Wightman, E., Tian, Y., Jack, K., Li, X., Zhong, H., Bond, P.L., Yuan, Z., Jiang, G.: Corrosion of reinforcing steel in concrete sewers. *Sci. Total Environ.* **649**, 739–748 (2019)
4. Jiang, G., Sharma, K.R., Guisasola, A., Keller, J., Yuan, Z.: Sulfur transformation in rising main sewers receiving nitrate dosage. *Water Res.* **43**, 4430–4440 (2009)
5. Hvitved-Jacobsen, T., Vollertsen, J., Nielsen, A.H.: *Sewer Processes: Microbial and Chemical Process Engineering of Sewer Networks*, 2nd edn. CRC Press (2013)
6. Jiang, G., Keller, J., Bond, P.L.: Determining the long-term effects of H₂S concentration, relative humidity and air temperature on concrete sewer corrosion. *Water Res.* **65**, 157–169 (2014)
7. Jiang, G., Sun, X., Keller, J., Bond, P.L.: Identification of controlling factors for the initiation of corrosion of fresh concrete sewers. *Water Res.* **80**, 30–40 (2015)
8. Jiang, G., Wightman, E., Donose, B.C., Yuan, Z., Bond, P.L., Keller, J.: The role of iron in sulfide induced corrosion of sewer concrete. *Water Res.* **49**, 166–174 (2014)
9. Song, Y., Tian, Y., Li, X., Wei, J., Zhang, H., Bond, P.L., Yuan, Z., Jiang, G.: Distinct microbially induced concrete corrosion at the tidal region of reinforced concrete sewers. *Water Res.* **150**, 392–402 (2019)
10. Song, Y., Wightman, E., Kulandaivelu, J., Bu, H., Wang, Z., Yuan, Z., Jiang, G.: Rebar corrosion and its interaction with concrete degradation in reinforced concrete sewers. *Water Res.* **182**, 115961 (2020)
11. Zivica, V.R., Bajza, A.: Acidic attack of cement based materials—a review.: Part 1. Principle of acidic attack. *Constr. Build. Mater.* **15**, 331–340 (2001)
12. Apgar, D., Witherspoon, J.: *Minimization of odors and corrosion in collection systems: Phase I*. Water Environment Research Foundation, Alexandria (2007)
13. Li, X., Khademi, F., Liu, Y., Akbari, M., Wang, C., Bond, P.L., Keller, J., Jiang, G.: Evaluation of data-driven models for predicting the service life of concrete sewer pipes subjected to corrosion. *J. Environ. Manag.* **234**, 431–439 (2019)
14. Liu, Y., Song, Y., Keller, J., Bond, P., Jiang, G.: Prediction of concrete corrosion in sewers with hybrid Gaussian processes regression model. *RSC Adv.* **7**, 30894–30903 (2017)
15. Grengg, C., Mittermayr, F., Ukrainczyk, N., Koraimann, G., Kienesberger, S., Dietzel, M.: Advances in concrete materials for sewer systems affected by microbial induced concrete corrosion: A review. *Water Res.* **134**, 341–352 (2018)

16. Sun, X., Jiang, G., Bond, P.L., Wells, T., Keller, J.: A rapid, non-destructive methodology to monitor activity of sulfide-induced corrosion of concrete based on H₂S uptake rate. *Water Res.* **59**, 229–238 (2014)
17. Chetty, K., Xie, S., Song, Y., McCarthy, T., Garbe, U., Li, X., Jiang, G.: Self-healing bioconcrete based on non-axenic granules: A potential solution for concrete wastewater infrastructure. *J. Water Process Eng.* **42**, 102139 (2021)
18. Li, X., Bond, P.L., O'Moore, L., Wilkie, S., Hanzic, L., Johnson, I., Mueller, K., Yuan, Z., Jiang, G.: Increased resistance of nitrite-admixed concrete to microbially induced corrosion in real sewers. *Environ. Sci. Technol.* **54**, 2323–2333 (2020)
19. Li, X., O'Moore, L., Wilkie, S., Song, Y., Wei, J., Bond, P.L., Yuan, Z., Hanzic, L., Jiang, G.: Nitrite admixed concrete for wastewater structures: Mechanical properties, leaching behavior and biofilm development. *Constr. Build. Mater.* **233**, 117341 (2020)
20. Song, Y., Chetty, K., Garbe, U., Wei, J., Bu, H., O'Moore, L., Li, X., Yuan, Z., McCarthy, T., Jiang, G.: A novel granular sludge-based and highly corrosion-resistant bio-concrete in sewers. *Sci. Total Environ.* **791**, 148270 (2021)
21. Gutierrez-Padilla, M.G.D., Bielefeldt, A., Ovtchinnikou, S., Pellegrino, J., Silverstein, J.: Simple scanner-based image analysis for corrosion testing: Concrete application. *J. Mater. Process. Technol.* **209**, 51–57 (2009)
22. Hasan, S., Rajganes, B., Sublette, K.L.: Large-scale cultivation of *Thiobacillus denitrificans* to support pilot and field-tests of a bioaugmentation process for microbial oxidation of sulfides. *Appl. Biochem. Biotechnol.* **45–6**, 925–934 (1994)
23. Herisson, J., van Hullebusch, E.D., Moletta-Denat, M., Taquet, P., Chaussadent, T.: Toward an accelerated biodeterioration test to understand the behavior of Portland and calcium aluminate cementitious materials in sewer networks. *Int. Biodeterior. Biodegradation* **84**, 236–243 (2013)
24. Monteny, J., de Belie, N., Vincke, E., Verstraete, W., Taerwe, L.: Chemical and microbiological tests to simulate sulfuric acid corrosion of polymer-modified concrete. *Cem. Concr. Res.* **31**, 1359–1365 (2001)
25. Monteny, J., Vincke, E., Beeldens, A., de Belie, N., Taerwe, L., van Gemert, D., Verstraete, W.: Chemical, microbiological, and in situ test methods for biogenic sulfuric acid corrosion of concrete. *Cem. Concr. Res.* **30**, 623–634 (2000)
26. Sun, X., Jiang, G., Bond, P.L., Keller, J.: Impact of fluctuations in gaseous H₂S concentrations on sulfide uptake by sewer concrete: The effect of high H₂S loads. *Water Res.* **81**, 84–91 (2015)
27. Sun, X., Jiang, G., Bond, P.L., Keller, J.: Periodic deprivation of gaseous hydrogen sulfide affects the activity of the concrete corrosion layer in sewers. *Water Res.* **157**, 463–471 (2019)
28. Valix, M., Mineyama, H., Chen, C., Cheung, W.H., Shi, J., Bustamante, H.: Effect of film thickness and filler properties on sulphuric acid permeation in various commercially available epoxy mortar coatings. *Water Sci. Technol.* **64**, 1864–1869 (2011)
29. Wu, L., Huang, G., Liu, W.V.: Methods to evaluate resistance of cement-based materials against microbially induced corrosion: A state-of-the-art review. *Cement Concr. Compos.* **123**, 104208 (2021)
30. Živica, V.R.: Acidic attack of cement based materials—a review Part 3: Research and test methods. *Constr. Build. Mater.* **18**, 683–688 (2004)
31. Jiang, G., Zhou, M., Chiu, T.H., Sun, X., Keller, J., Bond, P.L.: Wastewater-enhanced microbial corrosion of concrete sewers. *Environ. Sci. Technol.* **50**, 8084–8092 (2016)
32. Sun, X., Jiang, G., Chiu, T.H., Zhou, M., Keller, J., Bond, P.L.: Effects of surface washing on the mitigation of concrete corrosion under sewer conditions. *Cem. Concr. Compos.* **68**, 88–95 (2016)
33. Cayford, B.I., Jiang, G., Keller, J., Tyson, G., Bond, P.L.: Comparison of microbial communities across sections of a corroding sewer pipe and the effects of wastewater flooding. *Biofouling* **33**, 780–792 (2017)
34. Wells, T., Melchers, R.E.: An observation-based model for corrosion of concrete sewers under aggressive conditions. *Cem. Concr. Res.* **61–62**, 1–10 (2014)
35. Wells, T., Melchers, R.E.: Modelling concrete deterioration in sewers using theory and field observations. *Cem. Concr. Res.* **77**, 82–96 (2015)

36. Cayford, B.I., Dennis, P.G., Keller, J., Tyson, G.W., Bond, P.L.: High-throughput amplicon sequencing reveals distinct communities within a corroding concrete sewer system. *Appl. Environ. Microbiol.* (2012)
37. Joseph, A.P., Keller, J., Bustamante, H., Bond, P.L.: Surface neutralization and H₂S oxidation at early stages of sewer corrosion: Influence of temperature, relative humidity and H₂S concentration. *Water Res.* **46**, 4235–4245 (2012)
38. Satoh, H., Odagiri, M., Ito, T., Okabe, S.: Succession of sulfur-oxidizing bacteria in the microbial community on corroding concrete in sewer systems. *Appl. Environ. Microbiol.* **73**, 971–980 (2007)
39. Islander, R.L., Devanny, J.S., Mansfeld, F., Postyn, A., Shih, H.: Microbial ecology of crown corrosion in sewers. *J. Environ. Eng.* **117**, 751–770 (1991)
40. Satoh, H., Odagiri, M., Ito, T., Okabe, S.: Microbial community structures and in situ sulfate-reducing and sulfur-oxidizing activities in biofilms developed on mortar specimens in a corroded sewer system. *Water Res.* **43**, 4729–4739 (2009)
41. Sun, X., Jiang, G., Bond, P.L., Keller, J., Yuan, Z.: A novel and simple treatment for control of sulfide induced sewer concrete corrosion using free nitrous acid. *Water Res.* **70**, 279–287 (2015)
42. Vollertsen, J., Nielsen, A.H., Jensen, H.S., Wium-Andersen, T., Hvitved-Jacobsen, T.: Corrosion of concrete sewers—the kinetics of hydrogen sulfide oxidation. *Sci. Total Environ.* **394**, 162–170 (2008)
43. Keller-Lehmann, B., Corrie, S., Ravn, R., Yuan, Z., Keller, J.: Preservation and simultaneous analysis of relevant soluble sulfur species in sewage samples. In: *Proceedings of the Second International IWA Conference on Sewer Operation and Maintenance*, Vienna, Austria (2006)
44. Pomeroy, R.D.: *The Problem of Hydrogen Sulphide in Sewers*. Clay Pipe Development Association Limited, London (1990)

Modelling of Concrete Sewer Corrosion

Controlling Environmental Factors of Microbiologically Influenced Concrete Corrosion in Sewers



Guangming Jiang, Xiaoyan Sun, Xuan Li, Yarong Song, and Jurg Keller

Abstract Microbiologically influenced concrete corrosion occurs in sewers through two distinct stages, i.e., initiation and deterioration. Although different concretes have various corrosion resistance, both corrosion stages are known to be affected by the sewer environmental conditions, such as temperature, relative humidity, and most importantly gaseous hydrogen sulfide concentration. In addition, wastewater itself was also identified as an important factor in the corrosion process. The location of concrete surface relative to the wastewater level was also found to be critical in both lab experiments and field studies in real sewers. Recent research advance has identified, delineated, and quantified these controlling environmental factors and their variations on the MICC in sewers. The knowledge about controlling environmental factors is not only important for the operation and management of sewer systems, but also critical for the development of mathematical models for sewer concrete corrosion. This chapter summarizes recent findings about different environmental factors that are controlling the corrosion development.

G. Jiang (✉)

School of Civil, Mining, Environmental and Architectural Engineering, University of Wollongong, Wollongong, NSW 2522, Australia
e-mail: gjiang@uow.edu.au

X. Sun

School of Civil Engineering, Sun Yat-Sen University, Zhuhai 519082, China
e-mail: sunxy55@mail.sysu.edu.cn

X. Li

Centre for Technology in Water and Wastewater, School of Civil and Environmental Engineering, University of Technology Sydney, Ultimo, Sydney, NSW 2007, Australia
e-mail: xuan.li@uts.edu.au

Y. Song · J. Keller

Australian Centre for Water and Environmental Biotechnology, The University of Queensland, Brisbane, QLD 4072, Australia
e-mail: yarong.song@uq.edu.au

J. Keller

e-mail: j.keller@uq.edu.au

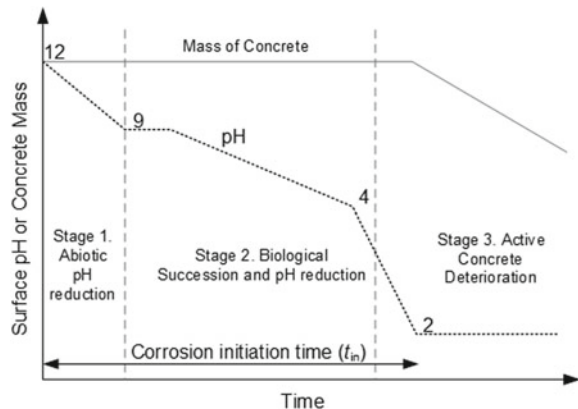
1 Introduction

The global population growth and increasing urbanization level require the construction of new sewer systems as an addition to existing wastewater infrastructure. The outdated sewers without proper functions due to the expiry of their service life need huge investment to be replaced. As a result, fresh concrete sewer pipes and auxiliary structures have been constructed globally, especially in developing countries, due to many advantages of concrete including excellent strength, low costs, and molding flexibility.

For microbiologically influenced concrete corrosion to develop on fresh concrete surface, the surface will go through an initiation stage. Gravity sewers provide amenable conditions for microbiologically influenced concrete corrosion to initiate, including the availability of water due to condensation or wastewater splashing or flooding, high concentrations of carbon dioxide and H_2S as corrosion precursors [1–3]. However, corrosion-causing microorganisms found it impossible to colonize on the fresh concrete surface after construction due to the high surface pH (a result of cement alkalinity). Therefore, sulfide oxidizing microorganisms can only develop after the initiation period when the surface reacts with corrosive compounds like CO_2 and H_2S in gravity sewers (stage 1 in Fig. 1).

During the corrosion initiation stage, the surface pH of concrete is reduced due to the neutralization of cement alkalinity ($Ca(OH)_2$) with weak acids like CO_2 , H_2S and organic acids in wastewater [5, 6]. Following stage 1, neutrophilic and acidiphilic sulfide oxidising-bacteria colonize and grow on the modified concrete surface with a pH below 9. Their microbial metabolism, primarily sulfide oxidation to produce sulfuric acid, would lead to the further loss of cement alkalinity [7–9]. The cement alkalinity is converted to corrosion products, including gypsum ($CaSO_4 \cdot 2H_2O$) primarily in the corrosion layer with a pH around 2, and ettringite ($(CaO)_3 \cdot Al_2O_3 \cdot (CaSO_4)_3 \cdot 32H_2O$) mostly near the corrosion front with a slightly higher pH [8, 10].

Fig. 1 The development of microbiologically influenced corrosion on new concrete sewer surfaces, adapted from [4], with the corrosion initiation period (indicated by the time t_{in}) including stage 1, 2 and a small part of stage 3

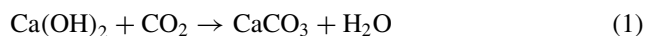


The total time span starting from fresh concrete surface to the active mass loss of concrete (deterioration) covers all the corrosion development stages. Many sewer environmental factors affect the physical (condensation), chemical (oxidation, neutralization) and biological (sulfide oxidation) processes related to the MICC development. These environmental conditions change due to the geographical locations, or the design and operation of the wastewater collection, and some corrosion control measures such as chemical dosing and ventilations. It is thus inevitable to establish a sound understanding of effects of environmental factors for a quantitative relationship being simulated using mathematical modelling.

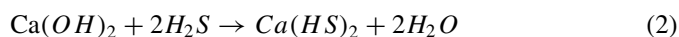
The well-known Pomeroy model was established to estimate the deterioration rate of concrete sewer pipes in early days with limited understanding of MICC in sewers [11]. Recent research advances and new knowledge of the relationship between corrosion initiation/deterioration and sewer environmental factors including H_2S concentration, relative humidity and temperature is critical for the overall prediction of sewer corrosion.

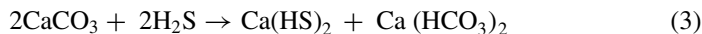
2 Controlling Environmental Factors for the Initiation Stage of Concrete Sewer Corrosion

At the very beginning of concrete sewer corrosion, carbonisation by CO_2 starts immediately after the cast of concrete. Theoretically, carbonation can lower the pH from 12 to 8.4 (pH of carbonate-bicarbonate-carbon dioxide equilibrium), as shown in Eq. (1). Our previous research found the surface pH of fresh concrete to be around 10.5, which indicates the effect of carbonation of the exposed surface during the cast, curing, transportation, and storage of the concrete sewer pipe to the laboratory [1, 6]. The CO_2 concentration in the open atmosphere is around 414 ppm. However, this could be much higher in the sewer system due to the anaerobic processes in wastewater, which was reported to be around 1.0% in the sewer head gas.



When concrete is exposed to the sewer environment, in the presence of H_2S , neutralisation of cement alkalinity would further reduce surface pH, as shown in Eqs. (2) and (3). Both $Ca(OH)_2$ and $CaCO_3$ react with H_2S as a weak acid. In comparison to H_2S , the contribution of CO_2 to the reduction of surface pH is insignificant. Within a period of 12 months, a decrease in surface pH by 1.8, 3.5, and 4.8 units was observed for coupons exposed to a temperature of 30, 25 and 18 °C and 50 ppm H_2S , respectively [6]. Elemental sulfur was found to be the major oxidation product of H_2S on the concrete surface. Higher levels of H_2S , temperature and relative humidity increased both surface pH reduction and sulfide oxidation.





A later long-term study over 4.5 years found that for concrete exposed to the gas-phase, like the sewer crowns, the corrosion initiation took similar time around 20 months for the different H_2S concentrations above 5 ppm [1]. No clear trend of decreasing corrosion initiation time was not observed with increasing gaseous H_2S concentrations. H_2S above 5 ppm was likely a critical point for the corrosion initiation, implicating a certain level of H_2S is required for significant corrosion development. It was pointed out that the corrosion of gas-phase coupons was determined by the sulfide oxidation rate, not the H_2S concentration. However, this long-term study indeed confirmed that for corrosion in the sewer crown regions, corrosion initiation was faster with higher temperature and higher humidity in sewer head gas.

In contrast to the corrosion initiation at the crown regions, the initiation at the tidal regions was observed to be faster with increased H_2S concentration in this 4.5 year study. The decrease of surface pH is more prominent on partially-submerged coupons for all H_2S gas levels than the gas-phase coupons. This is partially due to at the initial stages, the surface pH was lowered by H_2S and CO_2 , which was facilitated by high moisture levels at the tidal regions.

It was also reported that H_2S can be chemically oxidized into small crystal particles of elemental sulfur, owing to the presence of catalytic oxides on the new concrete surface [12, 13]. Overall, an important step is the dissociation of hydrogen sulfide to HS^- in the adsorbed film of water on the concrete surface. This dissociation is enhanced by the alkaline surface pH, which is an important factor for the uptake of gaseous hydrogen sulfide during this first stage [14]. Additionally, the chemical sulfide oxidation rate in the sewer is seen to double for a temperature increase of 9°C by the same study. Therefore, relative humidity, H_2S concentration and temperature all play a certain role in the corrosion initiation stage.

Following the chemical neutralization by CO_2 and H_2S at the initial stage, H_2S can then be oxidized to acids either chemically or biologically as the surface is conducive for the colonization of sulfide-oxidizing bacteria. It is reported that when surface pH is above the threshold of 8.3–9.4, H_2S is mainly oxidizing to elemental sulfur due to the oxygen limitation in the thin water film on concrete surface. Sulfate (or sulfuric acid) became the oxidation products when surface pH is below the threshold value [6]. The elemental sulfur formed would further promote the development of sulfur-oxidizing microorganisms on the concrete surface, which would further catalyze the formation of sulfuric acids [15]. During this time, both elemental sulfur and sulfate (in the form of corrosion products like gypsum) can be observed on the concrete surface. As a result, the corrosion initiation can be accelerated by these microorganisms. Another study also pointed out the inoculation by wastewater can accelerate the corrosion by providing nutrients, moisture and diverse microorganisms [5].

Collectively speaking, carbonization occurs as the first step, followed by further acidification by H_2S to reduce the surface pH. Sulfide oxidations produce both elemental sulfur and sulfate, depending on the surface pH is above or below 8.3–9.4, respectively. Microbial colonization occurs due to the wastewater inoculation and

supply of other essential nutrients. The biological sulfide oxidation leads to faster production of sulfuric acid than chemical reactions. The corrosion initiation finishes with the fully development of acidophilic sulfide oxidizing bacteria.

3 Controlling Environmental Factors for the Deterioration Stage of Concrete Sewer Corrosion

The corrosion initiation usually takes a few months, up to a few years, depending on the sewer conditions and the type of concrete product. In comparison, the designed service life of sewer systems is usually 50–100 years as they are highly expensive infrastructure. That also means, concrete sewers are subject to active corrosion and deterioration for most of its service life. It is thus critical to delineate the controlling factors for the deterioration stage of concrete sewer corrosion. The deterioration rate is directly correlated to the biological sulfide oxidation rates in sewers. Recent studies show that the biological sulfide oxidation rates correlate with H_2S concentration, relative humidity and temperature [8, 14, 16]. This section will discuss in details how these environmental factors, including the level and variations, affect the deterioration rates of concrete.

H_2S gas in sewers was initially generated by anaerobic sulfate-reducing bacteria mostly in the rising main (pumped) sewer biofilms or deeper layers of gravity sewer biofilm and sediments. Protonated sulfide, i.e. H_2S , in wastewater is emitted to the sewer head gas where it is diffused into the thin water film on the concrete surface (sides and crown of sewer pipes above the water line). Subsequently, biological oxidation of H_2S leads to the production of sulfuric acid [17–20], which is responsible for deterioration of the concrete [4, 21]. A highly diverse microbial community, composed of primarily sulfide-oxidizing bacteria, archaea and fungi, was reported to be involved in this acid production [7, 9, 15, 22–25].

The biologically generated sulfuric acid attacks the intact cement in concrete, mainly hydrated calcium silicate ($\text{CaO} \cdot \text{SiO}_2 \cdot 2\text{H}_2\text{O}$) and portlandite ($\text{Ca}(\text{OH})_2$), forming corrosion products including gypsum and ettringite [10, 26]. Both gypsum and ettringite, including recently reported iron precipitates, are believed to cause internal cracking near the corrosion front and hence accelerate the corrosion rates [26–28].

To control concrete sewer corrosion, different technologies were developed and widely used according to the local situations. The sulfide control technologies include liquid- and gas-phase technologies that use chemicals such as nitrates or iron salts to reduce the production and emission of H_2S into sewer head gas [29–33] or remove H_2S from sewer air through forced ventilation [34]. It is important to evaluate the effectiveness of these different treatment and control technologies, usually through the direct measurement of concrete sewer corrosion rate, in terms of the annual concrete depth loss (mm/year). In reality, dissolved sulfide in wastewater or gaseous H_2S concentrations in the head gas before and after treatment were used instead, due

to the difficulty to measure actual corrosion rates in operating sewers. However, H₂S concentration must be employed together with various sewer environmental factors such as relative humidity and temperature to evaluate and optimize the corrosion control strategies.

3.1 Gaseous Hydrogen Sulfide Concentration

The gaseous H₂S concentration in the head gas of sewers depends greatly not only on the factors related to production, such as hydraulic retention times, wastewater flow velocities and wastewater characteristics, but also on the factors related to dissipation like natural or forced ventilation, and corrosion itself as a H₂S consumer. In addition to a high relative humidity and high atmospheric oxygen content, a H₂S level > 2 ppm was suggested to be required for the sulfide oxidation to proceed on concrete sewers [35]. Conventionally, a simplified directly proportional relationship was assumed between the H₂S emission rate and concrete sewer corrosion rate [36]. An early model was developed to calculate the deterioration rate of concrete sewer pipes based on the acid production rate that was proportional to the hydrogen sulfide uptake rate [11]:

$$C_r = \frac{11.5k\phi_{sw}}{alk} \quad (4)$$

where C_r = concrete sewer corrosion rate (mm/year); k = factor related to the acid formation, based on climate conditions, 0.8 in moderate climates; ϕ_{sw} = hydrogen sulfide flux at the air-wall interface [g H₂S/(m² hr)]; and alk = alkalinity of the concrete pipe material (g CaCO₃/g concrete).

It is undoubtedly that gaseous H₂S concentration is a key factor determining the concrete corrosion rates during long-term exposure to sewer conditions, as the higher the concentration, the higher the sulfide flux to the sewer concrete wall. A recent long-term study over 45 months found that for both the initial corrosion rate (0–12 months) and the long-term corrosion rates (12–24 and 24–45 months), the increasing trend with increasing gaseous H₂S concentration is evident, with respective p-values of 8.6×10^{-5} , 1.5×10^{-6} , and 6.4×10^{-7} (Fig. 2). The results demonstrates that gaseous H₂S concentration is one of the primary controlling factors for the concrete sewer corrosion rates on a time scale of years. Similar to the Pomeroy model (Eq. 1), the concrete sewer corrosion rate is deemed directly proportional to the sulfide oxidation rate (SOR), which can be simulated using a power function of gaseous H₂S concentration [37, 38].

$$C_r = k_{SOR} \times SOR = kC_{H_2S}^n \quad (5)$$

where C_r is the concrete sewer corrosion rate (mm year⁻¹); C_{H_2S} is the gaseous H₂S concentration in the sewer head gas; k and n are model constants to be estimated

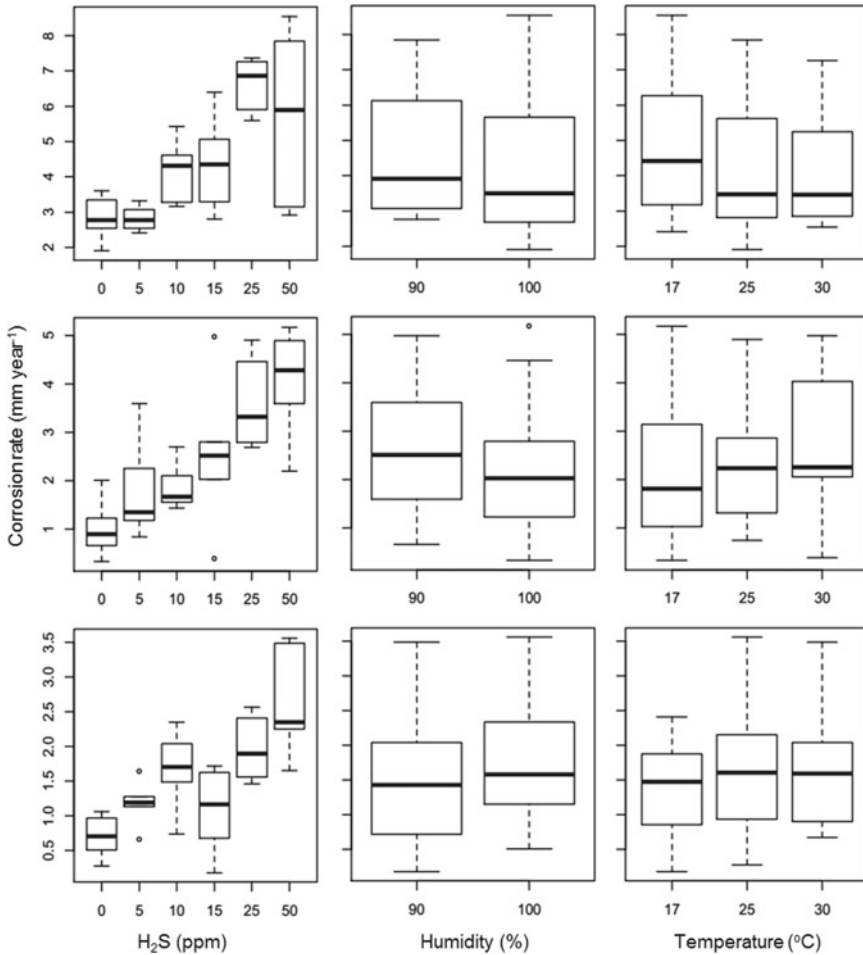


Fig. 2 Box-plots of corrosion rates of partially-submerged concrete coupons related to gaseous H₂S concentration, relative humidity and gas temperature in the corrosion chambers. Plots in the three rows are for corrosion rates during 0–12, 12–24, and 24–45 months, respectively. Reproduced from [8] with permission from Elsevier

from the experimental data. Theoretically, the corrosion layer can be assumed as a biofilm, of which the flux of hydrogen sulfide is usually diffusion limited. This would generally lead to a n value of 0.5.

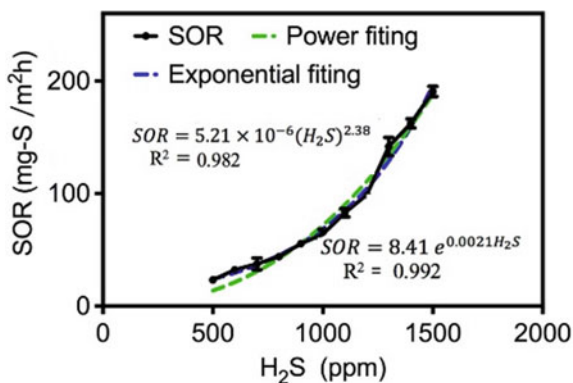
Although H₂S exists ubiquitously in the head gas of sewer systems, its concentrations vary temporally and spatially from a few ppm to several hundred ppm [8, 39]. In some sewers, hydrogen sulfide can accumulate to a very high concentration, i.e. > 800 ppm, not only leading to severe corrosion but also different deterioration mechanisms. At relatively low gaseous H₂S concentration, microbially catalyzed

sulfuric acid production is regarded as the primary cause for concrete sewer corrosion since the biological oxidation rate is much higher than the chemical oxidation rate [40]. However, the chemical sulfide oxidation can become important at very high concentrations of gaseous H_2S concentration, as it is a n th order reaction with n between 0.90 and 1.38 [41, 42]. Especially, when corrosion-resistant materials are adopted in sewers, instead of reacting with concrete, the gaseous H_2S in sewer air might accumulate to a very high concentration. Furthermore, many factors like high sulfate concentration in wastewater (e.g. the use of sea water for toilet flushing in Hong Kong [43]), extended hydraulic retention time could also lead to high H_2S concentrations [44, 45].

One study explored the chemically induced concrete corrosion in the presence of high gaseous H_2S concentration [46]. A corrosion rate around 3 mm year^{-1} was detected on fresh concrete being exposed to gaseous H_2S around 1000 ppm. The corrosion developed within one month, with the concrete surface pH being reduced to around 3. The fast concrete corrosion was mainly due to the chemical oxidation of H_2S to sulfuric acid as no sulfide-oxidizing bacteria were found in the corrosion products. The sulfide oxidation rate increased exponentially with hydrogen sulfide concentrations between 500 and 1500 ppm, which implies a high corrosion rate that cannot be predicted by conventional MICC mechanisms (Fig. 3).

Many studies on the effects of gaseous hydrogen sulfide concentration employed a constant value in the experiments or the model (e.g. Eq. 2). However, real sewers usually show highly dynamic gaseous hydrogen sulfide concentration due to diurnal wastewater flow and seasonal temperature changes etc. As shown in Fig. 4, the diurnal wastewater flow leads to fluctuations of dissolved sulfide in wastewater, and the gaseous H_2S concentration in the sewer head gas. This leads to periodic sudden increases of H_2S concentrations in the gravity pipe gas phase, creating so called 'spikes' or H_2S overload situations. The periodical pumping events and the temporal variation of sulfide concentrations can intermittently create gaseous H_2S levels up to 100 times as high as the average concentrations, most typically in the first pump cycles in the morning [31].

Fig. 3 Sulfide oxidation rate of concrete coupons before and after sterilization under 10–200 ppm H_2S (Left), and the sulfide oxidation rate of concrete coupons under 500–1500 ppm H_2S . Reproduced from [46] with permission from Elsevier



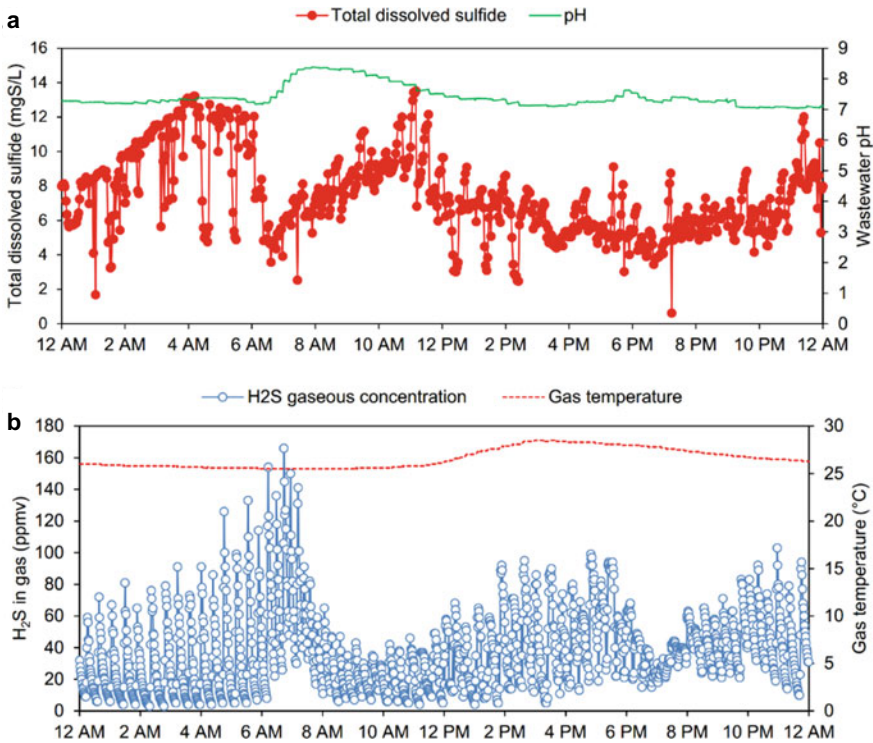


Fig. 4 Diurnal profiles of the total dissolved sulfide, pH and temperature at the end of a rising main sewer pipe located in the Gold Coast, Australia, and gaseous H₂S in the discharge manhole from the main. Reproduced from [47] with permission from Taylor & Francis

It was found both short and long H₂S overload events, i.e. spikes, decrease the sulfide uptake rate of concrete coupons. The latter leads to a larger temporary reduction of sulfide uptake rate whereas they cause similar persistent inhibition effects [48]. For the sulfur transformation in sewer concrete corrosion layer, the oxidation of sulfide or other reduced sulfur species is likely the rate-limiting step of the overall sulfide uptake process. This results in an initial increase in the sulfide uptake rate after a short-term (1 h) gaseous H₂S deprivation period, likely due to a depletion of the sulfur species previously accumulated in the corrosion layer. After the H₂S deprivation period, it will create a higher initial driving force and subsequent increase of sulfide uptake rate [49]. Because real sewers typically experience fluctuating gaseous H₂S concentration, the knowledge about dynamic sulfide uptake by concrete sewer is important for better estimation of corrosion rates and sewer service life.

3.2 *Relative Humidity*

The high relative humidity in the head gas of gravity sewer is mainly due to the relatively high (warm) wastewater temperature in comparison to the slightly cooler sewer walls, which also creates condensation on the concrete surface at crown regions [50]. However, the impact of relative humidity on the concrete sewer corrosion rate was not studied as thoroughly as gaseous H_2S concentrations. On one hand, it is usually difficult to measure the relative humidity with sensors continuously in sewer environment due to the working principle of these sensors. Indeed, the diurnal fluctuation of relative humidity is not as severe as the gaseous H_2S concentrations (Fig. 5). On the other hand, it is often assumed that relative humidity is very high, close to 100%, due to the wastewater flow and turbulence nature in sewer pipes. The usual relative humidity is indeed above 95%, with higher level in summer and lower in other seasons (Fig. 5).

Generally, it is no doubt that the bacteria causing concrete sewer corrosion would need a moist concrete surface to grow. The thin water film on concrete surface also facilitates the transfer of H_2S in the sewer head gas to the liquid where chemical and biological reactions happen. The relative humidity in the sewer head gas was linked to the moisture content of concrete by considering it as a porous material [39]. Early studies showed that the moisture of concrete surface reached a low state (descriptively as a “dry pipe”) that can complete halt sulfuric acid production by bacteria when relative humidity less than $\sim 85\%$ [52]. With the increase of relative humidity, water vapour starts to condense at 100% relative humidity. The condensed water initially fills the smaller diameter pores and then progressively in larger diameter pores, the pore space is completely filled. A visible condensate film forms on the concrete surface after filling all porous structures in the concrete.

As shown in Fig. 5, the relative humidity is an important factor affecting the moisture of concrete surface, especially in the crown regions. For the tidal regions, the fluctuation of water level and the wastewater splashing would be another source of moisture on concrete surface. The water and nutrients provided by wastewater are found to promote the microbial corrosion, especially for the area close to the water level in a sewer pipe [5, 53]. For the pipe surface further away from the water level, the relative humidity of the sewer air and the condensation process on the concrete surface would generate a water film for microbial growth. However, when the wastewater flushing becomes more frequent, it can also reduce the corrosion by washing away the sulfuric acid and corrosion-causing bacteria. This observation was reported in two real sewer sites in Sydney that were subject two frequent flooding due to heavy rainfall [54].

A long-term 3.5 year corrosion chamber study found that high relative humidity (100%), in comparison to low humidity at 90–95%, led to increased corrosion rates on concrete coupons located in the gas-phase (simulating crown regions), but did not affect the corrosion rate of the concrete coupons partially submerged in wastewater. This is because the wastewater level is constant and concrete coupons tend to absorb moisture from wastewater for those concrete surface in proximity to wastewater.

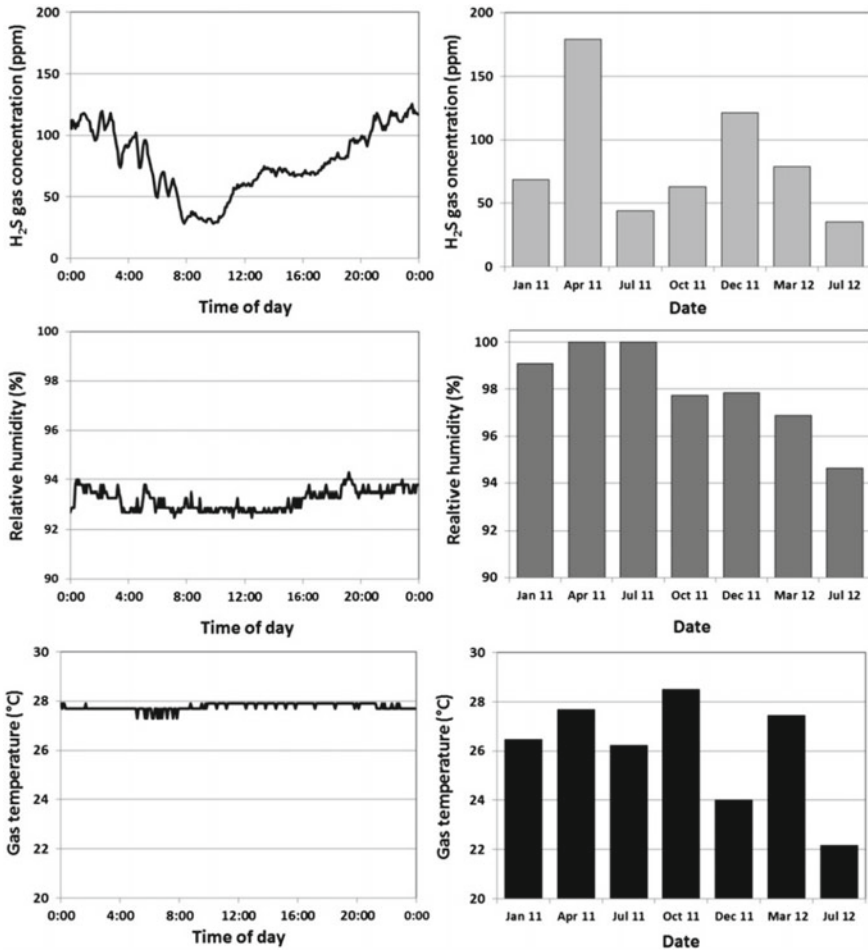


Fig. 5 Diurnal (left) and seasonal variation (right) of H₂S concentration (top), humidity (middle) and gas temperature (bottom) at the Perth sewer site. (The diurnal data shown was recorded on the 24th March 2012). Reproduced from [51] with permission from Elsevier

Collectively speaking, high relative humidity levels close to saturation is nearly inevitable in sewer systems due to the constant wastewater flow and its slightly higher temperature than the sewer gas (partly due to the cooler sewer wall). Only in rare occasions, the natural humidity might become lower than 90% due to the sewer system itself or the climate. Another possibility is that forced ventilation is adopted to reduce the humidity, together with odor treatment in many cases [47]. It is thus recommended to regard sewer head gas to be always at a 100% relative humidity when assessing the corrosion rates of concrete in sewers.

3.3 Location in the Sewer System and Wastewater Inoculation

The sewer pipe crown is a location which is reported to be highly susceptible to sulfide induced corrosion due to the high level of condensation and the high concentration of hydrogen sulfide [38, 53]. Another corrosion hotspots were usually observed on the concrete sewer pipe near the water level, which is also a region of high corrosion activity. This is generally attributed to the wastewater providing sufficient moisture, nutrients and microbial inoculum for the succession of corrosion biofilms. As shown in Fig. 6, our study in real sewer sites located in Sydney found close correlation of microbial community between tidal regions and wastewater, including its sediments. The 2011 ceiling or crown samples showed closer correlation to wastewater due to the flooding of the sewer pipes which becomes fully-filled flow during heavy rainfall before the sampling dates. The results clearly indicate the effects of wastewater on the dynamic changes of corrosion microbial communities.

Indeed, it was reported that sulfate concentrations detected in corrosion layers on concrete surface of partially-submerged coupons were twice as high as that of coupons located in the gas phase, for the same level of H_2S exposure [8]. After

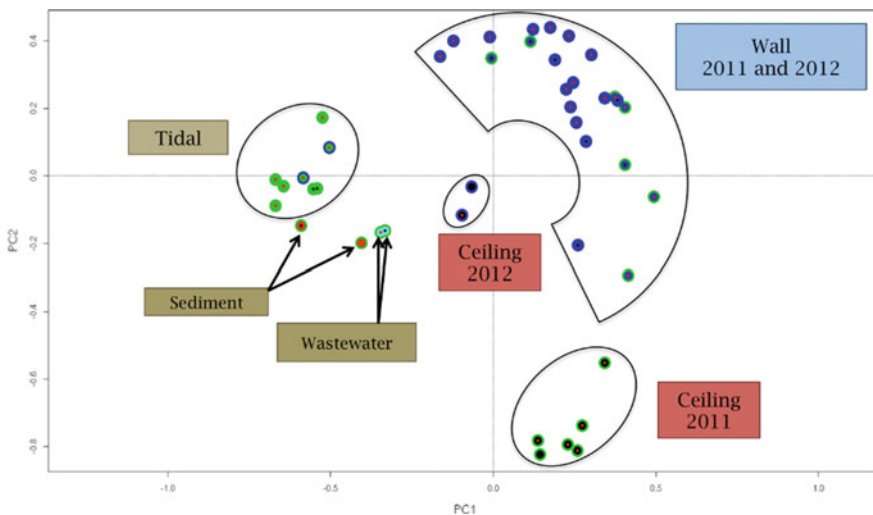


Fig. 6 PCA of microbial community compositions derived from corrosion layer samples at the tidal, wall and ceiling regions of the Sydney sewers, Pipe 1 and Pipe 2. PCA clustering analysis of samples shows relatedness between samples. Each coloured dot represents the community in the sample; similar samples cluster together. Each sample point is comprised of three concentric circles, the external represents the sampling date (green for September 2011 and dark blue for April 2012), the middle circle represents the location from which the sample was taken (black for ceiling, dark blue for wall and green, red and light blue for the tidal, sediment and wastewater respectively, the central dot represents which pipe the sample was from (black representing Pipe 1 and red Pipe 2). Reproduced from [54] with permission from Taylor & Francis

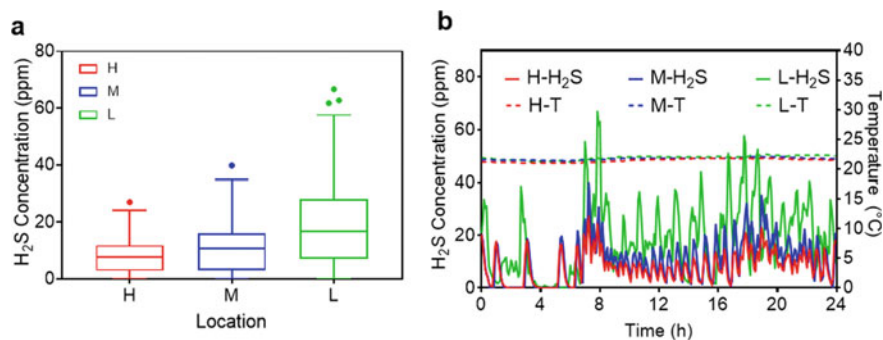


Fig. 7 A box and whiskers plot summarizing the profile of gaseous H₂S concentrations during the exposure in the manhole (a). The middle line of the box represents the median, the upper and lower lines represent the 25th and 75th percentile, the whiskers extending the box, and the outliers represent the data outside the interquartile range. And typical diurnal profiles of gaseous H₂S concentration (H-H₂S, M-H₂S and L-H₂S) and temperature (H-T, M-T, L-T) observed at three heights of the manhole (i.e. H, M, L) (b). Reproduced from [55] with permission from Elsevier

3.5 years of exposure to H₂S, corrosion loss on coupons located in the gas-phase was limited to 2–8 mm. In contrast, the partially-submerged coupons showed much higher levels of corrosion, i.e. between 3 and 15 mm after 45 months exposure. In a sewer manhole located in the Gold Coast, Australia, the H₂S concentrations at different heights varied greatly during the monitoring period, especially for the peak concentrations (Fig. 7). The average H₂S concentration was 8.0, 10.7, and 18.7 ppm at height H, M, and L of the manhole (being 1.5, 1, and 0.5 m from wastewater), respectively. Therefore, the higher corrosion rate at the tidal region was also likely related to the higher H₂S concentrations near the wastewater surface.

In addition to the higher average H₂S concentration at height L, being 0.75 and 1.4 times higher than that of M and H, respectively, a higher fluctuation range of H₂S concentrations were observed at deeper parts of the manhole. Moreover, the coupons at location L were more susceptible to wastewater splash. Enhanced biological sulfide oxidation on concrete surfaces with regular wastewater inoculation due to flooding or splashing has been commonly observed, which can also accelerate corrosion development [5]. Another explanation might be due to the shift of major sulfide oxidizing microorganisms on the concrete coupons placed at different heights of the manhole. *Ferroplasma* was more dominant than *Thiobacillus* at height L and height M than height H. Although both are acidophilic bacteria (pH < 3) [56], *Ferroplasma* has highly impermeable membranes composed of tetraether lipids which are highly adapted to lower or extreme pH conditions [15].

Another study characterized the physical-chemical conditions and corrosion products in the tidal region of concrete sewers [57]. The corrosion of concrete were found to be correlated with the succession of microorganisms, starting with the coexistence of conventional autotrophic sulfide oxidizing bacteria and acidophilic heterotrophic bacteria, and ending with the predominant colonization of *Mycobacterium* (75%) after 6 months. The microbial succession was a result of the imminent vicinity

of concrete surface to wastewater. The high water content, abundant organics and nutrients, continuous microbial inoculation, and persistent and gradual removal of corrosion products, collectively contribute to the severe corrosion in the tidal regions.

The 15-month field study reported concrete corrosion rate within 50 cm of wastewater surface was about 1.6–1.8 times higher than that of a location 1.5 m above the wastewater [55]. It is thus discernable to understand concrete sewer corrosion is not an even process even in one single sewer pipe. The location or distance to the wastewater level can be a critical factor accounting for the final corrosion rate. When assessing the concrete corrosion in sewers, it is prudent to take the hotspots with the highest corrosion rates, not the average rate for the whole pipe, for the estimation of the overall service life.

3.4 Temperature

As concrete sewer corrosion is largely due to biochemical reactions, which are inevitably affected by the temperature. The influence of sewer gas temperature on the chemical, physiochemical and biological processes involved in sewer corrosion was described as a function of the activation energy using the Arrhenius relationship [39], as shown in Eq. (6).

$$r \propto e^{-\frac{E_a}{RT}} \quad (6)$$

where r is the corrosion rate of concrete sewer (or sulfide oxidation rate) at temperature T (K), E_a is the activation energy for the process (J mol^{-1}), ranging from 35 to 80 kJ mol^{-1} have been reported for abiotic and biotic oxidation and for uptake of H_2S under aerobic conditions in wastewater environments. R is the universal gas constant ($=8.314 \text{ J mol}^{-1} \text{ K}^{-1}$).

In sewer systems, the diurnal temperature fluctuation is minimal as shown in Figs. 5 and 7. However, the seasonal change of temperature can be up to 10 °C or higher depending on the local climate. When ventilation is strong (naturally or due to forced ventilation), short-term changes of temperature can happen due to temperature differences and interactions between sewer systems and outer atmosphere [58]. One important process for sewer concrete corrosion is the air-water transfer of hydrogen sulfide, which was found to increase with increasing temperature due to higher diffusion coefficients [59].

It is widely accepted that the sulfide oxidation rate, both chemically and biologically, increases with temperature, which can be described with the Arrhenius relationship like Eq. (6) [14, 60]. The sulfide oxidation rate is reported to double for a temperature increase of 7–9 °C. In addition, sewer systems located in different climates may have biological activity that is acclimated to different temperatures. The sulfide oxidation rates, and accordingly corrosion rates, could thus be very different for different climatic regions. Although the theory is very clear and widely accepted,

in the 3.5 years long-term study, no clear effects of temperature were observed for surface pH, sulfate and corrosion loss [8]. This indicates the effects of temperature were likely masked by more prominent effects of gaseous H₂S concentration and relative humidity. The same was also observed in corrosion rates obtained in real sewers [39].

4 Summary

Concrete corrosion in sewers is an ultimate phenomenon due to a complex of physical, chemical and biological processes. It was divided into the initiation and deterioration stages, for which different impacting factors relevant to sewer environments were discussed in detail. A focus was put on the establishment of quantitative relationships so the knowledge would contribute to the development of a comprehensive mathematical modelling of concrete corrosion in sewers. Gaseous hydrogen sulfide concentration is the mostly important controlling factor of concrete sewer corrosion. Relative humidity can be detrimental to corrosion if it is lower than 90%, which usually indicates a dry concrete surface. The location of concrete surface relative to wastewater level is critical for corrosion development for a few reasons related to corrosion development. It should be recognized that current data available is still limited in many cases, so an accurate relationship is still impossible yet. For the evaluation of concrete service life, it should always consider the highest corrosion possible as the whole pipe needs to be replaced no matter which location was damaged first. Specifically, corrosion rates need to be determined close to wastewater levels, during the summer season with the highest gaseous temperature and with a saturated relative humidity (100%).

References

1. Jiang, G., Sun, X., Keller, J., Bond, P.L.: Identification of controlling factors for the initiation of corrosion of fresh concrete sewers. *Water Res.* **80**, 30–40 (2015)
2. Wei, S., Jiang, Z., Liu, H., Zhou, D., Sanchez-Silva, M.: Microbiologically induced deterioration of concrete: A review. *Braz. J. Microbiol.* (2014)
3. Wei, S., Sanchez, M., Trejo, D., Gillis, C.: Microbial mediated deterioration of reinforced concrete structures. *Int. Biodeterior. Biodegradation* **64**, 748–754 (2010)
4. Islander, R.L., Deviny, J.S., Mansfeld, F., Postyn, A., Shih, H.: Microbial ecology of crown corrosion in sewers. *J. Environ. Eng.* **117**, 751–770 (1991)
5. Jiang, G., Zhou, M., Chiu, T.H., Sun, X., Keller, J., Bond, P.L.: Wastewater-enhanced microbial corrosion of concrete sewers. *Environ. Sci. Technol.* **50**, 8084–8092 (2016)
6. Joseph, A.P., Keller, J., Bustamante, H., Bond, P.L.: Surface neutralization and H₂S oxidation at early stages of sewer corrosion: Influence of temperature, relative humidity and H₂S concentration. *Water Res.* **46**, 4235–4245 (2012)
7. Cayford, B.I., Dennis, P.G., Keller, J., Tyson, G.W., Bond, P.L.: High-throughput amplicon sequencing reveals distinct communities within a corroding concrete sewer system. *Appl. Environ. Microbiol.* **78**, 7160–7162 (2012)

8. Jiang, G., Keller, J., Bond, P.L.: Determining the long-term effects of H₂S concentration, relative humidity and air temperature on concrete sewer corrosion. *Water Res.* **65**, 157–169 (2014)
9. Okabe, S., Odagiri, M., Ito, T., Satoh, H.: Succession of sulfur-oxidizing bacteria in the microbial community on corroding concrete in sewer systems. *Appl. Environ. Microbiol.* **73**, 971–980 (2007)
10. O’Connell, M., McNally, C., Richardson, M.G.: Biochemical attack on concrete in wastewater applications: A state of the art review. *Cem. Concr. Compos.* **32**, 479–485 (2010)
11. Pomeroy, R.D.: *The Problem of Hydrogen Sulphide in Sewers*. Clay Pipe Development Association Limited, London (1990)
12. Bagreev, A., Bandosz, T.: Carbonaceous materials for gas phase desulphurization: Role of surface. *Am. Chem. Soc. Div. Fuel Chem.* **49**, 817–821 (2004)
13. Bagreev, A., Bandosz, T.J.: On the mechanism of hydrogen sulfide removal from moist air on catalytic carbonaceous adsorbents. *Ind. Eng. Chem. Res.* **44**, 530–538 (2005)
14. Nielsen, A.H., Vollertsen, J., Hvitved-Jacobsen, T.: Kinetics and stoichiometry of aerobic sulfide oxidation in wastewater from sewers: Effects of pH and temperature. *Water Environ. Res.* **78**, 275–283 (2006)
15. Li, X., Kappler, U., Jiang, G., Bond, P.L.: The ecology of acidophilic microorganisms in the corroding concrete sewer environment. *Front. Microbiol.* **8**, 683 (2017)
16. Nielsen, A.H., Hvitved-Jacobsen, T., Vollertsen, J.: Kinetics and stoichiometry of sulfide oxidation by sewer biofilms. *Water Res.* **39**, 4119–4125 (2005)
17. Parker, D.: The corrosion of concrete. 2. The function of *Thiobacillus concretivorus* (Nov-spec) in the corrosion of concrete exposed to atmospheres containing hydrogen sulfide. *Aust. J. Exp. Biol. Med. Sci.* **23**, 91–98 (1945)
18. Parker, D.: The corrosion of concrete. I. The isolation of a species of bacterium associated with the corrosion of concrete exposed to atmospheres containing hydrogen sulphide. *Aust. J. Exp. Biol. Med. Sci.* **23**, 81–90 (1945)
19. Parker, D.: Species of sulphur bacteria associated with the corrosion of concrete. *Nature (London)*, **159** (1947)
20. Pomeroy, R., Bowlus, F.D.: Progress report on sulfide control research. *Sewage Works J.* **18**, 597–640 (1946)
21. Ismail, N., Nonaka, T., Noda, S., Mori, T.: Effects of carbonation on microbial corrosion of concretes. *J. Constr. Manag. Eng.* **20**, 11–138 (1993)
22. Hernandez, M., Marchand, E.A., Roberts, D., Peccia, J.: In situ assessment of active *Thiobacillus* species in corroding concrete sewers using fluorescent RNA probes. *Int. Biodeterior. Biodegradation* **49**, 271–276 (2002)
23. Kelly, D.P., Wood, A.P.: Reclassification of some species of *Thiobacillus* to the newly designated genera *Acidithiobacillus* gen. nov., *Halothiobacillus* gen. nov and *Thermithiobacillus* gen. nov. *Int. J. Syst. Evol. Microbiol.* **50**, 511–516 (2000)
24. Nica, D., Davis, J.L., Kirby, L., Zuo, G., Roberts, D.J.: Isolation and characterization of microorganisms involved in the biodeterioration of concrete in sewers. *Int. Biodeterior. Biodegradation* **46**, 61–68 (2000)
25. Santo Domingo, J.W., Revetta, R.P., Iker, B., Gomez-Alvarez, V., Garcia, J., Sullivan, J., Weast, J.: Molecular survey of concrete sewer biofilm microbial communities. *Biofouling* **27**, 993–1001 (2011)
26. Jiang, G., Wightman, E., Donose, B.C., Yuan, Z., Bond, P.L., Keller, J.: The role of iron in sulfide induced corrosion of sewer concrete. *Water Res.* **49**, 166–174 (2014)
27. Monteny, J., Vincke, E., Beeldens, A., de Belie, N., Taerwe, L., van Gemert, D., Verstraete, W.: Chemical, microbiological, and in situ test methods for biogenic sulfuric acid corrosion of concrete. *Cem. Concr. Res.* **30**, 623–634 (2000)
28. Parande, A.K., Ramsamy, P.L., Ethirajan, S., Rao, C.R.K., Palanisamy, N.: Deterioration of reinforced concrete in sewer environments. *Proc. Inst. Civ. Eng. Municipal Eng.* **159**, 11–20 (2006)

29. Gutierrez, O., Mohanakrishnan, J., Sharma, K.R., Meyer, R.L., Keller, J., Yuan, Z.: Evaluation of oxygen injection as a means of controlling sulfide production in a sewer system. *Water Res.* **42**, 4549–4561 (2008)
30. Jiang, G., Gutierrez, O., Sharma, K.R., Keller, J., Yuan, Z.: Optimization of intermittent, simultaneous dosage of nitrite and hydrochloric acid to control sulfide and methane production in sewers. *Water Res.* **45**, 6163–6172 (2011)
31. Jiang, G., Sharma, K.R., Yuan, Z.: Effects of nitrate dosing on methanogenic activity in a sulfide-producing sewer biofilm reactor. *Water Res.* **47**, 1783–1792 (2013)
32. Jiang, G., Yuan, Z.: Synergistic inactivation of anaerobic wastewater biofilm by free nitrous acid and hydrogen peroxide. *J. Hazard. Mater.* **250–251**, 91–98 (2013)
33. Zhang, L., Keller, J., Yuan, Z.: Inhibition of sulfate-reducing and methanogenic activities of anaerobic sewer biofilms by ferric iron dosing. *Water Res.* **43**, 4123–4132 (2009)
34. Sivret, E., Stuetz, R.: Sewer odour abatement practices—an Australian survey. *Water* **37**, 77–81 (2010)
35. O’Dea, V.: Understanding biogenic sulfide corrosion. *Mater. Perform.* **46**, 36–39 (2007)
36. de Belie, N., Monteny, J., Beeldens, A., Vincke, E., van Gemert, D., Verstraete, W.: Experimental research and prediction of the effect of chemical and biogenic sulfuric acid on different types of commercially produced concrete sewer pipes. *Cem. Concr. Res.* **34**, 2223–2236 (2004)
37. Jensen, H.S., Nielsen, A.H., Hvitved-Jacobsen, T., Vollertsen, J.: Modeling of hydrogen sulfide oxidation in concrete corrosion products from sewer pipes. *Water Environ. Res.* **81**, 365–373 (2009)
38. Vollertsen, J., Nielsen, A.H., Jensen, H.S., Wium-Andersen, T., Hvitved-Jacobsen, T.: Corrosion of concrete sewers—the kinetics of hydrogen sulfide oxidation. *Sci. Total Environ.* **394**, 162–170 (2008)
39. Wells, T., Melchers, R.E.: Modelling concrete deterioration in sewers using theory and field observations. *Cem. Concr. Res.* **77**, 82–96 (2015)
40. Hvitved-Jacobsen, T., Vollertsen, J., Nielsen, A.H.: *Sewer Processes: Microbial and Chemical Process Engineering of Sewer Networks*. CRC Press (2013)
41. Chen, K.Y., Morris, J.C.: Kinetics of oxidation of aqueous sulfide by oxygen. *Environ. Sci. Technol.* **6**, 529–537 (1972)
42. Haaning Nielsen, A., Vollertsen, J., Hvitved-Jacobsen, T.: Chemical sulfide oxidation of wastewater-effects of pH and temperature. *Water Sci. Technol.* **50**, 185–192 (2004)
43. Liu, X., Dai, J., Wu, D., Jiang, F., Chen, G., Chui, H.K., van Loosdrecht, M.C.M.: Sustainable application of a novel water cycle using seawater for toilet flushing. *Engineering* **2**, 460–469 (2016)
44. Lahav, O., Lu, Y., Shavit, U., Loewenthal, R.E.: Modeling hydrogen sulfide emission rates in gravity sewage collection systems. *J. Environ. Eng.* **130**, 1382–1389 (2004)
45. Sharma, K.R., Yuan, Z., de Haas, D., Hamilton, G., Corrie, S., Keller, J.: Dynamics and dynamic modelling of H₂S production in sewer systems. *Water Res.* **42**, 2527–2538 (2008)
46. Li, X., O’Moore, L., Song, Y., Bond, P.L., Yuan, Z., Wilkie, S., Hanzic, L., Jiang, G.: The rapid chemically induced corrosion of concrete sewers at high H₂S concentration. *Water Res.* **162**, 95–104 (2019)
47. Jiang, G., Melder, D., Keller, J., Yuan, Z.: Odor emissions from domestic wastewater: A review. *Crit. Rev. Environ. Sci. Technol.* **47**, 1581–1611 (2017)
48. Sun, X., Jiang, G., Bond, P.L., Keller, J.: Impact of fluctuations in gaseous H₂S concentrations on sulfide uptake by sewer concrete: The effect of high H₂S loads. *Water Res.* **81**, 84–91 (2015)
49. Sun, X., Jiang, G., Bond, P.L., Keller, J.: Periodic deprivation of gaseous hydrogen sulfide affects the activity of the concrete corrosion layer in sewers. *Water Res.* **157**, 463–471 (2019)
50. Wells, T., Melchers, R.E., Bond, P.: Factors involved in the long term corrosion of concrete sewers. In: *Australasian Corrosion Association Proceedings of Corrosion and Prevention 2009, Corrosion and Prevention—2009*. Coffs Harbour, Australia (2009)
51. Wells, T., Melchers, R.E.: An observation-based model for corrosion of concrete sewers under aggressive conditions. *Cem. Concr. Res.* **61–62**, 1–10 (2014)

52. Thistlethwayte, D.: *The Control of Sulphides in Sewerage Systems*. Butterworth Pty. Ltd., Sydney (1972)
53. Mori, T., Nonaka, T., Tazaki, K., Koga, M., Hikosaka, Y., Noda, S.: Interactions of nutrients, moisture and pH on microbial corrosion of concrete sewer pipes. *Water Res.* **26**, 29–37 (1992)
54. Cayford, B.I., Jiang, G., Keller, J., Tyson, G., Bond, P.L.: Comparison of microbial communities across sections of a corroding sewer pipe and the effects of wastewater flooding. *Biofouling* **33**, 780–792 (2017)
55. Li, X., Johnson, I., Mueller, K., Wilkie, S., Hanzic, L., Bond, P.L., O’Moore, L., Yuan, Z., Jiang, G.: Corrosion mitigation by nitrite spray on corroded concrete in a real sewer system. *Sci. Total Environ.* **806**, 151328 (2022)
56. Southam, G., Beveridge, T.: Enumeration of *Thiobacilli* within pH-neutral and acidic mine tailings and their role in the development of secondary mineral soil. *Appl. Environ. Microbiol.* **58**, 1904–1912 (1992)
57. Song, Y., Tian, Y., Li, X., Wei, J., Zhang, H., Bond, P.L., Yuan, Z., Jiang, G.: Distinct microbially induced concrete corrosion at the tidal region of reinforced concrete sewers. *Water Res.* **150**, 392–402 (2019)
58. Vollertsen, J., Almeida, M.D.C., Hvitved-Jacobsen, T.: Effects of temperature and dissolved oxygen on hydrolysis of sewer solids. *Water Res.* **33**, 3119–3126 (1999)
59. Yongsiri, C., Vollertsen, J., Hvitved-Jacobsen, T.: Effect of temperature on air-water transfer of hydrogen sulfide. *J. Environ. Eng. ASCE* **130**, 104–109 (2004)
60. Nielsen, A.H., Vollertsen, J., Hvitved-Jacobsen, T.: Chemical sulfide oxidation of wastewater - effects of pH and temperature. *Water Sci. Technol.* **50**, 185–192 (2004)

Mathematical Modelling for the Concrete Corrosion of Sewer Systems



Guangming Jiang, Yiqi Liu, Xuan Li, and Xiaoyan Sun

Abstract Concrete corrosion in sewer systems is a complicated and dynamic process that involves wastewater, head gas, and concrete surfaces. The key process is the biological sulfide oxidation by corrosion microbial communities in the corrosion layer. Mathematical models are practically useful in designing new concrete sewer systems meeting the service life, or in planning the sewer rehabilitation and chemical dosing by estimating the corrosion rates. Theoretically, various corrosion models can also be employed to optimize the design of corrosion-resistant concrete or sewer operation. This chapter provides a review of models for the sulfide oxidation kinetics and different types of models for the service life, including corrosion initiation time and corrosion rate. As corrosion rate is the determining factor for concrete sewer service life, various models were discussed for its estimation, including empirical models, data-driven models, and process dynamic models. These mathematical modelling tools would enable better design, construction, operation, and management of sewer systems.

G. Jiang (✉) · X. Li

School of Civil, Mining, Environmental and Architectural Engineering, University of Wollongong, Wollongong, NSW 2522, Australia
e-mail: gjiang@uow.edu.au

X. Li

e-mail: xuan.li@uts.edu.au

Y. Liu

School of Automation Science and Engineering, South China University of Technology, Wushang Road, Guangzhou 510640, China
e-mail: aulyq@scut.edu.cn

X. Li

Centre for Technology in Water and Wastewater, School of Civil and Environmental Engineering, University of Technology Sydney, Ultimo, NSW 2007, Australia

X. Sun

School of Civil Engineering, Sun Yat-sen University, Zhuhai 519082, China
e-mail: sunxy55@mail.sysu.edu.cn

© The Author(s), under exclusive license to Springer Nature Switzerland AG 2023

G. Jiang (ed.), *Microbiologically Influenced Corrosion of Concrete Sewers*, Engineering Materials, https://doi.org/10.1007/978-3-031-29941-4_8

1 Introduction

The corrosion of concrete sewer pipes and other structures is mainly a result of the microbial oxidation of hydrogen sulfide in sewer air. As a predominant form of deterioration that reduces the service life of the concrete sewers, it is critical to model the corrosion processes for the planning of inspection, maintenance, and rehabilitation in the management of sewer assets. Due to the slow corrosion process and the transient dynamics of corrosion factors (gas flow, H_2S concentration, humidity etc.), the instant corrosion fluctuates for the same sewer location. It is fundamentally important to understand the corrosion processes by modelling such instantaneous corrosion rates. However, the long-term corrosion rate (mm/year), or alternatively the service life, is the primary objective for such corrosion models. The sewer service life (L , year) is determined by two stages, i.e. corrosion initiation and concrete deterioration (see Chap. 7 for detailed discussions). It is thus possible to calculate the concrete sewer service life using two key corrosion parameters: the time for corrosion to initiate (t_i , month) and the corrosion rate (r , i.e. concrete depth lost over time, mm/year) (Eq. 1).

$$L = \frac{t_i}{12} + \frac{D}{r} \quad (1)$$

where D is the depth (mm) of concrete cover that can be sacrificed before the end of sewer service life. It is thus possible to estimate the depth of sacrificial layer of concrete sewers when corrosion parameters and service life are designated. This equation of concrete sewer service life thus forms the base for further discussion about sewer corrosion models.

In the early research about concrete sewer corrosion, empirical models were established based on the understanding of concrete corrosion at that time, which mainly relies on the direct proportional relationship between sulfide uptake and concrete mass loss [40, 45, 46]. Although this fundamental principle of concrete sewer corrosion still applies nowadays, the empirical models have a few empirical parameters that would require careful considerations for their accuracy in using the models.

In addition to the conventional empirical models, there are different approaches to the corrosion modelling: (1) simplified process models mainly based on the kinetics of sulfide oxidation [14, 16, 47]; (2) physicochemical models including purely the reaction–diffusion system [5] or comprehensive models integrating surface neutralisation, biological sulfide oxidation, acid transport and chemical reactions [54, 55]; (3) data-driven models performing prediction based on sewer environmental factors [19, 29, 33, 48, 49].

2 Oxidation Kinetics of Hydrogen Sulfide in Sewer Environment

Although sulfur may exist as several oxidation states (Table 1), only three are significant in nature: -2 (sulfhydryl R-SH, and sulfide, HS^-), 0 (elemental sulfur, S), and $+6$ (sulfate, SO_4^{2-}). For sulfur cycle in sewers, sulfate can be reduced by many sulfate-reducing bacteria (SRB) via either dissimilatory or assimilatory pathways. On the other hand, sulfur compound oxidizing bacteria (SOB) are capable of oxidizing sulfide directly or indirectly to sulfate.

Some aerobic bacteria are capable of removing sulfate intracellularly to sulfide ($-\text{SH}$), which is then incorporated into new cellular materials (assimilatory sulfate reduction). However, biological sulfate reduction generally denotes the anaerobic dissimilatory sulfate reduction. Anaerobic sulfate reduction may occur in pressure sewer biofilms, and the deep layer of biofilms or sediments in gravity sewer environment [8, 10]. Sulfide oxidation is also widespread when oxygen and nitrate/nitrite are injected or added to sewer wastewater either naturally or artificially. In wastewaters, various sulfur compounds appear in the chemical and biological sulfur cycle [20, 25]. The sulfide production and sulfate reduction constitute a complete sulfur cycle as shown in Fig. 1.

Aeration in partially-filled gravity sewer pipes is a primary source of dissolved oxygen in wastewater. Oxygen in the sewer head gas is also available for any biological sulfide oxidation on the concrete surface exposed to the sewer air. The aerobic oxidation of hydrogen sulfide can happen both in the wastewater or on the concrete surface where oxygen is available. Sulfide oxidation in the wastewater phase is usually not considered harmful because it doesn't reduce the wastewater pH significantly due to the large volume of wastewater, limited hydraulic residence time in sewers (usually less than 10 h), and its high buffering capacity. In contrast, it is a highly damaging process on concrete surface due to the reaction is in a thin moisture layer with limited amount of condensation water and its relative stagnant nature. The corrosion of concrete sewer pipes and other structures is mainly a result of the microbial oxidation of hydrogen sulfide by oxygen mainly in gravity sewers. The reaction kinetics of aerobic sulfide oxidation is critical to the production rate of sulfuric acid,

Table 1 Oxidation states of sulfur, adapted from [9]

Oxidation state	Name	Formula
+ 6	Sulfate	SO_4^{2-}
+ 5	Dithionate	$\text{S}_2\text{O}_6^{2-}$
+ 4	Sulfite	SO_3^{2-}
+ 4	Disulfite	$\text{S}_2\text{O}_5^{2-}$
+ 3	Dithionate	$\text{S}_2\text{O}_4^{2-}$
+ 2	Thiosulfate	$\text{S}_2\text{O}_3^{2-}$
0	Elemental sulfur	S^0
- 2	Sulfide	S^{2-}

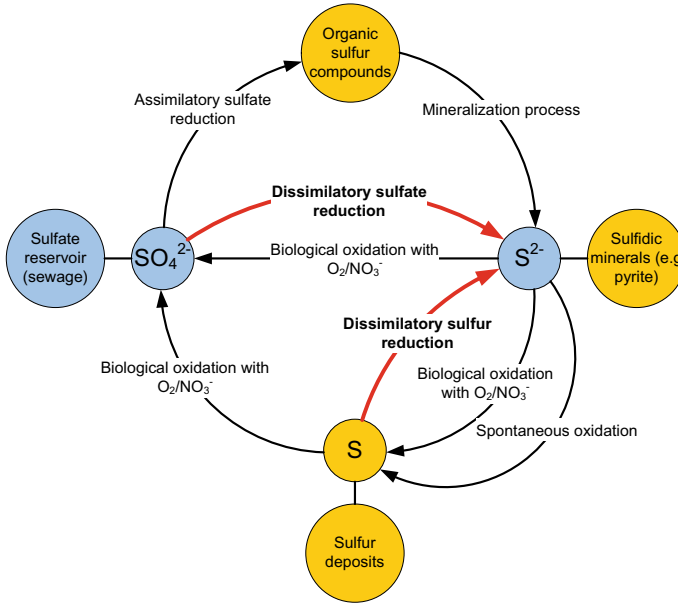
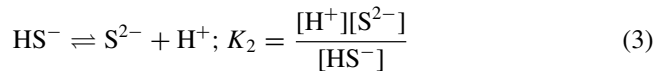
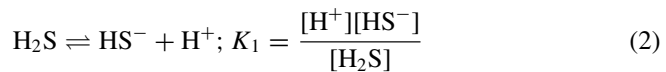


Fig. 1 The biological sulfur cycle in the sewer systems, adapted from [20, 23, 25]

which eventually causes the deterioration of concrete. This chapter focuses on the surface reactions that is directly relevant to the concrete corrosion.

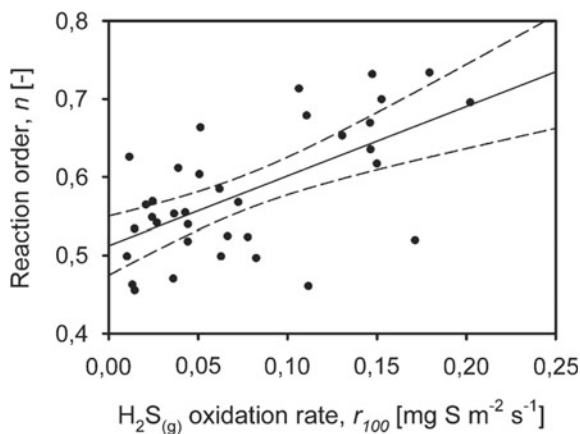
2.1 Oxidation Reactions and Products of Hydrogen Sulfide

As a weak acid, the speciation of sulfide (thus the reactants of sulfide oxidation) can affect the oxidation rates. Hydrogen sulfide (H_2S) can form different sulfide species in an aqueous solution, of which the equilibrium depends largely on the solution pH and its thermodynamic dissociation constants (Figs. 2 and 3).

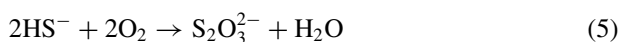


The aerobic sulfide oxidation products include elemental sulfur (S^0) and sulfate (SO_4^{2-}) through either biological or chemical processes [36, 38]. Many factors like temperature, pH have been investigated for their effects on aerobic sulfide oxidation [35]. The rate of sulfide oxidation was found to double with a temperature increase

Fig. 2 Correlation between the reaction order (n) and the hydrogen sulfide gas phase oxidation rate at 100 ppm. Regression line (solid) and 95% confidence intervals (dashed lines) are shown. Reproduced from [47] with permission from Elsevier



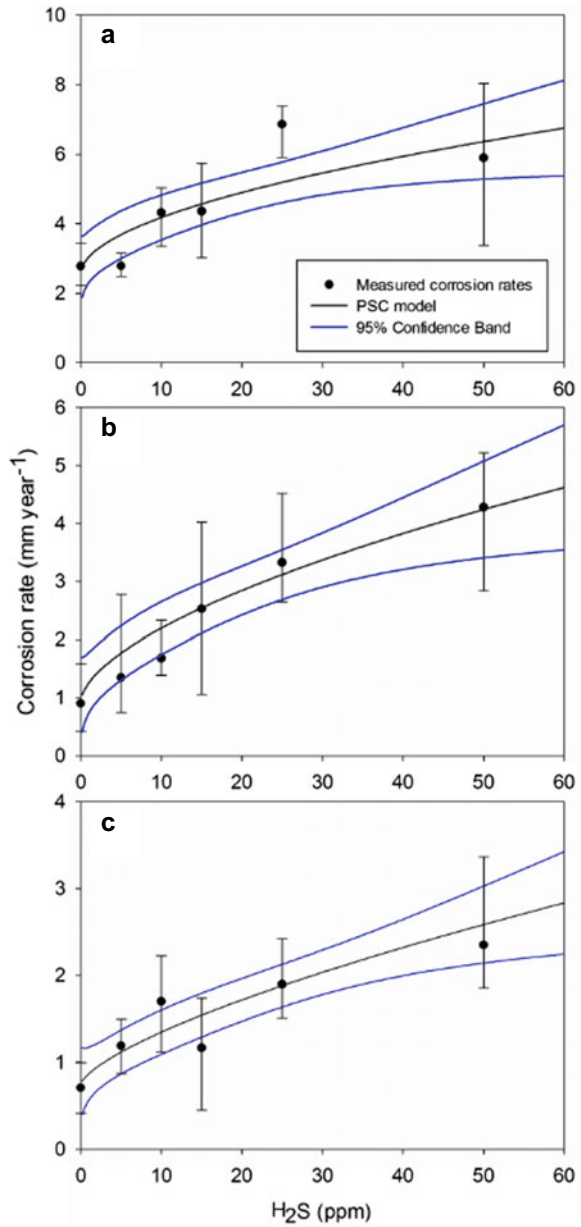
of 7–9 °C. The effect of pH is mainly related to the dissociation of H_2S to form bisulfide ion (HS^-), with HS^- being more easily oxidized chemically than H_2S .



Chemical sulfide oxidation was found to produce thiosulfate and sulfate, while elemental sulfur and sulfate is the main product of biological oxidation [6, 35]. Many efforts have been made to understand the kinetics and stoichiometry of aerobic sulfide oxidation [3, 37]. The stoichiometry of chemical oxidation of sulfide with oxygen varies with different intermediates and products, mainly elemental sulfur (S^0), thiosulfate ($\text{S}_2\text{O}_3^{2-}$), sulfite (SO_3^{2-}) and sulfate (SO_4^{2-}) [37].

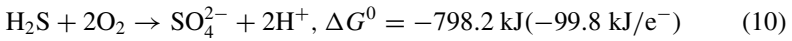
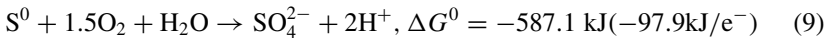
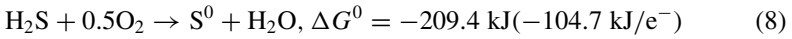
In the water phase, the chemical oxidation accounts for less than 5% of the total sulfide oxidation while biofilms accounted for the majority [35]. For the biological sulfide oxidation with oxygen by sewer biofilm, it is reported to be 0.5 g O_2 consumed for the oxidation of 1 g sulfide [36], corresponding to elemental sulfur being the oxidation product [39]. A detailed review of sulfide removal rate with O_2 , NO_3^- , and CO_2 as electron acceptors have been provided by [7].

Fig. 3 Corrosion rates of partially-submerged concrete coupons fitted with the PSC model for 0–12 (a), 12–24 (b), and 24–45 (c) months. Error bars are standard deviations of corrosion rates (•) determined for the same level of H₂S. Reproduced from [16] with permission from Elsevier



2.2 Thermodynamics and Kinetics of Sulfide Oxidation by Oxygen

Sulfide oxidation can occur abiotically in the absence of SOB, although biological sulfide oxidation dominates in the concrete sewer corrosion when gaseous H_2S concentration is limited to be less than 100 ppm [16, 28, 43]. At extremely high concentration like 500–1500 ppm, chemical sulfide oxidation might become the major contributor of concrete corrosion, especially on fresh concrete with a high surface pH [30]. The overall biological chemotrophic oxidation of sulfide by sulfide oxidizing bacteria in the presence of O_2 is described in Eqs. below [31].



For aerobic sulfide oxidation, the final sulfur products are largely dependent on the mass molar ratio between oxygen (O_2) and sulfide (O/S). When O/S ratio is below 0.6, aerobic sulfide oxidation mainly produce thiosulfate ($\text{S}_2\text{O}_3^{2-}$) through abiotic chemical oxidation, which can outcompete biological sulfide oxidation under such low oxygen conditions [2, 12, 13]. A higher O/S ratio around 0.7 would ensure S^0 being the primary final product through Eq. 8, which has a theoretical stoichiometry of 0.5. An even higher O/S ratio > 1 leads to the formation of sulfate (SO_4^{2-}) as the major final products of biological sulfide oxidation. The low O/S ratio means low energy production, which subsequently inhibits the growth of some sulfide-oxidizing bacteria [2] because of energy shortfall for the biomass synthesis [26].

Theoretically the corrosion rate is directly proportional to the biological sulfide oxidation rate (SOR), which is related to gaseous H_2S concentration in a power function [14, 47]. The uptake of hydrogen sulfide from the sewer head gas by corroding concrete was described using the n th-order kinetics, and was consequently normalized to the exposed concrete surface area [14]. The surface removal kinetics of gas phase hydrogen sulfide under varying temperature conditions were corrected to a temperature of 20 °C using an Arrhenius expression with a temperature coefficient applicable for a diffusion-limited process [11].

$$r_{\text{H}_2\text{S}} = k C_{\text{H}_2\text{S}}^n \frac{10^{-6} \times 101325 \times 32 \times V}{RTA} 1.03^{(T-293.16)} \quad (11)$$

where $r_{\text{H}_2\text{S}}$ is the hydrogen sulfide removal rate [$\text{g S m}^{-2} \text{ s}^{-1}$], k is the rate constant for hydrogen sulfide uptake [$(\text{ppm})^{-n+1} \text{ s}^{-1}$], $C_{\text{H}_2\text{S}}$ is the hydrogen sulfide concentration [ppm], n is the reaction order [-], V is the air volume for the concrete surface A [m^3],

R is the universal gas constant [$\text{J K}^{-1} \text{mol}^{-1}$], T is the absolute temperature [K], A is the area of concrete surface exposed to the gas phase [m^2].

By comparing the measured gas-phase hydrogen sulfide uptake rate and the batch reactor tests with corrosion products, it was concluded that hydrogen sulfide uptake by the concrete surface was governed by a combination of sorption and biological oxidation [15]. It is therefore prudent to differentiate sulfide uptake rate (SUR) and sulfide oxidation rate (SOR), when they are utilized to quantify the concrete corrosion rates in sewers. For a specific temperature and sewer system, Eq. 10 can be simplified as:

$$r_{\text{H}_2\text{S}} = k_A C_{\text{H}_2\text{S}}^n \quad (12)$$

where k_A is surface-specific process rate constant [$\text{mg S m}^{-2} \text{s}^{-1} \text{ppm}^{-n}$]. It was found that the reaction order (n) correlated weakly with the hydrogen sulfide oxidation rates [47]. Experimentally, the biological sulfide oxidation rates increased with increasing hydrogen sulfide concentrations and showed no tendency towards saturation, even at gas phase concentrations as high as 1000 ppm. The hydrogen sulfide oxidation kinetics followed simple n th order kinetics, with a process order in the range from 0.45 to 0.75 and an average rate constant of $0.005 \text{ mg S m}^{-2} \text{ s}^{-1} \text{ ppm}^{-n}$ (Fig. 2).

The measured hydrogen sulfide oxidation kinetics was extrapolated to gravity sewer systems by considering the transfer or release of hydrogen sulfide from wastewater [47]. It was found that the fast hydrogen sulfide oxidation rate was limited by the slower hydrogen sulfide release rate at rather low gaseous H_2S concentrations. This has a profound implication as that it is the hydrogen sulfide release rate that controls the corrosion rate and that high corrosion rates can occur even though hydrogen sulfide gas phase concentrations are low. The H_2S release was largely controlled by the wastewater pH, gravity sewer pipe diameter and slope. It is thus essential to simulate the H_2S release from wastewater.

2.3 Hydrogen Sulfide Release Rate from Wastewater

Sulfide is mostly generated in wastewater and H_2S is subsequently released from wastewater surface to the sewer head gas. This mainly takes place in sewer networks having a free water surface from which the gas can escape, e.g., gravity sewers, pumping stations and manholes [53, 54]. The key element in the emission process is molecular aqueous hydrogen sulfide, $\text{H}_2\text{S}_{\text{aq}}$. The ionized forms, bisulfide ion HS^- or sulfide ion S^{2-} due to H_2S dissociation, at typical pH values of domestic wastewater cannot pass across the air–water interface [11]. The concentration of S^{2-} is negligible because of its insignificant presence in the domestic wastewater, e.g., only approximately 0.1% present at a high pH value of 14 and even less with decreasing pH (Eqs. 2 and 3). The sulfide dissociation in wastewater depending on the pH is represented as below:

$$\log \frac{[HS^-]}{[H_2S_{(aq)}]} = pH - pK_a \quad (13)$$

where, pK_a is negative logarithm of the H_2S/HS^- equilibrium constant ($= 7.0$ for typical wastewater conditions). As shown in Eq. 2, lower wastewater pH shift the H_2S distribution toward higher $H_2S(aq)$ fractions, implying increased emission rates, while alkaline conditions diminish the $H_2S(aq)$ fraction. Based on the Henry's law constant of H_2S and the two-film or two-resistance theory [27], the mass transfer of H_2S from wastewater to air is mainly controlled by a thin water film at the air–water interface, i.e. resistance in the water phase being over 98% of the overall resistance [32, 34, 42]. Therefore, the release rate of H_2S from wastewater is not affected by the turbulence in the air phase except the gaseous H_2S concentration.

In sewers, the gaseous and aqueous H_2S concentrations are usually not equilibrated, i.e. no air–water mass transfer of H_2S . The release rate of H_2S is thus determined by the overall mass-transfer coefficient and concentration difference, i.e. the difference between the concentration in the water phase and the saturation concentration corresponding to the gaseous concentration.

$$r_{H_2S} = K_L a_{H_2S} (C_{w,H_2S} - \frac{C_a}{H_c}) \quad (14)$$

where, r_{H_2S} is H_2S release rate from wastewater ($gS\ m^{-3}\ h^{-1}$); $K_L a_{H_2S}$ is overall mass transfer coefficient of H_2S (h^{-1}); C_{w,H_2S} is dissolved H_2S concentration in the water phase ($gS\ m^{-3}$); C_a is gaseous H_2S concentration in the sewer head gas ($gS\ m^{-3}$); H_c is Henry's law constant of H_2S (m^3 of water phase m^{-3} of air phase). By considering dissolved H_2S as a part of total dissolved sulfide and the impact of temperature and correction for wastewater rather than clean water, the below equation was proposed by Yongsiri et al. [53].

$$r_{H_2S} = \alpha f K_L a_{H_2S} (C_w - \frac{C_a}{f H_c}) \theta_e^{(T-20)} \quad (15)$$

where, f is the ratio of dissolved H_2S to total dissolved sulfide; C_w is the total dissolved sulfide concentration ($gS\ m^{-3}$). α is the ratio of $K_L a_{H_2S}$ for domestic wastewater to that for clean water ($-$), being about 0.6; θ_e is temperature correction factor for H_2S mass transfer, being about 1.034 and T is temperature ($^{\circ}C$).

$K_L a_{H_2S}$ depends largely on the physical and hydraulic conditions of wastewater. [52] described an empirical equation to determine $K_L a_{H_2S}$ based on the $K_L a_{O_2}$ and wastewater pH.

$$K_L a_{H_2S} = (1.736 - 0.196pH) K_L a_{O_2} \quad (16)$$

$$K_L a_{O_2} = 0.86(1 + 0.2F^2)(su)^{3/8} d_m^{-1} \alpha_r^{(T-20)} \quad (17)$$

where, $K_L a_{O_2}$ is the overall mass-transfer coefficient of oxygen (reaeration coefficient) at 20 °C (h^{-1}). u is the mean wastewater flow velocity (m s^{-1}); s is the slope of sewer pipes (m m^{-1}); d_m is the mean hydraulic depth of wastewater in the sewer pipes, i.e., the water cross-sectional area divided by the width of the water surface (m); F is the Froude number, $F = u(gd_m)^{-0.5}$; g is the gravitational acceleration (m s^{-2}); α_r is the temperature coefficient for reaeration = 1.024; T is the wastewater temperature (°C).

3 Empirical Models

In the early time of concrete sewer corrosion research, some empirical models were developed to forecast the hydrogen sulfide production, accumulation, and corresponding corrosion rates based on data observed in wastewater and corroding concrete. Pomeroy [41] summarized different equations involved according to the best knowledge at that time. The well-known Pomeroy model calculates the corrosion rate of concrete sewer pipes based on the H_2S emission from wastewater and a few empirical parameters [41]:

$$C_r = \frac{11.5k\phi_{sw}}{alk} \quad (18)$$

where C_r = concrete sewer corrosion rate (mm/year); k = factor related to the acid formation, based on climate conditions, 0.8 in moderate climates; ϕ_{sw} = hydrogen sulfide flux at the air-wall interface [$\text{g H}_2\text{S}/(\text{m}^2 \text{ h})$]; and alk = alkalinity of the concrete pipe material ($\text{g CaCO}_3/\text{g concrete}$). As discussed above, the sulfide uptake rate by concrete tends to equilibrate with the release rate of H_2S from wastewater to the sewer head gas. The flux of H_2S to the wall equals to the flux of H_2S from sewage to sewer air, i.e. ϕ_{sf} (US [46]).

$$\phi_{sf} = 0.7(su)^{3/8}[\text{H}_2\text{S}_{aq}] = 0.7(su)^{3/8} f[\text{TDS}] \quad (19)$$

where ϕ_{sf} is the flux of H_2S at the wastewater-air interface ($\text{g m}^{-2} \text{ h}^{-1}$); s is the slope of sewer pipes (m m^{-1}); u is the wastewater flow velocity (m s^{-1}); f is the pH-dependent factor for proportion of H_2S in total dissolved sulfide; $[\text{TDS}]$ is the total dissolved sulfide concentration (mg L^{-1}).

This empirical equation has been widely used for the estimation of corrosion rate based on the H_2S emission from wastewater. Recent study also confirmed that the model estimated corrosion rate corresponds well with the measurements in a pilot-scale concrete sewer [47]. However, the estimated corrosion rate could be very different from the actual rate due to the local flow turbulence or the impact

of factors other than H_2S . Many environmental factors, including gaseous H_2S , relative humidity, temperature and wastewater inoculation, have been determined to be influential to the concrete corrosion rate observed in both lab-scale and real sewers [16, 18, 21, 49]. Therefore, some recent empirical models should consider other factors that play significant roles in determining the corrosion rate.

To accommodate the effects of relative humidity, it is assumed that the sulfide oxidate rate is proportional to the water content in the concrete because water is essential for possible biological and chemical reactions. The water content can be estimated from the relative humidity using a Brunauer–Emmett–Teller (BET) sorption isotherm [51]. Based on these considerations and the statistical analysis of long-term corrosion testing results obtained using lab-scale corrosion chambers, the following models were proposed to estimate corrosion rates.

$$\text{For sewer tidal regions : } C_r = kC_{H_2S}^n + C_{ri} \quad (20)$$

$$\text{For sewer crown regions : } C_r = kC_{H_2S}^n f_{BET}(RH) + C_{ri} \quad (21)$$

where C_r is the corrosion rate (mm year^{-1}); C_{H_2S} is the gaseous H_2S concentration; k and n are model constants that can be estimated from the experimental data. C_{ri} represents the corrosion caused due to previous exposure. $f_{BET}(RH)$ is a BET sorption isotherm. The sewer tidal region model was examined by fitting with the experimental data (Fig. 3). The empirical model can adequately describe the relationship between corrosion rates and H_2S concentrations.

Another study explored theoretical relationship between corrosion rate and gaseous concentration, relative humidity and temperature to establish an empirical model [50]. The effects of sewer head gas temperature on the chemical, physiochemical and biological processes involved in sewer corrosion was described as a function of the activation energy using the Arrhenius relationship:

$$r \propto e^{-E_a/RT} \quad (22)$$

where r , (mol s^{-1}), is the rate of the process in question at temperature = T (K), E_a is the activation energy for the process (J mol^{-1}) and R is the universal gas constant ($= 8.314 \text{ J mol}^{-1} \text{ K}^{-1}$). The value of E_a was estimated using the concrete corrosion data obtained in field conditions as a value at the midrange of reported values of $E_a = 45 \text{ kJ mol}^{-1}$, with literature values ranging from 35 to 80 kJ mol^{-1} for abiotic and biotic oxidation and for uptake of H_2S under aerobic conditions in wastewater environments [50].

To approximate the effects of sewer head gas relative humidity on concrete corrosion, a relationship between humidity and concrete moisture content was assumed as a function of the pore size distribution of the concrete, the geometry and tortuosity of the individual pores as well as the temperature of the pipe relative to the sewer head gas [50]. The maximum pore radius into which vapour will condense was estimated for relative humidities ranging from 85 to 100% using the Kelvin equation which

relates the maximum radius of a pore at which capillary condensation occurs to the partial pressure of water vapour.

$$r_{cond} = \frac{-2\gamma V_m}{\ln(P/P_{sat})RT} = \frac{-2\gamma V_m}{\ln(P_{RH})RT} \quad (23)$$

where, r_{cond} is the radius of the pore in which condensation occurs (m), P/P_{sat} is the partial pressure of the water vapour (equivalent to the relative humidity $P_{RH}(-)$), γ is the surface tension of water (N m^{-1}), V_m is the molar volume of water ($\text{m}^3 \text{mol}^{-1}$), R is the universal gas constant ($= 8.314 \text{ J mol}^{-1} \text{ K}^{-1}$), and T is the absolute temperature (K). It is also assumed that the concrete corrosion rate is directly proportional to the moisture content present in the concrete pores. Based on the previously reported relationship between sulfide oxidation and gaseous hydrogen sulfide concentration (Eq. 12), this study finally established an empirical model of the concrete corrosion rate for the specific concrete products as below.

$$r = A \times C_{\text{H}_2\text{S}}^{0.5} \times \frac{(0.1602P_{RH} - 0.1355)}{(1 - 0.977P_{RH})} \times e^{(-45000/RT)} \quad (24)$$

The value of the scaling constant, A ($= 207,750 \text{ mm year}^{-1} \text{ ppm}^{-1/2}$), was determined using the average humidity, temperature and gaseous H_2S concentration associated with corrosion measurements obtained in the study.

4 Dynamic Process Models

The corrosion of concrete sewers includes an initiation stage (no mass loss) and a deterioration stage evidenced by continuous formation of corrosion products and loss of intact concrete. Recent years have seen significant advancement in understanding the development of corrosion, detailed corrosion processes and impacting factors for the different corrosion stages. The initiation of corrosion on concrete starts with carbonation and neutralisation by H_2S . The initiation process might take a few years depending on the conditions [21]. Few models have tried to address this initiation period due to its insignificance compared to the whole service life [19, 56]. For the corrosion prevention in new sewers, more research is required to better understand and model the initiation processes.

The key process of concrete corrosion is the sulfide oxidation, both chemical and biological, in the corrosion layer. The simple approach for sulfide oxidation can be adequately modelled as a nth order kinetics with n around 0.5 [16, 47]. For the active deterioration stage, many complex process models have been developed not only for the modelling of corrosion rate but also the formation and distribution of different corrosion products. A multiple diffusion–reaction system with a moving boundary, i.e. the corrosion front, was employed to simulate the corrosion in sewer pipes [1].

Recently, similar comprehensive models were developed and validated with data from accelerated corrosion tests [5, 55, 56].

Yuan et al. [56] employed a set of reactive transport model to simulate the initial neutralization process of concrete surface, sulfuric acid (H_2SO_4) production by sulfide-oxidizing bacteria community, and H_2SO_4 degradation of concrete. This model is capable of predict the change of pH in corrosion products (SOB community), the composition of pipe concrete during the biodeterioration process, and the decrease of concrete depth during the MICC process.

For the neutralisation of concrete surface, the absorption of hydrogen sulfide and its various chemical reactions with cement were considered. The absorption of hydrogen sulfide was simulated by the n th order kinetics as described as follow

$$F_{\text{H}_2\text{S}} = k_{\text{abs}} p_{\text{H}_2\text{S}}^n \quad (25)$$

where, $p_{\text{H}_2\text{S}}$ is the gaseous H_2S concentration (ppm). k_{abs} is the surface specific H_2S absorption rate constant, which is reported to vary between 6.25×10^{-8} and $3.12 \times 10^{-7} \text{ mol S m}^{-2} \text{ s}^{-1} (\text{ppm H}_2\text{S})^{-n}$ depending on temperature. The chemical neutralization of cement by H_2S considered a set of different reactors as listed in Table 2.

Based on the equilibrium constants listed in the Table 2, the critical hydrogen sulfide concentration was estimated to be $8.90 \times 10^{-10} \text{ mol L}^{-1}$ for CaS precipitation, i.e., dissolution of portlandite takes place when aqueous H_2S concentration is higher than this critical level. With the above-described absorption of H_2S in gas phase and the chemical reactions of neutralization of concrete, the pH reduction of concrete surface can be calculated.

The biological production of sulfuric acid was simulated in a formality to the curve of succession of SOB at different pH range, which was fitted by a set of lognormal functions.

Table 2 Chemical reaction between cement and hydrogen sulfide

Aqueous reactions	Equilibrium constant (K)
$\text{H}_2\text{O} \rightleftharpoons \text{H}^+ + \text{OH}^-$	$K_{\text{H}_2\text{O}} = 10 \times 10^{-14}$
$\text{H}_2\text{S} \rightleftharpoons \text{H}^+ + \text{HS}^-$	$K_{\text{H}_2\text{S}} = 8.9 \times 10^{-8}$
$\text{HS}^- \rightleftharpoons \text{H}^+ + \text{S}^{2-}$	$K_{\text{HS}^-} = 1.2 \times 10^{-13}$
$\text{CaOH}^+ \rightleftharpoons \text{Ca}^{2+} + \text{OH}^-$	$K_{\text{CaOH}^+} = 1.66 \times 10^1$
$\text{Ca}^{2+} + \text{S}^{2-} \rightleftharpoons \text{CaS}$	$K_{\text{CaS}} = 3.5 \times 10^3$
$\text{Ca}^{2+} + 2\text{HS}^- \rightleftharpoons \text{Ca}(\text{HS})_2$	$K_{\text{Ca}(\text{HS})_2} = 1.276 \times 10^1$
$\text{Ca}^{2+} + \text{H}_2\text{SiO}_4^{2-} \rightleftharpoons \text{CaH}_2\text{SiO}_4$	$K_{\text{CaH}_2\text{SiO}_4} = 3.89 \times 10^4$
$\text{Ca}^{2+} + \text{H}_3\text{SiO}_4^- \rightleftharpoons \text{CaH}_3\text{SiO}_4^+$	$K_{\text{CaH}_3\text{SiO}_4^+} = 1.58 \times 10^1$
$\text{SiO}_2 + 2\text{H}_2\text{O} \rightleftharpoons \text{H}_4\text{SiO}_4$	$K_{\text{SiO}_2} = 1.94 \times 10^{-3}$
$\text{H}_4\text{SiO}_4 \rightleftharpoons \text{H}_3\text{SiO}_4^- + \text{H}^+$	$K_{\text{H}_4\text{SiO}_4} = 1.55 \times 10^{-10}$
$\text{H}_3\text{SiO}_4^- \rightleftharpoons \text{H}_2\text{SiO}_4^{2-} + \text{H}^+$	$K_{\text{H}_3\text{SiO}_4^-} = 4.68 \times 10^{-14}$

$$\text{NSOB} : R_{\text{H}_2\text{SO}_4} = \frac{\alpha_0}{\sigma\sqrt{2\pi}} e^{-\frac{(\text{pH}_{\text{NSOB}} - \text{pH}_{\text{ASOB}})^2}{2\sigma}} 10^{\text{pH}_{\text{NSOB}} - \text{pH}} \quad (26)$$

$$\text{ASOB} : R_{\text{H}_2\text{SO}_4} = \frac{\alpha_0}{\sigma\sqrt{2\pi}} e^{-\frac{(\text{pH} - \text{pH}_{\text{ASOB}})^2}{2\sigma}} \quad (27)$$

where, α_0 and σ are constants depending on SOB numbers and activity, which were determined using previous experimental data. When $\text{pH} \geq \text{pH}_{\text{ASOB}}$, $\alpha_0 = 8 \times 10^{-7} \text{ mol L}^{-1} \text{ s}^{-1}$, $\sigma = 0.48$; while $\alpha_0 = 4 \times 10^{-7} \text{ mol L}^{-1} \text{ s}^{-1}$, $\sigma = 0.24$ when $\text{pH} \leq \text{pH}_{\text{ASOB}}$.

The biologically produced sulfuric acid, as a strong acid, will penetrate the porous concrete react with concrete due to its alkalinity. This leads to the dissolution of the calcium hydroxide and production of gypsum and ettringite as a layer of white precipitate on the concrete surface. The modelling of these chemical reactions was simulated in a previous paper by Yuan et al. [54]. The coupling between the transport of different reactive species in porous concrete (assuming water saturation due to high relative humidity in sewers) and the bio-/chemical reactions were simulated by their mass balance equations. This model provides a prediction of the biodeterioration depth of concrete being exposed to hydrogen sulfide. As shown in Fig. 4, the model predicted biodeterioration depth during 8 cycles of submersion is consistent with the experimental results (Fig. 5).

Overall, the process models need to be validated with corrosion data from long-term tests under real sewer conditions. Some improvement in modelling the different physicochemical and biological processes may enhance the model performance. Process parameters of current models were not calibrated or properly verified with reliable experimental data due to the complexity and difficulty in obtaining such data. Some models assume the corrosion microbial community as one single species and the biological sulfide oxidation as a simple correlation to the pH. The relationship of the biological sulfide oxidation rate with the environmental factors needs to be accounted for adequately to ensure a good simulation of the acid production

Fig. 4 Concrete surface pH after exposure of 1 year and its model simulated values. Reproduced from [55] with permission from Elsevier

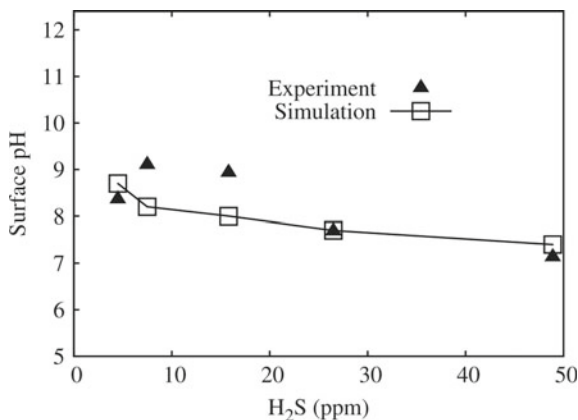
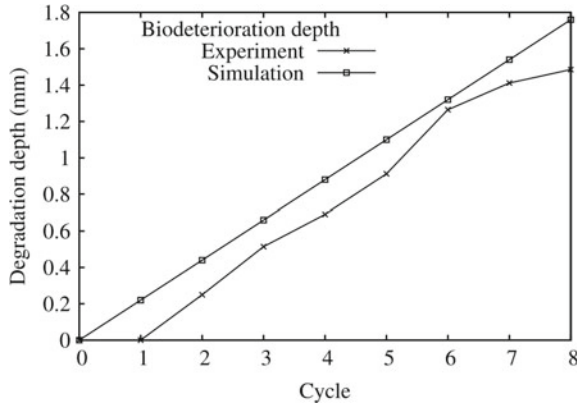


Fig. 5 The model predicted and measured corrosion depth of concrete. Reproduced from [55] with permission from Elsevier



rate, which is the most determining factor of corrosion rate. Especially, this should consider the diurnal fluctuation of H₂S load in real sewers [44].

For chemical reactions between sulfuric acid and concrete, cement has been assumed to be calcium carbonate (CaCO₃) or calcium hydroxide (Ca(OH)₂). A method for deciding the most appropriate chemical formula for different concrete types should be developed and validated to represent their alkalinity, acid neutralisation capacity and heterogeneity.

Some has considered the effects of humidity and water condensation [1], either on the biological sulfide oxidation or the diffusion/transport of H₂S and sulfate in the corrosion layer, other has consider the corrosion layer as water saturated [55]. The condensation might lead to the loss of sulfuric acid due to the dripping of excess surface water into the sewage, which has not been accounted in the existing process models. In addition, the expansion of the corrosion products (both gypsum and ettringite), which changes the porosity and thus the diffusion length of both H₂S and sulfuric acid, needs to be considered in the process models.

5 Data-Driven Models

As discussed above, it is difficult to use deterministic models for the simulation of the complex processes involved in corrosion, data-driven (black-box) type models can be used to obtain predictions with reasonable accuracy. This approach includes models based upon multiple linear regression (MLR), Gaussian processes regression (GPR), artificial neural network (ANN) and adaptive neuro fuzzy inference system (ANFIS) etc.

5.1 MLR Model

The multiple linear regression analysis generates the correlation in terms of a straight line which best approximates all the individual data points including target and output parameters [4, 24]. The general form of the MLR is thus given as:

$$\hat{Y} = a_0 + \sum_{j=1}^m a_j X_j \quad (28)$$

where, \hat{Y} is the MLR model output; X_j is the independent input variables to the MLR model; and $a_0, a_1, a_2, \dots, a_m$ are the partial regression coefficients.

The categorization of in-sewer location of corrosion hotspots (*Location*), relative humidity (*RH*, %), atmospheric temperature (*T*, °C) and H₂S gaseous concentration (*H₂S*, ppm) were chosen as input variables for the prediction of corrosion rate (*r*) and initiation time (*t_i*) using MLR models [19, 29]. The interaction between these variables were analyzed and significance of their interaction was assessed using F-test. The coefficients for each of the input variables in each model were determined with associated standard error. Due to the interaction between *Location* and *RH* on the prediction of corrosion initiation time, MLR models were established by either using separated locations, i.e., gas-phase (GP) or partially submerged (PS) data or introducing the *Location***RH* into the model (Table 3).

The MLR model for the GP location showed a good prediction with R² value around 0.76, while that for PS was pretty poor (R² = 0.42). After including the interaction term, i.e., *Location* * *RH*, into the MLR model, the model performance improved with R² increased from 0.54 to 0.62. Based on the coefficients of input variables, MLR models provide a way to evaluate the contribution from different sewer environmental factors. For example, higher impact of H₂S concentration and lower impact of gas temperature was found on PS than GP corrosion hotspots.

Table 3 MLR models built with full dataset and location specific data for the prediction of initiation time

Dataset	Interaction	Model	R ²
Full dataset	–	$t_i = 96.34 + 1.68 * \text{Location} - 0.18 * \text{H}_2\text{S} - 0.54 * \text{RH} - 0.84 * \text{T}$	0.54
Gas phase dataset	–	$t_i = 147.7 - 0.160 * \text{H}_2\text{S} - 1.01 * \text{RH} - 1.08 * \text{T}$	0.76
Partially Submerged dataset	–	$t_i = 44.94 - 0.208 * \text{H}_2\text{S} - 0.0708 * \text{RH} - 0.592 * \text{T}$	0.42
Full dataset	Location: RH	$t_i = 96.34 + 46.07 * \text{Location} - 0.184 * \text{H}_2\text{S} - 0.538 * \text{RH} - 0.835 * \text{T} - 0.467 * \text{Location} * \text{RH}$	0.62

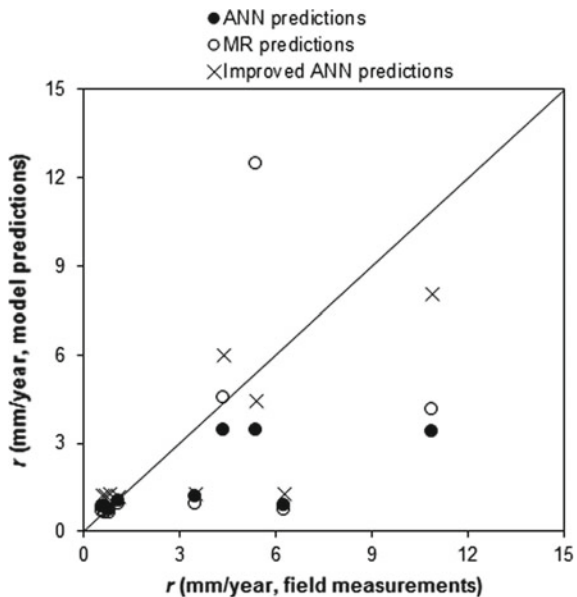
5.2 ANN Model

A semi-empirical model based on theoretical dependency of corrosion on environmental factors was proposed and the parameters determined using a small dataset obtained in field studies [49, 50]. This approach might suffer from the simplification of corrosion processes and the limited data availability. Generally, data-driven models should be based on a large dataset, especially those obtained under well-controlled experimental conditions. Recently, ANN was successfully used for the prediction of both the corrosion initiation time (t_i) and corrosion rate (r) based on data obtained over 4.5 years [19]. It was also found that ANN performs better than the MLR models due to the nonlinear nature of corrosion processes.

The ANN model trained with laboratory experimental data was further validated using corrosion rates measured in real sewer sites in Australia and those in literature reviewed by Wells and Melchers [50]. The ANN model demonstrated accurate predictions of corrosion rates for most sewer sites, while under-predicting the corrosion rates of two sites (Fig. 6). The mis-predictions occurred because the ANN was trained solely using data obtained from laboratory-scale corrosion chambers. The inclusion of the field and literature dataset in the model training significantly improved the ANN model prediction capability. The simple MLR model did show promising performance especially for corrosion rates lower than 4 mm/year.

ANN model was observed to give predictions of corrosion with relatively large deviations. The deviation from observations was likely due to either the negligence of some affecting factors and inherent variances in the corrosion data. One study

Fig. 6 Validation of the ANN and multiple regression (MR) models using corrosion rates observed in real sewers. The ANN predictions were improved by including corrosion rates observed in real sewers in the model training process. Reproduced from [19] with permission from Elsevier



found that, in comparison to constant gaseous H_2S concentrations, diurnal fluctuation occurring in real sewers can affect the H_2S oxidation pathway and the total amount of H_2S uptake by the sewer concrete [44]. Also, the periodic inoculation of the concrete surface by sewage due to changing water levels (e.g. flooding) and splashing can significantly change the corrosion process [22]. The wastewater inoculation accelerates the initiation of corrosion and corrosion rate on frequently wetted concrete. Additionally, different sewer pipes are made of different cements and aggregates with different water to cement ratios. Therefore, the concrete properties and other variables should be included for the improvement of the ANN sewer concrete corrosion model.

5.3 Gaussian Processes Regression (GPR) Model

However, there are still not many studies in the application of data-driven models for the prediction of sewer corrosion. The limiting factors are the source and quality of data. The water industry might have accumulated lots of data about corrosion rate, although without adequate data for the related sewer environmental conditions, like H_2S concentration, temperature, and humidity etc. Efforts should be invested to collect more data and future models should implement a strategy to enhance its capability and tolerance in utilizing the incomplete dataset. A major challenge in practice for such data-based models is the limited availability of reliable corrosion data obtained in well-defined sewer environments. To enhance the predictability of the hybrid Gaussian Processes Regression (GPR) model, an interpolation technique was implemented to extend the limited dataset [33].

GPR model is a simple and general class of functions, describing the distribution over functions such that a finite set of function values $\{f(x_1), f(x_2), \dots, f(x_n)\}$ have a joint Gaussian distribution. Given a new testing input x^* with a given training set $D = \{(x_i, y_i)|_{i=1}^n\}$ of n pairs of inputs x_i and noisy outputs y_i , GPR is usually formulated to compute the predictive distribution (distribution of possible unobserved values conditional on the incoming observed values) of f . Assuming that the noise is additive, independent and Gaussian, the relationship between the function $f(x_i)$ and the observed noisy targets y are derived by Rasmussen and Williams [42]:

$$y_i = f(x_i) + \varepsilon_i \quad (29)$$

$$\varepsilon \sim N(0, \delta_n^2) \quad (30)$$

$$f(\cdot) \sim GP(0, k(\cdot, \cdot)) \quad (31)$$

where $GP(0, k(\cdot, \cdot))$ represents a Gaussian process with mean and covariance matrix equaling to 0 and $k(\cdot, \cdot)$, respectively. The noise ε follows the Gaussian distribution

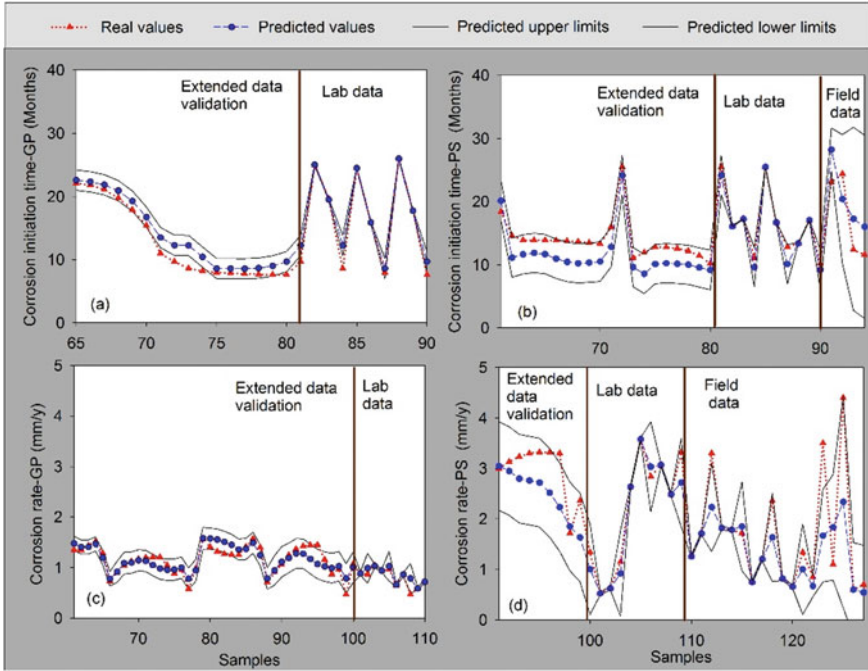


Fig. 7 Uncertainty analysis of GPR models based on laboratory and field corrosion data for both of gas-phase and partially submerged sewers. Reproduced from [33] with open access

with mean 0 and covariance σ_n^2 . A GP model was established for the corrosion initiation time and corrosion rate, which gave predictions together with its uncertainty, as shown in Fig. 7. This capability of prediction uncertainty was normally not addressed by ANN type models. Together with the uncertainty level from the GP model, the confidence of each prediction value can be accessed and quantified properly.

5.4 Model Robustness with Partial Input Data

The above discussed data-driven models usually need inputs such as gaseous H_2S concentration, gas temperature, relative humidity and other data. It is usually difficult to have reliable inputs and often only partial data are available in the real sewer environments. It is thus highly important for the robustness of the model subject to the incomplete dataset as the input. The resilience of data-driven models to the incompleteness of input data would be an important criterion in choosing the suitable corrosion models. Obviously, not all the environmental factors, i.e. input data, contribute equally to the prediction of sewer corrosion, in terms of t_i and r . In the aspect of t_i , H_2S and temperature are significant factors while RH has no-significant

effect [18]. For corrosion rate r , H_2S and RH were significant controlling factors for the corrosion rate of concrete coupons.

Based on the nature of data and also the limited availability of real data as inputs to the corrosion models, comprehensive assessments of 12 different partial input scenarios were tested using MLR, ANN, and ANFIS models [29]. The analysis showed that all the data-driven models for t_i are sensitive to the partial input data. It is thus essential to provide as much sewer environmental data as possible for the accuracy of prediction for t_i . In contrary, the data-driven models for predicting the corrosion rate are more robust when only partial inputs were provided. Among all inputs, location and H_2S concentration are the two key input parameters. This is also consistent to a previously identified minimum adequate models, which are also based on these two input parameters, which were able to predict corrosion rate reasonably well [17]. As the input of location only has two corrosion hotspots, i.e., the tidal zone or crown zones. The sewer service life based on concrete corrosion can be adequately estimated with only the hydrogen sulfide concentration as a model input.

6 Summary

Concrete corrosion in sewers is a complicated phenomenon that can be generally separated as a two-stage process, i.e., the corrosion initiation stage of mainly chemical neutralisation of concrete surface, and the following biodeterioration stage of mainly biological sulfuric acid production and reaction with concrete. The key corrosion parameters are thus corrosion initiation time (t_{in} in months or years) and corrosion rate (r in mm/year) for the two stages.

This chapter provides a summary of different modelling approaches that have been developed for the concrete corrosion in sewers. These models can be used in the estimation or prediction of corrosion rates, and thus the service life under a certain sewer environmental condition. The empirical and data-driven models are shown to be effective in achieving those predictions with confident accuracy. However, further development of mechanistic models is much needed with the increasing understanding of concrete corrosion in sewers. The integration of concrete corrosion model with other sewer process model would provide a useful capacity in the sewer corrosion management.

References

1. Bohm, M., Deviny, J., Jahani, F., Rosen, G.: On a moving-boundary system modeling corrosion in sewer pipes. *Appl. Math. Comput.* **92**, 247–269 (1998)
2. Bosch, P.L.F.V.D., Beusekom, O.C.V., Buisman, C.J.N., Janssen, A.J.H.: Sulfide oxidation at halo-alkaline conditions in a fed-batch bioreactor. *Biotechnol. Bioeng.* **97**, 1053–1063 (2007)
3. Chen, K. Y., Morris, J.C.: Kinetics of oxidation of aqueous sulfide by O_2 . *Environ. Sci. Technol.* **6**, 529–530 (1972)

4. Deshpande, N., Londhe, S., Kulkarni, S.: Modeling compressive strength of recycled aggregate concrete by artificial neural network, model tree and non-linear regression. *Int. J. Sustain. Built Environ.* **3**, 187–198 (2014)
5. Fatima, T., Muntean, A.: Sulfate attack in sewer pipes: Derivation of a concrete corrosion model via two-scale convergence. *Nonlinear Anal.-Real World Appl.* **15**, 326–344 (2014)
6. Fuseler, K., Cypionka, H.: Elemental sulfur as an intermediate of sulfide oxidation with oxygen by *Desulfobulbus-propionicus*. *Arch. Microbiol.* **164**, 104–109 (1995)
7. Gadekar, S., Nemati, M., Hill, G.A.: Batch and continuous biooxidation of sulphide by *Thiomicrospira sp* CVO: reaction kinetics and stoichiometry. *Water Res.* **40**, 2436–2446 (2006)
8. Garcia-de-Lomas, J., Corzo, A., Carmen Portillo, M., Gonzalez, J.M., Andrades, J.A., Saiz-Jimenez, C. Garcia-Robledo, E.: Nitrate stimulation of indigenous nitrate-reducing, sulfide-oxidising bacterial community in wastewater anaerobic biofilms. *Water Res.* **41**, 3121–3131 (2007)
9. Gerardi, M.H.: Sulfur-Oxidizing and sulfur-reducing bacteria. In: Gerardi, M.H. (ed.) *Wastewater Bacteria* (Chapter 13). Wiley, Hoboken, New Jersey (2006)
10. Gutierrez, O., Jiang, G., Sharma, K., Yuan, Z.: Biofilm development in sewer networks. In: Romani, A.M., Guasch, H., Balaguer, M.D. (eds.) *Aquatic Biofilms: Ecology, Water Quality and Wastewater Treatment* (Chapter 8). Caister Academic Press (2016)
11. Hvitved-Jacobsen, T., Vollertsen, J., Nielsen, A.H.: *Sewer Processes: Microbial and Chemical Process Engineering of Sewer Networks*, 2nd ed. CRC Press (2013)
12. Janssen, A.J.H., Ma, S.C., Lens, P., Lettinga, G.: Performance of a sulfide-oxidizing expanded-bed reactor supplied with dissolved oxygen. *Biotechnol. Bioeng.* **53**, 32–40 (1997)
13. Janssen, A.J.H., Sleyster, R., Vanderkaa, C., Jochemsen, A., Bontsema, J., Lettinga, G.: Biological sulfide oxidation in a fed-batch reactor. *Biotechnol. Bioeng.* **47**, 327–333 (1995)
14. Jensen, H.S., Nielsen, A.H., Hvitved-Jacobsen, T., Vollertsen, J.: Modeling of hydrogen sulfide oxidation in concrete corrosion products from sewer pipes. *Water Environ. Res.* **81**, 365–373 (2009)
15. Jensen, H.S., Nielsen, A.H., Lens, P.N.L., Hvitved-Jacobsen, T., Vollertsen, J.: Hydrogen sulphide removal from corroding concrete: comparison between surface removal rates and biomass activity. *Environ. Technol.* **30**, 1291–1296 (2009)
16. Jiang, G., Keller, J., Bond, P.L.: Determining the long-term effects of H₂S concentration, relative humidity and air temperature on concrete sewer corrosion. *Water Res.* **65**, 157–169 (2014)
17. Jiang, G., Keller, J., Bond, P.L.: Determining the long-term effects of H₂S concentration, relative humidity and air temperature on concrete sewer corrosion. *Water Res.* **65**, 157–169 (2014)
18. Jiang, G., Keller, J., Bond, P.L., Yuan, Z.: Predicting concrete corrosion of sewers using artificial neural network. *Water Res.* **92**, 52–60 (2016)
19. Jiang, G., Keller, J., Bond, P.L., Yuan, Z.: Predicting concrete corrosion of sewers using artificial neural network. *Water Res.* **92**, 52–60 (2016)
20. Jiang, G., Sharma, K.R., Guisasola, A., Keller, J., Yuan, Z.: Sulfur transformation in rising main sewers receiving nitrate dosage. *Water Res.* **43**, 4430–4440 (2009)
21. Jiang, G., Sun, X., Keller, J., Bond, P.L.: Identification of controlling factors for the initiation of corrosion of fresh concrete sewers. *Water Res.* **80**, 30–40 (2015)
22. Jiang, G., Zhou, M., Chiu, T.H., Sun, X., Keller, J., Bond, P.L.: Wastewater-Enhanced microbial corrosion of concrete sewers. *Environ. Sci. Technol.* **50**, 8084–8092 (2016)
23. Kato, M.T., Field, J.A., Lettinga, G.: High tolerance of methanogens in granular sludge to oxygen. *Biotechnol. Bioeng.* **42**, 1360–1366 (1993)
24. Khademi, F., Behfarnia, K.: Evaluation of concrete compressive strength using artificial neural network and multiple linear regression models. *Iran Univ. Sci. Technol.* **6**, 423–432 (2016)
25. Kleinjan, W.E., de Keizer, A., Janssen, A.J.H.: Biologically produced sulfur. In: Steudel, R. (ed.) *Elemental Sulfur and Sulfur-Rich Compounds I*. Springer, Berlin, Heidelberg (2003)
26. Klok, J.B., van den Bosch, P.L., Buisman, C.J., Stams, A.J., Keesman, K.J., Janssen, A.J.: Pathways of sulfide oxidation by haloalkaliphilic bacteria in limited-oxygen gas lift bioreactors. *Environ. Sci. Technol.* **46**, 7581–7586 (2012)

27. Lewis, W.K., Whitman, W.G.B.: Principles of gas absorption. *Ind. Eng. Chem.* **16**, 1215–1220 (1924)
28. Li, X., Kappler, U., Jiang, G., Bond, P.L.: The ecology of acidophilic microorganisms in the corroding concrete sewer environment. *Front. Microbiol.* **8** (2017)
29. Li, X., Khademi, F., Liu, Y., Akbari, M., Wang, C., Bond, P.L., Keller, J., Jiang, G.: Evaluation of data-driven models for predicting the service life of concrete sewer pipes subjected to corrosion. *J. Environ. Manage.* **234**, 431–439 (2019)
30. Li, X., O'Moore, L., Song, Y., Bond, P.L., Yuan, Z., Wilkie, S., Hanzic, L., Jiang, G.: The rapid chemically induced corrosion of concrete sewers at high H₂S concentration. *Water Res.* **162**, 95–104 (2019)
31. Lin, S., Mackey, H.R., Hao, T., Guo, G., van Loosdrecht, M.C.M., Chen, G.: Biological sulfur oxidation in wastewater treatment: a review of emerging opportunities. *Water Res.* **143**, 399–415 (2018)
32. Liss, P.S., Slater, P.G.: Flux of gases across the Air-Sea interface. *Nature* **247**, 181–184 (1974)
33. Liu, Y., Song, Y., Keller, J., Bond, P., Jiang, G.: Prediction of concrete corrosion in sewers with hybrid Gaussian processes regression model. *RSC Adv.* **7**, 30894–30903 (2017)
34. Matos, J.S., Aires, C.M.: Mathematical modelling of sulphides and hydrogen sulphide gas build-up in the Costa do Estoril sewerage system. *Water Sci. Technol.* **31**, 255–261 (1995)
35. Nielsen, A., Rn, H., Vollertsen, J., Hvitved-Jacobsen, T.: Kinetics and stoichiometry of aerobic sulfide oxidation in wastewater from sewers: effects of pH and temperature. *Water Environ. Res.* **78**, 275–283 (2006)
36. Nielsen, A.H., Hvitved-Jacobsen, T., Vollertsen, J.: Kinetics and stoichiometry of sulfide oxidation by sewer biofilms. *Water Res.* **39**, 4119–4125 (2005)
37. Nielsen, A.H., Vollertsen, J., Hvitved-Jacobsen, T.: Determination of kinetics and stoichiometry of chemical sulfide oxidation in wastewater of sewer networks. *Environ. Sci. Technol.* **37**, 3853–3858 (2003)
38. Nielsen, A.H., Vollertsen, J., Hvitved-Jacobsen, T.: Chemical sulfide oxidation of wastewater—effects of pH and temperature. *Water Sci. Technol.* **50**, 185–192 (2004)
39. Norsker, N.H., Nielsen, P.H., Hvitved-Jacobsen, T.: Influence of oxygen on biofilm growth and potential sulfate reduction in gravity sewer biofilm. *Water Sci. Technol.* **31**, 159–167 (1995)
40. Pomeroy, R., Bowlus, F.D.: Progress report on sulfide control research. *Sewage Works J.* **18**, 597–640 (1946)
41. Pomeroy, R.D.: *The Problem of Hydrogen Sulphide in Sewers*. Clay Pipe Development Association Limited, London (1990)
42. Rasmussen, C.E., Williams, C.K.I.: *Gaussian Processes for Machine Learning*. MIT Press, London (2006)
43. Smith, J.H., Bomberger, D.C., Haynes, D.L.: Prediction of the volatilization rates of high-volatility chemicals from natural water bodies. *Environ. Sci. Technol.* **14**, 1332–1337 (1980)
44. Song, Y., Tian, Y., Li, X., Wei, J., Zhang, H., Bond, P.L., Yuan, Z., Jiang, G.: Distinct microbially induced concrete corrosion at the tidal region of reinforced concrete sewers. *Water Res.* **150**, 392–402 (2019)
45. Sun, X., Jiang, G., Bond, P.L., Keller, J.: Impact of fluctuations in gaseous H₂S concentrations on sulfide uptake by sewer concrete: the effect of high H₂S loads. *Water Res.* **81**, 84–91 (2015)
46. Thistlethwayte, D.: *The Control of Sulphides in Sewerage Systems*. Butterworth Pty. Ltd., Sydney (1972)
47. US EPA: *Process design manual for sulfide control in sanitary sewer systems* (1974)
48. Vollertsen, J., Nielsen, A.H., Jensen, H.S., Wium-Andersen, T., Hvitved-Jacobsen, T.: Corrosion of concrete sewers—the kinetics of hydrogen sulfide oxidation. *Sci. Total Environ.* **394**, 162–170 (2008)
49. Wells, T., Melchers, R.E.: An observation-based model for corrosion of concrete sewers under aggressive conditions. *Cem. Concr. Res.* **61–62**, 1–10 (2014)
50. Wells, T., Melchers, R.E.: Modelling concrete deterioration in sewers using theory and field observations. *Cem. Concr. Res.* **77**, 82–96 (2015)

51. Xi, Y., Bažant, Z.P., Jennings, H.M.: Moisture diffusion in cementitious materials adsorption isotherms. *Adv. Cem. Based Mater.* **1**, 248–257 (1994)
52. Yongsiri, C., Hvitved-Jacobsen, T., Vollertsen, J., Tanaka, N.: Introducing the emission process of hydrogen sulfide to a sewer process model (WATS). *Water Sci. Technol.* **47**, 85–92 (2003)
53. Yongsiri, C., Vollertsen, J., Hvitved-Jacobsen, T.: Hydrogen sulfide emission in sewer networks: a two-phase modeling approach to the sulfur cycle. *Water Sci. Technol.* **50**, 161–168 (2004)
54. Yongsiri, C., Vollertsen, J., Hvitved-Jacobsen, T.: Influence of wastewater constituents on hydrogen sulfide emission in sewer networks. *J. Environ. Eng. ASCE* **131**, 1676–1683 (2005)
55. Yuan, H.F., Dangla, P., Chatellier, P., Chaussadent, T.: Degradation modelling of concrete submitted to sulfuric acid attack. *Cem. Concr. Res.* **53**, 267–277 (2013)
56. Yuan, H.F., Dangla, P., Chatellier, P., Chaussadent, T.: Degradation modeling of concrete submitted to biogenic acid attack. *Cem. Concr. Res.* **70**, 29–38 (2015)

Corrosion Control Strategies

Advances on Corrosion-Resistant Concrete for Sewers



Fengming Yang, Yazhou Zhao, Tian Wang, Yarong Song, Guangming Jiang, and Min Wu

Abstract This chapter discusses the advances on corrosion-resistant concrete for sewers from the viewpoint of binder materials, aggregates and additives. For binder materials, alkaline activated materials (AAM) and calcium aluminate cement (CAC) are not included, as they are presented in Chaps. 10 and 11. The performance of several other binder materials, including sulfate resistant cement, the use of supplementary cementitious materials, polymer modified cements, and sulfur binder, under (sulfuric) acidic conditions and sewers conditions are summarized. The possible benefits and limitations of each binder material are critically discussed. The importance of aggregate in corrosion resistant concrete is highlighted primarily due to the high-volume fraction (e.g. > 60%). Aggregates studied include siliceous and calcareous aggregates, crushed CAC clinker aggregate and polyethylene terephthalate (PET) aggregate. Additives may play a significant role in improving the corrosion resistance of concrete. The effects and limitations of using antimicrobial agents and novel corrosion-resistant bioconcrete are also discussed.

F. Yang · Y. Zhao · M. Wu (✉)

Department of Civil and Architectural Engineering, Aarhus University, 8000 Aarhus, Denmark
e-mail: mnwu@cae.au.dk

F. Yang

School of Materials Science and Engineering, Southeast University, Nanjing 211189, China

Y. Zhao

College of Harbour, Coastal and Offshore Engineering, Hohai University, Nanjing 210098, China

T. Wang

Department of Chemical and Biochemical Engineering, Technical University of Denmark, 2800 Denmark, Lyngby, Denmark

Y. Song

Australian Centre for Water and Environmental Biotechnology, The University of Queensland, Brisbane, QLD 4072, Australia

G. Jiang

School of Civil, Mining, Environmental and Architectural Engineering, University of Wollongong, Wollongong, NSW 2522, Australia

© The Author(s), under exclusive license to Springer Nature Switzerland AG 2023

G. Jiang (ed.), *Microbiologically Influenced Corrosion of Concrete Sewers*, Engineering Materials, https://doi.org/10.1007/978-3-031-29941-4_9

185

1 Binder Materials

1.1 Sulfate Resistant Cement

Sulfate resistant cement (SRC) is a type of Portland cement designed to mitigate associated problems for concrete exposed to aggressive sulfate environments (e.g., seaports, underground, tunnels, roads, and bridges). Compared to ordinary Portland cement (OPC), typically the C_3A ($3CaO \cdot Al_2O_3$) content is low in SRC. This is due to that C_3A phase can react with sulfate ions in the presence of water, resulting in volume expansion and crystallization pressure which can lead to cracking and destruction of hardened concrete. Therefore, by changing the mineral composition of cement clinker, i.e. reducing the C_3A content, the ability of the cement to resist sulfate attack is increased. Generally, standards for sulfate resistant cement set corresponding requirements on the limits of C_3A content. Table 1 shows the main physicochemical requirements on sulfate resistant cement in some countries/regions.

The application of SRC in concrete to increase the resistance against sulfate attack and durability of the concrete has been widely investigated and validated [58, 73]. Since the main acid generated in the MIC processes is sulfuric acid (sulfate ions contained), various studies have been performed to investigate if sulfate resistant cement can be beneficiary in improving the performance of concrete exposed to (chemical or biological) sulfuric acid conditions.

Table 1 Requirements on sulfate resistant cement in standards, adapted based on [155]

	ASTM-V	EN 197	GB 748
Loss on ignition/%	≤ 3	≤ 3	≤ 3
Insoluble matter/%	≤ 0.75	≤ 1.5	≤ 1.5
w(MgO) /%	≤ 6	≤ 5	≤ 5
w(SO ₃) /%	≤ 2.3	≤ 2.5	≤ 2.5
w(Na ₂ O + 0.658K ₂ O)	≤ 0.6	–	–
w(C ₃ A)/%	≤ 5	≤ 3.5	P-MSR ≤ 5 , P-HSR ≤ 3
w(C ₄ AF)/%	$2C_3A + C_4AF \leq 25$	–	–
Specific surface area/ m ² /kg	≥ 280	–	≥ 280
Initial setting time/min	≥ 45	≥ 60	≥ 45
Final setting time/min	≤ 375	–	≤ 600
Volume stability	Autoclave Expansion $\leq 0.8\%$	Expansion of Le Chatelier needles ≤ 10 mm	Boiling method is qualified

ASTM American Society for Testing and Materials; EN European standard; GB China national standard; P-MSR medium sulfate resistant Portland cement; P-HSR high sulfate resistant Portland cement

In the laboratory studies [11, 41], similar performance of concrete samples prepared by SRC and OPC was observed after the exposure to chemical sulfuric acid. Similarly, in another study [58], the improved resistance of concrete using SRC when exposed to chemical sulfuric acid was also not confirmed. Estokova et al. [40] performed investigations on the corrosion of SRC concrete by chemical and biological sulfuric acids. The acid induced deteriorations were evaluated through the leached quantities of the main chemical elements, e.g. Ca, Si, Fe and Al, sulfate ions in the solutions, and the surface and mineralogical changes of the samples. It was reported that the leaching behavior varied considerably under chemical and biological sulfuric acid attacks. Furthermore, the surface precipitates of the samples affected by the biological and chemical acids showed different morphologies (Fig. 1). The formation of surface compounds was found to be more significant in the case of the biological acid compared to the chemical counterpart. This could be linked to the fact that the concentrations of sulfate ions exposed to the biological acid were almost 5 times higher than that of the chemical acid. Analysis of the precipitates revealed the presence of Ca, Si, O, and S, indicating the existence of sulfate compounds, e.g. gypsum, anhydrite and/or bassanite, consistent with reported results elsewhere, e.g. in [117, 156]. In addition, the phosphorus, which was a component of the nutrient medium for the sulfur-oxidizing bacteria in the form of K_2HPO_4 , was also observed in the biologically affected samples. Overall, Estokova et al. [40] concluded that concrete prepared by SRC appeared to be more resistant to chemical than biological sulfuric acid, which might be related to the complex processes caused by bacteria and their micro-environmental effects. Harbulakova et al. [59] investigated the leaching of Ca, Si, Fe and Al elements from concrete prepared by SRC with the exposure to *Acidithiobacillus thiooxidans* strain. The correlation analysis of leaching trends of selected ions demonstrated that the leaching behavior strongly depends on the aggressiveness of bacterial medium.

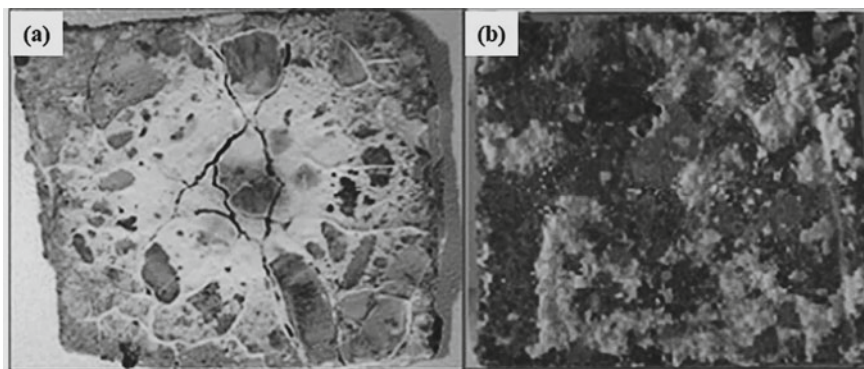


Fig. 1 New compounds (sulfate-based products exist in the form of white coating or discrete crystals) on the surface of the samples exposed to **a** biologically generated acid and **b** chemical sulfuric acid; reproduced from [40]

With respect to studies under site conditions, Grengg et al. [49] performed a case study from a combined sewer network in Austria. Even with the use of C₃A free (highly sulfate resistant) cement, the corrosion depth of the concrete after 9 years in service reached around 9 cm, corresponding to an average corrosion rate of 1 cm/year. El Gamal et al. [37] conducted a 24-month field research on the physical and chemical effects of the actual sewer environment on Portland cement concrete (PCC) and SRC concrete (SRCC). The results showed a reduction in the alkalinity of PCC and SRCC, due to the exposure to the sewer environment. SRCC showed higher corrosion depth in the beginning than PCC; however, after 24 months of exposure, SRCC had a lower corrosion depth than PCC (3.2 mm vs. 3.8 mm), see Fig. 2. The SEM examination of PCC in Fig. 3a showed obvious cracks at the paste-aggregate interface and in the surrounding matrix, which might be attributed to the attack caused by the sewer environment. Figure 3b demonstrated that thaumasite was one of the formed products in PCC. Figure 3c, d presented the SEM results for the SRCC. SRCC became porous after exposure to the sewer environment and crystal products, i.e. calcite and gypsum, were formed. The formation of gypsum was a consequence of the oxidation/hydration of sulfur and the interaction of the formed sulfuric acid with the concrete. In [74, 75], the deterioration observed in natural sewer conditions (North Head wastewater treatment plant in Sydney) and the effects of six-month sulfuric acid (1.5% H₂SO₄) attack on SRC mortar were compared. The study found that widespread crystallization of gypsum within the corroded regions of SRC mortar was responsible for the major micro-cracking, loss in strength, loss of mass and surface disintegration. However, by comparing the mechanisms of deterioration observed in natural aggressive sewer environment to that observed after exposure to chemical sulfuric acid solution, significant differences were highlighted. The mechanism of neutralization in natural sewer conditions was governed by the simultaneous carbonation and H₂S acidification in addition to the interactions with microorganisms, which produced sulfuric acid (biologically generated) and caused localized deteriorations within the mortar microstructure after the penetration of the biological acid. While with chemical sulfuric acid exposure, neutralization of mortar was due to the widespread diffusion of SO₄²⁻ and H⁺ ions from the acid solution, leading to an alkalinity loss and then the deterioration. Both mechanisms are schematically shown in Fig. 4. This is another example showing that the chemical tests based solely on sulfuric acid are not reliable to predict field behaviors in sewers.

Based on the discussions above, it seems that the use of SRC does not necessarily improve the acid resistance of concrete under MIC conditions. It should be highlighted that there is a major difference between sulfate attack and sulfuric acid attack. For concrete attacked by sulfuric acid, apart from the chemical reactions with the sulfate ions, the action of hydrogen ion has to be considered [58, 105]. In general, concrete deterioration caused by sulfuric acid attack is much more severe compared to that of sulfate attack [58].

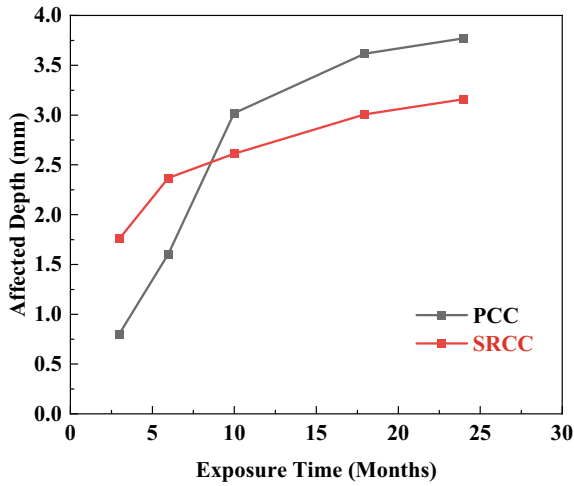


Fig. 2 Average affected (or corrosion) depth with time of exposure to sewerage environment for PCC and SRCC, data based on [37]

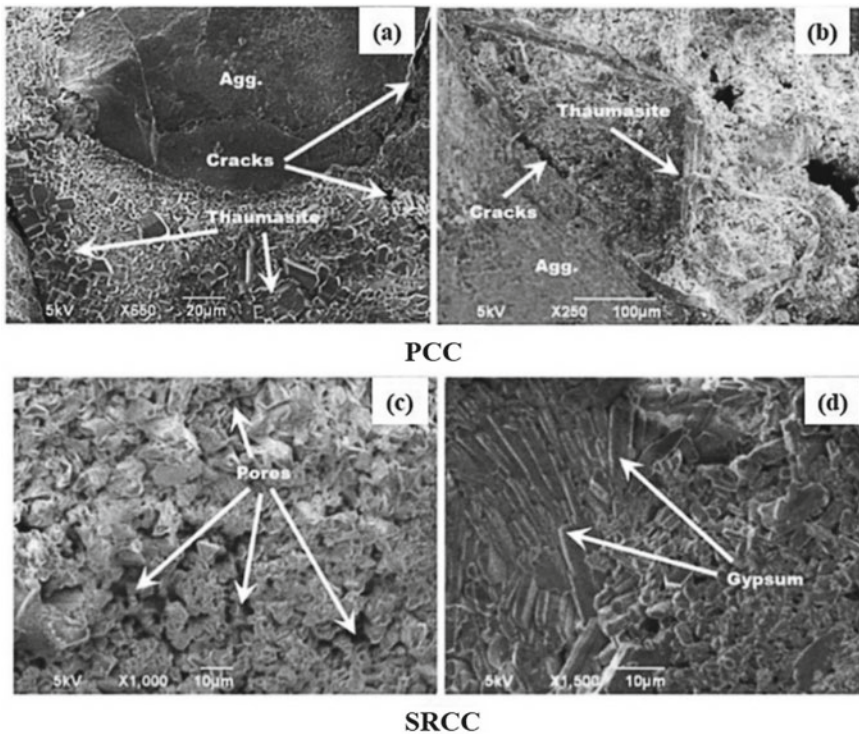


Fig. 3 SEM photos of specimens of Portland cement concrete (PCC) and SRC concrete (SRCC) after exposure to actual sewer environment for 24 months. Reproduced from [37] with permission from Elsevier

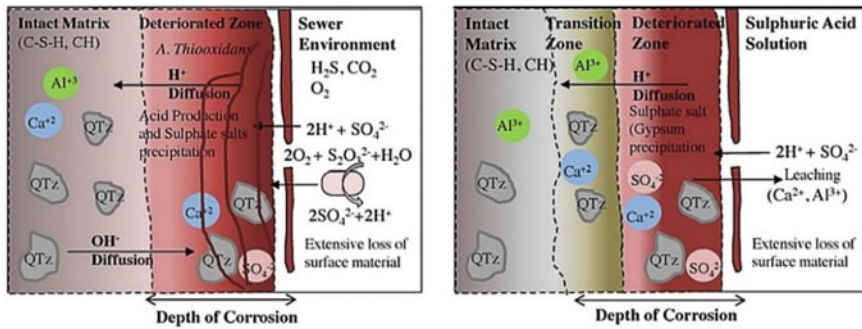


Fig. 4 Schematic models for deterioration of SRC mortar in two aggressive exposure conditions: **a** actual sewer environment; **b** sulfuric acid solution. Reproduced from [74] with permission from Elsevier

1.2 Supplementary Cementitious Materials

Ground granulated blast furnace slag (GGBFS), fly ash (FA) and silica fume (SF) are the most commonly used supplementary cementitious materials (SCMs). SCM acts as a partial replacement for cement clinker composition, to enhance the mechanical performance and durability of concrete. GGBFS has a similar chemical composition to OPC, while FA and SF have totally different compositions (Table 2) [68]. The replacement ratio of GGBFS to OPC can be up to 70–80% [85], while it is relatively lower for other types of SCMs, e.g. 20–40% for FA [66, 80, 92, 109, 153] and 2.5–10% for SF [78, 134]. During the cement hydration process, hydration products like calcium silicate hydrate (C–S–H) and calcium hydroxide (CH) are firstly formed due to the reactions between cement and water. The size of capillary pores in hardened cement/concrete can be reduced with the addition of GGBFS which reacts with the CH and facilitates the formation of C–S–H. The reduction of CH compacts or densifies the concrete matrix and hinders the penetration of aggressive ions [135]. Different from GGBFS, there is a low content of calcium oxide (CaO) in both FA and SF, where the main composition is silicon dioxide (SiO₂). Therefore, the formation of C–S–H is insufficient due to the lack of calcium source in the mix in the early stage, while a delayed strength evolution can be observed due to the pozzolanic reaction between CH and SiO₂. After the depletion of CH, the unreacted GGBFS and FA would only serve a role of filler in cementitious systems [135]. It is worth to mention that FA can promote the chemical reactivity of OPC clinker, especially at a later hydration time [29, 31, 82, 115].

Numerous investigations have been conducted to study the effect of SCMs in mitigating the deterioration of cementitious materials in simulated MIC conditions, where most of the studies adopted chemical sulfuric acid in laboratory conditions [68, 147]. In general, the addition of SCMs shows some positive effects in reducing corrosion to different extent based on most of the tests using chemical acids. Major mechanisms accounting for the positive effects can be summarized as follows:

Table 2 Typical chemical compositions and physical properties of OPC, GGBFS, FA and SF, data based on [68]

Oxide (%)	OPC	GGBFS	FA	SF
CaO	63.3	41.7	3.4	0.7
SiO ₂	20.2	31.7	57.6	91.2
Al ₂ O ₃	5.8	14.5	25.5	1.3
Fe ₂ O ₃	3.0	0.7	6.1	0.8
MgO	3.4	5.4	0.9	0.3
SO ₃	2.1	2.1	–	–
Density (g/cm ³)	3.15	2.92	2.39	2.20
Fineness (m ² /kg)	312	445	359	20 470

(a) optimized pore size and volume, (b) reduced permeability (or dense structure), (c) reduced CH content, and (d) improved interfacial transition zones (ITZs) between the hardened cement paste and the aggregates [6, 99]. Yoshida et al. [154] studied sulfuric acid attack on concrete with and without GGBFS. The results showed that concrete incorporating GGBFS significantly increased the resistance to acid attack. The mass loss after 26 weeks of the acid attack was reduced from 82% for Portland cement concrete to 45% for concrete with 60% GGBFS. Liu et al. [90] reported that the mass losses of Portland cement concrete, 10% SF concrete, and 20% FA concrete were 3.56%, 2.17%, and 2.32% after been immersed in 5.0% H₂SO₄ solution for 28 days. In a chemical sulfuric acid immersion study, House et al. [64] concluded that partial replacement of OPC by GGBFS, FA and SF all led to improved resistance to sulfuric acid compared to concrete made with OPC at an equivalent water to cementitious materials ratio. De Belie et al. [28] studied the effects of both chemical and biological sulfuric acids on concrete with and without SCMs. The results, however, showed limited impact of SCMs in the tests using chemical acids, and a slightly higher resistance of GGBFS cement concrete reported in other studies was not found. Further, Portland cement performed the best in the microbiological tests, echoing the conclusions drawn in previous work.

Several aspects should be considered in evaluating the effect of SCMs under laboratory conditions. Firstly, different metabolic activities of microbial communities occur in realistic sewage networks and the amount of acid production varies significantly in the MIC process, which is totally different from a stable sulfuric acid concentration used in laboratory conditions [35]. Besides, the corrosion layer (with the main composition of gypsum) in a MIC attack can be very different from that in pure sulfuric acid solutions. Bacteria and fungi can colonize and produce sulfuric acid on the corrosion layer in a MIC attack, but the formed gypsum layer can prohibit the further penetration of aggressive ions in a pure sulfuric acid solution. It is important to note that when exposed to biological conditions, addition of SCMs may not always show benefits in comparison with plain OPC samples, e.g. see [35]. Increased corrosion of concrete samples containing GGBFS under biological corrosion testing was also reported [120]. In-situ tests showed some differences

between concrete samples prepared by OPC, GGBFS and FA cements in the early measurements (i.e. up to 23 months); while almost no difference was noted in terms of neutralization depth after 35 months of exposure [5, 112]. In [76], concrete samples with different binder compositions including Portland cement (PC), PC + FA, PC + GGBFS and PC + SF were subjected to a “live” sewer for 127 months. The SCMs seemed to improve the resistance to some extent as far as the average corrosion rate was concerned, however, the relatively wide variation of the data made the conclusion somewhat ambiguous. Herisson et al. [62] studied the corrosion of OPC and OPC replaced by 75% GGBFS mortars placed in actual sewer headspace for 4 years, and the results indicated that the replacement of GGBFS improved the performance as GGBFS changed completely the evolution of microorganisms thriving onto the mortar surface compared to OPC alone. The results, however, are in contradiction with the biological tests reported in [28], where it was proposed that GGBFS cement concrete surface was more hospitable for microorganisms to colonize.

In summary, the effects of SCMs with respect to the concrete corrosion subject to MIC are not conclusive. Concrete samples with various SCMs have been subjected to the exposures of both chemical and biological sulfuric acid conditions. The obtained results are highly variable. One possible explanation may be related to the different test conditions and the many factors that could affect the final obtained results. Biological and in-situ tests consider at least one more aspect that is not possible to be accounted for in chemical acid immersion tests, i.e. the interactions between microorganisms and the concrete surfaces (e.g. bacteria colonization and proliferation). In this sense, they should be able to provide data more representative or closer to site conditions. However, such data reported so far are also not consistent and sometimes even contradictory. Apparently, further studies are needed to clarify the effects of SCMs and it seems that standardized tests which are currently missing are of extremely high value.

1.3 Polymer Modified Cements

Various polymers, including emulsions, liquid resins, water-soluble polymers, etc., can be used to modify cementitious materials, and the advantages include simple preparation, low cost and relatively good modification effects [10, 47, 60, 127]. In the 1950s, polymer modified cement was proposed for the uses in concrete structures and pipelines as high-performance materials [47]. There are two main methods of using polymers in this context. The first one is to add polymer(s) into a cementitious material and apply it to concrete surface to form a protective layer, e.g. similar to coating. The second one is to mix the polymer(s) directly into concrete as an admixture. The effects of polymers in concrete also can be divided into two categories, i.e. physical and chemical. The physical action is mainly manifested by the interweaving of polymer and cement hydration products into a mesh structure, improving the interfacial transition zones (ITZs, between aggregates and cement pastes) and pore structure. The chemical action mainly includes the reactions between the polymer

and cement hydration products or metal ions in concrete to produce bridge bonding, which improves the compactness and bonding of concrete [60, 65, 150]. The use of polymer modified cement/concrete has been promoted due to, e.g. high mechanical properties, fast curing and excellent bonding to cement [136, 137]. However, the performance of concrete is largely influenced by the type and the content of the added polymers, among others [150]. When used in the construction industry, concrete prepared by polymer modified cement is typically exposed to different harsh environments, e.g. wastewater, acid rain and seawater during the lifetime. These environments can affect the long-term durability of polymer materials. Therefore, the long-term behavior, durability, safety and serviceability of the materials are critical issues to be considered [47].

Several studies under laboratory conditions have shown that the introduction of polymers into concrete reduces the permeability and slows down the penetration of H_2S , CO_2 , and the entry of microorganisms and their metabolites. The reduction of permeability is mainly due to bridging of micro-cracks, reduction of pore size and blocking of the pores by polymer particles [22, 47, 60, 150]. Therefore, the purpose of using polymers is somehow similar to the addition of SCMs, i.e. to hinder the ingress of aggressive substances, see Sect. 1.2.

It has been reported that polymer modified cement mortars or concrete are resistant to aggressive compounds such as lactic acid, acetic acid and sulfuric acid [9, 15, 22]. Chang and Choi [22] developed a repair mortar with improved acid resistance which can be applied to partially damaged concrete sewer pipes. Accelerated tests were carried out to assess the performance of the mortar in a sulfuric acid environment. The results confirmed that the inclusion of polyvinyl acetate (PVA) resin powder in the binder improved the resistance to sulfuric acid. Küçük et al. [81] analyzed the acid resistance of dioctyl terephthalate (DOTP) cement mortar (DOCEM) and compared that with other polymer modified cement mortars, e.g. that containing polyvinyl chloride (PVC), polypropylene (PP) and polyethylene terephthalate (PET), where the results are shown in Table 3. The most successful polymers against sulfuric acid exposure were PVC, PET and PP because of their strong covalent bonds. Actually, PP and PVC were also successful in preventing compressive strength loss against hydrochloric and nitric acid exposure in the same study. Although modification with polymers reduces the permeability of concrete, the compatibility between the polymer and ingredients in the concrete mix can negatively alter the behavior of the polymer-modified cement concrete. Retarded cement hydration and reduced compressive strength of modified concrete have been reported at high polymer/cement ratios [143]. Moreover, significant improvement of concrete have been mostly achieved at the polymer/cement ratios in the range of 3–20%, which remarkably increases the overall material cost of concrete, and hence limits its application [79, 104]. However, Sakhakarmi [119] compared the costs of polymer modified cement concrete with conventional cement concrete in the sewer network of the city of Las Vegas, USA, and found that the use of polymer concrete was actually more cost effective in the long run compared to

conventional cement concrete. In addition, applying polymers in confined spaces such as sewage systems must also take into account an important health and safety aspect, as these polymer-containing materials often contain solvents and/or components that are potentially dangerous to human beings.

In the study [110], polymer materials including 2% melamine and 10% styrene-butadiene latex or emulsions were used to modify Portland cements to prepare mortar and concrete samples. The samples were tested in chemical sulfuric acid ($\text{pH} = 0.7$). It was concluded that the use of concrete with polymer addition during the mixing phase showed minor beneficial effect on the acid resistance. It was further stated that this solution was not economically attractive because the increase of costs was too high. Li et al. [87] studied the impact of chemical sulfuric acid on mortar samples for five years. The results showed that the compressive strength loss of polyvinyl acetate latex modified mortar was 29.4%, whereas the corresponding value for the reference mortar was as high as 50.6%. Vincke et al. [138] studied the performance of concrete samples subjected to both chemical and microbiological tests, where the Portland cement binders were modified by four different polymer types, i.e. styrene

Table 3 Results for sulfuric acid resistance of cement mortars containing different polymers, data based on [81]

pH	Polymer ^a	Properties		
		Loss in 28-day compressive strength (%)	Loss in 28-day electrical resistivity (%)	Loss in 28-day ultrasonic pulse velocity (%)
pH = 2	DOTP(10%)	- 74.2874	- 17.3410	22.577
	DOTP(20%)	- 74.3452	10.2427	23.781
	PP(20%)	- 10.0653	- 9.2144	- 31.543
	PET(20%)	- 2.2472	14.8803	11.673
	PVC(20%)	47.8114	- 0.7707	21.897
pH = 3	DOTP(10%)	- 27.7568	- 1.6725	4.793
	DOTP(20%)	- 32.4212	8.2610	24.113
	PP(20%)	- 3.8495	- 8.8264	- 51.711
	PET(20%)	15.5349	13.2154	- 44.990
	PVC(20%)	13.4680	- 5.0096	152.650
pH = 4	DOTP(10%)	- 7.0867	2.2939	3.030
	DOTP(20%)	- 0.5604	10.9021	22.600
	PP(20%)	12.9790	- 0.8729	- 49.010
	PET(20%)	12.9295	13.6316	3.657
	PVC(20%)	72.7647	10.5973	- 6.276

^aDOTP Diocetyl terephthalate; PP polypropylene; and PET polyethylene terephthalate; PVC polyvinyl chloride. The percentage in the bracket shows the cement replacement ratio. The loss of a property is calculated by the (value of the samples exposed to the acid—value of the samples cured in water)* 100%/value of the samples exposed to the acid

butadiene polymer (SBR), styrene acrylic ester polymer (SA), acrylic polymer (AC) and vinylcopolymer (VPV). In the chemical tests, all the concrete mixes showed the same pattern in terms of the change of the dimension (radius) of the cylinder samples, except the mix with SA. An increase of the radius was measured after the first few cycles and after a certain cycle, a breakpoint was reached with a resulting decrease in the radius. For the SA mix, expansion was recorded during all the cycles of measurements. The overall dimension reduction increased in the order of VPV, reference, AC and SBR. The obtained results were different from the microbiological tests, where only the addition of the SA resulted in an overall increase in resistance of the concrete. While for the concrete with addition of SBR or VPV, neither an increase nor a decrease in resistance was observed. However, the addition of AC had a negative influence on the resistance against microbiological sulfuric acid. That is, the addition of two of the selected polymers led to the same results concerning the resistance to sulfuric acid with both test methods, i.e. SA with an increased resistance and AC with decreased resistance in comparison with the reference mix. However, the other concrete mixes did not show the same results for both tests. Comparing with the reference mix, the addition of VPV led to a slight increase in resistance against the chemical sulfuric acid but no better resistance against the corrosion due to the microbiological sulfuric acid. The addition of SBR did not cause an increased resistance of the concrete using the microbiological procedure, while a decrease in resistance was reported in the chemical tests.

Similar to the discussions in Sects. 1.1 and 1.2, the benefits of using polymer modified cements against MIC are not confirmed. The results deviate significantly from each other in existing studies, where the relevant discussions included in the previous sections regarding the complexity of factors influencing MIC and the variations in the adopted test methods are applicable for polymer modified cements as well. Moreover, applications of polymer-modified cement concrete in practice are very limited, e.g. due to the associated high costs and health and safety risks. All these factors putting together makes the prospect of using polymer-modified cements for MIC related applications rather dim.

1.4 Sulfur Binder

With the considerable improvement in technologies for the removal of sulfur, e.g. from natural gas, crude oil and petroleum products, large amount of sulfur was separated from oil and natural gas industry [140]. According to US Geological Survey [43], China contributes the largest amount of sulfur production, reaching 17 million tons in 2018. After China, the sulfur production of USA, Russia, Saudi Arabia, and Canada are 9.7, 7.1, 6 million tons, with an annual world production of 80 million tons (Fig. 5a). As an industrial raw material, sulfur has been applied to different industries, e.g. agriculture, ore mining, and pharmaceuticals. The attempt to use sulfur as a binding material in civil engineering also attracts considerable interest

due to the increasing environment concerns about the cement production process as well as the depletion of raw materials (Fig. 5b) [42, 96].

Sulfur may be used as a binder in concrete manufacturing, e.g. as an alternative to OPC. Sulfur concrete (SC) consists of mineral aggregate, filler, and sulfur as the binder [48]. Relevant research has attracted extensive interest in the scientific community because of, e.g. its strong corrosion resistance, excellent mechanical properties and rapid setting characteristics. [33, 44, 48, 51, 98, 140, 152]. Table 4 summarizes the mechanical performance of some sulfur concretes with different compositions. Unfortunately, the low stability of SC, especially exposed to high humid environment, would induce the failure and degradation of the concrete [48]. Therefore, several attempts have been made to modify original SC, termed modified sulfur concrete (MSC) [13, 34, 53]. The most common modifiers used include dicyclopentadiene or a combination of dicyclopentadiene, cyclopentadiene and diphenylene, as well as olefin polysulfide additives, which can avoid the transfer of sulfur from monoclinic state to orthorhombic state [98]. According to [18], modification of sulfur was also performed by polymerization with cyclic hydrocarbon.

There are a number of experimental investigations on sulfur binder in laboratory conditions. Mass loss has been used as an important parameter to evaluate the corrosion resistance of sulfur concrete in simulated sewer environments. The reported mass loss varies considerably in existing literature, e.g. see some summarized results in Table 5. The results can be affected by various factors, depending on the sulfur concrete types and service conditions. Sulfur concrete is typically characterized by low permeability as water is not used in the mixing process [37]. The ingress of acid species, chloride and sulfate ions, oxygen, and water can be significantly hindered from the surrounding environment. Therefore, the mass loss of MSC is normally one order of magnitude smaller than Portland cement concrete (PCC) under the same exposure conditions. Another study conducted by [140] showed that filler in

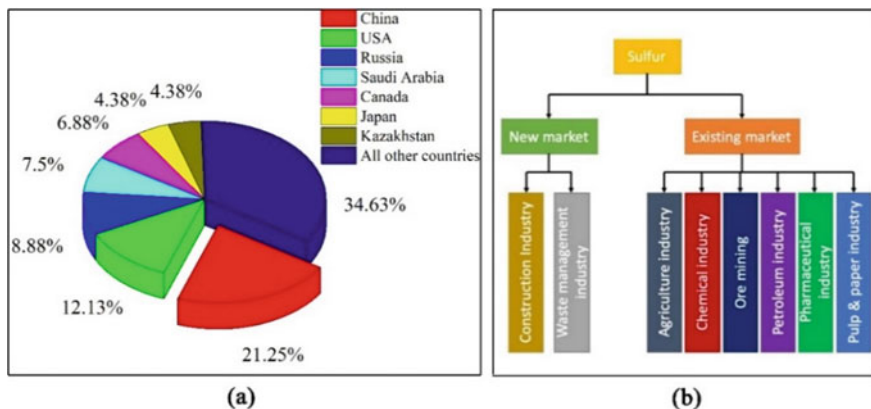


Fig. 5 **a** The major sulfur producing countries in the world, data from [43]; **b** Global new and existing sulfur application fields [42]

Table 4 Reported mechanical performance of some sulfur concrete

Composition (wt. %)		Mechanical properties					References		
Sulfur	Sulfur modifier	Binder	Coarse aggregate	Sand	Fillers	Compressive strength (MPa)	Flexural strength (MPa)	Tensile strength (MPa)	
30	-	-	-	63	7	55	8	3	[140]
12	-	6 (fly ash)	42	40	-	30	2	1	[3]
25	-	5 (slag)	-	70	-	70	12	5	[48]
15	-	13 (fly ash)	40	32	-	83	13	6	[121]
50	50 (phosphogypsum)	-	-	-	-	41	5	2	[42]
30	-	-	-	-	70	115	16	7	[142]
17	2 (polymer)	8 (soil)	24	49	-	60	13	6	[8]
25	5 (slag)	-	-	70	-	52	8	3	[34]
40	-	25 (binary cement)	-	35*	-	62	9	4	[53]
30	-	-	-	70*	-	43	5	2	[97]

Table 5 Mass loss reported in laboratory studies for sulfur concrete

Temp. (°C)	Exposure medium	Test duration	Concrete type	Mass loss (%)	References
N.A	20 wt% H ₂ SO ₄	1 year	MSC with 0.1% talc	~ 0	[140]
			MSC with 8% alumina ^a	8	
			MSC with 4% microsilica	7	
			MSC with 1% fly ash	1.1	
Room temperature	98 wt% H ₂ SO ₄	24 h	PCC	0.3	[152]
			MSC	3.5	
N.A	Biological acid condition	180 days	PCC	2.35	[118]
			MSC	8.85	
N.A	40 wt% H ₂ SO ₄	24 h	PCC	2.73	[98]
			MSC	0.29	

^a The specimen began to crumble after 100 days of exposure
Note Information not available is indicated by “N.A.”

sulfur concrete also plays a crucial role in the corrosion resistance and mechanical performance in various corrosion environments.

The performance of sulfuric based concrete has also been studied under (close to) sewer site conditions. In the study performed by El Gamal et al. [37], concrete specimens made from Portland cement, sulfate resistant cement, and modified sulfur (namely, PCC, SRCC, and MSC) were exposed to a realistic sewer environment with a H₂S concentration varying from 10 to 70 ppm for two years. The analysis of the pore systems of the studied concrete revealed that there was an increase in the number of pores and pore sizes and connectivity after the exposure in the cases of PCC and SRCC, while insignificant change was observed in the pore system of the MSC. The neutralization depths of PCC and SRC concretes, identified by the alkalinity tests (1% Phenolphthalein), were 3.8 mm and 3.2 mm, but there is no obvious change in alkalinity of MSC concrete (Fig. 6). Another site observation reported in [95] demonstrated that the mass loss of MSC was only 2.2%, while that for PCC and SRCC was as high as 8.0% and 13.6%, respectively, after exposure to sewer environment [95], also indicating that MSC is highly resistant to sewer environment compared to PCC and SRCC.

Almost all the existing work showed the superior acid and MIC resistance of MSC and/or SC and the suitability for sewer applications. There have been attempts to produce precast sewer pipes or linings for sewer pipes using the binder, e.g. see [83]. However, the applications in cast in-situ sewer structures have not been identified. One possible reason may be related to the manufacturing process

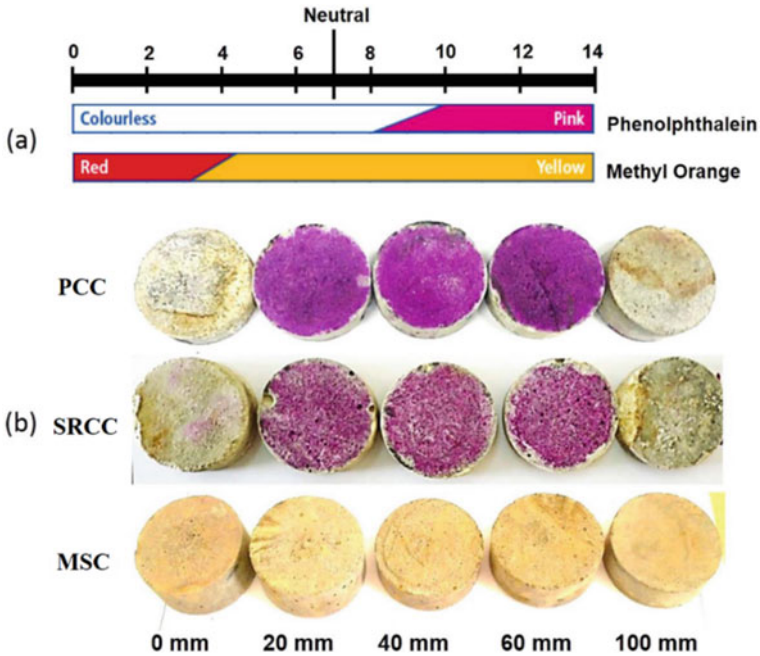


Fig. 6 a Acid and base scale range of 1% Phenolphthalein and 1% Methyl Orange; b Color change of concrete specimens along its depth after exposure to sewerage environments [37]. Reproduced with permission from Elsevier

where some high temperatures (130–150 °C) are required to melt sulfur [36]. The completely different casting procedures than the conventional concreting practices increases the challenges for application. Other hindrances may include, e.g. high costs and the lack of relevant design standards for sulfur concrete [141]. The potential health and safety risks, e.g. due to volatile compositions at high temperatures, may be another limiting factor since cast in-situ sewer structures typically require operations in confined underground spaces.

2 Aggregates

2.1 Siliceous and Calcareous Aggregates

Two types of aggregates are commonly used in concrete: calcareous aggregates that react easily with acids (where the main component in terms of oxide is CaO, e.g. limestone and dolomite) and siliceous aggregates that are rather inert when exposed to acids (where the main component in terms of oxide is SiO₂, e.g. granite and

gabbro). Aggregate volume content in concrete is typically high, e.g. > 60% [147, 149]. Consequently, aggregates can have a major impact on concrete performance.

It is generally believed that calcareous aggregates can improve the durability of concrete in acidic environments, e.g. MIC, and can even play a more critical role than cement types [6, 111, 125, 147, 149]. The acid resistance of concrete varies due to differences in the chemical composition of the aggregates, which can be largely attributed to the “alkalinity” of the concrete. Concrete with calcareous aggregates has a much higher alkalinity than concrete with siliceous aggregates, and the high alkalinity provides more material to react with the acid (the so-called neutralization capacity), thus slowing down the corrosion rate. Replacing siliceous aggregates by calcareous aggregates may significantly increase the concrete resistance to MIC. The resistance can be increased by a factor of 3 using calcareous aggregates [20, 61]. In concrete containing siliceous aggregates, only the cement paste can react with acid, therefore, the neutralization capacity of the concrete is limited when compared with the counterpart with calcareous aggregates [91, 111].

Under laboratory conditions, Xiao et al. [148] investigated the corrosion morphology of concrete specimens containing siliceous coarse aggregates exposed to sulfuric acid solution with a pH value of 0.95. The degradation pattern, as reflected by the change of the morphology during the 194 days, could be characterized by the loss of mainly cement paste/mortar with coarse aggregates protruding out. In the same study, concrete made with limestone coarse aggregates had a lower corrosion depth and less loss of thickness than that of the concrete with siliceous coarse aggregates. House et al. [64] revealed the improved acid resistance of concrete using limestone coarse aggregates. Pather et al. [111] stored Portland cement concrete (PCC) samples of two different strength classes containing siliceous granite and calcareous dolomite aggregates in sulfuric acid solutions for 84 days and evaluated the effect of the both types of aggregates on the acid resistance. The relevant results are shown in Figs. 7 and 8. It was concluded that calcareous aggregate (dolomite) was more effective in reducing the progression of acid attack for PCC. The effect was due to the sacrificial nature of dolomite (reacting with the acid) involving the simultaneous corrosion of both the cement paste and the dolomite aggregates, resulting in uniform surface wear and thus reducing the corrosion process of the acid attack. In the study performed by De Belie et al. [28], both chemical and microbiological tests showed that the aggregate type had the largest effect on degradation, i.e. concrete with limestone aggregates showed a smaller degradation depth than that of the concrete with inert gravel aggregates.

Studies under site conditions (or full-scale experiments) revealed that calcareous aggregates in general have a beneficiary role in reducing the MIC rate of concrete exposed to sewer environments [6, 113, 125]. In the classic Virginia Experimental Sewer in South Africa, the corrosion of concrete pipe sections prepared by different aggregate types (and binders, i.e. CAC and OPC) were studied [6]. The state of the pipe sections after 12 years in test are excerpted and illustrated in Fig. 9. It can be seen that for OPC concrete, the use of calcareous aggregates significantly slowed down the MIC rate, i.e. an average value of about 1.7–2.5 mm/year as compared to > 5 mm/year for the counterpart using siliceous aggregates. Pomeroy [113] reported

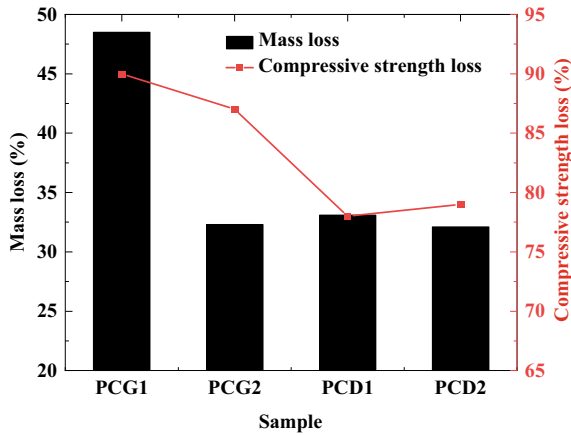


Fig. 7 Paired test analysis based on mass loss and strength loss results of PC concretes. *Note* PCG1—PC + granite, Strength C50; PCG2—PC + granite, Strength C35; PCD1—PC + dolomite, Strength C50; PCD2—PC + dolomite, Strength C35; data based on [111]

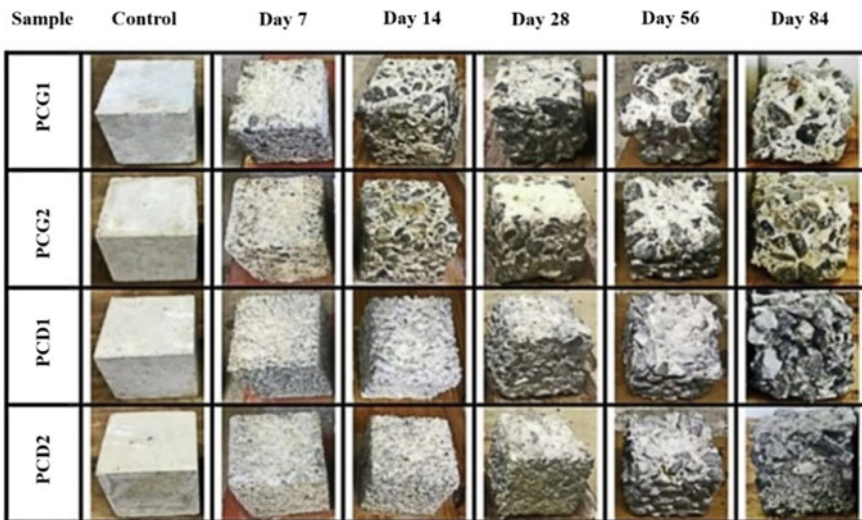


Fig. 8 PC concrete cubes before and after immersion in sulfuric acid, adapted from [111]. Reproduced from with permission from Elsevier

the results of five experimental concrete pipes placed in a by-pass line between two manholes after 7 years of exposure. The qualitative results can be seen in Fig. 10, where the corrosion was much less pronounced for the pipe with limestone aggregates compared to the pipes with granite aggregates. Slightly different results were found in [77], where concrete samples prepared by CAC together with both siliceous and calcareous aggregates were exposed to two different sewer environments. Mass loss

and sample thickness reduction were measured after more than 120 months. The average values for the CAC concrete containing the two types of aggregates were found to be similar. This might be explained by the fact that CAC was used. Besides the mechanism of providing neutralization capacity, other effects brought in by CAC may dominate in this case, especially the “bacteriostatic effect” which has been considered the most important one and accounts for largely the resistance against MIC [124].

As discussed in [144], the beneficiary effects of using calcareous aggregates instead of inert siliceous aggregates to mitigate MIC in general have been validated in both laboratory studies and field applications. The high-volume fraction of aggregates (60% or more) in concrete further magnifies the effects. The main mechanism is attributed to the increased “alkalinity” or acid neutralization capacity of concrete when calcareous aggregates are used. Nevertheless, local availability of calcareous aggregates may be a constraint for the wide adoption of this MIC mitigation measure in practice.

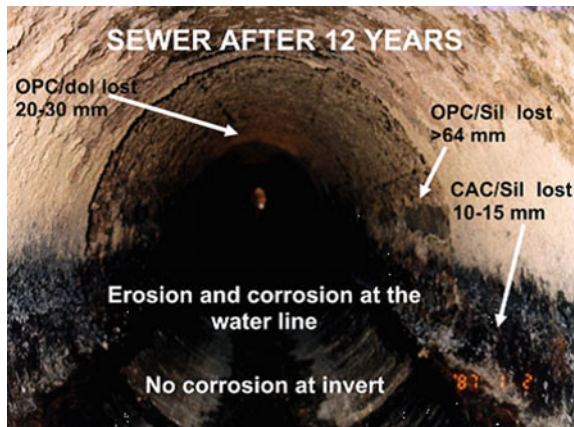


Fig. 9 Corrosion of the concrete pipe sections in the Virginia Experimental Sewer in South Africa after 12 years of test: “dol” indicates dolomite aggregates and “Sil” indicates siliceous aggregates [6]. Reproduced with permission from Springer

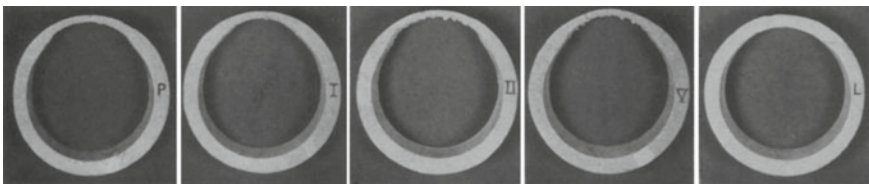


Fig. 10 Concrete pipes exposed to septic tank effluent for 7 years. Notation on the pipes (cement type according to ASTM C150): P– Type II cement with pozzolan and granite aggregates; I– Type I cement and granite aggregates; II– Type II cement and granite aggregates; V– Type V cement and granite aggregates; L– Type II cement and limestone aggregates, adapted based on [113]

2.2 Crushed CAC Clinker as Aggregates

Several studies have shown that 100% CAC based concrete or mortar (i.e. the aggregates are crushed CAC clinkers) performs better than CAC with either siliceous or calcareous aggregates in sewer conditions.

In [6, 35], various concrete mixes were prepared and the concrete samples were then installed in holders on the walls of the manhole in a sewer, directly above maximum sewage level. The samples were visually inspected and measured after 5 and 17 months, respectively, with the results shown in Table 6. It can be seen that after only 5 months, OPC concrete with siliceous aggregates already suffered from severe attack, while the attack on the samples of the other concrete mixes were negligible at this stage. After 17 months, both OPC mixes experienced notable (moderate to severe) attack, while both CAC mixes showed negligible attack. The trend of the attack was more evident by looking at the mass loss. The mass losses of the two CAC mixes were significantly lower than that of the OPC mixes after 17 months. There was some mass loss for the CAC mix with dolomite aggregate, even though the magnitude was rather small. It is worthwhile to highlight that the CAC/AlagTM mix, i.e. 100% CAC mix, showed completely no mass loss, indicating the excellent performance of the mix. In another study reported by Kiliswa [77], the average corrosion rate of 100% CAC mix after around 10 years exposure in the Virginia Experimental Sewer was compared with that of the CAC mixes with siliceous and calcareous aggregates, see Fig. 11. The corrosion rate of the 100% CAC mix was 0.23 mm/year, while the values for the other two mixes were 0.35 mm/year. The results also demonstrated the beneficiary effects of using 100% CAC mix.

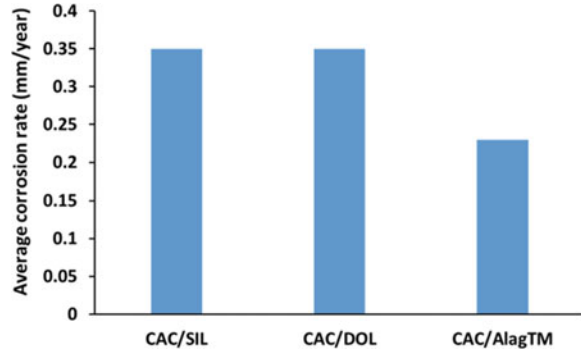
Regarding the mechanism, Saucier and Herisson [123] argued that it could be attributed to a uniform chemistry across the whole concrete surfaces, including that of the aggregates and the cement hydrates. Aggregate grains, e.g. sand, could act like “virgin islands” for relevant bacteria to generate sulfuric acid without being slowed down by the bacteriostatic effect imposed by the CAC chemistry. The acid produced at the sand surfaces can run off onto the surrounding cement hydrates leading to the

Table 6 Attack of concrete samples from various concrete mixes placed in the Virginia manhole after 5 and 17 months, adapted from [6]

Mix (% binder)	w/b	5 months		17 months		
		Attack	pH	Attack	pH	Mass loss (%)
OPC/Sil (23%)	0.32	Severe	–	Severe	6.70	6.09
OPC/Dolo (23%)	0.26	Negligible	6.00	Moderate	6.70	2.46
CAC/Dolo (23%)	0.26	Negligible	6.00	Negligible	6.70	0.35
CAC/Alag TM (23%)	0.26	Negligible	6.50	Negligible	7.14	0.00

Sil siliceous aggregate; *Dolo* dolomite aggregate; *AlagTM* artificial aggregate made from CAC clinker

Fig. 11 Average corrosion rates of different CAC concrete mixes after exposure in the Virginia Experimental Sewer for 120 months (10 years), data adopted from [77]



corrosion. As 100% CAC concrete has the same chemistry throughout the surfaces, there are no “virgin islands” for the bacteria to colonize and proliferate. That is, the process for generating sulfuric acid is interrupted/hindered by the bacteriostatic effect.

2.3 PET Aggregates

Plastic waste materials have caused severe environmental issues as the biodegradation process may last thousands of years [101]. Recycling of such wastes is a mainstream and meets the requirement for sustainable development. The possibility of using plastic materials in the construction industry has been studied. Polyethylene terephthalate (PET) is a common plastic waste that can be used as aggregates in concrete. Some recent studies showed that the lower specific gravity of PET compared to common aggregates leads to a reduction in concrete weight, which may be an advantage in designing lightweight structures [2, 46, 130, 146]. However, it has also been shown that the addition of PET particles may also negatively affect the quality of concrete, e.g. leading to decreased mechanical properties due to the weaker bonding and lower surface energy [4, 26, 94].

To the best knowledge of the authors, there has been no related work studying the performance of concrete containing PET aggregates in the context of MIC. However, there are some studies on acid resistance of concrete incorporating PET particles in laboratory conditions using chemical sulfuric acid [9, 17, 116]. Table 7 summarizes some of the reported mass loss of concrete with different content of PET particles under sulfuric acid attack. Based on the limited results, it seems that PET may be used as aggregates for concrete in aggressive environments, e.g. sewer conditions. PET aggregates may alter the mechanism of concrete corrosion under sulfuric acid attack and help concrete better maintain the load-bearing capacity and integrity [9, 17]. More stringent studies are needed to evaluate the performance of concrete with PET aggregates under real sewer conditions.

Table 7 Mass loss reported in laboratory studies of concrete with PET

Physical characteristics of PET		PET Content (%)	Exposure	Mass loss (%) after 60 days	References
Unit weight (kg/m ³)	Particle size (mm)				
464	< 7	0	5% H ₂ SO ₄	13.47	[9]
		5		10.26	
		10		8.98	
		15		6.57	
464	< 7	0	5% H ₂ SO ₄	14.47	[116]
		5		13.30	
		10		10.27	
		15		10.03	

3 Additives

3.1 Antimicrobial Agents

Antimicrobial agents, i.e., chemical substances toxic to a number of living organisms, may be added to increase the performance of concrete subject to MIC conditions. The concept of using antimicrobial agents in concrete to mitigate MIC has caught significant interests, and the principal mechanism is to inhibit the growth of microorganisms and thereby reduce the development of the corrosion [19, 104]. There are two main methods of using antimicrobial agents: one is to add antimicrobial agents into coating materials to protect underlying concrete; and the other is to mix antimicrobial agents directly into the concrete (as an admixture) [27, 158, 159].

Antimicrobial agents may be divided into two main types: inorganic and organic antimicrobial agents [72, 114]. Inorganic antimicrobial agents usually include heavy metals (silver, nickel, tungsten), metal compounds, silicate, free nitrite and nano inorganic antimicrobial materials. The antibacterial activity of metal or metal ions is in the order of: Ag > Hg > Cu > Cd > Cr > Ni > Pb > Co > Zn > Fe [72, 86, 88, 114, 157]. Antibacterial agents containing silver ions show strong effects, while broad use is hindered by the relatively high cost [72, 114]. Inorganic antimicrobial agents are characterized by long shelf time and high temperature resistance, while side effects such as toxicity cannot be neglected [89, 102, 108, 133]. Commonly used organic antimicrobial agents include, e.g. quaternary ammonium compounds and tertiary amines, mixtures of aldehydes, chlorine compounds, formalin, alcohols, peroxide compounds, nickel sulfide and calcium formate (toxic to thionic bacteria) and guanidine derivatives [50, 145]. Quaternary ammonium compounds are representative organic antimicrobial agents, e.g. silane quaternary ammonium chloride (SQA) [38] and cetyl-methyl ammonium bromide [7], both of which have been widely studied, e.g. see [67, 86].

In addition, it has been found that Cu_2O , CaCO_3 , TiO_2 , ZnO , CuO , Al_2O_3 , Fe_3O_4 and other nanoparticles also have shown good inhibitory effects on microorganisms [104, 128, 131, 139]. This is due to the fact that the ratio of surface area to volume increases significantly when the particle size is reduced to the nanoscale. This may result in superior antimicrobial properties due to, among others, greater interactions with the surrounding microorganisms and/or enhanced release of toxic ions from the surfaces [12, 14, 93, 104]. Some possible antimicrobial agents to mitigate MIC of concrete are summarized in Table 8. The use of antimicrobial agents in this context has both advantages and disadvantages [144]. The advantages include, e.g. good MIC mitigation effects can be expected when suitable antimicrobial agents are used and it is a technology with high potential, e.g. the use of nanoparticles. The potential disadvantages include, e.g. long-term effects not validated, potential environmental concerns due to the use of heavy metal bearing chemicals, and the high cost of using novel materials, e.g. nanoparticles.

4 Novel Corrosion-Resistant Bioconcrete

Conventionally, bioconcrete is an innovative type of concrete with admixed bacteria that is capable of microbially inducing calcite precipitation [160]. Calcite is a ‘bio-sealant’ to seal cracks and reduce concrete permeability. Different bacteria have been used for conventional bioconcrete, including sulfate-reduction bacteria [21, 39]. Previous bioconcrete studies mainly focused on crack-healing of concrete structures like buildings [126].

Sulfate-reducing bacteria has been long recognized for its diverse potential in biotechnology development [100]. Another study found that sulfate-reducing bacteria coexist with sulfide-oxidizing bacteria by inhabiting different layers of the corrosion biofilm on mortar samples located in a sewer manhole [122]. These findings support the potential use of sulfate-reducing bacteria in bioconcrete, for the purpose of enhancing the corrosion resistance in sewers. Some recent studies developed self-healing bioconcrete specifically for domestic sewer systems using sulfate-reducing bacteria and/or nitrate-reducing bacteria cultivated from wastewater [23, 25, 132].

A recent study evaluated the physiological suitability of sulfate-reducing bacteria granules for the development of bioconcrete [24]. The bioconcrete solution utilizes the sulfate reducing processes that can reverse the corrosion caused by sulfide-oxidizing bacteria. Sulfate-reducing bacteria can consume sulfate and increase the pH (Eqs. 1–3). The opposite microbial metabolisms of sulfate-reducing bacteria and sulfide-oxidizing bacteria (Eq. 4) can cycle a part of the total sulfur compounds on concrete surface, thus mitigate (or completely avoid ideally) the damaging effects of sulfuric acid to cement.

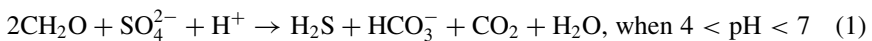


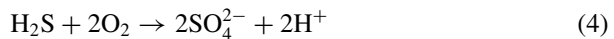
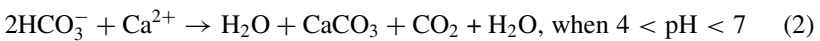
Table 8 Some possible antimicrobial agents to mitigate MIC of concrete

Antimicrobial agents	Effects	References
Sodium tungstate (Na_2WO_4)	Complete inhibition of five strains of ASOB at the concentration of 50 μM	[103]
Nickel, calcium tungstate (Ni , CaWO_4)	The addition of 0.075% metal nickel and 0.075% calcium tungstate significantly reduced the weight loss of cement samples after exposure to sewer atmosphere containing 28 ppm H_2S for two years, respectively	[103]
Metal (Ni , W) compounds, ZnSiF_6	Mortar with antimicrobial watertight admixture had higher pH (6.8) and lower concentration of sulfuric acid (3.78×10^{-8} mol/L) compared to that (6.6 and 2.56×10^{-7} mol/L) of plain mortar	[84]
Silver-loaded zeolite	Growth of planktonic and biofilm populations of <i>A.thiooxidans</i> was inhibited	[55]
Silver molybdate	The residual colony count of <i>E. coli</i> and <i>S. aureus</i> is 0 cfu/mL by addition of 0.004% silver molybdate	[157]
Silver-silica composite (Ag-Si)	Mortality for Gram positive and negative bacteria was 99%	[1]
Silver, zinc and copper ions contained in zeolites (Ag , Zn and Cu)	The efficiency of the silver ions was superior to the other single ionic systems. The binary Cu/Zn had similar antimicrobial efficiency as Ag	[72]
Zn oxide (ZnO), copper (Cu) slag, ammonium chloride (NH_4Cl) sodium bromide (NaBr), and cetyl-methyl ammonium bromide ($\text{C}_{17}\text{H}_{38}\text{BrN}$)	They all showed inhibition capabilities to algal. Addition of zinc oxide and ammonium chloride (10% each) in mortar mix showed comparable bacteriostatic properties to commercial biocides	[7]
Nickel, tungsten and fluosilicates (Ni , W and $\text{ZnSiF}_6/\text{MgSiF}_6$)	Inhibition effects on SOB growth were observed	[54]
Copper and copper oxide (Cu and CuO)	The samples were able to kill 95% of <i>E. coli</i> after 4 h contact	[30]
Copper oxide (CuO)	Leaching of copper from the nano copper oxide film significantly inhibited the growth of ASOB (<i>A. thiooxidans</i>)	[56]
Titanium dioxide (TiO_2)	16-week exposure study showed no visible algal growth on the surface of white cements containing a commercial TiO_2 nano-particles	[93]

(continued)

Table 8 (continued)

Antimicrobial agents	Effects	References
Nano sized TiO ₂ , CaCO ₃	Nano-TiO ₂ modified fly ash mortar and nano-sized TiO ₂ , CaCO ₃ modified fly ash mortar exhibited enhanced antibacterial activities compared to nano-CaCO ₃ modified fly ash mortar	[139]
SiO ₂ /TiO ₂ nano-composite	Bacteria inactivation after UV light irradiation and without illumination after 120 min was 67% and 42%, respectively	[129]
Aluminum ions (Al)	Impact of Al on the microbial activities has been proposed as a reason for high durability of calcium aluminate cements	[62, 63]
Calcium formate (Ca(HCOO) ₂)	The growth of the SOB (ASOB) was completely inhibited by formates, especially by calcium formate of concentrations more than 50 mM	[151]
Isothiazoline/cabamate (C ₃ H ₃ NS/NH ₂ COOH)	Outstanding antifungal effects (on the <i>Aspergillusniger</i>) were found for cement mortars with the isothiazoline/cabamate	[32]
Antimicrobial fibers	No growth of bacteria (<i>E. coli</i> and <i>S. aureus</i>) was observed within about 2–4 mm of the area surrounding the concrete samples	[45]
Free nitrous acid (FNA, i.e. HNO ₂)	H ₂ S uptake rate decreased by 84–92% 1–2 months and viable bacterial cells reduced from 84.6 ± 8.3% to 10.7 ± 4.3% within 39 h after FNA spray	[69]



Sulfate-reducing bacteria exist in wastewater systems due to the prevalence of carbon and sulfur substrates in wastewater for their growth and metabolisms [70]. Due to sulfur cycling, it is no surprise that sulfate-reducing bacteria and sulfide-oxidizing bacteria co-exist in the same natural environment [16, 52, 71]. Also, they were found to co-exist in the corrosion biofilms of a sewer manhole, where frequent wastewater inoculation happened [122]. The sulfate-reducing bacteria with relative abundance even lower than 1% in the corrosion layer significantly inhibited corrosion compared to those samples without sulfate-reducing bacteria. The less corrosion was detected on the gas-phase samples without wastewater inoculation, suggesting that

sulfate-reducing bacteria in the anerobic regions of the corrosion layer may reduce corrosion.

The concrete corrosion environment with elevated sulfate and calcium ions provides the sulfur substrate to sulfate-reducing bacteria. In sewers, the domestic wastewater can provide carbon substrate that is essential for dissimilatory sulfate reduction to happen (Eqs. 1 and 3). Sulfate-reducing bacteria can reduce sulfate to sulfide under anaerobic or microaerophilic environment [106, 107] generating calcite as well as consuming protons to produce H₂S and CO₂ [21, 122]. It was found that the spore-forming and haloalkaliphilic sulfate-reducing bacteria were active in alkaline environment with pH up to 11, which is similar to the fresh concrete condition [57]. It is thus highly possible to add sulfate-reducing bacteria as the bioagent of bioconcrete to mitigate corrosion. A recent study also found the abundance of sulfate-reducing bacteria increased significantly from ordinary concrete (0%) to two types of bioconcrete (2–7%) (as highlighted in Fig. 12).

A recent study tested a type of bioconcrete based on mixed sulfate-reducing bacteria and nitrate-reducing bacteria granules (originally developed for its self-healing capacity) for the corrosion rate in a corrosion chamber over 6 months [132]. It was found that the bioconcrete samples (B1 and B2, with 1% and 2% bacterial sludge) showed lower corrosion rate, up to 43% less, in comparison to a general Portland cement concrete (C0) (Fig. 13). This preliminary experiment demonstrates the potential of using sulfate-reducing bacteria in bioconcrete for enhanced corrosion resistance in sewer environment.

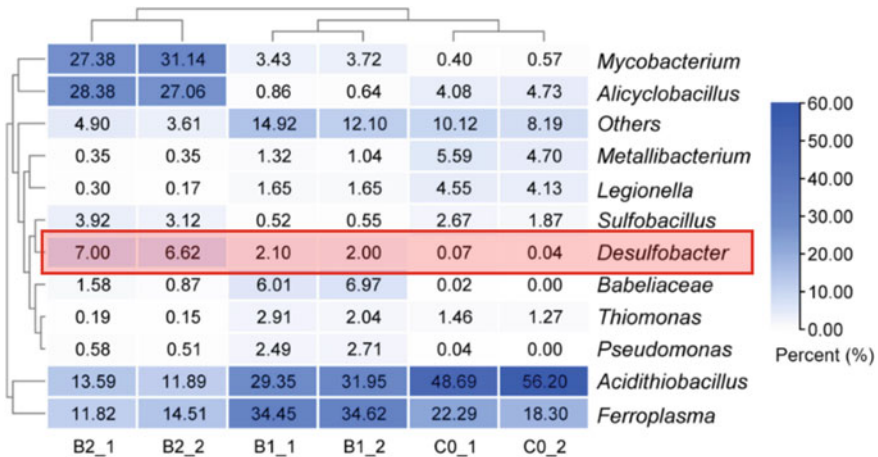


Fig. 12 Heatmap representing the relative abundance of the predominant bacterial types (> 2%) detected in the corrosion layer of portlandite concrete (C0) and two bioconcrete samples (B1 and B2) using 16S rRNA gene amplicon sequencing. The presence of sulfate-reducing bacteria is highlighted in the red box [132]. Reproduced with permission from Elsevier

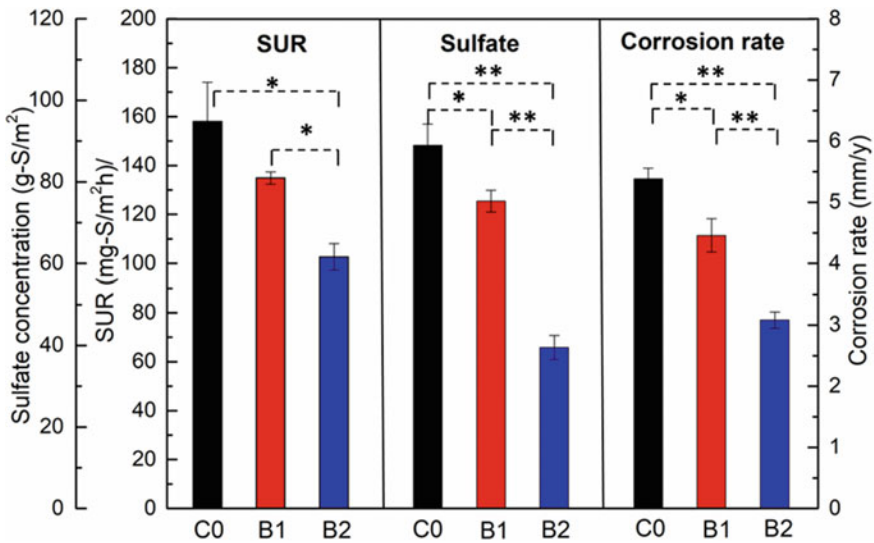


Fig. 13 The sulfide uptake rates (SUR), sulfate concentrations and corrosion rates after 6 months of exposure of control (C0) and bio-concrete mortar coupons (B1 and B2) after 0, 3 and 6 months of partially submerged exposure in the corrosion chamber. The error bars indicated the standard errors. Single-factor ANOVA analysis was used to calculate the significant difference among the groups (** $p < 0.01$; * $p < 0.05$) [132]. Reproduced with permission from Elsevier

5 Summary

Attempts have been made to improve the corrosion resistance of concrete under MIC conditions by using various different binder materials. Based on existing studies, the potential benefits of using sulfate resistant cement, supplementary cementitious materials and polymer modified cements against MIC are not conclusive, despite the positive results obtained in various laboratory studies. Almost all the existing work showed the superior acid and MIC resistance of sulfur concrete and the suitability for sewer applications, while the potential for field applications, especially for cast in-situ sewer structures, is challenged by practical issues, e.g. the casting procedures and potential health and safety risks.

Aggregate can contribute significantly to the corrosion resistance of concrete primarily due to the high-volume fraction (more than 60%). Concrete with calcareous aggregates has a much higher alkalinity than concrete with siliceous aggregates, and the high alkalinity provides more material to react with the acid (the so-called neutralization capacity), thus slowing down the corrosion rate. The use of crushed CAC clinker as aggregate together with CAC has shown better performance than CAC with either siliceous or calcareous aggregates in sewers, which is attributed to a uniform chemistry across the whole concrete surfaces. Laboratory studies have

shown improved acid resistance of concrete with PET aggregates, while more stringent studies are needed to evaluate the performance of the concrete under real sewer conditions.

The concept of using antimicrobial agents and additives in concrete to mitigate MIC have attracted significant interests, and the main mechanism is to inhibit the growth of microorganisms and thereby reduce the development of the corrosion. The advantages of using antimicrobial agents include good MIC mitigation effects when suitable products are used and the high potential of the technique, while the potential disadvantages include, e.g. long-term effects not validated, potential environmental concerns and the high cost of using novel materials, e.g. nanoparticles.

Corrosion-resistant bioconcrete is a novel technique that is at the early stage of the development. However, it holds a great potential as it provides a long-term protection of concrete in the sewer environment. Future research is needed to further develop and demonstrate this innovative technology.

References

1. Adak, D., Sarkar, M., Maiti, M., Tamang, A., Mandal, S., Chattopadhyay, B.: Antimicrobial efficiency of nano silver–silica modified geopolymer mortar for eco-friendly green construction technology. *RSC Adv.* **5**, 64037–64045 (2015)
2. Akçaözöğlü, S., Atiş, C.D., Akçaözöğlü, K.: An investigation on the use of shredded waste PET bottles as aggregate in lightweight concrete. *Waste Manage.* **30**, 285–290 (2010)
3. Al-Otaibi, S., Al-Aibani, A., Al-Bahar, S., Abdulsalam, M., Al-Fadala, S.: Potential for producing concrete blocks using sulphur polymeric concrete in Kuwait. *J. King Saud Univ-Eng. Sci.* **31**, 327–331 (2019)
4. Albano, C., Camacho, N., Hernández, M., Matheus, A., Gutiérrez, A.: Influence of content and particle size of waste pet bottles on concrete behavior at different w/c ratios. *Waste Manage.* **27**, 2707–2716 (2009)
5. Alexander, M., Bertron, A., de Belie, N.: *Performance of Cement-Based Materials in Aggressive Aqueous Environments*. Springer (2013)
6. Alexander, M., Fourie, C.: Performance of sewer pipe concrete mixtures with Portland and calcium aluminate cements subject to mineral and biogenic acid attack. *Mater. Struct.* **44**, 313–330 (2011)
7. Alum, A., Rashid, A., Mobasher, B., Abbaszadegan, M.: Cement-based biocide coatings for controlling algal growth in water distribution canals. *Cement Concr. Compos.* **30**, 839–847 (2008)
8. Anyszka, R., Bieliński, D. M., Siciński, M., Imiela, M., Szajerski, P., Pawlica, J., Walendziak, R.: Sulfur concrete—promising material for space-structures building. In: *Proceedings of the European Conference on Spacecraft Structures Materials and Environmental Testing*, Toulouse, France, pp. 27–30 (2016)
9. Araghi, H.J., Nikbin, I., Reskati, S.R., Rahmani, E., Allahyari, H.: An experimental investigation on the erosion resistance of concrete containing various PET particles percentages against sulfuric acid attack. *Constr. Build. Mater.* **77**, 461–471 (2015)
10. Assaad, J.J.: Development and use of polymer-modified cement for adhesive and repair applications. *Constr. Build. Mater.* **163**, 139–148 (2018)
11. Attiogbe, E.K., Rizkalla, S.H.: Response of concrete to sulfuric acid attack. *ACI Mater. J.* **85**, 481–488 (1988)

12. Azam, A., Ahmed, A.S., Oves, M., Khan, M.S., Habib, S.S., Memic, A.: Antimicrobial activity of metal oxide nanoparticles against Gram-positive and Gram-negative bacteria: a comparative study. *Int. J. Nanomed.* **7**, 6003 (2012)
13. Bae, S.G., Gwon, S.W., Kim, S.W., Cha, S.W.: Physical properties of sulfur concrete with modified sulfur binder. *KSCE J. Civil Environ. Eng. Res.* **34**, 763–771 (2014)
14. Batchelor-Mcauley, C., Tschulik, K., Neumann, C.C., Laborda, E., Compton, R.G.: Why are silver nanoparticles more toxic than bulk silver? Towards understanding the dissolution and toxicity of silver nanoparticles. *Int. J. Electrochem. Sci.* **9** (2014)
15. Beeldens, A., Monteny, J., Vincke, E., de Belie, N., van Gemert, D., Taerwe, L., Verstraete, W.: Resistance to biogenic sulphuric acid corrosion of polymer-modified mortars. *Cement Concr. Compos.* **23**, 47–56 (2001)
16. Bell, E., Lamminmäki, T., Alneberg, J., Andersson, A.F., Qian, C., Xiong, W., Hettich, R.L., Frutschi, M., Bernier-Latmani, R.: Active sulfur cycling in the terrestrial deep subsurface. *ISME J.* **14**, 1260–1272 (2020)
17. Benosman, A., Mouli, M., Taibi, H., Belbachir, M., Senhadji, Y.: Resistance of polymer (PET)-mortar composites to aggressive solutions. *Int. J. Eng. Res. Afr.* **1**, 1–15 (2011)
18. Blight, L., Currell, B.R., Nash, B.J., Scott, R.A.M., Stillo, C.: Preparation and properties of modified sulfur systems. *Abstr. Pap. Am. Chem. Soc.* **173**, 16–16 (1977)
19. Bryukhanov, A., Vlasov, D.Y., Maiorova, M., Tsarovtseva, I.: The role of microorganisms in the destruction of concrete and reinforced concrete structures. *Power Technol. Eng.* **54**, 609–614 (2021)
20. Cairns, J.: CMA publishes sewer design manual. *Civil Eng.* **17**, 61–62 (2009)
21. Chahal, N., Rajor, A., Siddique, R.: Calcium carbonate precipitation by different bacterial strains. *Afr. J. Biotech.* **10**, 8359–8372 (2011)
22. Chang, H.B., Choi, Y.C.: Accelerated performance evaluation of repair mortars for concrete sewer pipes subjected to sulfuric acid attack. *J. Market. Res.* **9**, 13635–13645 (2020)
23. Chetty, K., Garbe, U., Wang, Z., Zhang, S., Mccarthy, T., Hai, F. Jiang, G.: Bioconcrete based on sulfate-reducing bacteria granules: cultivation, mechanical properties, and self-healing performance. *J. Sustain. Cement-Based Mater.* 1–12 (2022a)
24. Chetty, K., McCarthy, T., Hai, F., Zhang, S., Song, Y., Jiang, G.: Physiological suitability of sulfate-reducing granules for the development of bioconcrete. *Biotechnol. Bioeng.* **119**, 2743–2756 (2022)
25. Chetty, K., Xie, S., Song, Y., Mccarthy, T., Garbe, U., Li, X., Jiang, G.: Self-healing bioconcrete based on non-axenic granules: a potential solution for concrete wastewater infrastructure. *J. Water Process Eng.* **42**, 102139 (2021)
26. Choi, Y.W., Moon, D.J., Kim, Y.J., Lachemi, M.: Characteristics of mortar and concrete containing fine aggregate manufactured from recycled waste polyethylene terephthalate bottles. *Constr. Build. Mater.* **23**, 2829–2835 (2009)
27. Dai, Y., Li, S.: Mechanism of action and development prospect of antibacterial concrete. **5** (2021)
28. de Belie, N., Monteny, J., Beeldens, A., Vincke, E., van Gemert, D., Verstraete, W.: Experimental research and prediction of the effect of chemical and biogenic sulfuric acid on different types of commercially produced concrete sewer pipes. *Cem. Concr. Res.* **34**, 2223–2236 (2004)
29. de Weerd, K., Haha, M.B., le Saout, G., Kjellsen, K.O., Justnes, H., Lothenbach, B.: Hydration mechanisms of ternary Portland cements containing limestone powder and fly ash. *Cem. Concr. Res.* **41**, 279–291 (2011)
30. Delgado, K., Quijada, R., Palma, R., Palza, H.: Polypropylene with embedded copper metal or copper oxide nanoparticles as a novel plastic antimicrobial agent. *Lett. Appl. Microbiol.* **53**, 50–54 (2011)
31. Deschner, F., Winnefeld, F., Lothenbach, B., Seufert, S., Schwesig, P., Dittrich, S., Goetz-Neunhoeffler, F., Neubauer, J.: Hydration of Portland cement with high replacement by siliceous fly ash. *Cem. Concr. Res.* **42**, 1389–1400 (2012)
32. Do, J., Song, H., So, H., Soh, Y.: Antifungal effects of cement mortars with two types of organic antifungal agents. *Cem. Concr. Res.* **35**, 371–376 (2005)

33. Dotto, J., de Abreu, A., dal Molin, D., Müller, I.: Influence of silica fume addition on concretes physical properties and on corrosion behaviour of reinforcement bars. *Cement Concr. Compos.* **26**, 31–39 (2004)
34. Dugarte, M., Martinez-Arguelles, G., Torres, J.: Experimental evaluation of modified sulfur concrete for achieving sustainability in industry applications. *Sustainability* **11**, 70 (2018)
35. Ehrich, S., Helard, L., Letourneux, R., Willocq, J., Bock, E.: Biogenic and chemical sulfuric acid corrosion of mortars. *J. Mater. Civ. Eng.* **11**, 340–344 (1999)
36. El Gamal, M., El-Sawy, K., Mohamed, A.-M.O.: Integrated mixing machine for sulfur concrete production. *Case Stud. Constr. Mater.* **14**, e00495 (2021)
37. el Gamal, M.M., El-Dieb, A.S., Mohamed, A.-M.O., el Sawy, K.M.: Performance of modified sulfur concrete exposed to actual sewerage environment with variable temperature, humidity and gases. *J. Build. Eng.* **11**, 1–8 (2017)
38. Erbektas, A.R., Isgor, O.B., Weiss, W.J.: Evaluating the efficacy of antimicrobial additives against biogenic acidification in simulated wastewater exposure solutions. *RILEM Techn. Lett.* **4**, 49–56 (2019)
39. Erşan, Y.Ç., Gruyaert, E., Louis, G., Lors, C., de Belie, N., Boon, N.: Self-protected nitrate reducing culture for intrinsic repair of concrete cracks. *Front. Microbiol.* **6**, 1228 (2015)
40. Estokova, A., Harbulakova, V.O., Luptakova, A., Kovalcikova, M.: Analyzing the relationship between chemical and biological-based degradation of concrete with sulfate-resisting cement. *Pol. J. Environ. Stud.* **28**, 2121–2129 (2019)
41. Fattuhi, N., Hughes, B.: The performance of cement paste and concrete subjected to sulphuric acid attack. *Cem. Concr. Res.* **18**, 545–553 (1988)
42. Fediuk, R., Mughahed Amran, Y., Mosaberpanah, M.A., Danish, A., El-Zeadani, M., Klyuev, S.V., Vatin, N.: A critical review on the properties and applications of sulfur-based concrete. *Materials* **13**, 4712 (2020)
43. Fediuk, R., Yevdokimova, Y. G., Smoliakov, A., Stoyushko, N.Y., Lesovik, V.: Use of geonics scientific positions for designing of building composites for protective (fortification) structures. In: *IOP Conference Series: Materials Science and Engineering*, p. 012011. IOP Publishing (2017)
44. Fontana, J.J., Farrell, L.J., Alexanderson, J., Ball Jr., H.P., Bartholomew, J.J., Biswas, M., Bolton, D.J., Carter, P.D., Chrysogelos Jr., J., Clapp, T.R.: *Guide for mixing and placing sulfur concrete in construction*. In: ACI: Farmington Hills, MI, USA (1988)
45. Freed, W.W.: Reinforced concrete containing antimicrobial-enhanced fibers. Google Pat. (2000)
46. Ge, Z., Sun, R., Zhang, K., Gao, Z., Li, P.: Physical and mechanical properties of mortar using waste Polyethylene Terephthalate bottles. *Constr. Build. Mater.* **44**, 81–86 (2013)
47. Ghassemi, P., Toufigh, V.: Durability of epoxy polymer and ordinary cement concrete in aggressive environments. *Constr. Build. Mater.* **234**, 117887 (2020)
48. Gracia, V., Vázquez, E., Carmona, S.: Utilization of by-produced sulfur for the manufacture of unmodified sulfur concrete. In: *International RILEM Conference on the Use of Recycled Materials in Buildings and Structures*, pp. 1–2. Citeseer (2004)
49. Grengg, C., Mittermayr, F., Baldermann, A., Bottcher, M.E., Leis, A., Koraimann, G., Grunert, P., Dietzel, M.: Microbiologically induced concrete corrosion: a case study from a combined sewer network. *Cem. Concr. Res.* **77**, 16–25 (2015)
50. Grengg, C., Mittermayr, F., Ukrainczyk, N., Koraimann, G., Kienesberger, S., Dietzel, M.: Advances in concrete materials for sewer systems affected by microbial induced concrete corrosion: a review. *Water Res.* **134**, 341–352 (2018)
51. Grugel, R.N., Toutanji, H.: Sulfur “concrete” for lunar applications—sublimation concerns. *Adv. Space Res.* **41**, 103–112 (2008)
52. Guibourdenche, L.: Deciphering sulfur cycling with multiple sulfur isotopes. *Nat. Rev. Earth Environ.* **3**, 163–163 (2022)
53. Gwon, S., Ahn, E., Shin, M.: Self-healing of modified sulfur composites with calcium sulfoaluminate cement and superabsorbent polymer. *Compos. B Eng.* **162**, 469–483 (2019)

54. Gyu-Yong, K., Eui-Bae, L., Bae-Su, K., Seung-Hun, L.: Evaluation of properties of concrete using fluosilicate salts and metal (Ni, W) compounds. *Trans. Nonferrous Met. Soc. China* **19**, s134–s142 (2009)
55. Haile, T., Nakhla, G.: The inhibitory effect of antimicrobial zeolite on the biofilm of *Acidithiobacillus thiooxidans*. *Biodegradation* **21**, 123–134 (2010)
56. Haile, T., Nakhla, G., Allouche, E., Vaidya, S.: Evaluation of the bactericidal characteristics of nano-copper oxide or functionalized zeolite coating for bio-corrosion control in concrete sewer pipes. *Corros. Sci.* **52**, 45–53 (2010)
57. Hammes, F., Verstraete, W.: Key roles of pH and calcium metabolism in microbial carbonate precipitation. *Rev. Environ. Sci. Biotechnol.* **1**, 3–7 (2002)
58. Harbulakova, V.O., Estokova, A., Kovalcikova, M.: Correlation analysis between different types of corrosion of concrete containing sulfate resisting cement. *Environments* **4**, 44 (2017)
59. Harbulakova, V.O., Estokova, A., Luptakova, A., Kovalcikova, M.: Leaching of Ca, Si, Fe and Al from concretes, based on sulphate resistant cement, due to bacterial attack—a correlation study. In: *IOP Conference Series: Earth and Environmental Science*. IOP Publishing, p. 012048 (2017b)
60. He, J., Yang, C.: Research of polymer modified concrete. *Concrete* **5**, 65–67 (2009)
61. Herisson, J., Guéguen-Minerbe, M., van Hullebusch, E.D., Chaussadent, T.: Behaviour of different cementitious material formulations in sewer networks. *Water Sci. Technol.* **69**, 1502–1508 (2014)
62. Herisson, J., Guéguen-Minerbe, M., van Hullebusch, E.D., Chaussadent, T.: Influence of the binder on the behaviour of mortars exposed to H₂S in sewer networks: a long-term durability study. *Mater. Struct.* **50**, 1–18 (2017)
63. Herisson, J., van Hullebusch, E.D., Moletta-Denat, M., Taquet, P., Chaussadent, T.: Toward an accelerated biodeterioration test to understand the behavior of Portland and calcium aluminate cementitious materials in sewer networks. *Int. Biodeterior. Biodegradation* **84**, 236–243 (2013)
64. House, M., Cheng, L., Banks, K., Weiss, J.: Concrete resistance to sulfuric acid immersion: the influence of testing details and mixture design on performance as it relates to microbially induced corrosion. *Adv. Civil Eng. Mater.* **8**, 20170134 (2019)
65. Hua, X., Wang, X., Hu, X.: Advances in polymer cement concrete: research and application. *J. Qingdao Univ. Technol.* **41**, 8 (2020)
66. Islam, M., Islam, M.: Strength and durability characteristics of concrete made with fly-ash blended cement. *Aust. J. Struct. Eng.* **14**, 303–319 (2013)
67. Javaherdashti, R., Alasvand, K.: An introduction to microbial corrosion—sciencedirect. *Biol. Treat. Microb. Corros.* 25–70 (2019)
68. Jeon, J.-K., Moon, H.-Y., Ann, K.-Y., Kim, H.-S., Kim, Y.-B.: Effect of ground granulated blast furnace slag, pulverized fuel ash, silica fume on sulfuric acid corrosion resistance of cement matrix. *Int. J. Concr. Struct. Mater.* **18**, 97–102 (2006)
69. Jiang, G., Bond, P.L., Sun, X., Yuan, Zhiguo, Keller: A novel and simple treatment for control of sulfide induced sewer concrete corrosion using free nitrous acid. *Water Res. A J. Int. Water Assoc.* (2015)
70. Jiang, G., Sharma, K.R., Guisasaola, A., Keller, J., Yuan, Z.: Sulfur transformation in rising main sewers receiving nitrate dosage. *Water Res.* **43**, 4430–4440 (2009)
71. Jørgensen, B.B., Findlay, A.J., Pellerin, A.: The biogeochemical sulfur cycle of marine sediments. *Front. Microbiol.* **10** (2019)
72. Kaali, P., Pérez-Madrigal, M., Stromberg, E., Aune, R.E., Czel, G., Karlsson, S.: The influence of Ag⁺, Zn²⁺ and Cu²⁺ exchanged zeolite on antimicrobial and long term in vitro stability of medical grade polyether polyurethane (2011)
73. Khademi, A.G., Sar, H.I.K.: Comparison of sulfur concrete, cement concrete and cement-sulfur concrete and their properties and application. *Curr. World Environ.* **10**, 63–68 (2015)
74. Khan, H.A., Castel, A., Khan, M.S.: Corrosion investigation of fly ash based geopolymer mortar in natural sewer environment and sulphuric acid solution. *Corros. Sci.* **168**, 108586 (2020)

75. Khan, H.A., Castel, A., Khan, M.S., Mahmood, A.H.: Durability of calcium aluminate and sulphate resistant Portland cement based mortars in aggressive sewer environment and sulphuric acid. *Cem. Concr. Res.* **124**, 105852 (2019)
76. Kiliswa, M.: Composition and microstructure of concrete mixtures subjected to biogenic acid corrosion and their role in corrosion prediction of concrete outfall sewers. University of Cape Town (2016a)
77. Kiliswa, M.W.: Composition and microstructure of concrete mixtures subjected to biogenic acid corrosion and their role in corrosion prediction of concrete outfall sewers. (2016b)
78. King, D.: The effect of silica fume on the properties of concrete as defined in concrete society report 74, cementitious materials. In: 37th Conference on Our World in Concrete and Structures, Singapore, pp. 29–31 (2012)
79. Kong, X.-M., Wu, C.-C., Zhang, Y.-R., Li, J.-L.: Polymer-modified mortar with a gradient polymer distribution: preparation, permeability, and mechanical behaviour. *Constr. Build. Mater.* **38**, 195–203 (2013)
80. Kou, S.C., Poon, C.S., Chan, D.: Influence of fly ash as cement replacement on the properties of recycled aggregate concrete. *J. Mater. Civ. Eng.* **19**, 709–717 (2007)
81. Küçük, V.A., Uğur, M., Korucu, H., Şimşek, B., Uygunoğlu, T., Kocakerim, M.M.: Chemical resistance of dioctyl terephthalate pozzolanic-cement mortar: comparative study with other waste polymers. *Constr. Build. Mater.* **263**, 120905 (2020)
82. Lawrence, P., Cyr, M., Ringot, E.: Mineral admixtures in mortars: effect of inert materials on short-term hydration. *Cem. Concr. Res.* **33**, 1939–1947 (2003)
83. Lee, D.Y.: Manufacturing methods for sulfur concrete sewer pipe. Final report to U.S. Environmental Protection Agency, National Center for Environmental Research, Washington D.C. (2000)
84. Lee, K.H.: Evaluation of properties of concrete using fluosilicate salts and metal (Ni, W) compounds. *Trans. Nonferrous Metals Soc. China* (2009)
85. Lee, Y.-J., Kim, H.-G., Kim, K.-H.: Effect of ground granulated blast furnace slag replacement ratio on structural performance of precast concrete beams. *Materials* **14**, 7159 (2021)
86. Li, C.P.: The antibacterial experiment study based on durability of concrete. Master Thesis, Ningxia University (2015)
87. Li, G., Xiong, G., Yin, Y.: The physical and chemical effects of long-term sulphuric acid exposure on hybrid modified cement mortar. *Cement Concr. Compos.* **31**, 325–330 (2009)
88. Li, W.: Progress of antibacterial materials. *New Chem. Mater.* (2003)
89. Li, X., Bond, P.L., O'Moore, L., Wilkie, S., Hanzic, L., Johnson, I., Mueller, K., Yuan, Z., Jiang, G.: Increased resistance of nitrite-admixed concrete to microbially induced corrosion in real sewers. *Environ. Sci. Technol.* **54**, 2323–2333 (2020)
90. Liu, W., Tan, H.L., Ni, C.L., Chen, Z.B., Luo, T.Z., Yu, L.: Effect of silica fume and fly ash on compressive strength and weight loss of high strength concrete material in sulfuric and acetic acid attack. *Key Eng. Mater. Trans Tech. Publ.* 301–310 (2017)
91. Makhloufi, Z., Kadri, E., Bouhicha, M., Benaissa, A.: Resistance of limestone mortars with quaternary binders to sulfuric acid solution. *Constr. Build. Mater.* **26**, 497–504 (2012)
92. Malhotra, V.M., Mehta, P.K.: High-performance, high-volume fly ash concrete: materials, mixture proportioning, properties, construction practice, and case histories (2002)
93. Maury-Ramirez, A., de Muynck, W., Stevens, R., Demeestere, K., de Belie, N.: Titanium dioxide based strategies to prevent algal fouling on cementitious materials. *Cement Concr. Compos.* **36**, 93–100 (2013)
94. Modro, N., Modro, N., Oliveira, A.: Evaluation of concrete made of Portland cement containing PET wastes. *Matéria (Rio de Janeiro)* **14**, 725–736 (2009)
95. Mohamed, A.-M.O., El-Dieb, A., Sawy, K.M.E., Gamal, M.M.E.: Durability of modified sulfur concrete in sewerage environment. *Environ. Geotech.* **2**, 95–103 (2015)
96. Mohamed, A.-M.O., El-Gamal, M.: Sulfur concrete for the construction industry: a sustainable development approach. J. Ross Publishing (2010)
97. Mohamed, A.-M.O., el Gamal, M.: Sulfur based hazardous waste solidification. *Environ. Geol.* **53**, 159–175 (2007)

98. Mohamed, A.-M.O., el Gamal, M.: Hydro-mechanical behavior of a newly developed sulfur polymer concrete. *Cement Concr. Compos.* **31**, 186–194 (2009)
99. Monteny, J., Vincke, E., Beeldens, A., de Belie, N., Taerwe, L., van Gemert, D., Verstraete, W.: Chemical, microbiological, and in situ test methods for biogenic sulfuric acid corrosion of concrete. *Cem. Concr. Res.* **30**, 623–634 (2000)
100. Muyzer, G., Stams, A.J.: The ecology and biotechnology of sulphate-reducing bacteria. *Nat. Rev. Microbiol.* **6**, 441–454 (2008)
101. Nampoothiri, K.M., Nair, N.R., John, R.P.: An overview of the recent developments in polylactide (PLA) research. *Biores. Technol.* **101**, 8493–8501 (2010)
102. Navarro, C.A., von Bernath, D., Jerez, C.A.: Heavy metal resistance strategies of acidophilic bacteria and their acquisition: importance for biomining and bioremediation. *Biol. Res.* **46**, 363–371 (2013)
103. Negishi, A., Muraoka, T., Maeda, T., Takeuchi, F., Kanao, T., Kamimura, K., Sugio, T.: Growth inhibition by tungsten in the sulfur-oxidizing bacterium *Acidithiobacillus thiooxidans*. *Biosci. Biotechnol. Biochem.* **69**, 2073–2080 (2005)
104. Noeiaghahi, T., Mukherjee, A., Dhama, N., Chae, S.-R.: Biogenic deterioration of concrete and its mitigation technologies. *Constr. Build. Mater.* **149**, 575–586 (2017)
105. O’Connell, M., McNally, C., Richardson, M.G.: Biochemical attack on concrete in wastewater applications: a state of the art review. *Cement Concr. Compos.* **32**, 479–485 (2010)
106. Okabe, S., Ito, T., Sugita, K., Satoh, H.: Succession of internal sulfur cycles and sulfur-oxidizing bacterial communities in microaerophilic wastewater biofilms. *Appl. Environ. Microbiol.* **71**, 2520–2529 (2005)
107. Okabe, S., Itoh, T., Satoh, H., Watanabe, Y.: Analyses of spatial distributions of sulfate-reducing bacteria and their activity in aerobic wastewater biofilms. *Appl. Environ. Microbiol.* **65**, 5107–5116 (1999)
108. Orell, A., Remonsellez, F., Arancibia, R., Jerez, C.A.: Molecular characterization of copper and cadmium resistance determinants in the biomining thermoacidophilic archaeon *Sulfolobus metallicus*. *Archaea* (2013)
109. Owaid, H.M., Hamid, R.B., Taha, M.R.: A review of sustainable supplementary cementitious materials as an alternative to all-Portland cement mortar and concrete. *Aust. J. Basic Appl. Sci.* **6**, 287–303 (2012)
110. Pacheco-Torgal, F., Jalali, S.: Sulphuric acid resistance of plain, polymer modified, and fly ash cement concretes. *Constr. Build. Mater.* **23**, 3485–3491 (2009)
111. Pather, B., Ekolu, S., Quainoo, H.: Effects of aggregate types on acid corrosion attack upon fly-Ash geopolymer and Portland cement concretes—comparative study. *Constr. Build. Mater.* **313**, 125468 (2021)
112. Pluym-Berkhout, J., Mijnsbergen, J., Polder, R.: Riolerings (II), biogene zwavelzuuraantasting. *Cement* **9**, 16–20 (1989)
113. Pomeroy, R.D.: Calcareous pipe for sewers. *J. Water Pollut. Control Fed.* 1491–1493 (1969)
114. Qiu, L., Dong, S., Ashour, A., Han, B.: Antimicrobial concrete for smart and durable infrastructures: a review. *Constr. Build. Mater.* **260**, 120456 (2020)
115. Rahhal, V., Talero, R.: Early hydration of Portland cement with crystalline mineral additions. *Cem. Concr. Res.* **35**, 1285–1291 (2005)
116. Rahimi, S., Nikbin, I.M., Allahyari, H., Habibi, S.: Sustainable approach for recycling waste tire rubber and polyethylene terephthalate (PET) to produce green concrete with resistance against sulfuric acid attack. *J. Clean. Prod.* **126**, 166–177 (2016)
117. Rozière, E., Loukili, A., el Hachem, R., Grondin, F.: Durability of concrete exposed to leaching and external sulphate attacks. *Cem. Concr. Res.* **39**, 1188–1198 (2009)
118. Sabour, M., Dezvareh, G., Bazzazzadeh, R.: Corrosion prediction using the weight loss model in the sewer pipes made from sulfur and cement concretes and Response Surface Methodology (RSM). *Constr. Build. Mater.* **199**, 40–49 (2019)
119. Sakhakarmi, S.: Cost Comparison of Cement Concrete and Polymer Concrete Manholes in Sewer Systems. University of Nevada, Las Vegas (2017)

120. Sand, W., Dumas, T., Marcdargent, S.: Accelerated biogenic sulfuric-acid corrosion test for evaluating the performance of calcium-aluminate based concrete in sewage applications. In: *Microbiologically Influenced Corrosion Testing*. ASTM International (1994)
121. Santos, M.C., Nunes, C., Saraiva, J.A., Coimbra, M.A.: Chemical and physical methodologies for the replacement/reduction of sulfur dioxide use during winemaking: Review of their potentialities and limitations. *Eur. Food Res. Technol.* **234**, 1–12 (2012)
122. Satoh, H., Odagiri, M., Ito, T., Okabe, S.: Microbial community structures and in situ sulfate-reducing and sulfur-oxidizing activities in biofilms developed on mortar specimens in a corroded sewer system. *Water Res.* **43**, 4729–4739 (2009)
123. Saucier, F., Herisson, J.: Use of calcium aluminate cement in H₂S biogenic environment. In: *Institute of Concrete Technology. Yearbook 2015–2016*, pp. 67–80 (2015a)
124. Saucier, F., Herisson, J.: Use of calcium aluminate cements in H₂S biogenic environment (2015b)
125. Scrivener, K., Belie, N.D.: Bacteriogenic sulfuric acid attack of cementitious materials in sewage systems. In: *Performance of Cement-Based Materials in Aggressive Aqueous Environments*. Springer (2013)
126. Seifan, M., Samani, A.K., Berenjian, A.: Bioconcrete: next generation of self-healing concrete. *Appl. Microbiol. Biotechnol.* **100**, 2591–2602 (2016)
127. Shi, C., Zou, X., Yang, L., Wang, P., Niu, M.: Influence of humidity on the mechanical properties of polymer-modified cement-based repair materials. *Constr. Build. Mater.* **261**, 119928 (2020)
128. Sikora, P., Augustyniak, A., Cendrowski, K., Nawrotek, P., Mijowska, E.: Antimicrobial activity of Al₂O₃, CuO, Fe₃O₄, and ZnO nanoparticles in scope of their further application in cement-based building materials (2018)
129. Sikora, P., Cendrowski, K., Markowska-Szczupak, A., Horszczaruk, E., Mijowska, E.: The effects of silica/titania nanocomposite on the mechanical and bactericidal properties of cement mortars. *Constr. Build. Mater.* **150**, 738–746 (2017)
130. Singh, S., Shukla, A., Brown, R.: Pullout behavior of polypropylene fibers from cementitious matrix. *Cem. Concr. Res.* **34**, 1919–1925 (2004)
131. Singh, V.P., Sandeep, K., Kushwaha, H.S., Powar, S., Vaish, R.: Photocatalytic, hydrophobic and antimicrobial characteristics of ZnO nano needle embedded cement composites. *Constr. Build. Mater.* **158**, 285–294 (2018)
132. Song, Y., Chetty, K., Garbe, U., Wei, J., Bu, H., O'Moore, L., Li, X., Yuan, Z., McCarthy, T., Jiang, G.: A novel granular sludge-based and highly corrosion-resistant bio-concrete in sewers. *Sci. Total Environ.* **791**, 148270 (2021)
133. Sun, X., Jiang, G., Bond, P.L., Keller, J., Yuan, Z.: A novel and simple treatment for control of sulfide induced sewer concrete corrosion using free nitrous acid. *Water Res.* **70**, 279–287 (2015)
134. Thomas, J.E., Carter, R.D., Whidden, J.A.: Pozzolanic composition used in concrete and cementitious mixture for concrete product or structure, comprises non-spec fly ash combined with natural pozzolan. US2019047913-A1 US151622 04 Oct 2018 US10377667-B2 US151622 04 (2018)
135. Tokyay, M.: *Cement and Concrete Mineral Admixtures*. CRC Press (2016)
136. Toufigh, V., Hosseinali, M., Shirkhorshidi, S.M.: Experimental study and constitutive modeling of polymer concrete's behavior in compression. *Constr. Build. Mater.* **112**, 183–190 (2016)
137. Toufigh, V., Toufigh, V., Saadatmanesh, H., Ahmari, S., Kabiri, E.: Behavior of polymer concrete beam/pile confined with CFRP sleeves. *Mech. Adv. Mater. Struct.* **26**, 333–340 (2019)
138. Vincke, E., van Wansele, E., Monteny, J., Beeldens, A., de Belie, N., Taerwe, L., van Gemert, D., Verstraete, W.: Influence of polymer addition on biogenic sulfuric acid attack of concrete. *Int. Biodeterior. Biodegradation* **49**, 283–292 (2002)
139. Vishwakarma, V., Sudha, U., Ramachandran, D., Anandkumar, B., George, R.P., Kumari, K., Preetha, R., Mudali, U.K., Pillai, C.S.: Enhancing antimicrobial properties of fly ash mortars specimens through nanophase modification. *Mater. Today Proc.* **3**, 1389–1397 (2016)

140. Vlahovic, M.M., Martinovic, S.P., Boljanac, T.D., Jovanic, P.B., Volkov-Husovic, T.D.: Durability of sulfur concrete in various aggressive environments. *Constr. Build. Mater.* **25**, 3926–3934 (2011)
141. Vroom, A., Aarsleff, L., Vroom, C.: Sulfur concrete for corrosion-resistant sewer pipe. *ASTM Spec. Tech. Publ.* 11–20 (2000)
142. VROOM, A. H.: Sulfur concrete goes global. *Concr. Int.* **20**, 68–71 (1998)
143. Wang, R., Wang, P.: Function of styrene-acrylic ester copolymer latex in cement mortar. *Mater. Struct.* **43**, 443–451 (2010)
144. Wang, T., Wu, K., Kan, L., Wu, M.: Current understanding on microbiologically induced corrosion of concrete in sewer structures: a review of the evaluation methods and mitigation measures. *Constr. Build. Mater.* **247**, 118539 (2020)
145. Wei, S., Jiang, Z., Liu, H., Zhou, D., Sanchez-Silva, M.: Microbiologically induced deterioration of concrete: a review. *Braz. J. Microbiol.* **44**, 1001–1007 (2013)
146. Won, J.-P., Jang, C.-I., Lee, S.-W., Lee, S.-J., Kim, H.-Y.: Long-term performance of recycled PET fibre-reinforced cement composites. *Constr. Build. Mater.* **24**, 660–665 (2010)
147. Wu, M., Wang, T., Wu, K., Kan, L.: Microbiologically induced corrosion of concrete in sewer structures: a review of the mechanisms and phenomena. *Constr. Build. Mater.* **239**, 117813 (2020)
148. Xiao, J., Wen-Jun, Q.U., Zhu, P.: Research on concrete sulfuric acid resistance with different types of coarse and fine aggregates. *J. Archit. Civil Eng.* (2016)
149. Xiao, J., Xu, Z., Murong, Y., Wang, L., Lei, B., Chu, L., Jiang, H., Qu, W.: Effect of chemical composition of fine aggregate on the frictional behavior of concrete–soil interface under sulfuric acid environment. *Fractal Fractional* **6**, 22 (2021)
150. Xiao, L., Zhou, J.: Formation mechanism and properties of polymer cement concrete composite. *J. Jilin Archit. Civil Eng. Inst.* **3**, 33–41 (2001)
151. Yamanaka, T., Aso, I., Togashi, S., Tanigawa, M., Shoji, K., Watanabe, T., Watanabe, N., Maki, K., Suzuki, H.: Corrosion by bacteria of concrete in sewerage systems and inhibitory effects of formates on their growth. *Water Res.* **36**, 2636–2642 (2002)
152. Yang, C., Lv, X., Tian, X., Wang, Y., Komarneni, S.: An investigation on the use of electrolytic manganese residue as filler in sulfur concrete. *Constr. Build. Mater.* **73**, 305–310 (2014)
153. Yerramala, A., Desai, B.: Influence of fly ash replacement on strength properties of cement mortar. *Int. J. Eng. Sci. Technol.* **4**, 3657–3665 (2012)
154. Yoshida, S., Taguchi, F., Nawa, T., and Watanabe, H.: Sulfuric acid resistance of belite-cased cement concrete mixed with GGBFS. In: *Proceeding of the 6th International Conference on Concrete Under Severe Conditions*. Merida, Mexico (2010)
155. Zang, Z.: Performance characteristics and requirements of production technology of Sulfate resistant cement. *Cem. Eng.* 25–26, 39 (2015)
156. Zhang, M., Chen, J., Lv, Y., Wang, D., Ye, J.: Study on the expansion of concrete under attack of sulfate and sulfate–chloride ions. *Constr. Build. Mater.* **39**, 26–32 (2013)
157. Zhang, W.: The novel inorganic antibacterial agent silver molybdate. *New Chem. Mater.* (2004)
158. Zhang, X.W., Zhang, X.: Present and prospect of microbial corrosion prevention of concrete. *Mater. Prot.* (2005)
159. Zhang, X.W., Zhang, X.: Mechanism and research approach of microbial corrosion of concrete. *J. Build. Mater.* **9**, 52–58 (2006)
160. Zhu, T., Dittrich, M.: Carbonate precipitation through microbial activities in natural environment, and their potential in biotechnology: a review. *Front. Bioeng. Biotechnol.* **4**, 4 (2016)

Corrosion Resistance of Calcium Aluminate Cements in Sewer Environments



Neven Ukrainczyk and Cyrill Grengg

Abstract This chapter provides a compact overview of the durability of calcium aluminate cements (CAC) in comparison to Portland cements (PC) in the context of (bio)chemically aggressive sewers. Special focus is on the CAC dissolution—precipitation reactions of alumina phases during acid attack and corresponding overall material response. Furthermore, the H₂S adsorption behaviour and the impact of high Al³⁺ content on microbial growth is discussed.

1 CAC Classification and Uses

Calcium aluminate cements (CAC), also termed high-alumina cements, are cements based on limestone and (low-silica) bauxite. The main mineral in CAC is mono-calcium aluminate CA (CaO·Al₂O₃, where Al is substituted up to ~ 5% with Fe as a solid solution). Some other minerals are gehlenite C₂AS (2CaO·Al₂O₃·SiO₂), mayenite C₁₂A₇ (12CaO · 7Al₂O₃), ferrite phase (with variable iron content: C₄AF·C₆AF₂), di-calcium aluminate CA₂ (2CaO · Al₂O₃), β-C₂S, pleochroite, perovskite, etc. Several commercial CAC classes are available, typically separated by the aluminate and iron content. The (very) high aluminate content CACs are relevant for refractory industry, and not used for sewer applications due to higher costs. Differences in raw materials, hydration and properties of CACs are detailed by Pöllmann [26], Scrivener [31] and Robson [29].

Most common usage of CACs as a construction material for wastewater infrastructure is twofold: (1) in pre-cast industry to coat PC-based concrete (or even steel) elements such as pipes or other, e.g. manhole structures or (2) to repair existing bio-deteriorated wastewater systems [29, 34]. Less common is to manufacture a full

N. Ukrainczyk (✉)

Institute of Construction and Building Materials, Technische Universität Darmstadt,
Franziska-Braun-Straße 3, 64287 Darmstadt, Germany
e-mail: ukrainczyk@wib.tu-darmstadt.de

C. Grengg

Institute of Applied Geosciences, Graz University of Technology, Rechbauerstraße 12, 8010 Graz,
Austria

structure based on CAC concrete, due to economic reasons, as CAC is typically 3–5 times more expensive than Portland Cement (PC). Nevertheless, full CAC concrete pipes were installed in Australia 1950 [31, 34].

2 Durability of CAC Versus PC in (Bio) Corrosive Sewer Environments

Calcium aluminate cements (CACs) are a well-used, initially costlier alternative to Portland-based cements that pays off when durability (to sulfates and sewer conditions) is to be considered. CACs have repeatedly been demonstrated to perform significantly better in field sewer environments, as well as in accelerated lab tests. Reported on-site corrosion rates vary significantly depending on the type of binder material, aggregates and environmental conditions (Table 1) [2, 6, 7, 10, 14, 17, 23–25, 28, 30, 32, 33, 40, 41, 43], and for CACs the biodegradation rates (R_{CAC}) are found to range from 0.4 to 5.4 mm/year whereas for PC (R_{PC}) based cements they range from 0.8 to 11.2 mm/year. The improved durability of CAC over PC is shown in Table 1, calculated individually from each reference, namely as the ratio of the (bio)degradation rates R_{PC}/R_{CAC} . For on-site and lab tests, the R_{PC}/R_{CAC} improvement factors range from 1.1 to 5.17 and 1.1 to 10.3, respectively. The exception of worse performance of the CAC than PC reference ($R_{PC}/R_{CAC} = 0.27$), reported by Ding et al. [7] could be attributed to the unknown mix design parameters used in commercial prebagged CAC dry mortar. From individual studies following major findings could be summarized. Kiliswa and Alexander [20] and Kiliswa et al. [22] highlighted the importance of the aggregate type, silicious vs. carbonaceous, demonstrated by on-site corrosion rates for PC of > 7.5 versus 3.1, respectively, while for CAC the rates are 1.9 versus 0.6, respectively. Wack et al. [42] and Herisson et al. [19] demonstrated the improved durability by use of CAC clinker instead of sand aggregates (Table 1). Kiliswa et al. [22] quantified the positive effect of increased PC or CAC binder content ($a/c = 5.25$ and 3.35 in Table 1) to reduce the corrosion rates. Buvignier et al. [3] compared the durability of CAC with PC and 70% slag PC, resulting in a corrosion rate (R_{PC}/R_{CAC}) improvement factors of 2.13 and 1.88, respectively, due to the beneficial effect of slag in PC blend.

Examples of excellent performance of CAC coatings (typically 25 mm thick) in real life applications on PC-based concretes are projects in Durban of South Africa [34] and Malaysia [31]. The better performance of CAC-based compared to PC based mortars and concretes is primarily explained by the different chemistry, mineralogy and microstructure of the cement pastes. These results in different (pH dependent) pore-filling and acid neutralization capacity, both mainly attributed to secondary precipitation and dissolution of alumina gel, discussed in following sub-sections. Moreover, the biofilm-material interaction should also be put in focus [12, 27], discussed later in separate sub-sections.

Table 1 Reported CAC corrosion rates based on various testing conditions: on-site or (accelerated) lab experiments [2, 6, 7, 10, 14, 17, 23–25, 28, 30, 32, 33, 40, 41, 43]

Reference (1st author and year)	Type	Aggregate	a/c	w/c	H ₂ S, ppm (or S _{equi})	T °C	R.H	Method (acceleration factor)	Biodeg. rate R _{CAC} , mm/year	R _{PC} /R _{CAC}	Portland cement type
Lors17 [23]	M	Si	3	0.5	(11.4 mol/m ²)	30		Lab (PC; 2.37, CAC; 1.78)	1.4*	2	I
Lors18 [24]	M	Si	3	0.5	5	–	–	On-site	0.7–1.0	1.1–1.3	I
Khan19 [19]	M	CAC (Si for PC)	2	0.4	0–880	14–34	0.78–1	On-site	2.25	2.11	V
Kiliswa19 [22]	C	carb	5.25 3.35	0.33	10–40	12–16	–	On-site	0.60 0.35	4.49 1.87	I
Kiliswa14 [20]	C	Si carb	–	–	40–75	27–35		On-site	1.9 0.6	> 3.95 5.17	
Greng20 [12]	M(C-PC)	Si (carb. PC)	3	0.45	65(– 722)	2.5–22.5	0.69–1	On-site	5.4	2.08	V
Aboule18 [2]	M	Si	3	0.5				Lab (BAC-test)	3.5	1.1	50% slag
Buvigni19 [3]	Pastes	None	0	0.3 (0.4 PC)	(S ~ 5.81 mol/m ² /d)			Lab (up to 3.1)	2.19	2.13 1.88	White PC 70% slag
Ding17 [7]	Prebagged	–	–	–	150	30	> 0.99	Lab (up to 5.3)	3.71	0.27	I
Herisson18 [19]	M	Si CAC	2.35	0.4		30	1	Lab (PC < 20.6 CAC < 6.6)	4.6 3.0	3.59 5.5	I

(continued)

Table 1 (continued)

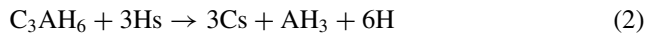
Reference (1st author and year)	Type	Aggregate	a/c	w/c	H ₂ S, ppm (or S _{equi})	T °C	R.H	Method (acceleration factor)	Biodeg. rate R _{CAC} , mm/year	R _{pc} /R _{CAC}	Portland cement type
Peyre15a [27]	M lining	Si			(1–6 mmol/L)	20		Lab (CAC < 0.8)	0.55	4.35	III
Peyre15b [28]	M	Si			(5 mmol/L)	20		Lab (CAC < 0.7)	0.49	4.65	Slag
Wack18 [42]	M	Si CAC				30		Lab (PC:8–12)	3.1 1.4	4.65 10.3	I

M mortar; *C* concrete; *Si* silicious; carb. Carbonaceous; *CAC* calcium aluminate cement; c-binder; a-aggregate

*Ficks law extrapolation

2.1 Precipitation-Dissolution Reactions (and Alumina Gel)

Both the initial CAC hydration and later concrete/mortar interactions with harsh sewer environments fundamentally rely on reaction-transport mechanisms taking place within the material's porous microstructure. Such chemical changes are driven by a reaction thermodynamic potential, while kinetic rates of the main reaction mechanisms tell us how fast the microstructure is changing. The main (stable) hydration products in CAC hardened pastes are hydrogarnet (C_3AH_6) and gibbsite (AH_3 or alumina gel). Monocarbonate (C_3ACcH_{11} , where c denotes CO_2) and Stratlingite (C_2ASH_8) may also form in case of significant amounts of CO_2 (e.g. calcite, Goergens and Goetz-Neunhoeffer [13]) and silica [5], respectively are blended with CACs (Valix SP2 Report on SCMs). In simplified form, considering only C_3AH_6 and AH_3 , the neutralization reaction of the attacking (biogenic) sulfuric acid (H_2SO_4 , or H_s shortened in cement chemistry notation) can be expressed with reaction Eqs. 1–3.



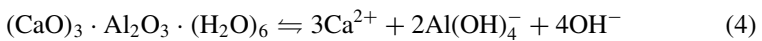
At pH below (3–4), alumina gel neutralization reaction (1) produces alunogenite ($Al_2(SO_4)_3 = As_3$) crystals. At higher sulfuric acid (H_s) concentrations, corresponding to the outer zones closer (or in) biofilm, C_3AH_6 transforms into $CaSO_4$ (Cs) and additional alumina gel (2), while in more inner zones (lower H_s concentrations) sulfates crystallize to gypsum (CsH_2) and ettringite ($C_3A \cdot 3Cs \cdot H_{32}$) according to Eq. 3. Although stratlingite (C_2ASH_8) is a more stable, i.e. a less soluble phase than C_3AH_6 , it has a lower neutralization capacity [3, 18]. In iron rich CACs, $C_2(AF)H_8$ is favorably formed over C_2AH_8 , which together with stratlingite exhibit greater resistance to sewer corrosion than C_3AH_6 (Valix SP2 Report on Reactions of CAC, Part 2).

The biodegradation process of CAC materials may also be related to the process of conversion of the metastable (CAH_{10} and C_2AH_8 , not considered in Eq. 1–3) into stable aluminate hydrates (C_3AH_6 and AH_3). The conversion process is accelerated by temperature and humidity [35–39]. A full conversion was reported to lower the biodeterioration resistance (by a factor from 1 to 1/4) (Valix SP2 Report on SCMs). However, the effect of conversion depends highly on the mix designs, primarily on the water to cement ratio, i.e. porosity of the binder matrix material. For the same reason increasing the content of silicates in CAC, especially when adding pozzolans, must be carefully proportioned to benefit in precipitation of stable stratlingite while minimizing the porosity and conversion effects. Lowering the water to cement mass ratio below a critical value of 0.4 is a promising way to minimize the well-known deleterious effect of the conversion reactions on porosity, and thus durability. To

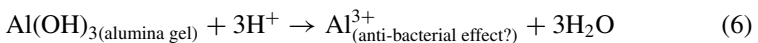
achieve this, while maintaining good workability (i.e. fresh rheological) properties, a superplasticizer polymer may be ad-mixed. To avoid side-effects like segregation and CAC hydration reaction retardation, a combined usage of polycarboxylate ether-based superplasticizer with methyl cellulose and lithium carbonate showed promising rheological/mechanical properties for CAC-based materials [39].

Concomitant to acid attack, another important degradation mechanism is sulfate attack. Namely, the ingress of sulfates through the pore solution of the cement matrix and chemical reactions with solid phases induces precipitation of sulfate-based phases, mostly as gypsum and ettringite (Eqs. 2 and 3) [12]. Crystallization of ettringite (Eq. 3) is expected to be more destructive than that of gypsum, due to higher swelling, i.e. lower density of the secondary crystals (1.77 vs. 2.32 g/cm³). Kiliswa et al. [21] studied the durability of calcium aluminate cement (CAC) compared to (sulfate resistant) Portland cement mortar in natural wastewater treatment plant environment. After 12 and 24 months of field exposure, microstructural analyses revealed that crack inducing precipitation of gypsum was the major reason behind the deterioration for both PC and CAC types of binders, though much less pronounced for CAC.

During (biogenic) acid attack the pH of the pore solution decreases, increasing the solubility equilibrium concentrations of calcium and aluminum ions in the cement paste matrix, according to Le Chatelier's principle of equilibrium law. For example, the solubility of hydrogarnet (C₃AH₆) in equilibrium reaction (Eq. 4) is thermodynamically defined by a solubility product ($K_{sp} = a_{Ca^{2+}}^3 a_{Al(OH)_4^-}^2 a_{OH^-}^4$, for simplicity activity a can be viewed as concentration in diluted case) having a strictly constant value, namely $K_{sp} = 3.2 \times 10^{-21}$ [11]. However, the ingress of H⁺ ions removes OH⁻ from the equilibrium (Eq. 4) by forming water molecule with an equilibrium (water auto-protolysis) reaction Eq. 5 ($K_w = 10^{-14}$). Thus, in order to maintain the constant value of K_{sp} , more C₃AH₆ has to dissolve in order to increase the equilibrium concentrations of calcium and aluminum ions in solution.



Moreover, the reactive-transport mechanism involved in the diffusion and dissolution-precipitation reaction (Eq. 2) due to acid attack on the CAC porous hardened paste matrix seems to be the key for the improved performance. Herisson et al. [15] suggested that alumina gel and calcite secondary precipitations (interactions with atmospheric CO₂) fill the pores of the CAC matrix. Namely, both precipitates remain stable to buffer the pH in a range between 4 and 10, thus dissolving only when the pore solution pH decreased further (below pH 4) due to the continuous ingress of acid and depletion of AH₃ (Eq. 6).



This is a key contrast to the PC matrix where the cement hydrates [mainly Portlandite ($\text{Ca}(\text{OH})_2$) and C–S–H] are entirely dissolved during initial reactions ($\text{pH} < 10$). In other words, although CACs have a lower total neutralization capacity (than PC), the secondarily precipitated alumina gel fills in (i.e. blocks) the pores, enabling a protective barrier. At lower pH values (around 4) the dissolution of alumina gel buffers the pH resulting in higher neutralization capacity at that pH range [3, 15, 22].

Rapid dissolution of cement hydration products leads to a severe degradation of the materials properties, driven by intricate mechanisms of coupled reactive transport through porous concrete. As this degradation process proceeds, the thickness of the affected layer and hence its protective performance increases, shifting the dissolution reaction to a diffusion-controlled mechanism. The degradation process of CAC mortar and concrete is typically described by different zones (qualitatively similar to PC-based case), which move into the undamaged material with time [8]. The first, most degraded zone, is a zone of erosion, in which the bigger insoluble aggregates are left protruding outwards, having a pH of the pore solution close to the biofilm. The solubility and the grain shape of aggregates have a great influence on the depth of degradation [1]. In a 2nd zone a porous degraded layer of low mechanical strength contains (a) calcium sulfate salts (gypsum, anhydrite CaSO_4 , and possibly the hemihydrate bassanite: $\text{CaSO}_4 \cdot 0.5\text{H}_2\text{O}$, depending on the activity of the water in the solution), (b) amorphous ferric (pH 1–2) and/or silica hydroxides (in iron and/or silica rich CACs) and (c) alumina hydroxide gel which buffers a pH of the pore solution to a value around 3–4. Third zone is a transition zone, being a mechanically sound region due to remaining C_3AH_6 and AH_3 , where the pH is increasing until reaching the value of the undamaged core material.

Recent studies [3, 12, 21, 22], e.g. using elemental maps, confirmed the dissolution of the alumina microstructure within the low pH decomposition layers at low rates (with time). In turn, significant amounts of amorphous alumina and silica gel phases were observed to form within the decomposition layers. Secondary precipitation of alumina gel thus effectively reduced the open porosity and preserved the cohesion of the CAC material, resulting in lower acid diffusion rates. An example of the different dissolution behavior of an OPC and CAC mortar after 18 months exposure within a sewer system strongly affected by MICC is shown in Fig. 1.

2.2 H_2S Affinity

Gaseous $\text{H}_2\text{S}_{(\text{g})}$ released in headspaces of a sewer absorbs into moisture films and water filled porosity on the concrete surfaces above the waterline in sewer systems. Absorbed H_2S chemically reacts by a number of abiotic and biotic reactions, leading to the generation of sulfuric acid and ultimately corrosion of the concrete. CAC-based concrete surface has a lower affinity to H_2S gas than PC-based one (proposed by Herisson et al. [15, 16]), exhibiting less deposition of elemental sulfur (S^0) on the CAC matrix and thus less formation of biogenic acids through the oxidization of

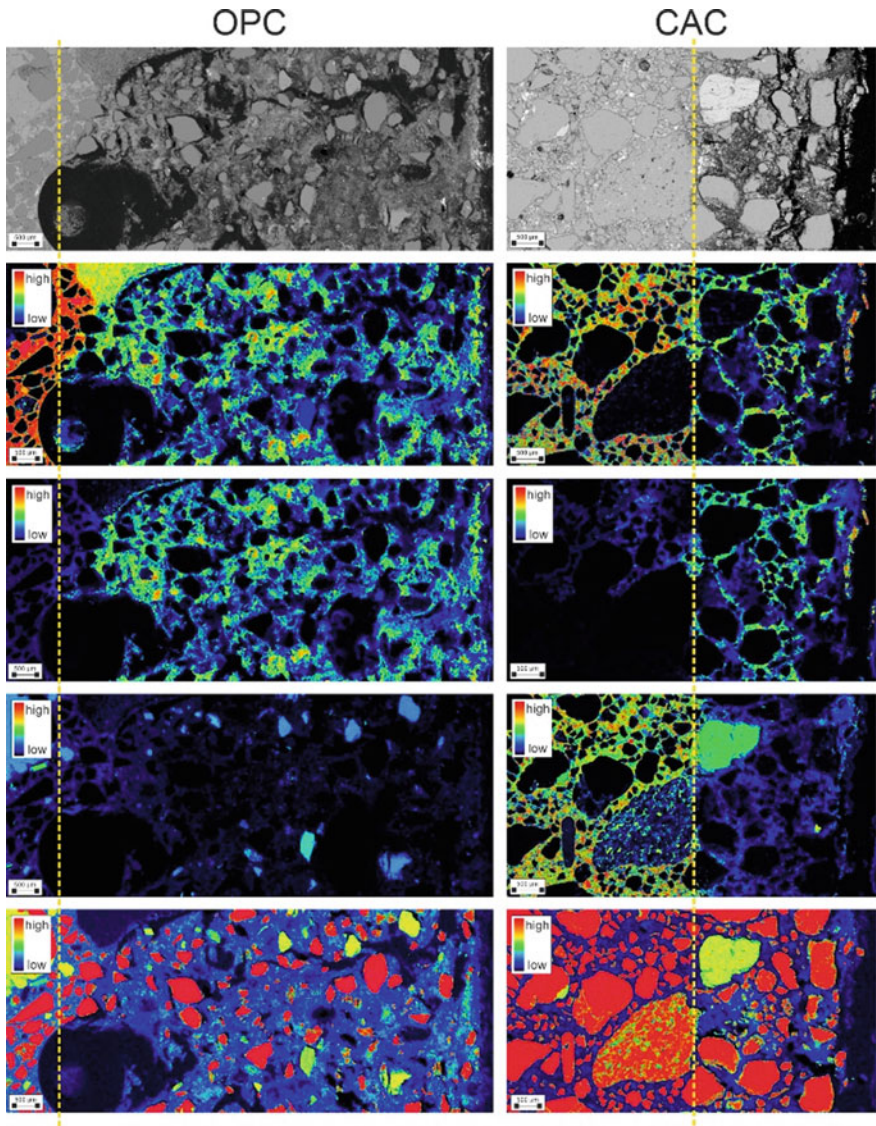


Fig. 1 BSE images of cross sections throughout the deteriorated layers of an OPC and CAC mortar, together with the elemental distribution of Ca, S, Al and Si within the same areas. The transition between the corroded and intact microstructure is marked with the yellow dotted line (data adopted from [12]. Reproduced with permission from Elsevier

sulfur compounds. Here it should be noted that the abiotic reactions of H_2S (intermediate) oxidation with the cement-based matrix may produce several sulfur compounds with different degrees of oxidation, e.g. beside S^0 also thiosulfate. [15] argued the different CAC binder chemistry (compared to PC) results in a different H_2S oxidation/deposition behavior which in turn plays a major role in the overall biodegradation processes. This was explained by a catalyst-based reaction, where the H_2S oxidation into elemental sulfur is kinetically assisted by Ca^{2+} and Fe^{x+} metallic cations. Thus Cu, Zn, and other metallic cations, which are interesting from their retardation effects on biofilm activity, could play also a second role on (accelerating) sulfur deposition. More research is needed in this direction. The presence of iron may also affect the development of some acidophilic bacteria [3].

2.3 Biofilm Affinity

Some studies have highlighted a bacteriostatic effect of Al^{3+} [15, 18] on biofilm activity, a still hypothetical mechanism whose chemical origin can also be attributed to the alumina gel dissolution reaction (Eq. 6). However, the bacteriostatic effect of Al^{3+} on the growth of relevant acid producing (acidophilic sulfur-oxidizing) bacteria has not yet been confirmed [3, 4].

The biofilm observed on CAC materials after up to 18 months of in situ exposure [12] consisted almost exclusively of relevant acid-producing (acidophilic sulfur-oxidizing) bacteria that spread over the entire depth of degradation. In addition, the biofilm had by far the lowest species diversity compared to the Portland cement and geopolymer materials tested. This suggests that although Al^{3+} has no clear conclusions for acidophilic sulfur-oxidizing bacteria, it may inhibit the growth of symbiotic microorganisms such as heterotrophic organisms and fungi, which could have long-term effects on the mechanisms of biogenic metabolism.

Harrison et al. [18] also reported that microbial diversity varies with binder types (PC, slag, CAC) and with exposure time, as mortar/concrete surface chemistry interacts with microbial colonization. In their study, the existing results on the possible mechanism of aluminum on the microorganisms involved in the biodegradation process were summarized. The following points are worth highlighting here, while readers are referred to [18] and the citations therein for more details. Different threshold concentrations (50–250 mg/L) of Al^{3+} ions are required to trigger a decline in activity in different species of *Thiobacillus* bacteria. The growth kinetics (and metabolic activity) of the species *A. thiooxidans* was slowed down (using 56–112 mg/L Al^{3+}), but not inhibited completely. However, similar retardation effects were also attributed to the simultaneous increase in ionic strength of the different test solutions without Al^{3+} , e.g. using only Na, K-based salts. Buvignier et al. [4] also demonstrated more recently that total dissolved-aluminum concentrations (up to 2698 mg/L) were not inhibitory, but more likely that the cell growth is (slightly) influenced by ionic strength.

In conclusion, the improved CAC resistance over PC binders should thus mainly be linked to the intrinsic chemistry driven reactive-transport process, as also suggested by recent findings [3, 12, 21, 22]. This means that dissolution of cement hydration phases initially present or secondarily precipitated during the acid attack process (detailed in the previous sub-section) plays a much more dominant role over biofilm affinity when explaining the impact of a binder type.

2.4 CAC Clinker Aggregates

Ehrich et al. [9], and later Alexander and Fourie [1] have demonstrated that CAC based concretes or mortars comprising merely crushed CAC clinker aggregates perform better in sewers than with either sand or calcareous aggregates. Saucier and Herisson [34] hypothesized that this could be explained by bacteriostatic effect, due to similarity (compatibility) in materials surface chemistry that interacts with biofilm, which is similar for the aggregates and the binder matrix. In case of conventional ‘inert’ sand, its surface is more favorable for producing sulfuric acid without being slowed down by the bacteriostatic Al^{3+} .

3 Summary

To date, CAC materials are the most effective commercially available inorganic binder type to be used in (bio)chemically aggressive sewers. Their increased performance in (bio)acid environments is mainly correlated to higher intrinsic acid resistance of the CAC microstructure, lower porosity due to the formation of alumina gel under acid attack, higher acid buffer capacity at low (3–4) pH and lower affinity of H_2S surface adsorption. Furthermore, bacteriostatic effects of Al^{3+} may also impact the activity of microbes and corresponding biogenic acid production rates.

Author Contribution N. Ukrainczyk: Conceptualization, Investigation, Formal analysis, Writing—original draft, Writing—review and editing. C. Grenng: Writing—review and editing.

References

1. Alexander, M., Fourie, C.: Performance of sewer pipe concrete mixtures with portland and calcium aluminate cements subject to mineral and biogenic acid attack. *Mater. Struct.* **44**, 313–330 (2011)
2. Aboulela, A., Peyre-Lavigne, M., Patapy, C., Bertron, A., Alexander, M., Beushausen, H., Dehn, F., Moyo, P.: Evaluation of the resistance of CAC and BFSC mortars to biodegradation: laboratory test approach. In: *MATEC Web Conference*, vol. 199, p. 02004 (2018)

3. Buvignier, A., Patapy, C., Lavigne, M.P., Paul, E., Bertron, A.: Resistance to biodeterioration of aluminium-rich binders in sewer network environment: study of the possible bacteriostatic effect and role of phase reactivity. *Cem. Concr. Res.* **123**, 105785 (2019)
4. Buvignier, A., Peyre-Lavigne, M., Robin, O., Bounouba, M., Patapy, C., Bertron, A., Paul, E.: Influence of dissolved-aluminum concentration on sulfur-oxidizing bacterial activity in the biodeterioration of concrete. *Appl. Environ. Microbiol.* **85**, 1–12 (2019)
5. Ding, J., FU, Y., Beaudoin, J.J.: Stratlingite formation in high alumina cement—silica fume systems: significance of sodium ions. *Cem. Concr. Res.* **25**(6), 1311–1319 (1995)
6. De Belie, N., Monteny, J., Beeldens, A., Vincke, E., Van Gemert, D., Verstraete, W.: Experimental research and prediction of the effect of chemical and biogenic sulfuric acid on different types of commercially produced concrete sewer pipes. *Cem. Concr. Res.* **34**, 2223–2236 (2004)
7. Ding, L., Weiss, W.J., Blatchley, E.R.: Effects of concrete composition on resistance to microbially induced corrosion. *J. Environ. Eng.* **143**, 4017014 (2017)
8. Drugă, B., Ukrainczyk, N., Weise, K., Koenders, E., Lackner, S.: Interaction between wastewater microorganisms and geopolymer or cementitious materials: biofilm characterization and deterioration characteristics of mortars. *Int. Biodeterior. Biodegradation* **134**, 58–67 (2018)
9. Ehrich, S., Helard, L., Letourneux, R., Willocq, J., Bock, E.: Biogenic and chemical sulfuric acid corrosion of mortars. *J. Mater. Civ. Eng.* **11**, 340–344 (1999)
10. Geoffroy, V., Bachelet, M., Crovisier, J., Aouad, G., Damidot, D.: Evaluation of aluminium sensitivity on a biodegrading bacteria acidithiobacillus thiooxidans: definition of a specific growth medium. In: Proceedings of the Centenary Conference of Calcium Aluminate Cements, Avignon (France), pp. 309–319 (2008)
11. Grandclerc, A., Gueguen-Minerbe, M., Chaussadent, T.: Accelerated biodeterioration test of cementitious materials in sewer networks. In: Bertron, A., Jonkers, H. (eds.) Proceedings of Final Conference of RILEM TC 253-MC (2018)
12. Grengg, C., Ukrainczyk, N., Koraimann, G., Mueller, B., Dietzel, M., Mittermayr, F.: Long-term in situ performance of geopolymer, calcium aluminate and Portland cement-based materials exposed to microbially induced acid corrosion. *Cem. Concr. Res.* **131**, 106034 (2020)
13. Goergens, J., Goetz-Neunhoeffer, F.: Temperature-dependent late hydration of calcium aluminate cement in a mix with calcite—Potential of G-factor quantification combined with GEMS-predicted phase content. *Cement* **5**, 100011 (2021)
14. Hormann, K., Hofmann, F., Schmidt, M.: Stability of concrete against biogenic sulfuric acid corrosion, a new method for determination. In: Proceedings of the 10th International Congress on the Chemistry of Cement, Gothenburg (1997)
15. Herisson, J., Van Hullebusch, E.D., Moletta-Denat, M., Taquet, P., Chaussadent, T.: Toward an accelerated biodeterioration test to understand the behavior of portland and calcium aluminate cementitious materials in sewer networks. *Int. Biodeterior. Biodegradation* **84**, 236–243 (2013)
16. Herisson J., Van Hullebusch E., Minerbe M.G., Chaussadent, T.: Biogenic corrosion mechanism: study of parameters explaining calcium aluminate cement durability. In: CAC 2014-International Conference on Calcium Aluminates, pp. 633–644 (2014)
17. Herisson, J., Guéguen-Minerbe, M., Van Hullebusch, E., Chaussadent, T.: Behaviour of different cementitious material formulations in sewer networks. *Water Sci. Technol.* **69**, 1502–1508 (2014)
18. Herisson, J., Gueguen-Minerbe, M., Van Hullebusch, E.D., Chaussadent, T.: Influence of the binder on the behaviour of mortars exposed to H₂S in sewer networks: a longterm durability study. *Mater. Struct.* **50**, 8 (2017)
19. Herisson J., Guinot D., Saucier F.: Accelerated biodeterioration of various cementitious materials through an accelerated laboratory chamber. In: Proceedings of Final Conference of RILEM TC 253-MC, (2018)
20. Kiliswa, M.W., Alexander, M.: Biogenic corrosion of concrete sewer pipes: a review of the performance of cementitious materials. In: Conference: XIII DBMC International Conference at Sao Paulo, p. 9 (2014)
21. Khan, H.A., Castel, A., Khan, M.S.H., Mahmood, A.H.: Durability of calcium aluminate and sulphate resistant Portland cement based mortars in aggressive sewer environment and sulphuric acid. *Cem. Concr. Res.* **124**, 105852 (2019)

22. Kiliswa, M.W., Scrivener, K.L., Alexander, M.G.: The corrosion rate and microstructure of Portland cement and calcium aluminate cement-based concrete mixtures in outfall sewers: a comparative study. *Cem. Concr. Res.* **124**, 105818 (2019)
23. Lors, C., Hondjuila Miokono, E., Damidot, D.: Interactions between *Halothiobacillus neapolitanus* and cementitious materials: comparison of the biodeterioration between Portland and calcium aluminate cement mortars. *Int. Biodeterior. Biodegradation* **121**, 19–25 (2017)
24. Lors, C., Aube, J., Guyoneaud, R., Vandembulcke, F., Damidot, D.: Biodeterioration of mortars exposed to sewers in relation to microbial diversity of biofilms formed on the mortars surface. *Int. Biodeterior. Biodegradation* **130**, 23–31 (2018)
25. Miokono, H.: Biodétérioration de mortiers avec une succession de bactéries sulfo-oxydantes neutrophiles et acidophiles, Ph.D. thesis, Université Lille 1, Science Technology (2013)
26. Pollmann, H.: Calcium aluminate cements—raw materials, differences, hydration and properties. *Rev. Mineral. Geochem.* **74**, 1–82 (2012)
27. Peyre, L.M., Bertron, A., Auer, L., Hernandez-Raquet, G., Foussard, J.-N., Escadeillas, G., Cockx, A., Paul, E.: An innovative approach to reproduce the biodeterioration of industrial cementitious products in a sewer environment Part I: test design. *Cem. Concr. Research* **73**, 246–256 (2015)
28. Peyre, L.M., Bertron, A., Patapy, C., Lefebvre, X., Paul, E.: Accelerated test design for biodeterioration of cementitious materials and products in sewer environments. *Mater. Tech.* **103**, 204 (2015)
29. Robson, T.D.: *High-Alumina Cement and Concrete*. Wiley (1962)
30. Sand, W., Dumas, T., Marcargent, S.: Accelerated biogenic sulfuric-acid corrosion test for evaluating the performance of calcium-aluminate based concrete in sewage applications. In: *Microbiologically Influenced Corrosion Testing*, vol. 1232, pp. 234–234. ASTM International (1994)
31. Scrivener, K.L., Capmas, A.: *Calcium Aluminate Cements*, 4th edn, pp. 713–782. Elsevier Science & Technology (1998)
32. Saricimen, H., Shameem, M., Barry, M., Ibrahim, M., Abbasi, T.: Durability of proprietary cementitious materials for use in wastewater transport systems. *Cem. Concr. Compos.* **25**, 421–427 (2003)
33. Scrivener, K., De Belie, N.: Bacteriogenic sulfuric acid attack of cementitious materials in sewage systems. In: *RILEM State of the Art Report—Performance of Cement-Based Materials in Aggressive Aqueous Environments*, Springer, 2013, pp. 305–318
34. Saucier, F., Herisson, J.: Use of calcium aluminate cement in H₂S biogenic environment. In: *Institute of Concrete Technology, Yearbook 2015–2016*, 2015, pp. 67–80
35. Strauss Rambo, D.A., Ukrainczyk, N., de Andrade Silva, F., Koenders, E., Toledo Filho, R.D., da Fonseca Martins Gomes, O.: Calcium-aluminate mortars at high temperatures: overcoming adverse conversion effects using clinker aggregates, *Cem. Concr. Compos.* **96**, 212–224 (2019)
36. Ukrainczyk, N., Matusinović, T.: Thermal properties of hydrating calcium aluminate cement pastes. *Cem. Concr. Res.* **40**, 128 (2010)
37. Ukrainczyk, N.: Kinetic modeling of calcium aluminate cement hydration. *Chem. Eng. Sci.* **65**, 5605–5614 (2010)
38. Ukrainczyk, N., Rogina, A.: Styrene-Butadiene latex modified calcium aluminate cement mortar. *Cement Concr. Compos.* **41**, 16–23 (2013)
39. Ukrainczyk, N.: Effect of polycarboxylate superplasticiser on properties of calcium aluminate cement mortar. *Adv. Cem. Res.* **27**(7), 388–398 (2015)
40. Valix, M.: SP2 Report on reactions of CAC in the field hydration, conversion, carbonation and corrosion Part 2: XRD and SEM/EBSD analysis. <https://water360.com.au/wp-content/uploads/2022/02/SP2-Report-5-Reactions-of-CAC-in-the-Field-Part-2.pdf>
41. Valix, M.: SP2 Report on use of supplementary Cementitious materials (Pozzolan) in arresting the conversion of CAC and its effect on CAC corrosion based on accelerated corrosion tests. <https://water360.com.au/wp-content/uploads/2022/02/SP2-Report-5-Effect-of-Pozzolan-on-CAC-Conversion-and-Corrosion.pdf>

42. Wack, H., Gehrke, T., Sand, W., Pape, F., Hintemann, D., Brill, F., Deckret, S.: Accelerated testing of materials under the influence of biogenic sulphuric acid corrosion (BSA). In: Proceedings of Final Conference of RILEM TC 253-MC (2018)
43. Xie, Y., Lin, X., Ji, T., Liang, Y., Pan, W.: Comparison of corrosion resistance mechanism between ordinary Portland concrete and alkali-activated concrete subjected to biogenic sulfuric acid attack. *Constr. Build. Mater.* **228**, 117071 (2019)

Alkali-Activated Materials for Sewers



Cyrill Grengg, Gregor J. G. Gluth, and Florian Mittermayr

Abstract This chapter aims to give a brief introduction into the field of alkali activated materials (AAM) and their physicochemical material behavior when exposed to sulfuric acid and in biochemically aggressive sewer environments. Additionally, the differences in material behavior within chemical (abiotic) and microbially induced acid environments are highlighted. Finally, existing data on overall performance of AAM, compared to conventional concrete-based building materials in sewer systems will be discussed.

1 AAM Classification and Synthesis

Alkali-activated materials (AAM), also often referred to as geopolymer materials (GP; for simplification reasons hence, the term AAM will be used) in the literature [46], represent a promising alternative to conventional ordinary Portland cement (OPC)-based construction materials due to generally higher durability in (bio) chemical aggressive environments, as well as due to lower greenhouse gas emissions during production and associated lower environmental footprint. Generally, the global warming potential of AAMs is estimated to be between 10 and 80% lower compared to OPC, depending on precursors and activators used for the syntheses [31, 40, 43, 63].

A detailed description of the nature of AAM chemistry is not focus of this chapter and the readers are referred to numerous descriptive literatures e.g. [15, 16, 44, 49,

C. Grengg (✉)

Institute of Applied Geosciences, Graz University of Technology, Rechbauerstraße 12, 8010 Graz, Austria

e-mail: cyrill.grengg@tugraz.at

G. J. G. Gluth

Division 7.4 Technology of Construction Materials, Bundesanstalt für Materialforschung und -prüfung (BAM), Unter den Eichen 87, 12205 Berlin, Germany

F. Mittermayr

Institute of Technology and Testing of Building Materials, Graz University of Technology, Inffeldgasse 24, 8010 Graz, Austria

© The Author(s), under exclusive license to Springer Nature Switzerland AG 2023

233

G. Jiang (ed.), *Microbiologically Influenced Corrosion of Concrete Sewers*, Engineering Materials, https://doi.org/10.1007/978-3-031-29941-4_11

51]. In the following, central aspects, relevant to decipher the material behavior of AAMs in (bio) chemical aggressive environments, will be elucidated.

In the most general description, AAM consist of two main components—a precursor and an alkaline activator. Due to very few requirements for precursors suitability (and lacking standardizations), there are many kinds of source materials potentially applicable to be used, such as metakaolin [14], kaolin [8], calcined clays [47], fly ashes [52], various slags [1], red muds [7], volcanic ashes [19], different types of mineral and glass wools [5], and others. Frequently used activators comprise sodium and potassium hydroxide (NaOH, KOH) or different types of waterglass (K/Na silicates). Alkali activation (geopolymerization) takes place in three steps: (i) dissolution of the aluminosilicate precursor via alkaline hydrolysis in an alkaline medium, producing aluminate and silicate species, (ii) solution and supersaturation due to rapid precursor dissolution, triggering aluminosilicate monomers formation and subsequent gel nucleation (binding of Al and Si with O into tetrahedral structure), and (iii) polycondensation, rearrangement and dehydration into the amorphous aluminosilicate network [21, 53], generally referred to as polymeric framework.

Based on the relative concentrations of the cementitious components in the system ($\text{CaO-SiO}_2\text{-Al}_2\text{O}_3\text{-Na}_2\text{O-K}_2\text{O}$), AAMs may be grouped into three main categories:

- (1) High calcium AAMs (e.g. blast furnace slag, BFS, as a precursor), in which calcium silicate hydrate (C-(A)-S-H) gel forms the main structural framework [60]. However, the chain structure of this gel may differ significantly from C-S-H formed in OPC, due to low Ca/Si ratio and coval high Al content [50]. Additionally, layered double hydroxides (LDHs) form, especially in Mg-rich mixtures. High calcium AAMs are defined by Ca/(Si + Al) ratio of approximately 1 [48].
- (2) Low calcium AAMs (metakaolin or fly ash), with sodium/potassium aluminosilicate hydrate [(K/N-A-S-(H))] gel as the main reaction product, whereas H is not a major component of the gel structure (accordingly denoted in parenthesis).
- (3) A combination of the two (hybrid materials), in which co-existing C-(A)-S-H and K/N-A-S-(H) gels are present e.g. in blended slag-fly ash binders [35].

Figure 1 displays a schematic overview of the different process pathways and reaction products during alkali activation for low and high calcium systems.

As seen in Fig. 1 the raw materials choice and mix design centrally control the chemistry and reaction product composition of AAMs. Besides compositional aspects, AAM microstructure and corresponding overall performance (mechanical properties and durability) are furthermore strongly dependent on various factors such as the curing regime, particle size distribution, type and concentration of the activator, etc. [12, 22, 56, 58, 61].

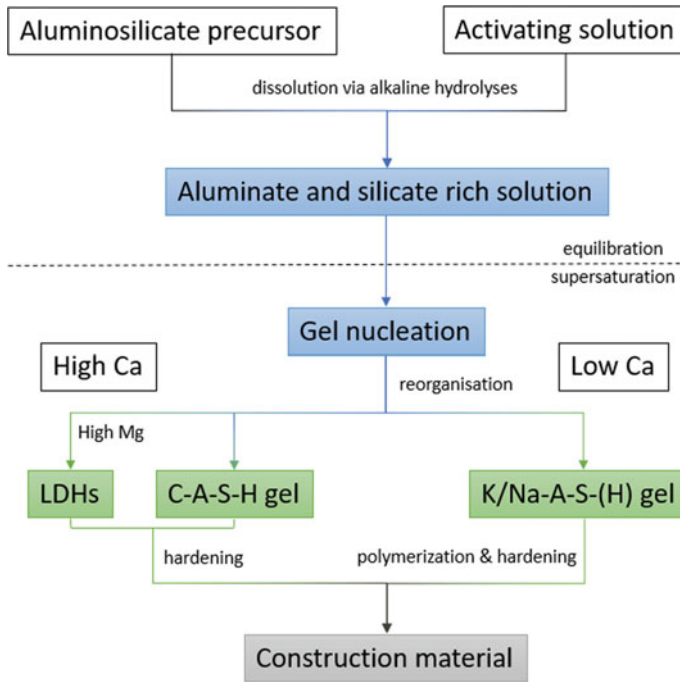


Fig. 1 A simplified conceptual model of the process and reaction products of alkali activation, showing the pathway for low and high calcium (and Mg) containing systems, modified after [21, 48]

2 Application and Durability of AAM in Sewers

Many studies have reported an overall higher durability of well-designed AAMs in acidic environments [6, 24, 38, 57, 59]. Reasons for that are mainly related to the difference in phase assemblages and corresponding higher phase stability under acid attack, as well as due to different physical material properties such as lower permeability. Furthermore, frequently augmented reasons are that in contrast to the acid induced dissolution of Ca-rich phases such as C-S-H, $\text{Ca}(\text{OH})_2$, Aft and AFm [55] in OPC-based systems and corresponding formation of a highly porous corrosion layer, in AAM a coherent layer of aluminosilicate gel may remain even after decalcification, which in combination with newly formed amorphous Si-gel may reduce/hinder further acid ingress [9, 38, 50].

At the same time data on AAM durability in biochemically aggressive sewer environments are scarce. Therefore, in this chapter the overall AAM response to sulfuric acid (H_2SO_4) exposure will be discussed based on mainly (abiotic) chemical laboratory tests setups, followed by an overall durability evaluation of AAM based on in situ exposure and field studies in sewer systems, also recognizing microbial impact.

2.1 (Abiotic) Sulfuric Acid Environments

2.1.1 Chemical AAM Dissolution in Sulfuric Acid

The deterioration of AAMs, when exposed to H_2SO_4 , can be subcategorized in several process steps. Initially, the diffusion of acid into the porous microstructure triggers leaching of the charge balancing, non-framework alkali cations [Na^+ , K^+ , (Ca^{2+})] coinciding with a decalcification of the microstructural framework (for high Ca AAM), resulting in the formation of a leached layer at the acid—material interface [25]. As a result, the pH within the affected layers decreases significantly, destabilizing the polymeric framework and triggering a subsequent dealumination of the aluminosilicate framework by hydrolysis and exchange of Al^{3+} with H_3O^+ . Thereby, the decomposition kinetics strongly depend on the concentration of the sulfuric acid and corresponding prevailing pH conditions, as well as on hydrochemical reactions, such as complexation, within the latter [17, 18]. For instance, dissolved Al ions are known to strongly interact with silicic acids forming dissolved hydroxylalumosilicate colloids (HAS), which strongly retard the depolymerization of polymeric species to monosilicic acid [23, 62] and references therein). Described processes result in a leached layer which is characterized by low Al, Ca and Na/K concentrations and high Si content.

The exact mechanistic dissolution behavior of the aluminosilicate framework under continued H_2SO_4 exposure, e.g. incongruent vs. congruent material dissolution, has remained undefined for decades. Recent studies, focusing on the detailed formation process of the leached layer, strongly argue for a largely congruent dissolution behavior of the polymeric framework which proceeds through the breaking of the Si–O–Si bonds and subsequent precipitation of a secondary Si-gel phase within the last stage of the acid attack. For instance, Sturm et al. [54], described an almost complete transformation of the $\text{Q}^4(m\text{Al})$ species of the binder phase to Q^3 and Q^4 units, using ^{29}Si MAS NMR and ^1H - ^{29}Si CP MAS NMR spectra of silica/sodium aluminate-based AAMs with and without 25% GGBFS addition. This indicates that these units had formed via the precipitation of a silica gel. This conclusion is further supported by Grengg et al. [27], studying metakaolin-based AAMs under H_2SO_4 exposure. Applying a multi-proxy approach including oxygen isotope analyses they observed a strong oxygen isotopic fractionation of up to 13 ‰, which can only be explained by a breakdown of the Si–O–Si bonds and corresponding oxygen exchange with the solution. Furthermore, they observed increased Si concentrations within the leached layer, compared to the initial framework composition, as well as a strong decrease in Si/Al ratios within the solution after an initial equilibration time period, from values similar to the Si/Al ratio of the material, close to zero. These findings clearly indicate an overall congruent material dissolution behaviour and the formation of a secondary Si-gel phase as the final deterioration product.

Described observations coincide with studies on the dissolution behaviour of natural aluminosilicates and glasses in acidic environments, describing a hydrolysis-based breaking of the Si–O–Si bonds as the final step of dissolution, and an overall

congruent dissolution behaviour [32, 33, 42]. Consistently, [25] pointed out the alike material behaviour of manmade AAMs and natural aluminosilicates and glasses in acidic environment, suggesting a stronger consideration of disciplines such as mineralogy and geochemistry to advance the understand of acid resistance of AAMs in the future.

Besides leaching and framework dissolution, the precipitation of secondary minerals plays a crucial role during the acid attack of AAMs. This is especially true for H_2SO_4 environments, where the sulfate ion provides a useful anion to react with particularly Ca and Al. Depending on the composition, in primarily the Ca content, of the exposed AAM, the formation of calcium sulfates (mainly gypsum, but also basanite and anhydrite) and Na/K-alum proceeds. In low-Ca systems also the formation of alunite and syngenite was reported [26], whereas Khan et al. [36] additionally reported the formation of the Na-phases thenardite and natron. Described mineral precipitations are described to occur mainly within the transition zone between the leached layer and the intact AAM matrix, as well as on the surface of the material [3, 4, 26]. A list of frequently reported secondary minerals to form during the progressing sulfuric acid attack in AAMs, associated with an expansive behavior, is presented in Table 1.

Due to the expansive behavior of many of these secondary minerals, they play a central role in respect to the formation of micro and macro cracks and corresponding acid diffusion into the AAM material. In this context, the elemental leaching kinetics and consistent timespan to reach supersaturation of relevant mineral phases within the pore solutions is crucial determining AAM durability. For instance, in the previously described experiments of [26], the saturation state of different sulfate salts with time were calculated based on the chemical evolution of the exposure solution (H_2SO_4 , $pH_{stat} = 2$). The first supersaturation of relevant sulfate salts was already reached within the first 8 h of the experiments. Accordingly, the overall deterioration kinetics of the exposed AAMs were subcategorized in an initial (short) dissolution-controlled phase, followed by a main diffusion—precipitation-controlled phase (Fig. 2).

Table 1 Secondary mineral phases frequently reported to precipitated during sulfuric acid attack of AAMs

Mineral	Chemical formula
Gypsum	$CaSO_4 \cdot 2H_2O$
Basanite	$CaSO_4 \cdot 0.5H_2O$
Anhydrite	$CaSO_4$
Natron	$NaCO_3 \cdot 10H_2O$
Thenardite	Na_2SO_4
Ettringite	$3CaO \cdot Al_2O_3 \cdot 3CaSO_4 \cdot 32H_2O$
Syngenite	$K_2Ca(SO_4)_2 \cdot H_2O$
Sodium alum	$NaAl(SO_4)_2 \cdot 12H_2O$
Potassium alum	$KAl(SO_4)_2 \cdot 12H_2O$
Alunite	$KAl_3(SO_4)_2(OH)_6$
Jurbanite	$AlSO_4(OH) \cdot 5H_2O$

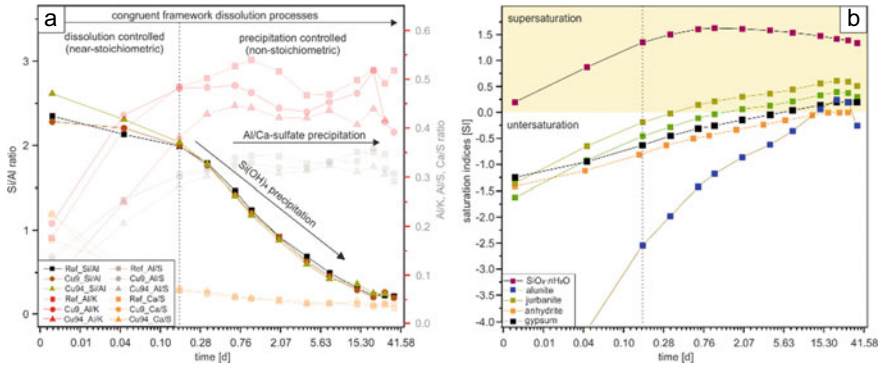


Fig. 2 a Conceptual description of the elemental evolution in a sulfuric acid solution with exposure time and corresponding shift from a dissolution controlled (near-stoichiometric) to a precipitation controlled (non-stoichiometric) process regime. b Corresponding calculated saturation indices (SI) of relevant mineral phases with time (data from [26])

2.1.2 Durability Evaluation of AAM in Sulfuric Acid

Existing literature on the overall performance of AAMs in sulfuric acid environments has been recently summarized by Gluth et al. [25] and is presented in Table 2. Due to the wide range of raw materials used and different experimental setups (pH conditions, solid/liquid ratio, open/closed system etc.) and criteria of evaluation applied, such as weight loss, strength loss, width of leached layer, a general characterization of AAM performance in sulfuric acid is difficult to determine. However, several studies reported significantly higher durability of well-designed AAMs compared to standard OPC materials [2, 11, 36, 41]. As previously described, several physicochemical material properties influence the performance of AAM when exposed to sulfuric acid. Among them are porosity, soluble silica content, Si/Al ratio, alkali content, acid buffer capacity, type of aggregates and water-to-binder ratio (w/b). A detailed emphasis of single parameters on the overall durability is difficult, however several properties are reported to increase AAM durability in sulfuric acid environments [38]:

- Low porosity and corresponding low permeability
- High amount of soluble silicate in the activating solution
- High alkali content
- Low w/b ratio.

2.2 AAM Durability in Biochemically Aggressive Sewers

To date only a limited number of studies exists focusing on the durability of AAM in biochemical aggressive sewer environments. Interestingly, most of them are focusing

Table 2 Studies on the resistance of AAMs against sulfuric acid attack, compared to OPC-based materials (data adopted from [25])

References	AAM starting material(s)	pH	Acid resistance relative to OPC ^b
[11]	GGBFS/fly ash	1.0	++
[41]	Fly ash (class F)	0.6	++
	Fly ash (class C)	0.6	++
	Metakaolin	0.6	+
[10]	GGBFS	3.0	≈
[2]	GGBFS	1.0 ^a	≈ ^c
	GGBFS	0.5 ^a	≈ ^c
	GGBFS	0.3 ^a	≈ ^c
	Fly ash	1.0 ^a	≈
	Fly ash	0.5 ^a	++
	Fly ash	0.3 ^a	++
	[36]	Fly ash/GGBFS	0.8 ^a

^a pH calculated from the given concentration of H₂SO₄
^b Two plus signs (++) indicate that a relevant parameter (thickness of corroded layer, mass loss, or decrease of compressive strength) was > 50% better than for OPC; one plus sign (+) indicates that a relevant parameter was between approx. 25% and 50% better than for OPC; ≈ indicates that the performance of AAM and OPC was similar
^c Dissolution/mass loss for OPC mortar; expansion and cracking for GGBFS-based AAM

on low-Ca, metakaolin/fly ash-based formulations. A summary of existing literature is presented in Table 3.

Table 3 Summary of existing studies of AAM exposure in biochemically aggressive sewer systems

References	Mix design	Duration	Characterization techniques
[37]	fly ash, blast furnace slag, NaOH + Na ₂ SiO ₃	12 months	Corrosion depths, pH, mass change
[30]	Metakaolin, trass, K-waterglass	18 months	pH, mass change, corrosion depth, microbial communities
[36]	fly ash, blast furnace slag, NaOH + Na ₂ SiO ₃	24 months	Corrosion depths, pH, mass change
[27]	Metakaolin, K-waterglass (CuSO ₄ · 5H ₂ O) (ZnO)	20 months	pH, mass change, corrosion depth, microbial communities

2.2.1 AAM Deterioration Process: Biotic Versus Abiotic

The overall deterioration mechanisms of AAM in sewer system overlap largely with the multistage process described for AAMs when exposed to (abiotic) sulfuric acid exposure. This comprises the leaching of alkali ions, the formation of a leached layer and the precipitation of (expansive) secondary minerals. However, the deterioration kinetics may differ greatly due to numerous additional environmental and biological factors contributing to the material degradation and corresponding significantly higher complexity. For instance, Khan et al. [36] observed significant differences in the material response of fly ash-based AAM when exposed to sulfuric acid and within a biochemically aggressive sewer system. Accordingly, they concluded that standard chemical tests are insufficient in estimating the service life of sewage infrastructure. In the following, the major differences in between the exposure environments and corresponding differences in material behaviour are discussed.

Combined Carbonation and Acidification

As described in Chap. 2 the initial stage of microbial induced acid corrosion proceeds via abiotic diffusion and dissolution of CO_2 and H_2S within the pore solutions of the exposed material and corresponding reduction of the surface-near pH [29, 34]. Continued gas penetration triggers, besides the leaching of alkali ions due to the formation of weak acids (thiosulfuric & polythionic acid), the carbonation of the polymeric framework and corresponding formation of carbonates, such as calcite and natron [36, 37]. This, in turn may lead to changes in the microstructure of the AAM, impacting further material response with progressing exposure time.

Microbial Activity and Biogenic Sulfuric Acid Production

The central aspect controlling material performance in biochemically aggressive sewers is the development and activity of acid-producing microorganisms. For instance, Grengg et al. [26, 27] found that the addition of Cu ions, added to enhance bacteriostatic material properties, altered the physicochemical material properties (e.g. increase in porosity), reducing the overall performance when exposed to sulfuric acid (abiotic). However, they observed significantly higher material durability of Cu-doped AAMs when exposed to a real sewer system. Hence, the authors concluded that the bacteriostatic effect of Cu addition overcompensates its negative impact on physicochemical material properties.

In this context, a detailed understanding regarding the microorganisms–AAM interaction is key to understanding material behaviour in the latter. While much research on conventional cement-based material (OPC and CAC) has been conducted in this regard, only very limited data pertaining to the effects of AAMs on the abundance and activity of microorganisms is available [20, 27, 30].

The overall microbial evolution within AAMs corresponds to the ones reported for OPC-based materials. Therein, autotrophic, sulphur oxidizing bacteria (SOBs) dominate the prevailing biofilms in and on AAMs, with a time and pH depending shift from neutrophilic to acidophilic species. The overall biodiversity within the biofilms is reported to decrease with exposure time [27, 30]. An example of dominant

Species	Family	material	OPC		CAC		GP_K1T		GP_K2	
			6	12	9	12	6	12	12	18
<i>Halothiobacillus</i> sp.	<i>Halothiobacillaceae</i>	autotrophs	33.1 %	14.7 %	0.02 %	0.22 %	66.6 %	0 %	0 %	0.07 %
<i>Acidithiobacillus ferrooxidans</i>	<i>Acidithiobacillaceae</i>		0 %	0 %	9.3 %	29.1 %	0.57 %	31.4 %	21.2 %	12.0 %
<i>Acidithiobacillus thiooxidans</i>	<i>Acidithiobacillaceae</i>		0 %	0.12 %	50.6 %	26.7 %	3.4 %	48.9 %	2.2 %	3.8 %
<i>Acidiphilium</i> sp.	<i>Acetobacteraceae</i>		0 %	0 %	31.2 %	34.1 %	2.9 %	1.5 %	0.44 %	0 %
<i>Acidocella</i> sp.	<i>Acetobacteraceae</i>		0.06 %	0.22 %	0.23 %	0.67 %	1.0 %	0.19 %	27.0 %	3.7 %
<i>Corynebacterium variabile</i>	<i>Corynebacteriaceae</i>		0 %	0.08 %	0 %	0.12 %	0 %	0.19 %	13.6 %	0.38 %
<i>Brevundimonas</i> sp.	<i>Caulobacteraceae</i>		18.1 %	5.4 %	0.01 %	0.04 %	1.5 %	0.02 %	0.50 %	0.11 %
<i>Romboutsia</i> sp.	<i>Peptostreptococcaceae</i>		1.3 %	35.8 %	0.69 %	1.8 %	1.9 %	9.3 %	8.3 %	43.2 %
<i>Clostridium</i> sp.	<i>Clostridiaceae 1</i>		0.11 %	16.2 %	0.26 %	0.74 %	0 %	4.3 %	2.2 %	16.4 %
Shannon Index H'			5.48	4.02	1.85	2.44	3.50	2.42	4.14	3.86

Fig. 3 Distribution of dominant bacterial species on the investigated field samples after 6, 12 and 18 months of exposure within a biochemically aggressive sewer system. Only species that were found at a relative abundance of more than 10% in at least one sample, are shown in the heatmap matrix. White: no OTU/ASV present; blue: < 1%; green: 1–5%; yellow: 5–20%; red: > 20%. As an estimation for bacterial alpha-diversity, the Shannon index (H') is given (data from [30])

bacterial species on various metakaolin-based AAMs, compared to an OPC and CAC formulation after different exposure durations within a strongly biochemically aggressive sewer system is presented in Fig. 3.

Besides autotroph species, the occurrence of several heterotrophs, such as *Acidiphilium* sp. and *Acidocella* sp., as well as fungi [13] are reported, especially at later corrosion stages within highly deteriorated AAMs. These heterotrophs are frequently observed in the microbial communities within acidic environments, such as acid mine drainage, where they commonly co-exist with *At. ferrooxidans* [39]. Nevertheless, their exact role on the microbial community structure and corresponding effects on AAMs in sewer environments still remain uncertain.

At early stages of corrosion, the biofilms form at the surface and in large pore voids of the exposed material. With time they expand throughout the pore spaces and cracks of the leached layer, providing in situ sulfuric acid production at and in close vicinity of the transition zone to the intact microstructure. This strongly impacts further material deterioration towards higher dissolution rates and presents one major difference compared to the process mechanisms in abiotic acid environments. An example of a highly evolved biofilm in an AAM with progressing corrosion is presented in Fig. 4.

Cyclic Environmental Changes

In most of the chemical setups for the accelerated testing of cementitious materials in sulfuric environments the experimental parameters, such as acid concentration, temperature, solution/solid ratio, are controlled and stabilized. This is in direct

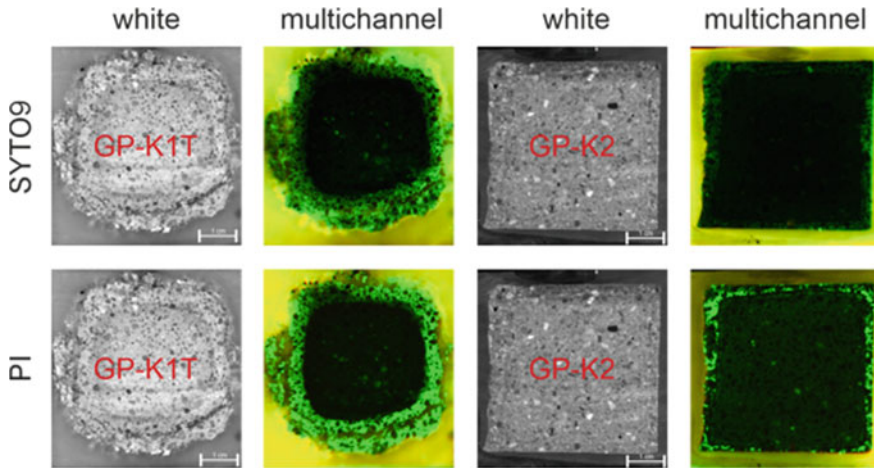


Fig. 4 Multichannel biofilm distribution images of two metakaolin-based AAMs exhibiting different deterioration degrees after 18 months of exposure within a biochemically aggressive sewer system. Fluorescence microscope images were recorded prior to staining (no stain, white) and after staining (multichannel) using two different staining agents (SYTO9 and PI) (data from [30])

contrast to the behaviour of the environmental parameters observed on site, which frequently exhibit continuous, inconstant cyclic variations.

Relevant parameters, such as concentrations of gases [H_2S , CO_2 , (CH_4), (VOC)], temperature and relative humidity, strongly change in dependency of climatic changes due to day/night, seasonal and annual variations, weather changes and operational and network specific reasons (e.g. pumping rates, retention times, flow rates and turbulences). This, on the one hand strongly impacts the microbial activity and corresponding biogenic acid production, and on the other hand the overall mineralogical and hydrochemical kinetics of the exposed material.

For instance, variation in relative humidity and corresponding degree of water saturation within the pore spaces, impacts the diffusion kinetics of deleterious gases and acids, as well as the leaching of species out of the material [45].

Furthermore, described variations have a strong impact on the saturation state of the pore solutions in respect to (expansive) secondary mineral precipitation and subsequent micro and macro crack formation. Overall higher cyclic changes in relative humidity and temperature, e.g. in sewer manholes due to day/night periods, and resulting in cyclic supersaturation of secondary mineral phases are which are reported to significantly increase the deterioration kinetics of AAM materials and cementitious materials [28, 30].

2.2.2 Durability Evaluation of AAM in Sewers

As described, only a few studies exist on the durability evaluation of AAM in biochemically sewers describing limited types of AAMs [27, 30, 36, 37]. Accordingly, currently a general conclusion in this regard cannot be made, and further research is needed on that topic.

However, existing data describe that AAMs with a low calcium content showed good to excellent resistance against biogenic induced acid corrosion in sewer environments [30, 36, 37]. This is particularly interesting since sometimes opposing findings were described for AAMs when exposed to abiotic acids [38].

Finally, of two metakaolin-based AAMs, the one with a lower water content and made from the metakaolin with a higher SiO₂ content (mainly due to a higher quartz content) performed better in a sewer environment, which was linked to a lower porosity and a finer pore structure as well as to higher Si/Al ratios [30].

3 Summary

The dissolution of AAMs in sulfuric acid can be described by a multistage deterioration process which is governed by (i) acid diffusion and corresponding leaching of alkali ions, (ii) decalcification of C-(A)-S-H and dealumination of N/K-A-S-(H), (iii) microstructural damage related to precipitation of expansive (K, Ca, Al)-sulfate-hydrate phases, (iv) complete dissolution of the microstructural framework, and (v) formation of silica gel in the leached layers. A schematic description of the deterioration process for a low-Ca AAM is presented in Fig. 5.

The overall deterioration mechanisms of AAM observed via abiotic acid tests coincide with the material response when exposed in biochemically aggressive sewer environments. However, the significantly higher complexity of the natural setting due to numerous additional environmental and biological factors may alter the deterioration mechanisms and kinetics.

Further research is needed to characterize AAM durability in biochemically aggressive sewer systems. Nevertheless, existing data on their general acid resistance, as well as first studies of on-site exposure demonstrate an overall high potential for such applications.

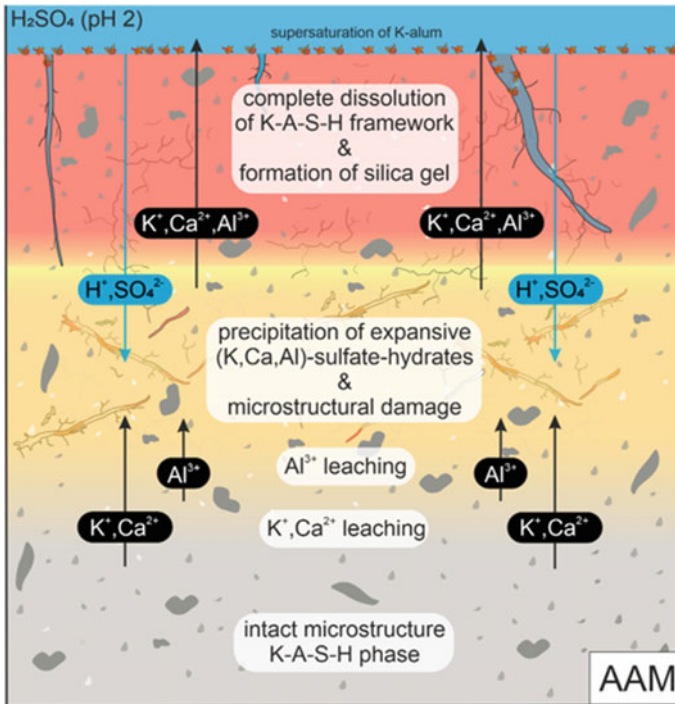


Fig. 5 Schematic description of the dissolution behaviour of a low-Ca AAM exposed to sulfuric acid (data from [26])

References

1. Adesanya, E., Ohenoja, K., Kinnunen, P., Illikainen, M.: Alkali activation of ladle slag from steel-making process. *J. Sustain. Metall.* **3**(2), 300–310 (2017). <https://doi.org/10.1007/s40831-016-0089-x>
2. Aliques-Granero, J., Tognonvi, T.M., Tagnit-Hamou, A.: Durability test methods and their application to AAMs: case of sulfuric-acid resistance. *Mater. Struct.* **50**(1), 36 (2016). <https://doi.org/10.1617/s11527-016-0904-7>
3. Allahverdi, A., Škvára, F.: Sulfuric acid attack on hardened paste of geopolymer cement: Part 1. Mechanism of concrete corrosion at relatively high concentrations. *Ceram.-Silik.* **9**, 225–229 (2005)
4. Allahverdi, A., Škvára, F.: Sulfuric acid attack on hardened paste of geopolymer cements: Part 2. Corrosion mechanism at mild and relatively low concentrations. *Ceram.-Silik.* **50**, 1–4 (2006)
5. Alzaza, A., Mastali, M., Kinnunen, P., Korat, L., Abdollahnejad, Z., Ducman, V., Illikainen, M.: Production of lightweight alkali activated mortars using mineral wools. *Materials* **12**(10), 1695 (2019). <https://doi.org/10.3390/ma12101695>
6. Awoyera, P., Adesina, A.: Durability properties of alkali activated slag composites: short overview. *SILICON* **12**(4), 987–996 (2020). <https://doi.org/10.1007/s12633-019-00199-1>
7. Badanoiu, A.I., Al Saadi, T.H.A., Stoleriu, S., Voicu, G.: Preparation and characterization of foamed geopolymers from waste glass and red mud. *Constr. Build. Mater.* **84**, 284–293 (2015)

8. Balczár, I., Korim, T., Kovács, A., Makó, É.: Mechanochemical and thermal activation of kaolin for manufacturing geopolymer mortars—comparative study. *Ceram. Int.* **42**(14), 15367–15375 (2016). <https://doi.org/10.1016/j.ceramint.2016.06.182>
9. Bernal, S.A., Rodríguez, E.D., de Gutiérrez, R.M., Provis, J.L.: Performance of alkali-activated slag mortars exposed to acids. *J. Sustain.Cement-Based Mater.* **1**(3), 138–151 (2012). <https://doi.org/10.1080/21650373.2012.747235>
10. Bernal, S.A., Rodríguez, E.D., Mejía de Gutiérrez, R., Provis, J.L.: Performance of alkali-activated slag mortars exposed to acids. *J. Sustain. Cement-Based Mater.* **1**(3), 138–151 (2012). <https://doi.org/10.1080/21650373.2012.747235>
11. Blaakmeer, J.: Diabind: An alkali-activated slag fly ash binder for acid-resistant concrete. *Adv. Cement Based Mater.* **1**(6), 275–276 (1994). [https://doi.org/10.1016/1065-7355\(94\)90036-1](https://doi.org/10.1016/1065-7355(94)90036-1)
12. Češnovar, M., Traven, K., Horvat, B., Ducman, V.: The potential of ladle slag and electric arc furnace slag use in synthesizing alkali activated materials; the influence of curing on mechanical properties. *Materials* **12**(7), 1173 (2019)
13. Cho, K.-S., Mori, T.: A newly isolated fungus participates in the corrosion of concrete sewer pipes. *Water Sci. Technol.* **31**(7), 263–271 (1995). [https://doi.org/10.1016/0273-1223\(95\)00343-L](https://doi.org/10.1016/0273-1223(95)00343-L)
14. Clausi, M., Tarantino, S. C., Magnani, L. L., Riccardi, M. P., Tedeschi, C., Zema, M.: Metakaolin as a precursor of materials for applications in cultural heritage: geopolymer-based mortars with ornamental stone aggregates. *Appl. Clay Sci.* **132–133**, 589–599 (2016). <https://doi.org/10.1016/j.clay.2016.08.009>
15. Davidovits, J.: Geopolymer cement, a review. *Geopolymer Inst. Libr.* 1–11 (2013)
16. Davidovits, J.: *Geopolymer Chemistry and Applications*, 4th ed. Springer (2013)
17. Dietzel, M.: Dissolution of silicates and the stability of polysilicic acid. *Geochim. Cosmochim. Acta* **64**(19), 3275–3281 (2000). [https://doi.org/10.1016/S0016-7037\(00\)00426-9](https://doi.org/10.1016/S0016-7037(00)00426-9)
18. Dietzel, M., Usdowski, E.: Depolymerization of soluble silicate in dilute aqueous solutions. *Colloid Polym. Sci.* **273**(6), 590–597 (1995). <https://doi.org/10.1007/BF00658690>
19. Djobo, J.N.Y., Elimbi, A., Tchakouté, H.K., Kumar, S.: Mechanical properties and durability of volcanic ash based geopolymer mortars. *Constr. Build. Mater.* **124**, 606–614 (2016)
20. Drugă, B., Ukrainczyk, N., Weise, K., Koenders, E., Lackner, S.: Interaction between wastewater microorganisms and geopolymer or cementitious materials: biofilm characterization and deterioration characteristics of mortars. *Int. Biodeterior. Biodegrad.* **134**, 58–67 (2018). <https://doi.org/10.1016/j.ibiod.2018.08.005>
21. Duxson, P., Fernández-Jiménez, A., Provis, J.L., Lukey, G.C., Palomo, A., van Deventer, J.S.J.: Geopolymer technology: the current state of the art. *J. Mater. Sci.* **42**(9), 2917–2933 (2007). <https://doi.org/10.1007/s10853-006-0637-z>
22. Duxson, P., Provis, J.L., Lukey, G.C., Mallicoat, S.W., Kriven, W.M., Van Deventer, J.S.J.: Understanding the relationship between geopolymer composition, microstructure and mechanical properties. *Colloids Surf., A* **269**(1–3), 47–58 (2005). <https://doi.org/10.1016/j.colsurfa.2005.06.060>
23. Farmer, V.C., Lumsdon, D.G.: An assessment of complex formation between aluminium and silicic acid in acidic solutions. *Geochim. Cosmochim. Acta* **58**(16), 3331–3334 (1994). [https://doi.org/10.1016/0016-7037\(94\)90088-4](https://doi.org/10.1016/0016-7037(94)90088-4)
24. Fernandez-Jimenez, A., García-Lodeiro, I., Palomo, A.: Durability of alkali-activated fly ash cementitious materials. *J. Mater. Sci.* **42**(9), 3055–3065 (2007). <https://doi.org/10.1007/s10853-006-0584-8>
25. Gluth, G.J.G., Grengg, C., Ukrainczyk, N., Mittermayr, F., Dietzel, M.: Acid resistance of alkali-activated materials: recent advances and research needs. *RILEM Tech. Lett.* **7**, 58–67 (2022). <https://doi.org/10.21809/rilemtechlett.2022.157>
26. Grengg, C., Gluth, G.J.G., Mittermayr, F., Ukrainczyk, N., Bertmer, M., Guilherme, A., Radtke, M., Leis, A., Dietzel, M.: Deterioration mechanism of alkali-activated materials in sulfuric acid and the influence of Cu: a micro-to-nano structural, elemental and stable isotopic multi-proxy study. *Cem. Concr. Res.* **142**, 106373 (2021). <https://doi.org/10.1016/j.cemconres.2021.106373>

27. Grengg, C., Koraimann, G., Ukrainczyk, N., Rudic, O., Luschnig, S., Gluth, G.J.G., Radtke, M., Dietzel, M., Mittermayr, F.: Cu- and Zn-doped alkali activated mortar—properties and durability in (bio)chemically aggressive wastewater environments. *Cem. Concr. Res.* **149**, 106541 (2021). <https://doi.org/10.1016/j.cemconres.2021.106541>
28. Grengg, C., Mittermayr, F., Baldermann, A., Böttcher, M.E., Leis, A., Koraimann, G., Dietzel, M.: Stable isotope signatures within microbial induced concrete corrosion: a field study. *Procedia Earth Planet. Sci.* **13**, 68–71 (2015). <https://doi.org/10.1016/j.proeps.2015.07.016>
29. Grengg, C., Mittermayr, F., Ukrainczyk, N., Koraimann, G., Kienesberger, S., Dietzel, M.: Advances in concrete materials for sewer systems affected by microbial induced concrete corrosion: a review. *Water Res.* **134**, 341–352 (2018). <https://doi.org/10.1016/j.watres.2018.01.043>
30. Grengg, C., Ukrainczyk, N., Koraimann, G., Mueller, B., Dietzel, M., Mittermayr, F.: Long-term in situ performance of geopolymer, calcium aluminate and Portland cement-based materials exposed to microbially induced acid corrosion. *Cem. Concr. Res.* **131**, 106034 (2020). <https://doi.org/10.1016/j.cemconres.2020.106034>
31. Habert, G., d'Espinose de Lacaillerie, J.B., Roussel, N.: An environmental evaluation of geopolymer based concrete production: reviewing current research trends. *J. Cleaner Prod.* **19**(11), 1229–1238 (2011). <https://doi.org/10.1016/j.jclepro.2011.03.012>
32. Hartman, R.L., Fogler, H.S.: Understanding the dissolution of zeolites. *Langmuir* **23**(10), 5477–5484 (2007). <https://doi.org/10.1021/la063699g>
33. Hartman, R.L., Lecefer, B., Frenier, W.W., Ziauddin, M., Fogler, H.S.: Acid-sensitive aluminosilicates: dissolution kinetics and fluid selection for matrix-stimulation treatments. *SPE Prod. Oper.* **21**(2), 194–204 (2006). <https://doi.org/10.2118/82267-pa>
34. Islander, B.R.L., Deviny, J.S., Member, A., Mansfeld, F., Postyn, A., Shih, H.: Microbial ecology of crown corrosion in sewers. *J. Environ. Eng.* **117**(6), 751–770 (1991)
35. Ismail, I., Bernal, S.A., Provis, J.L., San Nicolas, R., Hamdan, S., van Deventer, J.S.J.: Modification of phase evolution in alkali-activated blast furnace slag by the incorporation of fly ash. *Cem. Concr. Compos.* **45**, 125–135 (2014). <https://doi.org/10.1016/j.cemconcomp.2013.09.006>
36. Khan, H.A., Castel, A., Khan, M.S.H.: Corrosion investigation of fly ash based geopolymer mortar in natural sewer environment and sulphuric acid solution. *Corros. Sci.* **168**, 108586 (2020). <https://doi.org/10.1016/j.corsci.2020.108586>
37. Khan, H.A., Khan, M.S.H., Castel, A., Sunarho, J.: Deterioration of alkali-activated mortars exposed to natural aggressive sewer environment. *Constr. Build. Mater.* **186**, 577–597 (2018). <https://doi.org/10.1016/j.conbuildmat.2018.07.137>
38. Lloyd, R.R., Provis, J.L., van Deventer, J.S.J.: Acid resistance of inorganic polymer binders. 1. Corrosion rate. *Mater. Struct. Materiaux et Constructions* **45**(1–2), 1–14 (2012). <https://doi.org/10.1617/s11527-011-9744-7>
39. Lukhele, T., Selvarajan, R., Nyoni, H., Mamba, B.B., Msagati, T.A.M.: Acid mine drainage as habitats for distinct microbiomes: current knowledge in the Era of molecular and Omic technologies. *Curr. Microbiol.* **77**(4), 657–674 (2020). <https://doi.org/10.1007/s00284-019-01771-z>
40. McLellan, B.C., Williams, R.P., Lay, J., van Riessen, A., Corder, G.D.: Costs and carbon emissions for geopolymer pastes in comparison to ordinary Portland cement. *J. Cleaner Prod.* **19**(9), 1080–1090 (2011). <https://doi.org/10.1016/j.jclepro.2011.02.010>
41. Montes, C., Allouche, E.N.: Evaluation of the potential of geopolymer mortar in the rehabilitation of buried infrastructure. *Struct. Infrastruct. Eng.* **8**(1), 89–98 (2012). <https://doi.org/10.1080/15732470903329314>
42. Oelkers, E.H.: General kinetic description of multioxide silicate mineral and glass dissolution. *Geochim. Cosmochim. Acta* **65**(21), 3703–3719 (2001)
43. Ouellet-Plamondon, C., Habert, G.: 25—Life cycle assessment (LCA) of alkali-activated cements and concretes. In: Pacheco-Torgal, F., Labrincha, J.A., Leonelli, C., Palomo, A. (eds.) *Chindaprasirt Mortars and Concretes*, pp. 663–686. Woodhead Publishing (2015). <https://doi.org/10.1533/9781782422884.5.663>

44. Pacheco-Torgal, F., Abdollahnejad, Z., Miraldo, S., Baklouti, S., Ding, Y.: An overview on the potential of geopolymers for concrete infrastructure rehabilitation. *Constr. Build. Mater.* **36**, 1053–1058 (2012). <https://doi.org/10.1016/j.conbuildmat.2012.07.003>
45. Page, C.L., Page, M.M.: *Durability of Concrete and Cement Composites*. CRC Press (2007)
46. Provis, J.L.: Alkali-activated materials. *Cem. Concr. Res.* **114**, 40–48 (2018)
47. Provis, J.L.: Alkali-activation of calcined clays—past, present and future. In: *Calcined Clays for Sustainable Concrete*, pp. 372–376. Springer (2018)
48. Provis, J.L., Bernal, S.A.: Geopolymers and related alkali-activated materials. *Annu. Rev. Mater. Res.* **44**, 299–327 (2014). <https://doi.org/10.1146/annurev-matsci-070813-113515>
49. Provis, J.L., Palomo, A., Shi, C.: Advances in understanding alkali activated materials. *Cement Concr. Compos.* **78**, 110–125 (2015)
50. Provis, J.L., Palomo, A., Shi, C.: Advances in understanding alkali-activated materials. *Cem. Concr. Res.* **78**, 110–125 (2015). <https://doi.org/10.1016/j.cemconres.2015.04.013>
51. Provis, J.L., van Deventer, J.S.J. (eds.): *Geopolymers: Structure, Processing, Properties and Industrial Applications*. CRC Press, Boca Raton (2009). <https://doi.org/10.1533/9781845696382>
52. Rakngan, W., Williamson, T., Ferron, R.D., Sant, G., Juenger, M.C.G.: Controlling workability in alkali-activated class C fly ash. *Constr. Build. Mater.* **183**, 226–233 (2018)
53. Škvára, F.: Alkali activated material–geopolymer. In: *International Conference Alkali Activated Materials—Research, Production and Utilization, Česká Rozvojová Agentura, Praha*, pp. 21–22 (2007)
54. Sturm, P., Gluth, G.J.G., Jäger, C., Brouwers, H.J.H., Kühne, H.C.: Sulfuric acid resistance of one-part alkali-activated mortars. *Cem. Concr. Res.* **109**, 54–63 (2018). <https://doi.org/10.1016/j.cemconres.2018.04.009>
55. Taylor, H.F.W.: *Cement Chemistry*, 2nd edn. Thomas Telford Publishing (1997). <https://doi.org/10.1680/cc.25929>
56. Traven, K., Češnovar, M., Ducman, V.: Particle size manipulation as an influential parameter in the development of mechanical properties in electric arc furnace slag-based AAM. *Ceram. Int.* **45**(17, Part B), 22632–22641 (2019). <https://doi.org/10.1016/j.ceramint.2019.07.296>
57. Ukrainczyk, N., Muthu, M., Vogt, O., Koenders, E.: Geopolymer, calcium aluminate, and Portland cement-based mortars: comparing degradation using acetic acid. *Materials* **12**(19) (2019). <https://doi.org/10.3390/ma12193115>
58. Van Deventer, J.S.J., Provis, J.L., Duxson, P.: Technical and commercial progress in the adoption of geopolymer cement. *Minerals Eng.* **29**, 89–104 (2012). <https://doi.org/10.1016/j.mineng.2011.09.009>
59. Wang, A., Zheng, Y., Zhang, Z., Liu, K., Li, Y., Shi, L., Sun, D.: The durability of alkali-activated materials in comparison with ordinary Portland cements and concretes: a review. *Engineering* **6**(6), 695–706 (2020). <https://doi.org/10.1016/j.eng.2019.08.019>
60. Wang, S.-D., Scrivener, K.L.: Hydration products of alkali activated slag cement. *Cem. Concr. Res.* **25**(3), 561–571 (1995)
61. Williams, R.P., Van Riessen, A.: Determination of the reactive component of fly ashes for geopolymer production using XRF and XRD. *Fuel* **89**(12), 3683–3692 (2010)
62. Wonisch, H., Gérard, F., Dietzel, M., Jaffrain, J., Nestroy, O., Boudot, J.P.: Occurrence of polymerized silicic acid and aluminum species in two forest soil solutions with different acidity. *Geoderma* **144**(3–4), 435–445 (2008). <https://doi.org/10.1016/j.geoderma.2007.11.022>
63. Yang, K.-H., Song, J.-K., Song, K.-I.: Assessment of CO₂ reduction of alkali-activated concrete. *J. Cleaner Prod.* **39**, 265–272 (2013). <https://doi.org/10.1016/j.jclepro.2012.08.001>

Surface Treatment for Corroding Concrete Sewers



Xuan Li and Guangming Jiang

Abstract To mitigate the corrosion on existing corroding sewers, various approaches of surface treatment have been developed including surface coating or lining, chemical spraying, and surface washing. These approaches target at isolating concrete from corrosive environments, inhibiting or removing the corrosion-inducing microorganisms, or increasing the corrosion resistance of the surfaces. Different coating/lining materials have been applied in corroding sewers, including polymer-based and cement-based materials. Polymer-based materials isolate the concrete from the corrosive environment, while cement-based materials generally have higher corrosion resistance, slowing down the corrosion development on concrete surfaces. For the same type of coating material, the corrosion mitigation performance varies in different studies. The chemical spraying majorly uses alkaline solutions or slurry such as magnesium hydroxide liquid and sodium. These solutions increase the surface pH of concrete, inhibiting re-establishment and activity of corrosion-inducing microorganisms. Although chemical spraying exhibit promising results in corrosion control, a frequent re-spray is required due to the wash-off of chemicals. Surface washing aims to remove the corrosion layer, which is the major habitat of corrosion-inducing microorganisms. However, in ordinary Portland cement-based concrete, the effect of surface washing on corrosion control is often temporal.

X. Li

School of Civil and Environmental Engineering, Centre for Technology in Water and Wastewater, University of Technology Sydney, Ultimo, NSW 2007, Australia
e-mail: xuan.li@uts.edu.au

X. Li · G. Jiang (✉)

School of Civil, Mining, Environmental and Architectural Engineering, University of Wollongong, Wollongong, NSW 2522, Australia
e-mail: gjiang@uow.edu.au

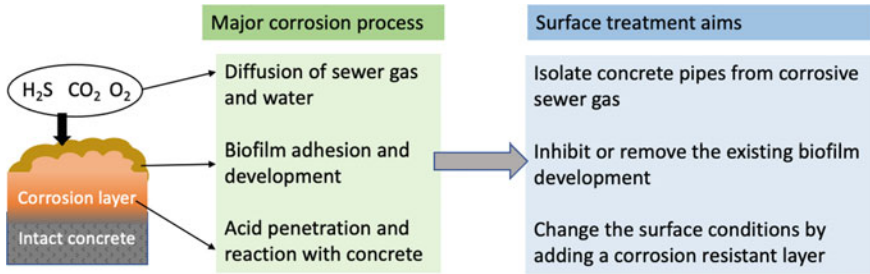


Fig. 1 Overview of major corrosion processes, and major aims of surface treatment with corrosion processes

1 Introduction

Concrete corrosion leads to structural deterioration and early failure of sewers globally, which shortens the life expectancy of sewer structures by more than 50% [27]. To mitigate the corrosion and extend the service life of sewers, surface treatment on existing corroding sewers is of high research interest and applicational benefits. As detailed in previous chapters, the concrete corrosion in sewers is predominately caused by the sulfuric acid produced by sulfide-oxidizing microorganisms (SOM) on concrete surfaces. Three major processes are involved in the corrosion process: (1) the diffusion of sewer gas and water into concrete, (2) the biofilm adhesion and development on concrete surface; and (3) the acid penetration and reaction with concrete (Fig. 1). Thus, surface treatment techniques majorly aim at (1) isolating the sewer pipes from the corrosive sewer gas; (2) changing the surface condition by adding a corrosion resistant layer; and (3) inhibiting or removing the existing biofilm development (Fig. 1). The first two targets are achieved by surface coating (Sect. 2) while the later one is usually achieved by chemical spraying (Sect. 3) or surface washing (Sect. 4).

2 Surface Coating and Lining

In corroding sewers, surface coating or lining has been widely applied to provide a protective layer on top of the concrete. Based on the coating materials, the liners/coating materials can be classified as, polymer-based materials and cement-based materials. Polymer-based coating/lining materials include epoxy resin coating, polyurea coating, polyurethane coating, unsaturated polyester resin coating, polyvinyl chloride (PVC), fiberglass, and high-density polyethylene (HDPE) [3, 31]. These materials are not susceptible to acid attack and are thus resistant to corrosion. Furthermore, they also isolate the concrete from the sewer environment by reducing

the ingress of corrosive gas (i.e. H_2S and CO_2) and moisture [42]. In addition, they also have sufficient bond strength to the concrete structure as required by most of the water utilities.

Even though polymer-based coatings are highly corrosion-resistant, their performance is reduced by the presence of pinholes, pores, and other defects [41]. Pinholes are small holes that typically form when bubbles within the coating rupture. Pores that travel through the coating are particularly detrimental as they can result in premature failure of the coating. The morphology of some polymer-based coating (i.e., epoxy) is shown as an example in Fig. 2a, b. Most of the coatings in Fig. 2a, b have small holes ($\sim 10\text{--}500\ \mu\text{m}$) on the surface. These appear to be generated by air bubbles that have escaped during curing. The presence of pinholes could provide access for the ingress of corrosive sewer gas, which reduces the protective effect on the concrete. With the ingress of corrosive gases, the corrosion development under the coating layer would further lead to other defects including blisters, delamination (shown in the red circle in Fig. 2c), and peeling of the coating layer (Fig. 2d) [10]. Therefore, the effectiveness of liners and coatings is highly dependent on the material itself, the thickness of the application and quality of the application (workmanship), and whether a completely sealed system is established [42]. In addition, the debonding areas and defects have been found to be acting as habitats for bacteria to grow, which may further accelerate the structural failure of the coating [21].

To date, there are numerous products regarding the same type of polymer-based coating materials. For instance, the epoxy coating in Figs. 2a (EA) and 2b (EB) are both epoxy-based coating. However, their morphology (Fig. 2), composition, hydrophobicity, and biodegradability vary depending on the product. EA has higher porosity, higher sulfur content, lower hydrophobicity, and earlier biofilm attachment on the coating surface than that of EB. To represent the biogenic acids generated by fungi, sulfur, and ammonia oxidizing bacteria that are of frequent presence in wastewater, citric acid, sulfuric and nitric acid were used for the acid uptake rate (an indicator of acid diffusion) test for concrete coated with EA and EB (Fig. 3). Depending on the exposure time to the corrosive reagent, the acid uptake rate of EB was about 10–100% higher than that of EA (Fig. 3). Furthermore, the dynamic sewer environment with varying H_2S concentration, relative humidity, and temperature also affects the corrosion development and structural failure of the coatings [8]. Therefore, inconsistent results are commonly observed from different studies. Under acid attack, the chemical resistance of epoxy resin-based surface coatings was shown to be better than acrylic resin-based coatings [2], but worse in another study [37]. Thus, the type of product and also the corrosive environments shall be taken into consideration when selecting the suitable coating materials.

Calcium aluminate cement (CAC) is the most used cement-based material for corroding concrete. The biofilm adhesion and development are affected by the surface quality, texture, and bacteriostatic properties of concrete. Calcium aluminate cement is a specialty cement principally made up of lime (CaO) and alumina (Al_2O_3). These components are reacted to generate calcium aluminates ($CaAl_2O_4$) as a hydration product. CAC shows significant advancement in corrosion resistance in comparison to ordinary Portland cement (OPC) based concrete [11, 20]. This is majorly attributed

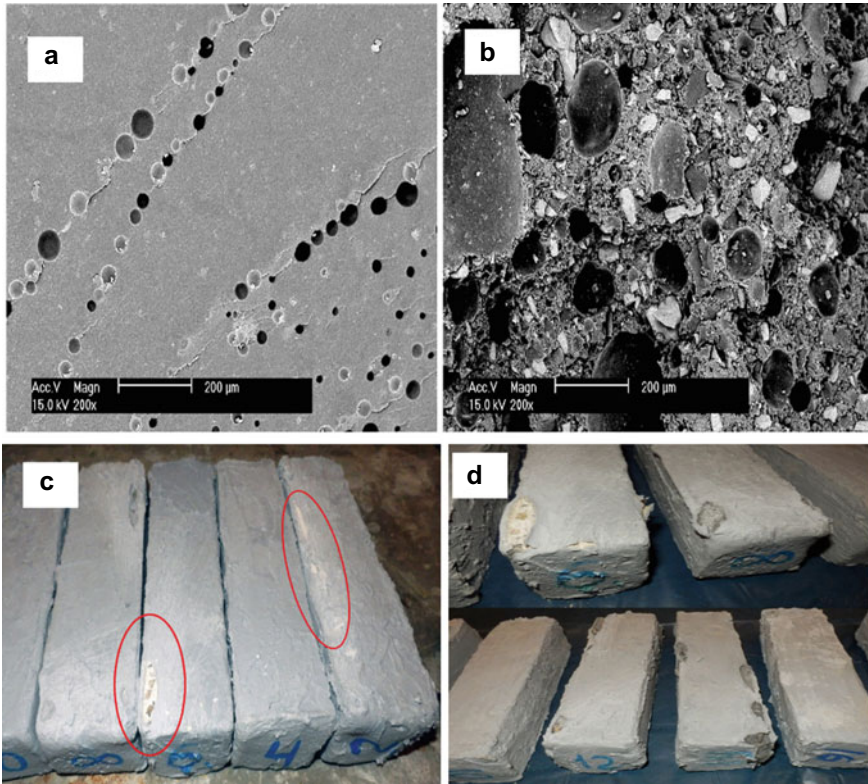


Fig. 2 Scanning electron microscopy image of epoxy coatings EA (a) and EB (b). The appearance of the samples with the epoxy coating exposed to sulfuric acid after 60 days (c) and 120 days (d) [10] (open access)

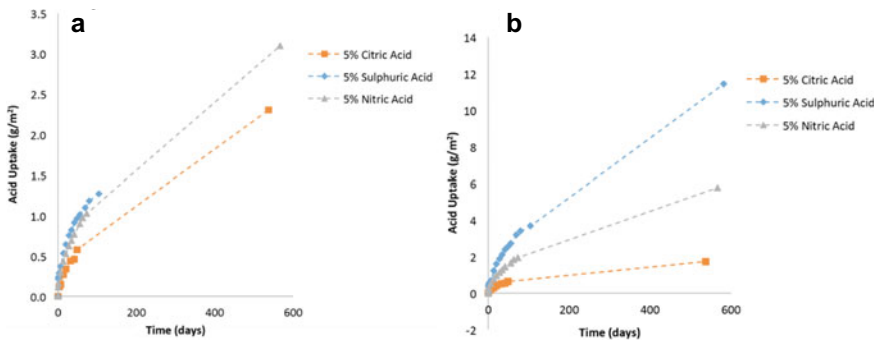


Fig. 3 Relative uptake of 5% citric, nitric and sulfuric acid on EA (a) and EB (b) [10] (open access)

to the bacteriostatic properties of aluminum content in CAC, which inhibits the growth of most microorganisms [20]. Compared with the corrosion layer from OPC concrete under the same sewer environment, the diversity of the microbes attached onto the CAC concrete surface tends to be single and specific, while the corrosion resistance is improved in CAC concrete [12]. Furthermore, under acid attack, CAC concrete could form aluminum hydroxide gel in the corrosion product. Compared to the general porous corrosion product (i.e. gypsum) in OPC concrete, the aluminum hydroxide gel is stable above pH 4 and decreases porosity and associated ingress of aggressive species [11]. In addition, CAC concrete also exhibits a higher acid neutralization capacity than OPC concrete under the same concrete mix [19]. These benefits make CAC suitable to be applied as an effective coating layer. Concrete pipes that suffer from microbially induced concrete corrosion were coated with CAC mortar in Durban of South Africa, and no evidence of corrosion was noted in an inspection after 31 years in use [36]. However, it should be recognized that concrete is intrinsically a porous material, despite the improvements on its formulation and quality control to the best possible extent, it is not possible to prevent completely the ingress of potentially harmful agents. Thus, CAC could slow down but not completely stop the corrosion development.

Polymer-modified mortar has also been applied as a coating material for corrosion control. Polymer-modified mortar is made of cement with polymer and aggregates. The incorporation of polymers to cement mortar improves strength, adhesion, resilience, and decreases water absorption, and the ingress of corrosive agents [1]. Using polymer-modified mortars on concrete is of vital importance in applications such as repair, flooring, waterproofing or corrosion protection of concrete structures [34]. Berndt [7] evaluated the performance of epoxy coatings (two different products), water-based epoxy-modified cementitious mortar coating, latex-modified mortar coating, and CAC mortar coatings under the microbially induced corrosion caused by typical sulfur-oxidizing bacteria (*Thiobacillus ferrooxidans*) and the corrosive environment in a cooling tower under SOM-induced corrosion. All the epoxy coatings and mortars showed good adhesion to the concrete substrates, suggesting the possibility of using all these materials for coating purposes. However, under the sulfuric acid attack generated by *Thiobacillus ferrooxidans* or the corrosive environment in the field, epoxy coatings and CAC mortar coating exhibited excellent durability, while epoxy- and latex-modified mortar coatings underwent some deterioration [7]. Thus, epoxy coating and CAC mortar coating were recommended for applications. However, it is highly worthy to note that, as mentioned earlier, the performance of each type of coating is dependent on the product itself, the thickness of the application, the quality of the application (workmanship), and the corrosive environment. Thus, the comparison and performance of these materials are limited to the specific products and environmental conditions in that study. Future selection of coatings for microbially induced concrete corrosion control still requires comparison and pre-testing for localized application.

3 Chemical Spraying

Another approach for surface treatment is chemical spraying. In contrast to the surface coating, chemical spraying requires no surface preparation before application. The aim of chemical spraying is to (1) deactivate the SOM; (2) render the surface conditions unfavourable for regrowth and recolonization of SOM. The chemical spraying is usually performed using a float mounted with a spray head that is pulled along the sewer at a controlled rate to spray the crown regions of sewers at a predetermined application rate [29]. Various alkaline chemicals and biocides such as phenol derivatives, quaternary ammonium salts, and monochloramine have been investigated in real sewers, where magnesium hydroxide liquid (MHL) was found as the most environmental-friendly and effective chemical [33, 40]. Magnesium hydroxide slurry is a non-hazardous chemical, which inherently has a high pH (9–10). Application of a 50% MHL slurry to the crown of a highly corroded active sewer (pH of 1–3) has maintained the surface pH at or greater than 9 for approximately 9 months [40]. The microbiological analysis further confirmed a reduction in the population of SOM, reaching to $10\text{--}10^2$ cells/g of corrosion product (below detectable levels) for about 9 months after treatment [40]. The major aim of MHL spraying is to increase the surface pH, neutralize the acidic surface condition, and maintain an alkaline condition to inhibit the SOM development. Depending on the concentration of MHL slurry, various products have been proposed and widely applied in water utilities in Australia and the USA for corrosion mitigation in gravity sewer pipes (Fig. 4a) and manholes (Fig. 4b) [5].

For concrete manufacturing, nitrite has been widely used to prevent rebar corrosion caused by chloride attacks and to accelerate the hydration process of cement [18, 32]. However, until recently, the inhibition of nitrite on SOM was observed after a nitrite solution was sprayed onto a corroding concrete surface [38]. After spraying the nitrite solution, the H_2S uptake rates of concrete coupons reduced by 84–92% within 39 h, and no obvious recovery was seen in up to 12 months [38]. This is likely caused

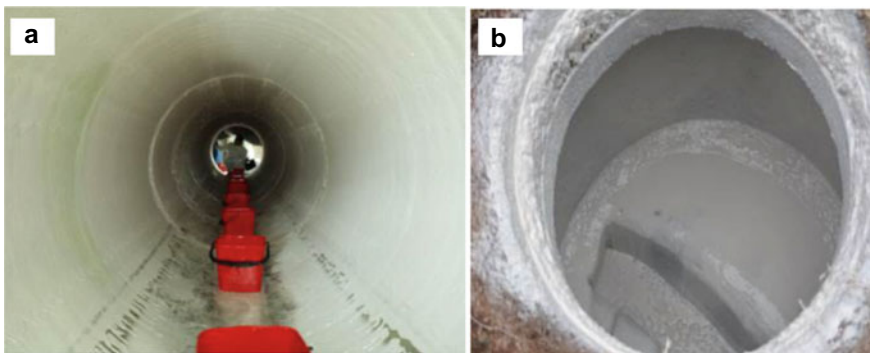


Fig. 4 A sewer pipe (a) and manhole (b) coated after the MHL spray, adapted from Apté [5] (open access)

by the inhibitory effect of free nitrous acid (FNA, HNO_2) formed by the nitrite solution on the acidic corrosion surface. FNA, the protonated form of nitrite ($\text{H}-\overset{\cdot\cdot}{\text{O}}-\overset{\cdot\cdot}{\text{N}}=\overset{\cdot\cdot}{\text{O}}$), is a weak monobasic acid ($pK_a = 3.16$, 25°C) [6]. In the past several decades, FNA has generally been recognized as an inhibitor of metabolisms of various groups of bacteria in wastewater environment, such as ammonium-oxidizing bacteria, nitrite-oxidizing bacteria, denitrifiers and polyphosphate-accumulating organisms [35, 44, 45]. Recent studies revealed that the level of bactericidal effect is strongly related to the FNA concentration and the exposure time. At ppb levels, FNA has a strong inhibitory effect on both the anabolic and catabolic processes of a broad range of microorganisms, while at ppm levels, FNA is a strong biocidal agent, due to the formation of reactive nitrogen intermediates and strong free radicals [9, 17]. In particular, FNA has been applied for sulfide control in sewers for several years. A long-term laboratory study reported that FNA concentration at 0.26 mg-N/L or above, with an exposure time of 12 h or longer, could suppress sulfide and methane production by sewer biofilms [14]. This is also evident in the results of viable bacterial cells in the corrosion layer after the nitrite spraying. The viable bacterial cells decreased by > 80%, 39 h after the nitrite spray, and remained at an undetectable level, 700 h after the spraying [38]. This showed a promising application of using FNA (nitrite sprayed on acid surfaces) to inactive the SOM development and mitigate the concrete corrosion. Compared with conventional approaches for corrosion control, FNA application on concrete limited the health concerns as nitrite is easily consumed by denitrifying organisms in the wastewater systems [24, 15].

A follow-up study investigated the effect of nitrite spraying on two types of concrete in a sewer manhole for 21 months. A nitrite solution was sprayed on the corroding surfaces of concrete at the 6th month. After the spraying, the sulfide uptake rate of sprayed coupons was reduced by about 35%, leading to 1–2 units higher surface pH, and 40–90% of reduction in corrosion loss for six months [22]. The abundance of SOM on nitrite sprayed coupons was also reduced on the sprayed coupons. However, after longer-term exposure, the corrosion mitigation effect became negligible in 15 months after the nitrite spraying [22]. The reduced corrosion mitigation effect during long-term exposure is likely caused by the wash-off of the nitrite due to the flooding or the condensation water dripping. The wash-off of corrosion inhibitors sprayed onto the sewer has also been observed with other chemicals such as MHL. Thus, re-spraying is required at suitable time intervals to restore the effectiveness of protection over a long period, and this adds to the maintenance cost of the sewerage system [29]. Further research on the anti-wash-off property of sprayed corrosion inhibitors is needed.

4 Surface Washing

To date, the role of corrosion layers on the microbially induced corrosion development is largely unclear and debatable. Some researchers point out that the bulk of biogenic acids is produced on the exposed surface of the corrosion layer, i.e. the produced acids must have to penetrate into the corrosion layer before reacting with the sound concrete underneath [43]. In this case, the increasing thickness of the corrosion layer can to some extent hinder the corrosion process. However, other studies consider the corrosion layer as an excellent medium for microorganisms/bacteria to grow and consequently accelerates the corrosion process [13, 26, 28]. Surface washing was thus proposed to remove the corrosion layers from corroded surfaces to control the corrosion development. Compared to the surface coating, the surface washing approach is generally regarded as a cost-effective approach by water utilities.

However, the effect of surface washing on corrosion control is found as limited and temporary for Ordinary Portland Cement (OPC) concrete. It is worthy to mention that although many types of corrosion-resistant concrete have been proposed, OPC concrete is still the most common and widely used concrete for sewers, especially for existing sewers. In a real sewer, the sulfide oxidizing activity of washed concrete reached the pre-washing level in 30–40 days [30]. Another study monitored the surface washing effect on corrosion control for 54 months on OPC concrete. In this study, the surface pH of washed and unwashed coupons was identical after 54 months and the sulfide oxidizing activity of washed concrete reached the pre-washing level in 60–140 days [39]. Thus, the temporal effect of surface washing is majorly attributed to the quick recovery/re-establishment of SOM on OPC concrete surfaces. It is commonly observed that after surface washing, the surface pH of concrete increases from 1 to 3 to around 5, which is still an acidic condition that allows the re-colonization and development of sulfide oxidizing microorganisms.

The surface washing effect was also investigated on calcium nitrite admixed concrete. As discussed in Sect. 2, FNA (formed by spraying nitrite on the acidic concrete surface) showed promising results in the corrosion mitigation of microbially induced corrosion, but the wash-off of the sprayed nitrite led to the temporal effect of the nitrite spraying. Thus, the potential solution is to add calcium nitrite into concrete during manufacture. Calcium nitrite has been widely used as a corrosion inhibitor against chloride attack of rebar steel for several decades. The addition of calcium nitrite aimed at increasing the chloride threshold level and also the corrosion-free life of rebar inside the concrete [4]. The effect of calcium nitrite admixture on microbially influenced concrete corrosion in sewers was only observed recently by Li et al. [25] through a 16-month monitoring of corrosion development in a real sewer manhole. During the exposure time in the sewer manhole, calcium nitrite admixed concrete constantly had a higher surface pH, lower sulfide uptake rate, and corrosion loss, confirming the inhibitory effect of nitrite leached from the inner part of concrete to the acidic surface [25].

More importantly, the effect of surface washing on OPC concrete and nitrite-admixed concrete was investigated and compared in a pilot-scale gravity sewer [23].

Concrete coupons with and without nitrite were exposed in the corrosive environment in the pilot sewer for 6 months for the development of microbially induced corrosion before the surface washing. Then the washed coupons were continuously monitored for another 10 months. In this study, the sulfide-oxidizing activity on concrete surface reached the comparable level to unwashed coupons within 4 months on OPC concrete but 8–10 months on nitrite calcium admixed concrete. The corrosion loss of OPC concrete showed no difference between washed and unwashed coupons, but surface washing reduced the corrosion loss by 20–30% in nitrite admixed concrete [23]. This is likely attributed to the inhibitory effect of nitrite on the development of SOMs. In particular, the OPC and calcium nitrite admixed concrete had a similar pH after surface washing, normally around 5–6 [13, 23, 39], which is still much lower than that of the intact concrete (*c.a.* 13). In a previous study, a pH transition zone was observed near the corrosion front ($\text{pH} < 4$), where the pH increased dramatically from around 5–11 within 5 mm [16]. Visually, some light-colored corrosion production can still be observed in the post-washing surface of the concrete (Fig. 5). Thus, it suggests that surface washing can only remove the loose structure ($\text{pH} < 4$) on the concrete surface but not reach the intact concrete surface. Compared with OPC concrete, the post-washing surface of calcium nitrite admixed concrete has a higher content of nitrite, which likely inhibited the re-development of SOM. This is also consistent with the microbial community analysis, where an incomplete development of SOM was observed on calcium nitrite admixed concrete 10 months after the surface washing [23]. Therefore, the corrosion-resistant concrete with inhibitors potentially can reach a synergic corrosion mitigation effect with the assistance of intermittent surface washing, which is recommended for future research.

5 Summary

This chapter summarized the surface treatment approaches on corroding concrete sewers for corrosion control. To date, surface coating/lining, chemical spraying, and surface washing have been applied to mitigate the concrete corrosion in sewers.

Two major types of materials are commonly used for the surface coating/lining, namely polymer-based materials and cement-based materials. Polymer-based materials include epoxy resin coating, polyurea coating, polyurethane coating, unsaturated polyester resin coating, polyvinyl chloride (PVC), fiberglass, and high-density polyethylene (HDPE). These materials isolate concrete from the corrosive sewer gas and are often corrosion resistant. However, for the same type of materials, various products are supplied from different companies. Their morphology, composition, hydrophobicity, and biodegradability vary depending on the product. Calcium aluminate cement (CAC) is the most used cement-based material, while polymer-modified mortar has also been occasionally used as a coating or lining material. Generally, CAC-based coating shows an excellent corrosion mitigation effect than other materials. However, like polymer-based materials, the composition of CAC-based coating materials varies depending on the product. Thus, for the application of coating/lining



Fig. 5 Surface characteristics of two OPC concrete (a) and calcium nitrite admixed concrete (b) samples after surface washing

in sewers, the quality of the production, the thickness and quality of the application, and dynamic sewer conditions shall be taken into consideration when selecting a suitable product.

Various alkaline chemicals and biocides such as phenol derivatives, quaternary ammonium salts, and monochloramine have been investigated in real sewers, where magnesium hydroxide liquid and sodium nitrite solution were found as the most environmental-friendly and effective chemical. However, the effect of chemical spraying is often affected by the wash-off of chemicals due to the flooding or the condensation water dripping. Thus, re-spraying at suitable intervals is required for effective corrosion mitigation.

The surface washing aims to remove the acidic corrosion product along with the corrosion-inducing microorganisms. However, the effect of surface washing is commonly found as temporal due to the fast re-development of sulfide oxidizing microorganisms. A recent study suggests that the concrete with microbial inhibitor (calcium nitrite) can achieve a longer corrosion mitigation effect of surface washing due to the slower re-establishment of sulfide oxidizing microorganisms in comparison to ordinary Portland land cement concrete. Thus, the surface washing effect on other corrosion-resistant concrete with microbial inhibitors is recommended for future research.

References

1. Aggarwal, L.K., Thapliyal, P.C., Karade, S.R.: Properties of polymer-modified mortars using epoxy and acrylic emulsions. *Constr. Build. Mater.* **21**, 379–383 (2007)
2. Al-Dulaijan, S., Maslehuddin, M., Al-Zahrani, M., Sharif, A., Al-Juraifani, E., Al-Idi, S.: Performance evaluation of resin based surface coatings. In: *Deterioration and Repair of Reinforced Concrete in the Arabian Gulf*. Preceeding of 6th ACI International Conference, pp. 342–62. Bahrain (2000)
3. Almusallam, A.A., Khan, F.M., Dulaijan, S.U., Al-Amoudi, O.S.B.: Effectiveness of surface coatings in improving concrete durability. *Cem. Concr. Compos.* **25**, 473–481 (2003)
4. Angst, U.M., Elsener, B., Larsen, C.K., Vennesland, Ø.: Chloride induced reinforcement corrosion: electrochemical monitoring of initiation stage and chloride threshold values. *Corros. Sci.* **53**, 1451–1464 (2011)
5. Apté, N.: Know your sewer-corrosion protection of sewer assets. In: *Proceedings 9th WIOA, NSW Water Industry Operations Conference and Exhibition*, vol. 24, pp. 129–135. Orange PCYC (2015)
6. Bastidas-Arteaga, E., Sánchez-Silva, M., Chateauneuf, A., Silva, M.R.: Coupled reliability model of biodeterioration, chloride ingress and cracking for reinforced concrete structures. *Struct. Saf.* **30**, 110–129 (2008)
7. Berndt, M.: Evaluation of coatings, mortars and mix design for protection of concrete against sulphur oxidising bacteria. *Constr. Build. Mater.* **25**, 3893–3902 (2011)
8. Delozanne, J., Desgardin, N., Coulaud, M., Cuvillier, N., Richaud, E.: Failure of epoxies bonded assemblies: comparison of thermal and humid ageing. *J. Adhes.* (2018)
9. Duan, H., Gao, S., Li, X., Ab Hamid, N.H., Jiang, G., Zheng, M., Bai, X., Bond, P.L., Lu, X., Chislett, M. M., Hu, S., Ye, L., Yuan, Z.: Improving wastewater management using free nitrous acid (FNA). *Water Res.* **171**, 115382 (2020)
10. Goncharenko, D., Aleinikova, A., Kabus, O., Kolomiets, Y.: Study of the efficiency of epoxy coating protection of concrete surfaces from sulfuric acid corrosion. In: *IOP Conference Series: Materials Science and Engineering*, p. 012081. IOP Publishing (2019)
11. Grengg, C., Mittermayr, F., Ukrainczyk, N., Koraimann, G., Kienesberger, S., Dietzel, M.: Advances in concrete materials for sewer systems affected by microbial induced concrete corrosion: a review. *Water Res.* **134**, 341–352 (2018)
12. Herisson, J., Guéguen-Minerbe, M., van Hullebusch, E.D., Chaussadent, T.: Influence of the binder on the behaviour of mortars exposed to H₂S in sewer networks: a long-term durability study. *Mater. Struct.* **50**, 1–18 (2017)
13. Islander, R.L., Deviny, J.S., Mansfeld, F., Postyn, A., Shih, H.: Microbial ecology of crown corrosion in sewers. *J. Environ. Eng.* **117**, 751–770 (1991)
14. Jiang, G., Gutierrez, O., Sharma, K.R., Keller, J., Yuan, Z.: Optimization of intermittent, simultaneous dosage of nitrite and hydrochloric acid to control sulfide and methane productions in sewers. *Water Res.* **45**, 6163–6172 (2011)
15. Jiang, G., Gutierrez, O., Sharma, K.R., Yuan, Z.: Effects of nitrite concentration and exposure time on sulfide and methane production in sewer systems. *Water Res.* **44**, 4241–4251 (2010)
16. Jiang, G., Wightman, E., Donose, B.C., Yuan, Z., Bond, P.L., Keller, J.: The role of iron in sulfide induced corrosion of sewer concrete. *Water Res.* **49**, 166–174 (2014)
17. Jiang, G., Yuan, Z.: Inactivation kinetics of anaerobic wastewater biofilms by free nitrous acid. *Appl. Microbiol. Biotechnol.* **98**, 1367–1376 (2014)
18. Justnes, H., Nygaard, E.C.: Technical calcium nitrate as set accelerator for cement at low temperatures. *Cem. Concr. Res.* **25**, 1766–1774 (1995)
19. Kiliswa, M.W.: *Composition and Microstructure of Concrete Mixtures Subjected to Biogenic Acid Corrosion and Their Role in Corrosion Prediction of Concrete Outfall Sewers* (2016)
20. Kong, L., Zhao, W., Xuan, D., Wang, X., Liu, Y.: Application potential of alkali-activated concrete for antimicrobial induced corrosion: a review. *Constr. Build. Mater.* **317**, 126169 (2022)

21. Kopteva, Z.P., Zanina, V., Kozlova, I.: Microbial corrosion of protective coatings. *Surf. Eng.* **20**, 275–280 (2004)
22. Li, X., Johnson, I., Mueller, K., Wilkie, S., Hanzic, L., Bond, P.L., O'Moore, L., Yuan, Z., Jiang, G.: Corrosion mitigation by nitrite spray on corroded concrete in a real sewer system. *Sci. Total Environ.* **806**, 151328 (2022)
23. Li, X., Kulandaivelu, J., O'Moore, L., Wilkie, S., Hanzic, L., Bond, P.L., Yuan, Z., Jiang, G.: Synergistic effect on concrete corrosion control in sewer environment achieved by applying surface washing on calcium nitrite admixed concrete. *Constr. Build. Mater.* **302**, 124184 (2021)
24. Li, X., O'Moore, L., Wilkie, S., Song, Y., Wei, J., Bond, P.L., ... & Jiang, G.: Nitrite admixed concrete for wastewater structures: Mechanical properties, leaching behavior and biofilm development. *Constr. Build. Mater.* **233**, 117341 (2020)
25. Li, X., Bond, P., O'Moore, L., Wilkie, S., Hanzic, L., Johnson, I., Mueller, K., Yuan, Z., Jiang, G.: Increased resistance of nitrite-admixed concrete to microbially induced corrosion in real sewers. *Environ. Sci. Technol.* **54**(4):2323–2333 (2020)
26. Mansfeld, F., Shih, H., Postyn, A., Devlin, J., Islander, R., Chen, C.: Corrosion monitoring and control in concrete sewer pipes. *Corrosion* **47**, 369–376 (1991)
27. Monteiro, P.J., Kurtis, K.E.: Time to failure for concrete exposed to severe sulfate attack. *Cem. Concr. Res.* **33**, 987–993 (2003)
28. Monteny, J., Vincke, E., Beeldens, A., de Belie, N., Taerwe, L., van Gemert, D., Verstraete, W.: Chemical, microbiological, and in situ test methods for biogenic sulfuric acid corrosion of concrete. *Cem. Concr. Res.* **30**, 623–634 (2000)
29. Ng, P.L., Kwan, A.K.H.: Improving concrete durability for sewerage applications. In: Tse, P.W., Mathew, J., Wong, K., Lam, R., Ko, C.N. (eds.) *Engineering asset management—systems, professional practices and certification*, pp. 1043–1053. Springer International Publishing, Cham (2015)
30. Nielsen, A.H., Vollertsen, J., Jensen, H.S., Wium-Andersen, T., Hvitved-Jacobsen, T.: Influence of pipe material and surfaces on sulfide related odor and corrosion in sewers. *Water Res.* **42**, 4206–4214
31. Noeiaghahi, T., Mukherjee, A., Dhama, N., Chae, S.-R.: Biogenic deterioration of concrete and its mitigation technologies. *Constr. Build. Mater.* **149**, 575–586 (2017)
32. Okeniyi, J.O., Omoniyi, O.M., Okpala, S.O., Loto, C.A., Popoola, A.P.I.: Effect of ethylene-diaminetetraacetic disodium dihydrate and sodium nitrite admixtures on steel-rebar corrosion in concrete. *Eur. J. Environ. Civ. Eng.* **17**, 398–416 (2013)
33. Parande, A.K., Ramsamy, P.L., Ethirajan, S., Rao, C.R.K., Palanisamy, N.: Deterioration of reinforced concrete in sewer environments, pp. 11–20. Published for the Institution of Civil Engineers by Thomas Telford Services, c1992-, London (2006)
34. Peier, W.H.: Adhesion testing of polymer modified cement mortars. In: Sasse, H.R. (ed.) *Adhesion between polymers and concrete/Adhésion entre polymères et béton: Bonding · Protection · Repair/Revêtement · Protection · Réparation*. Springer US, Boston, MA (1986)
35. Saito, T., Brdjanovic, D., van Loosdrecht, M.: Effect of nitrite on phosphate uptake by phosphate accumulating organisms. *Water Res.* **38**, 3760–3768 (2004)
36. Saucier, F., Herisson, J.: Use of calcium aluminate cement in H₂S biogenic environment. In: Hewlett, P., Mangabhai, R., Taylor, G., Domone, P., Trout, E., Goodier, C., Berrie, I., Killoran, D. (eds.) *Yearbook, 2016*, pp. 67–80. Institute of Concrete Technology (2015)
37. Sharmin, E., Imo, L., Ashraf, S.M., Ahmad, S.: Acrylic-melamine modified DGEBA-epoxy coatings and their anticorrosive behavior. *Prog. Org. Coat.* **50**, 47–54 (2004)
38. Sun, X., Jiang, G., Bond, P.L., Keller, J., Yuan, Z.: A novel and simple treatment for control of sulfide induced sewer concrete corrosion using free nitrous acid. *Water Res.* **70**, 279–287 (2015)
39. Sun, X., Jiang, G., Chiu, T.H., Zhou, M., Keller, J., Bond, P.L.: Effects of surface washing on the mitigation of concrete corrosion under sewer conditions. *Cement Concr. Compos.* **68**, 88–95 (2016)
40. Sydney, R., Esfandi, E., Surapaneni, S.: Control concrete sewer corrosion via the crown spray process. *Water Environ. Res.* **68**, 338–347 (1996)

41. Vipulanandan, C., Liu, J.: Performance of polyurethane-coated concrete in sewer environment. *Cem. Concr. Res.* **35**, 1754–1763 (2005)
42. Wang, T., Wu, K., Kan, L., Wu, M.: Current understanding on microbiologically induced corrosion of concrete in sewer structures: a review of the evaluation methods and mitigation measures. *Constr. Build. Mater.* **247**, 118539 (2020)
43. Wells, T., Melchers, R.: An observation-based model for corrosion of concrete sewers under aggressive conditions. *Cem. Concr. Res.* **61**, 1–10 (2014)
44. Yoshida, Y., Takahashi, K., Saito, T., Tanaka, K.: The effect of nitrite on aerobic phosphate uptake and denitrifying activity of phosphate-accumulating organisms. *Water Sci. Technol.* **53**, 21–27 (2006)
45. Zhang, S.-H., Huang, Y., Hua, Y.-M.: Denitrifying dephosphatation over nitrite: effects of nitrite concentration, organic carbon, and pH. *Biores. Technol.* **101**, 3870–3875 (2010)